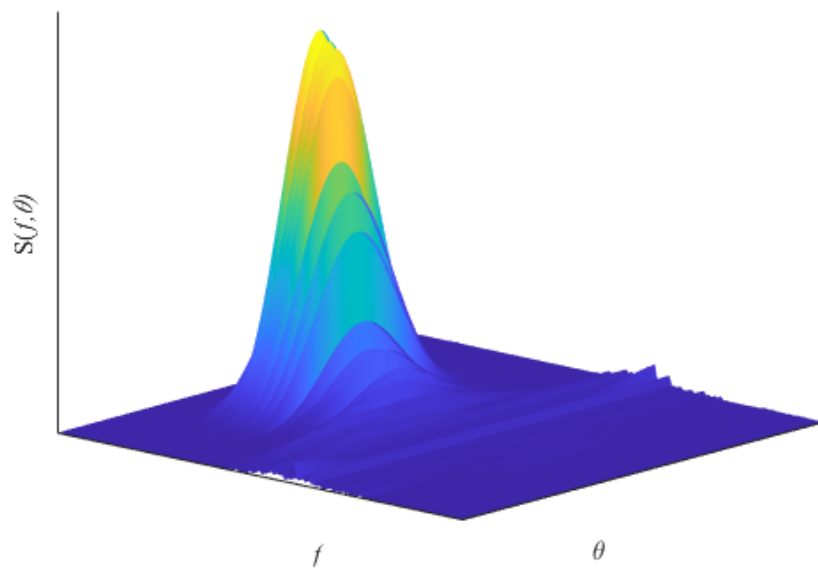


Aalborg University

Directional Analysis of Nonlinear Waves

Nonlinear Effects in Relation to Estimation of Directional Parameters



Master Thesis
Louise Vixø and Sarah Krogh Iversen
Structural and Civil Engineering
Aalborg University
June 9th 2022



**AALBORG
UNIVERSITY**

STUDENT REPORT

**4th semester, M.Sc. programme in
Structural and Civil Engineering**

Thomas Manns Vej 23
9220 Aalborg Øst

Title:

Directional Analysis of Nonlinear Waves

Topic:

Nonlinear Effects in Relation to Estimation of Directional Parameters

Project:

Master project

Project period:

August 2021 - June 2022

Attendees:

Louise Vixø
Sarah Krogh Iversen

Supervisors:

Thomas Lykke Andersen
Peter Frigaard

Number of pages: 701

Hand in: 9th of June 2022

Abstract

The purpose of this master thesis is to study if nonlinearity will have an influence on the directional wave analysis, when the analysis is based on linear wave theory. Two methods are considered; a simple method containing a geometrical solution of the wave propagation direction using the phase difference of the waves, in which only long-crested waves are possible to analyse. A statistical method with the directional parameters including the mean wave direction and the spreading when analysing the spectral density using the method containing cross-spectral analysis and the fitting method of maximum likelihood estimation of directional spectrum in standard form, which is determined as the Mitsuyasu-type directional spreading function. This analysis manages both long-crested and short-crested waves.

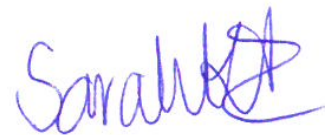
The analyses are performed for different cases placed in different water depths related to the Diagram of Le Mehaute, which contain different amount of second order energy when including this, and the cases similarly have different amount of amplitude dispersion. Furthermore, different generation methods produce different accuracy of the directional parameters. In this master thesis both long-crested and short-crested waves are considered. From the analyses of the waves fields, an impact of the nonlinearity is discovered for the cases including most second order energy or containing a faster wave celerity than predicted by linear wave theory. The directional analyses of the wave fields show a correlation between the amount of second order energy and the errors on the estimated directions.

For further investigation of the sensibility of the directional analysis of the waves, other effects are added including noise, calibration error and missing gauges. These analyses show random errors related when including noise, more organised errors related to calibration errors depending on the affected gauge, even larger than if a gauge is missing. This is also placed in context with both the second order waves and the waves with amplitude dispersion. The worst error is discovered for Method 1 including second order energy. Overall, Method 1 has a high accuracy from only three gauges and seems to be a fine estimation of long-crested waves, but is quite sensitive to second order waves, especially, for cases which do not fulfill the requirement of linear theory or Stokes second order wave theory. This method is however not implemented in practice. Method 2 seems more robust but must contain more wave gauges measurements. When using Method 2, all results show an accuracy within $\pm 5^\circ$, except for cases for which the combination of a relative high wave steepness, shallow water depth and more than 12% of second order energy compared to first order energy, which results in an inaccurate estimation of the directional parameters from a directional analysis.

Aalborg University, 9th of June 2022



Louise Vixø
lvixø20@student.aau.dk
20200900



Sarah Krogh Iversen
sivers20@student.aau.dk
20200921

Table of Contents

| | | |
|-----------|---|----|
| I | Introduction | |
| Chapter 1 | Introduction | 1 |
| Chapter 2 | Generation of Synthetic Data | 3 |
| 2.1 | Linear Wave Theory | 3 |
| 2.2 | Second Order Wave Theory | 6 |
| 2.3 | Nonlinear Effects | 10 |
| Chapter 3 | Analysis Methods | 13 |
| 3.1 | Method 1 | 13 |
| 3.2 | Method 2 | 16 |
| Chapter 4 | Test Cases for Generation of Data | 22 |
| 4.1 | Relative Wave Parameters of Test Cases | 22 |
| II | Nonlinear Effects | |
| Chapter 5 | Method 1: Long-Crested Waves | 26 |
| 5.1 | Analysis of First Order Waves | 26 |
| 5.2 | Analysis of Second Order Waves | 30 |
| 5.3 | Analysis of Waves With Amplitude Dispersion | 33 |
| 5.4 | Summary of Long-Crested Waves - Method 1 | 35 |
| Chapter 6 | Method 2: Long-Crested Waves | 37 |
| 6.1 | Analysis of First Order Waves | 37 |
| 6.2 | Analysis of Second Order Waves | 38 |
| 6.3 | Analysis of Waves With Amplitude Dispersion | 40 |
| 6.4 | Summary of Long-Crested Waves - Method 2 | 42 |
| Chapter 7 | Method 2: Short-Crested Waves | 44 |
| 7.1 | Generation Models of Synthetic Waves | 45 |
| 7.2 | Analysis of First Order Waves | 47 |
| 7.3 | Analysis of Second Order Waves | 49 |
| 7.4 | Analysis of Waves With Amplitude Dispersion | 52 |
| 7.5 | Summary of Short-Crested Waves | 55 |
| Chapter 8 | Evaluation of Methods and Nonlinear Effects | 58 |

| | |
|-----|---------------|
| III | Other Effects |
|-----|---------------|

| | | |
|------------|---|----|
| Chapter 9 | Noise | 65 |
| 9.1 | Long-Crested Waves | 65 |
| 9.2 | Short-Crested Waves | 68 |
| 9.3 | Summary of Noise Error | 70 |
| Chapter 10 | Errors Related to Calibration | 72 |
| 10.1 | Long-Crested Waves | 72 |
| 10.2 | Short-Crested Waves | 75 |
| 10.3 | Limitation of Application | 76 |
| Chapter 11 | Wave Gauge Arrangement | 77 |
| Chapter 12 | Analysis of Laboratory Tests | 81 |

| | |
|----|------------|
| IV | Evaluation |
|----|------------|

| | | |
|------------|--|----|
| Chapter 13 | Discussion | 83 |
| 13.1 | Nonlinearity Including Other Effects | 83 |
| 13.2 | Application of Data | 84 |
| 13.3 | Further Investigation | 85 |
| Chapter 14 | Conclusion | 87 |
| Chapter 15 | References | 89 |

| | |
|---|------------|
| V | Appendix I |
|---|------------|

| | | |
|------------|---|-----|
| Appendix A | Generation of Synthetic Waves | 94 |
| A.1 | Long-Crested Waves | 94 |
| A.2 | Nonlinear Wave | 101 |
| A.3 | Short-crested Waves | 107 |
| Appendix B | Fourier Analysis | 111 |
| B.1 | Cosine Taper Data Window | 112 |
| Appendix C | Directions | 113 |
| C.1 | Method 1 | 113 |
| C.2 | Method 2 | 113 |
| Appendix D | Second Order Wave Field | 115 |
| D.1 | Bichromatic Wave Field | 115 |
| D.2 | Irregular Wave Field | 117 |

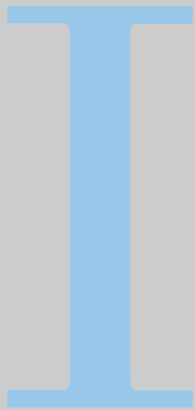
| | | |
|------------|---|-----|
| Appendix E | Convergence Study | 119 |
| E.1 | Single Summation Model | 119 |
| E.2 | Double Summation Model | 121 |
| Appendix F | Short-Crested Waves in More Directions | 124 |
| F.1 | First Order Waves | 124 |
| F.2 | Second Order Waves | 125 |
| F.3 | Waves with Amplitude Dispersion | 126 |
| Appendix G | Variability due to Number of Subseries | 128 |
| Appendix H | Analysis of Signal with Noise Added | 132 |
| H.1 | Long-Crested Waves | 132 |
| H.2 | Short-Crested Waves | 135 |
| Appendix I | Errors Related to Calibration | 141 |
| I.1 | Long-Crested Waves | 141 |
| I.2 | Short-Crested Waves | 156 |
| Appendix J | Improvements Related to Calibration Error | 169 |
| J.1 | Detection of Calibration Error | 169 |

| | |
|----|--------------------|
| VI | Appendix II - Data |
|----|--------------------|

| | | |
|-------------|---|-----|
| Appendix AA | Data: Long-Crested Waves - Method 1 | 173 |
| Appendix AB | Data: Long-Crested Waves - Method 2 | 287 |
| Appendix AC | Data: Short-Crested Waves | 359 |
| Appendix AD | Data: Long-Crested Waves incl. Noise | 373 |
| Appendix AE | Data: Short-Crested Waves incl. Noise | 436 |
| Appendix AF | Data: Long-Crested Waves incl. Errors Related to Calibration | 449 |
| Appendix AG | Data: Short-Crested Waves incl. Errors Related to Calibration | 655 |
| Appendix AH | Data: Wave Gauge Arrangement | 678 |
| Appendix AI | Data: Variability of Double Summation Model | 692 |

Nomenclature

| | |
|---------------------|---|
| a | Wave amplitude [m] |
| A | Fourier coefficient related to the real part of wave amplitude [m] |
| B | Fourier coefficient related to the imaginary part of wave amplitude [m] |
| C | Co-spectrum [m ² s] |
| $D(\omega, \theta)$ | Directional spreading function [1/rad] |
| f | Frequency [Hz] |
| f_p | Peak frequency [Hz] |
| f_s | Sample frequency [Hz] |
| g | Gravitational acceleration [m/s ²] |
| $G^{(2)\pm}$ | Transfer function [-] |
| h | Water depth [m] |
| H_{m0} | Significant wave height based on frequency domain analysis [m] |
| J | Number of subseries [-] |
| k | Wave number [m ⁻¹] |
| L | Wavelength [m] |
| M | Number of direction components [-] |
| N | Number of frequency components [-] |
| p | Probability density function [-] |
| P | Number of gauge positions [-] |
| Q | Quad-spectrum [m ² s] |
| r | Distance between two gauges [m] |
| s | Spreading parameter [-] |
| $S(\omega)$ | Variance spectrum [m ² s] |
| $S(\omega, \theta)$ | Directional wave spectrum [m ² s/rad] |
| t | Time [s] |
| T | Wave period [s] |
| T_0 | Duration [s] |
| x | x -coordinate [m] |
| y | y -coordinate [m] |
| | |
| β | Angle between wave gauges [rad] |
| η | Surface elevation [m] |
| γ | Peak enhancement factor [-] |
| κ | Cross-covariance [-] |
| \mathcal{L} | Likelihood function [-] |
| ω | Angular frequency [rad/s] |
| ϕ | Phase [rad] |
| ρ | Water density [kg/m ³] |
| σ^2 | Variance [m ²] |
| σ | Spreading [°] |
| θ | Wave propagation angle [rad] |
| θ_0 | Mean wave direction [rad] |



Introduction

| | | |
|-----------|---|----|
| Chapter 1 | Introduction | 1 |
| Chapter 2 | Generation of Synthetic Data | 3 |
| 2.1 | Linear Wave Theory | |
| 2.2 | Second Order Wave Theory | |
| 2.3 | Nonlinear Effects | |
| Chapter 3 | Analysis Methods | 13 |
| 3.1 | Method 1 | |
| 3.2 | Method 2 | |
| Chapter 4 | Test Cases for Generation of Data | 22 |
| 4.1 | Relative Wave Parameters of Test Cases | |

1 | Introduction

In which direction sea waves travel might be a simple question to answer for simple wave models, but the question gets much more complicated to answer for more complex wave models or in a real sea. A sea in severe weather might be unstructured and disordered, and a lot of different parameters can be used to describe the sea. A random sea state can be described by a directional surface elevation spectrum, where the energy distribution of a sea state is presented as a function of wave frequency and wave propagation direction. The directional wave spectrum is a significant parameter when designing offshore structures, estimating direction and magnitude of sediment transport by waves, determining the wave disturbance in harbours or determining the ship motions. Further, it is relevant for making wind-wave models or calculating the stability of breakwater roundheads.

In this master thesis, directional analysis of waves and the reliability hereof will be investigated further by use of different models. The development of the computational capacity has enabled the inclusion of more complex wave theory in wave analysis. So far nonlinear effects in wave analysis have been evaluated in relation to separation of incident and reflected components in regular waves by Andersen et al. (2017), which is an extension of the method by Lin and Huang (2004), which takes into account the bound higher harmonics and amplitude dispersion. The method has been extended to also cover irregular waves by Andersen and Eldrup (2019) using a narrowband approximation, through which the method has proven from numerical and physical models to cover highly nonlinear, long-crested, uni-directional, irregular waves as well. It has yet to be investigated how the nonlinearity affects the estimation of short-crested multi-directional waves.

The effects of the nonlinearity, when determining the direction of waves, are in this thesis investigated using different assumptions and models to describe the phenomena directional waves. The wave models used in this project will be of different level of detail, and therefore also different level of complexity. Initially, irregular long-crested waves are considered, making it possible to determine the direction and the effect of the nonlinearity from a low number of unknown sea parameters and the same number of equations.

Further, three-dimensional wave models are used where the short-crested waves are generated based on the directional spectrum. The directional wave spectrum, also stated as the directional variance spectrum of the surface elevation, is given in Equation (1.1) and sketched in Figure 1.1 to illustrate the principle of the energy spectrum.

$$S_{\eta}(\omega, \theta) = D(\omega, \theta) S_{\eta}(\omega) \quad \text{with} \quad \int_0^{2\pi} D(\omega, \theta) d\theta = 1 \quad (1.1)$$

where

| | | |
|---------------------|--|--------------------------------|
| $D(\omega, \theta)$ | | Directional spreading function |
| $S_{\eta}(\omega)$ | | Frequency variance spectrum |

The frequency variance spectrum, $S_{\eta}(\omega)$, is represented in the plane of the energy and the angular frequency, ω , and describe the wave elevation process, while the directional spreading function, $D(\omega, \theta)$, is represented in the depth of the figure with varying direction, θ .

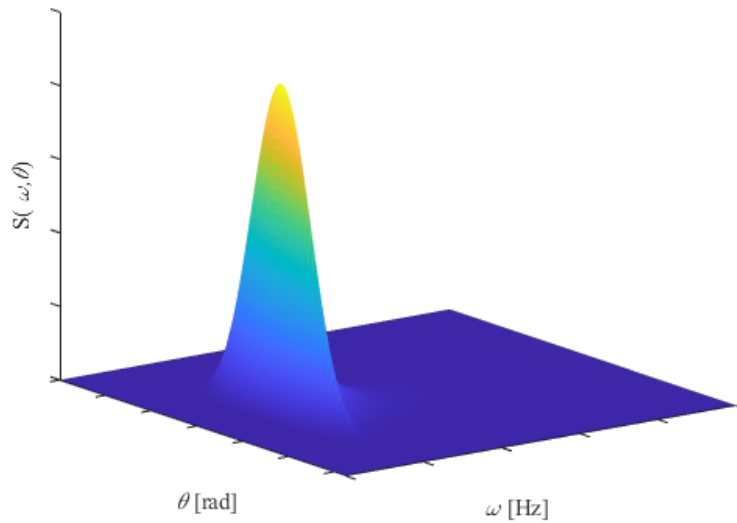


Figure 1.1: Directional Wave Spectrum.

The directional spectrum, $S(\omega, \theta)$, can be related to data, which in this thesis consists of surface elevation measurements. This is done through stochastic analysis methods. Different methods have been developed to solve this relation and some of them have been classified and discussed by Benoit et al. (1997), in which it is concluded, that methods in the directional wave analysis that fit to the data using a statistical method are to be preferred. Common for all methods is however, that they are based on linear wave theory, which is valid for waves of small steepness with a high relative water depth. For other conditions, other wave theories will have to be applied, which can be done based on the diagram of Le MéHauté (1976). In this thesis, the statistical fitting method will be used to fit the two directional parameters, a mean wave direction, θ_0 , and a spreading, σ . These parameters are characteristic for the directional spreading function.

The aim of this thesis is therefore to investigate the reliability of using linear wave theory in directional wave analysis of nonlinear waves.

Common for all approaches in this thesis is, that they are performed on synthetic waves in order to control the amount of degrees of freedom during the different approaches. The generation of synthetic waves enables the inclusion of for instance nonlinearity, multidirectionality and choice of variance spectra. The nonlinear wave theory used in the generation of synthetic data for this thesis is limited to Stokes second order wave theory. For inclusion of higher order effects, the wavelength is adjusted according to stream function theory in order to include simplified amplitude dispersion. Further, the generation of synthetic data is limited to eight different cases of sea states with different relative water depth and wave steepness, which are considered to investigate the consequences hereof. Breaking waves are not included in any of the cases considered in this project.

Additionally, this thesis is delimited to handling measurements of surface elevations from different gauge positions. Other signals than surface elevations can be included using transfer functions. It is furthermore assumed that the waves being analysed are incident. Reflection in the wave field can be included as given by Isobe and Kondo (1984) and Christensen and Sørensen (1994) but is not within the scope of this project.

2 | Generation of Synthetic Data

In this chapter, the wave theory used to generate synthetic data in the present thesis is described. The synthetic waves are generated by a program produced for the purpose of this master thesis. A more detailed description is stated further in Appendix A. The chapter is separated into linear wave theory, which is described in section 2.1. This is followed by second order wave theory and the inclusion of this in the synthetic wave generation in section 2.2. Lastly, higher order effects are discussed including amplitude dispersion in section 2.3.

2.1 Linear Wave Theory

To determine the direction of a wave with a certain direction of propagation, the measurements of heave, pitch and roll motions can be used to determine velocity components and surface elevation as a function of time at a location. A possible method to measure the wave direction from one measurement point is to measure two horizontal velocity components in perpendicular directions, which have to be correlated to the surface elevation measurements, simultaneously. In the present thesis only measurements of the surface elevation are used to estimate the direction, and therefore only surface elevations are generated, but more than one position is then required.

2.1.1 Generation of Synthetic Long-Crested Waves

The waves analysed in the present thesis are synthetically generated waves as mentioned in chapter 1, which are generated by the mathematical technique; Random phase method described by Tuah and Hudspeth (1982), which is expounded in Appendix A.

Linear Regular Wave - Monochromatic Wave

The most simple wave is a long-crested, linear, regular wave. The surface elevation of an oblique wave is stated in Equation (2.1) with the wave traveling with the direction of propagation, θ .

$$\eta(\vec{x}, t) = C \cos(\vec{k} \vec{x} - \omega t + \phi) \quad (2.1)$$

where

| | |
|-----------|---|
| C | Wave amplitude, $C = \sqrt{A^2 + B^2}$ |
| A | Real part of wave amplitude |
| B | Imaginary part of wave amplitude |
| \vec{k} | Wave number vector, $k[\cos(\theta), \sin(\theta)]$ |
| k | Wave number, $k = 2\pi/L$ |
| θ | Direction of propagation, [rad] |
| \vec{x} | Position of measuring the surface elevation, $\vec{x} = [x, y]^T$ |
| ω | Angular frequency, $\omega = 2\pi/T$ |
| t | Time [s] |
| ϕ | Initial phase [rad] |

The wave number is calculated based on the wavelength, which for linear wave theory is calculated using linear dispersion, $L = \frac{gT^2}{2\pi} \tanh(\frac{2\pi h}{L})$. The synthetic generated waves in this section are all

based on this formula. In the frequency domain, the surface elevation can be expressed through energy as the spectral density. For this simple regular wave, the energy is distributed over just a single frequency corresponding to the frequency step, Δf , and a single direction, which will generate one component in the directional wave spectrum. This is illustrated in Figure 2.1, where the energy in the auto-spectrum is described by Equation (2.2) which is based on the wave amplitude and expressed by the natural frequency, $f = \omega/2\pi$.

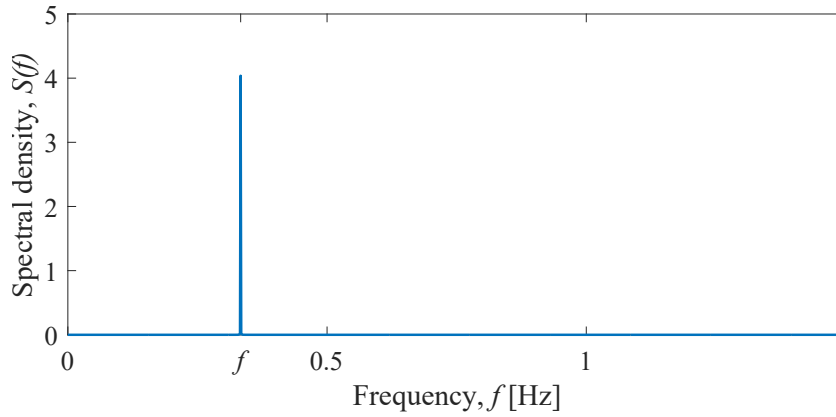


Figure 2.1: Sketch of the energy distribution from one regular wave appearing at one frequency.

$$S_{\eta}(f) = \frac{\frac{1}{2}C^2}{\Delta f} \quad (2.2)$$

where

$$\begin{array}{l|l} \Delta f & \text{Frequency width, } \Delta f = \frac{1}{T_0} \text{ [Hz]} \\ T_0 & \text{Duration of sample [s]} \end{array}$$

To obtain energy at only one frequency, a complete number of periods for the sample duration of the cosine wave is required. From the energy, which appears in the auto-spectrum, it is possible to calculate Fourier coefficients. The coefficients are calculated for each frequency, which result in just one pair of Fourier coefficients, A and B , existing for a regular wave. The coefficients are then used to generate the surface elevation by using an Inverse Fast Fourier Transform, where the energy is transformed from the frequency domain into the time domain.

Uni-directional Irregular Waves

A long-crested, linear, irregular wave field is considered as the sum of a number of regular, linear waves. An irregular wave can mathematically be described from the Fourier coefficients as stated in Equation (2.3), which is a number of linear wave components, N , generated by linear wave theory superposed. This surface elevation appears thus from the sum of the wave components with a frequency distribution as the auto-spectrum.

$$\eta(t) = \sum_{i=0}^{N-1} A_i \cos(\vec{k}_i \vec{x} - \omega_i t) + B_i \sin(\vec{k}_i \vec{x} - \omega_i t) \quad (2.3)$$

As the Fourier transform yields the frequency characteristics of a given sea state, the Fast Fourier transform is used to generate the surface elevation based on a given spectrum. The energy is

distributed over a frequency range as shown in Figure 2.2 with one direction of propagation, θ , which will cause a flat two-dimensional directional wave spectrum, described by Equation (2.4) which is based on the wave amplitudes and expressed by the natural frequencies, $f_i = \omega_i/2\pi$.

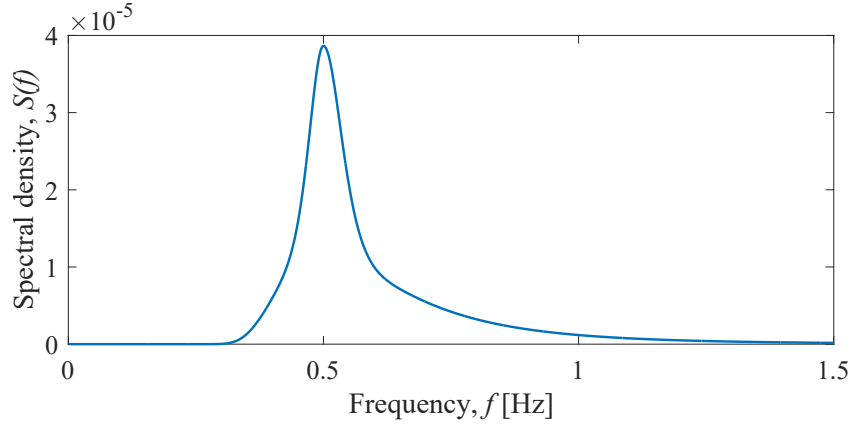


Figure 2.2: Sketch of energy distribution of an irregular wave.

$$S_{\eta}(f_i) = \frac{\frac{1}{2}C_i^2}{\Delta f} \quad \text{for } i = 0, 1, 2, \dots, N - 1 \quad (2.4)$$

The wave field is generated based on the empirical JONSWAP type spectrum suggested by Hasselmann et al. (1973) which depend on the significant wave height, H_{m0} , peak frequency, f_p , and peak enhancement factor, in the present thesis, $\gamma = 3.3$ is assumed, which is typical for waves in the North Sea. These synthetic generated wave fields are further used in the analysis of the directional spectrum of the long-crested waves in chapter 5 and 6.

2.1.2 Generation of Synthetic Short-Crested Waves

The short-crested wave field is generated as irregular waves with a spatial energy spectrum as shown in the introduction in Figure 1.1. The energy distribution is based on the empirical auto-spectrum, $S_{\eta}(\omega)$ and a directional spreading function, $D(\omega, \theta)$ as stated in Equation (2.5). The product of the directional spreading function, $D(\omega, \theta)$ and the auto-spectrum, $S_{\eta}(\omega)$ results in the directional wave spectrum, $S_{\eta}(\omega, \theta)$.

$$S_{\eta}(\omega, \theta) = D(\omega, \theta)S_{\eta}(\omega) \quad (2.5)$$

Theoretically, to assure identical wave energy in the directional wave spectrum and the uni-directional auto-spectrum, it is required that the result of integrating the directional spreading function from 0 to 360° becomes equal to 1.

Multi-directional Irregular Waves

Similar to the two-dimensional irregular waves generated by linear wave theory, the irregular three-dimensional waves are described as a linear superposition of a certain number of wave components. Just as the two-dimensional irregular wave, the waves are generated based on the frequency distribution of the JONSWAP spectrum, $S_{\eta}(\omega)$. The direction of the wave components are in the present thesis generated with the distribution of the directional spreading function

as the Mitsuyasu-type directional spectrum proposed by Mitsuyasu et al. (1975) with mean direction, θ_0 , and with the spreading parameter, s , as a cosine power function. This distribution of the directional spreading function is shown in Equation (2.6) and is an empirical proposal to the formulation of the directional spectrum.

$$D(\omega, \theta) = \frac{2^{2s-1} \Gamma^2(s+1)}{\pi \Gamma(2s+1)} \left[\cos \left(\frac{\theta - \theta_0}{2} \right) \right]^{2s} \quad (2.6)$$

where

$$\begin{array}{l|l} s & \text{Spreading parameter} \\ \theta_0 & \text{Mean direction} \end{array}$$

In the present thesis, the standard deviation of the spreading function, σ , which describes the directional spreading of the waves, is calculated based on the estimated spreading parameter, s , and the spreading function, $D(\omega, \theta)$. When generating irregular, short-crested waves, two different wave models exists, single and double summation models. In the single summation wave model, each of the f_i frequency components are assigned a single direction, θ_i . This is mathematically expressed in Equation (2.7), where the surface elevation, η , is summed over the number of frequencies, N , times the number of directions, M , which for a single summation model will be $M = 1$ for each of the N frequency components.

$$\eta(\vec{x}, t) = \sum_{i=0}^{(N-1) \cdot M} C_i \cos(\vec{k}_i \vec{x} - \omega_i t + \phi_i) \quad (2.7)$$

The direction, θ_i , is chosen based on the desired distribution of the spreading function, $D(\omega, \theta)$, which in this case is the directional spreading function from Equation (2.7), by choosing a random number with a probability density function equal to the spreading function based on a Monte Carlo simulation. In the double summation model, multiple directions, θ_j , are assigned to each frequency component, f_i . In this model, the directional components are chosen equally distributed from 0 to 2π . This is mathematically expressed in Equation (2.8), where the surface elevation, η , is summed over the number of frequencies, N and summed over the number of directions, M .

$$\eta(\vec{x}, t) = \sum_{i=0}^{N-1} \sum_{j=1}^M C_{ij} \cos(\vec{k}_{ij} \vec{x} - \omega_i t + \phi_{ij}) \quad (2.8)$$

These synthetic generated wave fields are further used in the analysis of the directional spectrum of the short-crested waves in chapter 7.

2.2 Second Order Wave Theory

The energy spectrum shown in Figure 1.1 is derived from linear wave theory and do not include second or other higher order energy contributions. These contributions will affect the energy and redistribute energy to other frequencies and frequencies where no energy is expected. When

including Stokes second order wave theory, the total surface elevation become the sum of the first order solution and the second order contribution as stated in Equation (2.9).

$$\eta(\vec{x}, t) = \eta^{(1)}(\vec{x}, t) + \eta^{(2)}(\vec{x}, t) \quad (2.9)$$

where

$$\begin{array}{l|l} \eta^{(1)} & \text{Surface elevation derived from linear wave theory and expressed in Equation (2.3)} \\ \eta^{(2)} & 2^{nd} \text{ order contribution to surface elevation derived from Stokes second order wave theory} \end{array}$$

The second order contribution of the surface elevation occurs when two wave components interact with each other. The second order contribution similarly depend on the wave generation model that is used. For the generation of long-crested waves and short-crested waves based on the single summation model, the contribution appears from Equation 2.10. For short-crested waves generated based on the double summation model, the second order contribution appears from Equation 2.11.

$$\eta^{(2)\pm}(\vec{x}, t) = \sum_{n=0}^{N-1} \sum_{m=n}^{N-1} \eta_{nm}^{(2)+}(\vec{x}, t) + \sum_{n=0}^{N-1} \sum_{m=n+1}^{N-1} \eta_{nm}^{(2)-}(\vec{x}, t) \quad (2.10)$$

$$\eta^{(2)\pm}(\vec{x}, t) = \sum_{n=0}^{N-1} \sum_{m=n}^{N-1} \sum_{j=1}^M \sum_{k=j}^M \eta_{nmjk}^{(2)+}(\vec{x}, t) + \sum_{n=0}^{N-1} \sum_{m=n+1}^{N-1} \sum_{j=1}^M \sum_{k=j}^M \eta_{nmjk}^{(2)-}(\vec{x}, t) \quad (2.11)$$

where

$$\begin{array}{l|l} \eta^{(2)+} & \text{Superharmonic component} \\ \eta^{(2)-} & \text{Subharmonic component} \end{array}$$

According to second order wave theory, the energy is redistributed and more energy components will be generated, including superharmonics and subharmonics. The nonlinear subharmonic appears from the interaction between two or more wave components at difference frequencies, where the nonlinear superharmonics appear at sum frequencies. This means that the interaction between two components at different frequencies will results in four second order components including one subharmonic and three superharmonics.

2.2.1 Generation of Second Order Waves

As mentioned earlier, the effect from the second order contribution will be studied for both a very simple model with an long-crested irregular wave field including Stokes second order wave theory and then further for short-crested waves based on a single summation model where each frequency has one direction and based on a double summation model where each frequency has multiple directions. First, the principle is described by a bichromatic wave field.

Bichromatic waves

When considering two regular waves, which are generated based on linear wave theory, this will result in the sum of the two wave components with each a wave height and a wave period. The two wave components are in the following described as wave component n and wave component

m . The surface elevation of the sum of the wave components is shown in Equation (2.12), where each component has a wave amplitude, wave number and frequency.

$$\begin{aligned}\eta_{nm}^{(1)}(\vec{x}, t) &= \eta_n(\vec{x}, t) + \eta_m(\vec{x}, t) \\ &= A_n \cos(\vec{k}_n \vec{x} - \omega_n t) + B_n \sin(\vec{k}_n \vec{x} - \omega_n t) \\ &\quad + A_m \cos(\vec{k}_m \vec{x} - \omega_m t) + B_m \sin(\vec{k}_m \vec{x} - \omega_m t)\end{aligned}\quad (2.12)$$

The surface elevation of first order wave components are plotted in Figure 2.3 which shows the two wave components without their interaction.

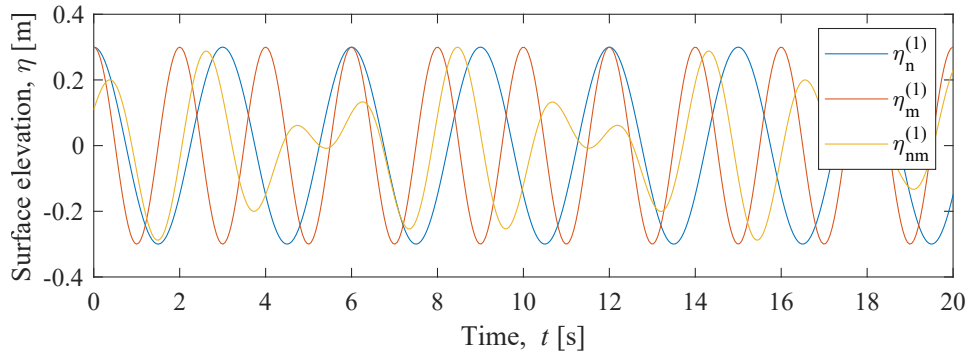


Figure 2.3: Sketch of surface elevation based on the components of η_n and η_m .

When two wave components interact with each other, a second order contribution will occur by nonlinear interaction. This gives rise to sub- and superharmonics for each interaction. Considering the two wave components having the frequencies, ω_n and ω_m , and directions, θ_n and θ_m , as described by Equation (2.13).

$$\begin{aligned}\eta_{nm}^{(2)\pm}(\vec{x}, t) &= G_{nm}^{\pm} \left[(A_n A_m \mp B_n B_m) \cos((\vec{k}_n \pm \vec{k}_m) \vec{x} - (\omega_n \pm \omega_m) t) \right. \\ &\quad \left. + (A_m B_m \pm A_n B_m) \sin((\vec{k}_n \pm \vec{k}_m) \vec{x} - (\omega_n \pm \omega_m) t) \right]\end{aligned}\quad (2.13)$$

where
 G_{nm}^{\pm} | 2nd order surface elevation transfer function

The surface elevation of the first order contribution, second order contribution and the sum hereof are likewise plotted in Figure 2.4.

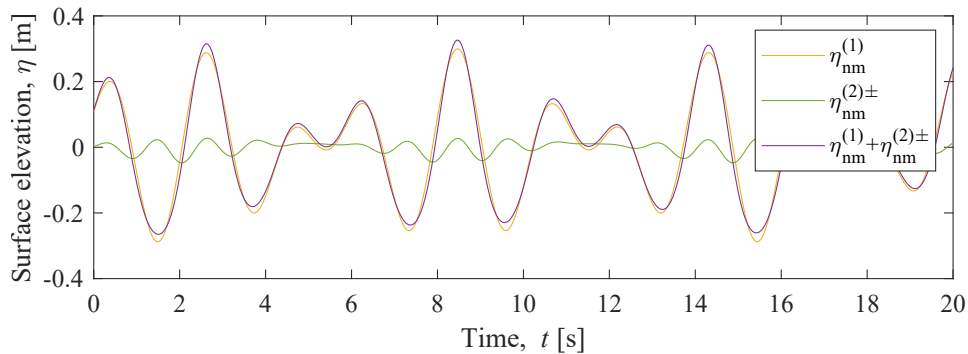


Figure 2.4: Sketch of surface elevation based on 1st and 2nd order components of η .

The transfer function G_{nm}^{\pm} , presented by Schäffer and Steenberg (2002), appears from the assumption that the second order contribution of the wave has the order of $O\left(\left(\frac{H}{h}\right)^2\right)$. By considering the equation of horizontal motion, the equation of continuity, the equation of momentum, the first order expression for the surface elevation, $\eta^{(1)}$, the velocities, $u^{(1)}$ and $v^{(1)}$, and the pressure, $p^{(1)}$, the transfer function is shown in Equation (2.14). The parameters H_{nm}^{\pm} , D_{nm}^{\pm} and L_{nm}^{\pm} are further expressed in Appendix A.

$$G_{nm}^{\pm} = \frac{\delta_{nm}}{g} \left((\omega_m \pm \omega_n) \cdot \frac{H_{nm}^{\pm}}{D_{nm}^{\pm}} - L_{nm}^{\pm} \right) \quad (2.14)$$

where

$$\delta_{nm} \left| \begin{array}{l} \text{where } \delta_{nm} = \begin{cases} \frac{1}{2}, & \text{for } \omega_n = \omega_m \\ 1, & \text{otherwise} \end{cases} \\ g \quad \text{Gravity acceleration, } g = 9.82 \text{ m/s}^2 \end{array} \right.$$

The raised \pm symbolizes the super- and subharmonics which occur from the combination of frequencies. The plus represents the superharmonics, $\omega_n + \omega_m$, while the minus represents the subharmonic, $\omega_n - \omega_m$. All the super- and subharmonics are summed to get the second order contribution as shown in Equation (2.10) and (2.11), and the total surface elevation, η , is given by the sum of the first and second order contributions as given in Equation (2.9). The energy of the bichromatic wave field will occur at the frequencies, ω_n , ω_m and $\omega_n \pm \omega_m$ which include both linear and nonlinear energy as sketched in Figure 2.5. The spectral density, $S_{\eta}(f)$, is calculated from Equation (2.2) including the second order wave amplitudes to obtain all components.

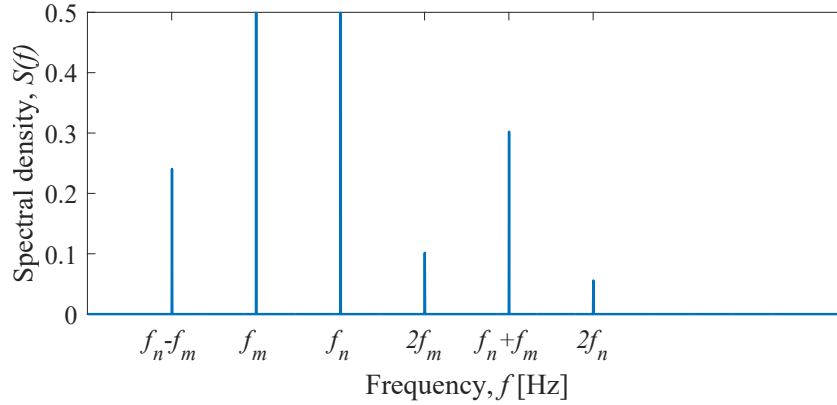


Figure 2.5: Sketch of energy peaks from two regular waves at 6 frequencies. Zoomed for illustration of second order components.

Nonlinear Irregular Wave

A nonlinear, irregular wave is similarly considered as the sum of a number of regular, nonlinear waves, in this case second order waves. A second order irregular wave is sketched in Figure 2.6 for a wave field based on a JONSWAP spectrum.

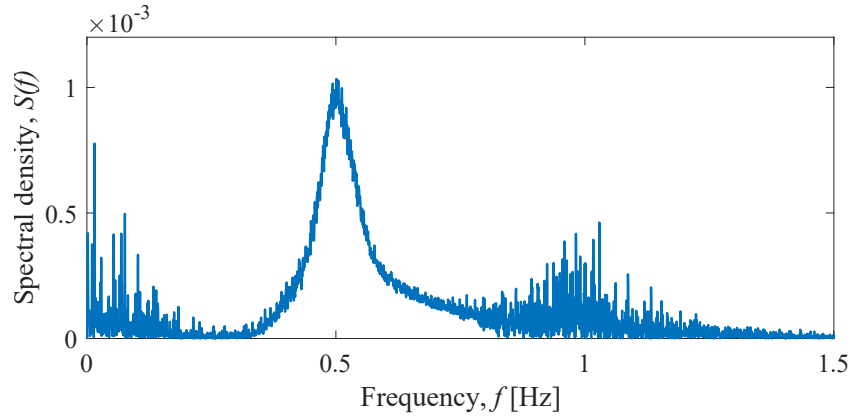


Figure 2.6: Wave energy spectrum containing 1st and 2nd order energy.

To generate short-crested, nonlinear waves the surface elevation must be summed as like either the single or double summation model, this is shown in Equation (2.15) and Equation (2.16).

$$\eta(\vec{x}, t) = \sum_{n=0}^{(N-1) \cdot M} \eta_{nm}^{(1)}(\vec{x}, t) + \sum_{n=0}^{(N-1) \cdot M} \sum_{m=n}^{(N-1) \cdot M} \eta_{nm}^{(2)+}(\vec{x}, t) + \sum_{n=0}^{(N-1) \cdot M} \sum_{m=n+1}^{(N-1) \cdot M} \eta_{nm}^{(2)-}(\vec{x}, t) \quad (2.15)$$

$$\eta(\vec{x}, t) = \sum_{n=0}^{N-1} \sum_{j=1}^M \eta_{nm}^{(1)}(\vec{x}, t) + \sum_{n=0}^{N-1} \sum_{m=n}^{N-1} \sum_{j=1}^M \sum_{k=j}^M \eta_{nmjk}^{(2)+}(\vec{x}, t) + \sum_{n=0}^{N-1} \sum_{m=n+1}^{N-1} \sum_{j=1}^M \sum_{k=j}^M \eta_{nmjk}^{(2)-}(\vec{x}, t) \quad (2.16)$$

Second order wave theory is derived to have an unchanged propagation velocity, $c = L/T$, because the second order component is equal to zero as shown in Svendsen and Jonsson (1980). The wavelength, L , must therefore be the same as for first order wave theory and is possible to calculate using linear dispersion. This conduct a wave number, $k = 2\pi/L$, which is then equal for first and second order wave theory.

2.3 Nonlinear Effects

In order to determine the reliability of directional wave analysis based on linear wave analysis, the influence of the nonlinear effects is considered. As the generation of synthetic data is limited to second order wave theory as described above, the influence hereof is quantified by determining the amount of second order energy relative to the total amount of energy in the wave field. Afterwards, the amplitude dispersion is investigated to include some of the effects from higher order wave theory as well.

2.3.1 Second Order Energy

To quantify the influence of the second order contribution, the amount of second order energy out of the total amount of energy for a regular wave of second order wave theory is determined. The amount of second order energy depends on the wave height, H , and water depth, h . The result is illustrated in Figure 2.7.

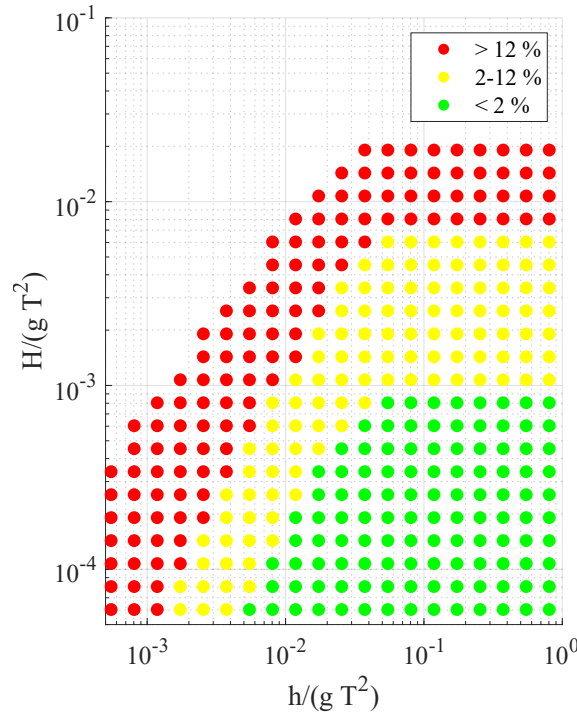


Figure 2.7: Amount of second order contribution out of total energy of regular waves as function of wave height, H , water depth, h , and wave period, T .

In Figure 2.7 it is indicated, when the second order contribution exceeds 2% and 12%, respectively, of the total energy. The separation of these intervals is chosen such that the yellow intervals corresponds more or less to where second order wave theory is valid according to Le MéHauté (1976) for intermediate depth and deep water waves. Generally, the amount of second order energy is though below 2% for waves where first order theory is valid in the green area, between 2 and 12% for waves where second order theory is valid, and above 12% for waves where only higher order theory is valid symbolised by the red area. For the further analyses, the characteristics of the wave field will be taken into account in relation to the reliability, as the energy contribution from second order energy depends on the wave steepness and relative water depth as illustrated in Figure 2.7.

2.3.2 Amplitude Dispersion

As mentioned in the previous sections, the generation of nonlinear waves in the present thesis is limited to second order wave theory, which means that no amplitude dispersion is included in the synthetic data. In the following, the amplitude dispersion will be investigated for a range of regular waves with varying wave height and water depth in order to determine the influence hereof under different conditions also including highly nonlinear waves.

The wavelength is here determined for linear theory as well as stream function theory. In opposition to linear theory, stream function theory estimates the wavelength and wave kinematics rather well under all conditions in relation to wave steepness and relative water depth according to Lin (2008). The wavelength is determined using linear wave theory, where the wavelength is determined based on the linear dispersion relation, $\omega^2 = gk \tanh kh$. The wavelength according to stream function theory is determined in WaveLab Aalborg University (2022).

The results appear from Figure 2.8, with indication of when the wavelengths, and thereby also wave celerities calculated based on stream function theory are within 0.1 % and 5 % larger than predicted by linear wave theory.

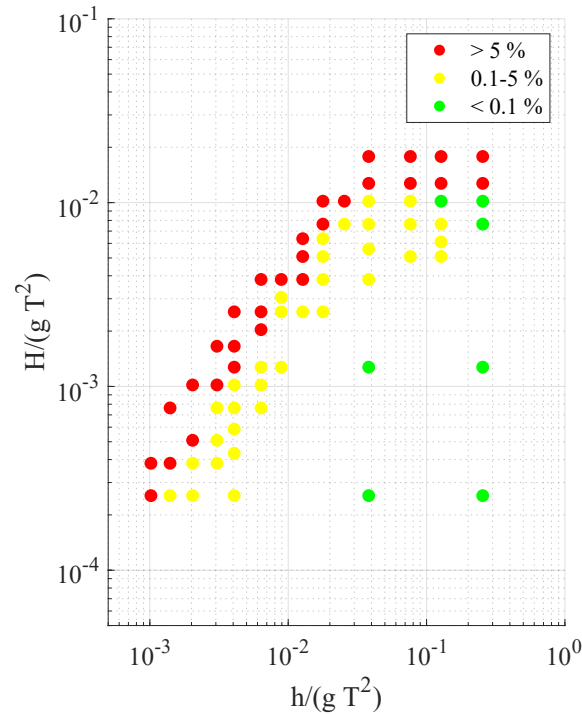


Figure 2.8: Difference in wave celerity for stream function theory compared to linear wave theory for regular waves as function of wave height, H , and water depth, h .

From Figure 2.8 it appears that the effect depends on the wave steepness and relative water depth. With these factors increasing, the more amplitude dispersion is experienced. Furthermore, Figure 2.8 supports the fact that the amplitude dispersion is especially relevant to consider for waves outside of the second order wave theory region as stated by Le Méhauté (1976). The synthetic data are produced for different position in the Diagram of Le Méhauté with different amount of second order energy contribution and different difference of wave celerity compared to the stream function theory. These cases are described further in chapter 4.

3 | Analysis Methods

In this chapter, the methods used in the present thesis for the directional analysis of waves are presented. Overall, this project will include two analysis methods of different complexity. Method 1 is a simple analysis, which makes it possible to determine the direction of propagation, θ , for long-crested waves. Method 2 is a stochastic analysis method, in which it is possible to determine the directional spreading function, $D(\omega, \theta)$, in standard form, which makes it applicable for short-crested waves as well. All analyses are conducted from programs for both methods, that have been programmed for the purpose of this thesis.

Common for the analyses of the present thesis is, that they are based on the assumption, that the wave field can be expressed as a sum of random phase processes. The processes are stated as surface elevations, $\eta(\vec{x}, t)$, relative to the mean water level (MWL) as function of position, $\vec{x} = [x, y]^T$, and time, t , as stated in Equation (3.1).

$$\eta(\vec{x}, t) = \sum_{i=1}^N \sum_{j=1}^M a_{ij} \cos(\vec{k}_{ij} \vec{x} - \omega_i t + \phi_{ij}) \quad (3.1)$$

The wave field is described in terms of the amplitude, a_{ij} , the wave number vector $k_i[\cos(\theta_j), \sin(\theta_j)]$, with the direction of propagation for the wave components, θ_j , the angular frequency of the wave component, ω_i , and a phase, ϕ_{ij} , which is uniformly distributed over $[0; 2\pi]$. This is summed over the number of frequency components, N , and the number of directions, M .

The amplitude of the sinusoidal wave, a_{ij} , can be expressed based on the directional variance spectrum of the wave. Letting the resolution of the wave direction and angular frequency go from discrete to continuous limit values, $\Delta\theta \rightarrow d\theta$ and $\Delta\omega \rightarrow d\omega$, from 0 to 2π and from 0 to ∞ , respectively and inserting this in Equation (3.1) yields Equation (3.2).

$$\eta(\vec{x}, t) = \int_0^\infty \int_0^{2\pi} \cos(\vec{k} \vec{x} - \omega t + \phi) \sqrt{2S(\omega, \theta)} d\theta d\omega \quad (3.2)$$

Based on this assumption, the determination of the direction of the long-crested waves can then be found based on the phase difference between signals of surface elevations in different gauge positions. This can be reduced to a simple analysis method described in section 3.1. The determination of the mean direction of the short-crested waves is a more complex affair, where a stochastic analysis method is used, which is described further in section 3.2.

3.1 Method 1

From measurements of surface elevation in two different gauge positions, it is possible to determine the direction within a span of 180° . In order to determine whether the wave travels one way or the other, surface elevations measurements from a third position, which is not in line with the two other positions, is required. The distance between the measuring positions is therefore also limited to half of the wavelength of the regular wave, or wave component in irregular waves, in order to determine the direction correctly. The inputs used to analyse

time-series of surface elevations are the surface elevation, water depth, gravitational acceleration and the sample frequency. The direction of the long-crested waves, θ , is defined as the positive angle between the direction of propagation and the x -axis of the coordinate system as illustrated in Figure 3.1. The angle is defined as a positive angle between 0 and 2π .

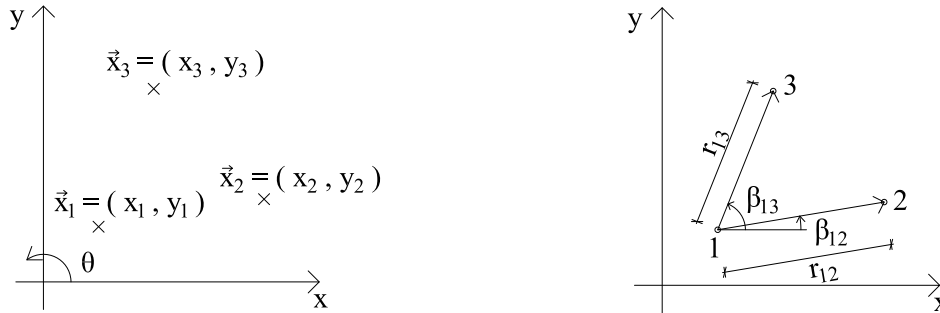


Figure 3.1: Geometry for analysis of long-crested waves.

A frequency domain analysis is performed of the time-series of surface elevation measurements, assuming that the surface elevations for irregular waves can be described as a sum of random phase processes. The Fourier components, $C = A + i \cdot B$, for each frequency component, are determined by Fast Fourier Transform of the discrete signals of surface elevation. The resolution, N , of the frequency domain solution is governed by the duration, T_0 , and sample frequency, f_s .

The direction of the waves is determined from the phase difference between the surface elevation of two different wave gauge positions. The phase of the individual wave components is found from the Fourier coefficient as shown in Equation (3.3). The operational sign of the phase difference, $\Delta\phi_i$, is determined from the sign of the Fourier coefficients. If the difference of both A_i and B_i from the frequency domain analysis of the surface elevation in two measurement points are positive, the phase difference will be defined as positive and therefore be placed in the first quadrant and so on. The principle is shown in Figure 3.2, which shows the definition of the operational sign of the phase, ϕ_i .

$$\phi_i = \tan^{-1} \left(\frac{B_i}{A_i} \right) \quad i = 1..N \quad (3.3)$$

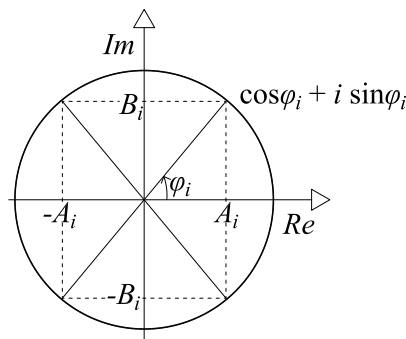


Figure 3.2: Definition of the operational sign of the phase, ϕ_i .

From the phase difference between two gauges, $\Delta\phi_i$, the distance between the two gauges in the direction of the wave, Δx_i , is determined in Equation (3.4) from the ratio between the wave length and the cycle of a phase, which is sketched in Figure 3.3.

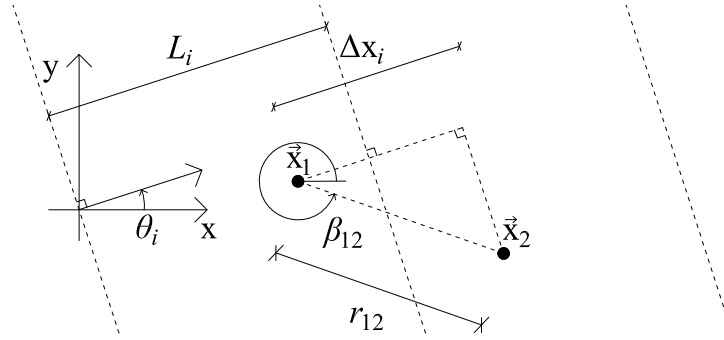


Figure 3.3: Sketch of the principle of Method 1.

$$\Delta x_i = \Delta \phi_i \cdot \frac{L_i}{2 \cdot \pi} \quad \text{for } i = 0, 1, \dots, N \quad (3.4)$$

where

| | |
|-------|---|
| L_i | Wave length based on linear dispersion, $L_i = g \cdot T_i^2 / (2 \cdot \pi) \cdot \tanh(2 \cdot \pi \cdot h / L_i)$, conducted by an iterative procedure. |
| T_i | Wave period, $T_i = T_0 / i$ [s] |
| T_0 | Duration, $T_0 = N / f_s$ [s] |

The direction of the wave in relation to a gauge pair, θ_{local_i} , is then determined from the distance Δx in the direction of the wave and the distance between the two gauges, r_{12} .

$$\Delta x_i = \cos(\theta_{local_i}) \cdot r_{12} \quad \Rightarrow \quad \theta_{local_i} = \cos^{-1} \left(\frac{\Delta x_i}{r_{12}} \right) \quad (3.5)$$

This direction is a local direction according to the two gauges considered, where gauge 1 is placed in the origin and gauge 2 is placed in position $(r_{12}, 0)$ as illustrated in Figure 3.4.

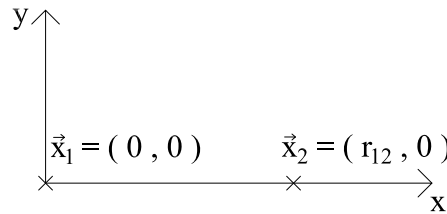


Figure 3.4: Local coordinate system for analysis of direction relative to gauge pair position.

The direction of the wave is then transformed to the global coordinate system using the angle between the considered gauges and the x -axis, β_{12} , as illustrated in Figure 3.1. The global direction, θ_i , is similarly calculated as a positive angle between 0 and 2π in the counter-clockwise direction starting from the x -axis.

$$\theta_i = \theta_{local_i} + \beta_{12} \quad (3.6)$$

As the direction is determined based on a cosine-relation, two different directions are possible outcomes of the analysis, when measurements from two gauge positions are used. The possible directions appear from Figure 3.5.

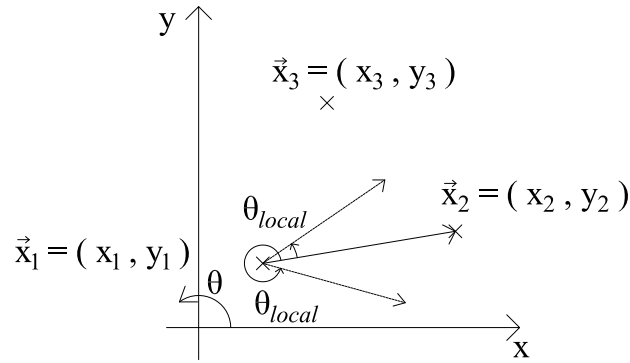


Figure 3.5: Possible outcomes of θ_{local} from analysis based on two wave gauge measurements.

To determine a unique direction, measurements from a third wave gauge position is therefore required. The third wave gauge cannot be in line with the two other gauges in order to determine which of the two directions from Figure 3.5 is correct.

Based on few degrees of freedom and an equal amount of equations, it is though possible to determine the direction of the wave, θ_i , based on the relation between the phase difference, $\Delta\phi_i$, between the signals in the two positions, and the wavelength, L_i . Generally, the wavelength is therefore of significant influence in this approach, wherefore the influence of a miscalculation of the wavelength will be investigated.

3.2 Method 2

Method 2 is introduced as a method that fits to the data in a statistical sense, wherefore a larger amount of gauge positions is required. Furthermore, the present method enables the analysis of short-crested waves, as it fits to a directional spreading distribution. The method contains a stochastic analysis method, which is based on the cross-correlation between two measuring positions. In the present thesis, it is chosen to use the CERC6, which contain six measurement positions as shown in Figure 3.6.

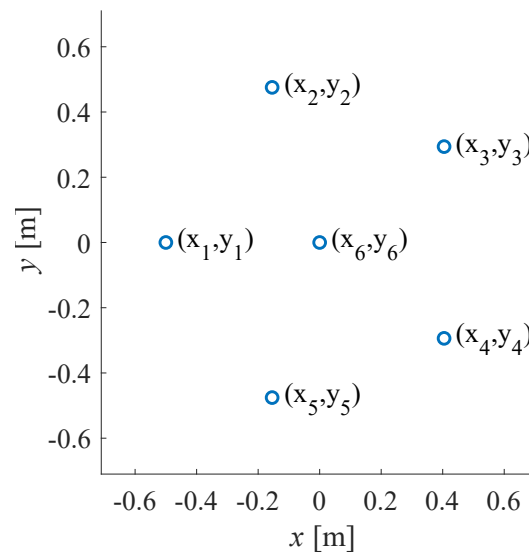


Figure 3.6: Wave gauge arrangement of CERC6.

The stochastic analysis method consists of two steps; a cross-spectral analysis of recorded time-series as specified below followed by determination of the directional spectrum using a given method.

3.2.1 Cross-Spectral Analysis

In the cross-spectral analysis, the correlation between a pair of wave signals is considered. Here surface elevations at different locations recorded simultaneously, $\eta_m(t)$ and $\eta_n(t)$, are considered as illustrated in Figure 3.7.

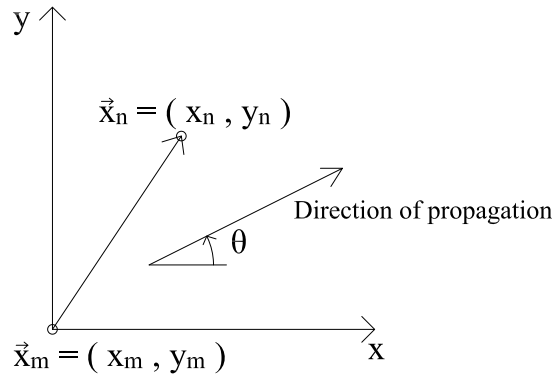


Figure 3.7: Definition of geometrical parameters.

The recorded signals are measured for a given duration, T_0 , and with a sample frequency, f_s , corresponding to a step of Δf . The correlation between the pair of signals measured is calculated from the cross-spectrum, $S_{mn}(\omega)$, in Equation (3.7) which is obtained by the surface elevation signals.

$$S_{mn}(\omega) = \lim_{T \rightarrow \infty} \frac{1}{T} \int_0^T \eta_m(t) \eta_n(t + \tau) dt \exp(-i\omega\tau) d\tau \quad (3.7)$$

Substituting the formulation for the surface elevation from Equation (3.2) into the cross-spectrum and assuming linear wave theory and that the phases of the wave components are randomly distributed over $[0; 2\pi]$, the relationship between the measurements and the unknown directional spectrum $S(\omega, \theta)$ is given in Equation (3.8).

$$S_{mn}(\omega) = \int_0^{2\pi} S(\omega, \theta) \exp\left(i \vec{k} \cdot (\vec{x}_m - \vec{x}_n)\right) d\theta \quad (3.8)$$

When normalised, the relation appears as in Equation (3.9), which relates the known data from the measured surface elevations on the left hand side with the unknown directional spreading function, $D(\omega, \theta)$, from Equation (1.1) on the right hand side. The auto-spectrum, $S(\omega)$, is measured in six different gauge positions where from the mean spectrum, $\bar{S}(\omega)$, is calculated, which results in 15 unique cross-spectra. Theoretically, the auto-spectra in each points are identically, but due to uncertainties, the mean is used for the further analyses.

$$\boxed{\frac{S_{mn}(\omega)}{\bar{S}(\omega)} = \int_0^{2\pi} D(\omega, \theta) \exp\left(-i \vec{k} \cdot (\vec{x}_m - \vec{x}_n)\right) d\theta} \quad (3.9)$$

Equation (3.9) cannot be solved analytically, wherefore further assumptions have to be made. Various methods have been developed based on different assumptions and also with difference in implementation and computation time. In the following, the method, *Maximum Likelihood Estimation of Directional Spectrum in Standard form* suggest by Isobe (1990), is used for further analysis of this thesis.

3.2.2 Maximum Likelihood Estimation of Directional Spectrum in Standard Form

For the following analysis, a maximum likelihood estimation of the directional spectrum in standard form is performed of the synthetic data of surface elevations based on the theory from chapter 2.

The Mitsuyasu-type directional spreading function, $D(\omega, \theta)$, suggest by Mitsuyasu et al. (1975) is used in the present thesis, describing the direction of the waves in terms of a mean wave direction, θ_0 , and a spreading parameter, s , as expressed in Equation (3.10) and illustrated in Figure 3.8. The parameters are to be estimated from the synthetic data generated in the CERC6 array chosen for the present thesis.

$$D(\omega, \theta) = \frac{2^{2s-1} \Gamma^2(s+1)}{\pi \Gamma(2s+1)} \left[\cos \left(\frac{\theta - \theta_0}{2} \right) \right]^{2s} \quad (3.10)$$

This spreading function represents a cosine power function with one peak, which describes waves coming from one mean direction, without considering any kind of reflection or other effects which could generate waves from an opposite direction.

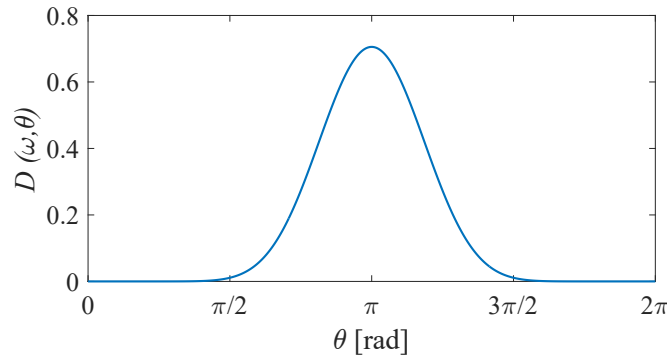


Figure 3.8: Mitsuyasu-type directional spectrum with mean direction $\theta_0 = \pi$ and spreading parameter $s = 6$.

The present maximum likelihood method uses an established relation between the cross-correlation of the six measurements of surface elevations and the directional spectrum to estimate a solution of Equation (3.9). Generally, this method uses the Fourier sums of the surface elevations as they are assumed stationary. From the Fourier coefficients, the mean value vector and the cross-correlation matrix are determined. The elements in the cross-correlation matrix are given in terms of the cross-spectral density of the six surface elevations. The cross-spectral density can be described as a function of the directional spectrum, which can be stated as the distribution of Fourier coefficients as a function of the unknown directional spectrum. The formulation of the likelihood function contains a probability density function of the Fourier coefficients, which estimates the unknown parameters in the directional spectrum based on the maximum likelihood method by maximising the probability of the Fourier coefficients obtained

from the synthetic generated data. Furthermore, it allows for the presence of reflection in the wave field, which is however not included in the present analysis.

To determine the unknown parameters, θ_0 and s , measurements of surface elevations, $\eta(\vec{x}, t)$, in six different positions are considered. It is assumed that the elevation processes in a point can be considered as a sum of harmonic components with Rayleigh distributed amplitudes and uniformly distributed phases. All phases and amplitudes are assumed independent, which means that the elevation processes become normally distributed. The processes are therefore assumed to be joint stationary, ergodic and Gaussian distributed with mean value functions equal to 0. Equation (3.11) expresses the six time series of surface elevations as Fourier sums.

$$\eta_n(\vec{x}, t) = \sum_{i=1}^N (A_{n,i} \cos(\omega_i t) + B_{n,i} \sin(\omega_i t)) \quad n = 1, 2, \dots, P \quad (3.11)$$

where

| | |
|------------|--|
| P | Number of gauges, $P = 6$ for the present thesis using CERC6 |
| ω_i | Cyclic frequency of the i 'th component, $\omega_i = \frac{2\pi}{T_i}$ [rad/s] |
| T_i | Wave period of i 'th component |

The measured surface elevations in each of the P positions are divided into J subseries, from where the spectra are found from Fourier analysis as described in Appendix B. It is assumed that the duration, T_0 , of each of the J subseries is sufficient in order to gain a representative estimate of the cross-spectral density function, since an infinite duration is not possible. The J subseries are modified by the cosine taper data window, as given in Appendix B as well, before the Fourier analysis is performed. The subseries overlap within the span that they are tapered. When dividing the measurements into J subseries, it will be a compromise between resolution and reliability. The total duration of the measurements then governs the number of components in frequency domain, N . The time series are analysed one frequency at a time, to allow for the unknown parameters in the directional spectrum to be frequency dependent. For each of the frequencies, the Fourier coefficients can be expressed as a vector as stated in Equation (3.12).

$$\vec{A}^T = [A_1 \ A_2 \ \dots \ A_P \ B_1 \ B_2 \ \dots \ B_P] \quad (3.12)$$

The cross-covariance between the coefficients can, as done by Isobe (1990), be shown to be related to the co- and quad-spectra at a given frequency, ω_i . The relation is based on the assumption that the coefficients are joint Gaussian distributed, meaning that the mean value function vector, $E[\vec{A}]$, is equal to the frequency distribution function, and that the cross-covariance is expressed as $\vec{\kappa}_{\vec{A}\vec{A}^T} = E[\vec{A} \ \vec{A}^T]$. The Wiener-Khinchine relation then leads to the expression stated in Equation (3.13).

$$\vec{\kappa}_{\vec{A}\vec{A}^T}(\omega_i) = \frac{\Delta\omega}{2\pi} \begin{bmatrix} \vec{C} & \vec{Q} \\ -\vec{Q} & \vec{C} \end{bmatrix} = \frac{\Delta\omega}{2\pi} \cdot \vec{\Omega}(\omega_i) \quad (3.13)$$

where

| | |
|-----------|---|
| \vec{C} | Co-spectrum matrix of the size of $P \cdot P$ |
| \vec{Q} | Quad-spectrum matrix of the size of $P \cdot P$ |

Considering the $2P$ elements in the vector \vec{A} having a joint normal distribution as a stochastic process, the probability density function, p , for this vector with joint Gaussian elements with mean value vector of $\vec{E}(\vec{A}) = 0$ can be calculated by Equation (3.14) using the cross-covariance function matrix, $\vec{\kappa}_{\vec{A}\vec{A}^T}$, and the actual Fourier coefficients, \vec{A}_{rea} .

$$p_{\vec{A}}(\vec{A}_{rea}) = \frac{1}{(\sqrt{2\pi})^{2P} \left| \vec{\kappa}_{\vec{A}\vec{A}^T}(\tau) \right|^{1/2}} \exp \left(-\frac{1}{2} \vec{a}^T \vec{\kappa}_{\vec{A}\vec{A}^T}(\tau)^{-1} \vec{A}_{rea} \right) \quad (3.14)$$

An estimate $\vec{A}_{rea}^{(j)}$ of $\vec{A}^{(j)}$ is obtained from each of the J subseries, with the probability of obtaining the estimate, $\vec{A}_{rea}^{(j)}$, given by Equation (3.14). Based on the assumption that the J subseries are statistically independent, the joint probability for obtaining the J observed estimates $\vec{A}_{rea}^{(j)}$ is given as the product of the probabilities. Isobe (1990) has suggested a likelihood function, \mathcal{L} , as the J^{th} root of the product of the probability that the Fourier coefficients from Equation (3.14) occur at the same time. In the maximum likelihood method, the cross-spectral density matrix, $\vec{\Omega}$, is determined so that the possibility is maximised.

$$\begin{aligned} \mathcal{L}(\vec{A}_{rea}^{(1)}, \dots, \vec{A}_{rea}^{(J)}, \vec{S}) &= \left(p_{\vec{A}}(\vec{A}_{rea})^{(1)} \cdot \dots \cdot p_{\vec{A}}(\vec{A}_{rea})^{(J)} \right)^{1/J} \\ &= \frac{1}{(\Delta\omega)^P \sqrt{\det(\vec{\Omega})}} \exp \left(-\frac{1}{2} \sum_{h=1}^{2P} \sum_{l=1}^{2P} \Omega_{hl}^{-1} \tilde{\Omega}_{lh} \right) \end{aligned} \quad (3.15)$$

where

| | | |
|-----------------------|--|--|
| Ω_{hl} | | Element in h^{th} row and l^{th} column of the estimated cross spectral density matrix |
| $\tilde{\Omega}_{lh}$ | | Element in l^{th} row and h^{th} column of the measured cross spectral density matrix |

The relationship between the directional spreading function and the cross spectral densities was found in Equation (3.9). The measured cross spectral density matrix, $\vec{\Omega}$, is established from the Fourier analysis of the measurements. The mean value over the J time series is then found as stated in Equation (3.16).

$$\vec{\Omega}_{lh} = \frac{1}{J} \sum_{q=1}^J \begin{bmatrix} \vec{C}_{lh} & \vec{Q}_{lh} \\ -\vec{Q}_{lh} & \vec{C}_{lh} \end{bmatrix}_q \quad (3.16)$$

The estimated cross-spectral density matrix is established from the cross-spectral density given in terms of the unknown parameters; the mean wave direction, θ_0 , and the spreading parameter, s , by Equation (3.9). The mean of the measured auto-spectral densities, $\bar{S}(\omega)$, used in the relation is determined as the mean value of all subseries as well as gauges. Numerical integration is used to solve the relation. Similarly, $\vec{\Omega}$ is then established from the co- and quad-spectra of the cross-spectral densities.

The optimal choice of the unknown parameters and thereby the directional spreading function, $S(\omega, \theta)$, is then obtained by maximising the likelihood function in Equation (3.15). First, the peak frequency is considered, which is found from frequency domain analysis using the mean value from all subseries and gauges. The likelihood function is then determined for a range of

the mean direction, θ_0 , with an interval size of 1° and for a range of the spreading parameter, s , with an interval size of 0.2. For further optimisation of the likelihood function, the values of θ_0 and s that corresponds to the maximum of $\mathcal{L}(\cdot)$ are used as initial values in the 0th order method as given by Nelder and Mead (1965) and suggested by Christensen and Sørensen (1994). For computational reasons, the minimum of the negative likelihood function is determined. Based on this, the most optimal choice of parameters for the peak frequency is determined, which corresponds to the maximum value of the likelihood function, $\mathcal{L}(\cdot)$. The optimisation by Nelder and Mead (1965) is then repeated for all other frequencies. For the frequencies below and above the peak frequency, the values from the previous frequency, above and below respectively, are used as initial values in the optimisation instead of the ranges that are used for the peak frequency as explained above.

For frequencies where a very wide spreading of the waves is detected, the result of the optimisation seems to depend solely on the initial guess. In these situations, a grid of different directions and spreading parameters is again used though with a coarser resolution in relation to θ_0 due to computational reasons. The values yielding the highest likelihood function are then used as results. In case the use of ranges detected several maxima of the likelihood function, the initial guesses from the peak frequency is used as initial values for the next frequency in order to avoid approaching local extremes.

At last, the mean direction, θ_0 , and spreading parameter, s , for each of the considered frequencies are weighted in relation to the spectral density of each component, which leads to a single weighted value of each of the two parameters that is then used for comparison in the investigation of the nonlinear effects.

4 | Test Cases for Generation of Data

In this chapter, different test cases are presented with different wave parameters, and the different generation models, which is used to produce the synthetic waves based on the theory described in chapter 2.

4.1 Relative Wave Parameters of Test Cases

For the analyses of the present thesis, a selection of different test cases is used. The test cases are chosen based on a regular wave with wave height, H , wave period, T , and water depth, h , which will give an indication of what wave theory is valid for the given case. For generation of irregular waves, the significant wave height, H_{m0} , and the peak frequency, f_p , are assumed to correspond to the wave height and period of the regular waves. The test cases, A to H, are chosen such that they represent the validity of different orders of wave theory at different water depths. As breaking waves are not considered in this project, all cases are chosen such that they are not placed too close to the breaking limit. The cases are illustrated with respect to these parameters in Figure 4.1, with parameters stated in Table 4.1.

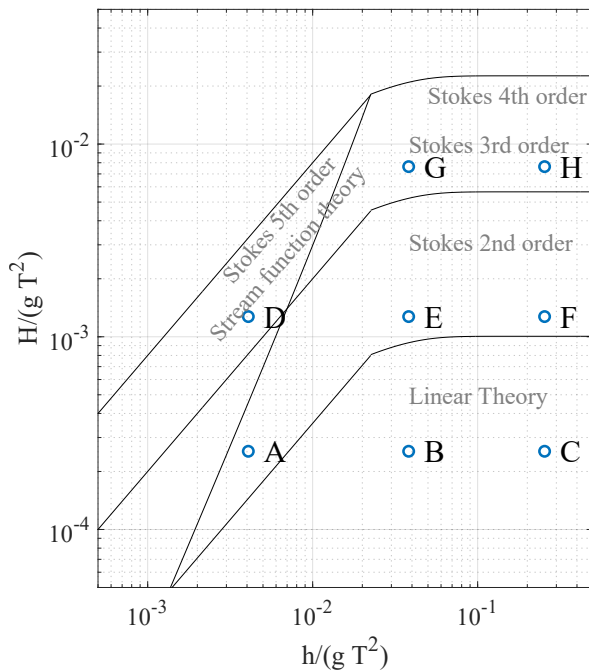


Table 4.1: Parameters for generation of test cases.

| Case | H_{m0} [m] | T_p [s] | h [m] |
|------|--------------|-----------|---------|
| A | 0.01 | 2 | 0.16 |
| B | 0.01 | 2 | 1.5 |
| C | 0.01 | 2 | 10 |
| D | 0.05 | 2 | 0.16 |
| E | 0.05 | 2 | 1.5 |
| F | 0.05 | 2 | 10 |
| G | 0.3 | 2 | 1.5 |
| H | 0.3 | 2 | 10 |

Figure 4.1: Position of test cases as function of wave height, H , and water depth, h .

The diagram suggested by Le MéHauté (1976) shows that cases B and C, are within the area of linear wave theory, while the cases A, E and F are in the area of second order wave theory and the cases D, G and H are in higher order wave theory, wherefore the different cases will be of interest in the different approaches presented in the following. As described in section 2.3, the wavelengths are determined based on linear as well as stream function theory, which leads to the results in Table 4.2 for the respective cases.

Table 4.2: Evaluation of wavelength.

| Case | Wave Steepness [-] $\frac{H}{L}$ | Relative Wave Height [-] $\frac{H}{h}$ | Wavelength Linear [m] | Wavelength Stream Function Theory [m] | Difference [%] |
|------|-------------------------------------|---|-----------------------|---------------------------------------|----------------|
| A | 0.004 | 0.062 | 2.440 | 2.448 | 0.3 |
| B | 0.002 | 0.007 | 5.788 | 5.786 | 0.0 |
| C | 0.002 | 0.001 | 6.252 | 6.249 | 0.0 |
| D | 0.019 | 0.313 | 2.440 | 2.589 | 6.1 |
| E | 0.009 | 0.033 | 5.788 | 5.790 | 0.0 |
| F | 0.008 | 0.005 | 6.252 | 6.253 | 2.5 |
| G | 0.051 | 0.200 | 5.788 | 5.930 | 0.0 |
| H | 0.048 | 0.030 | 6.252 | 6.249 | 0.0 |

The cases are evaluated based on the findings in section 2.3 in relation to the amount of second order energy and the difference in wave celerity according to stream function theory relative to linear theory as seen in Figure 4.2 and Figure 4.3.

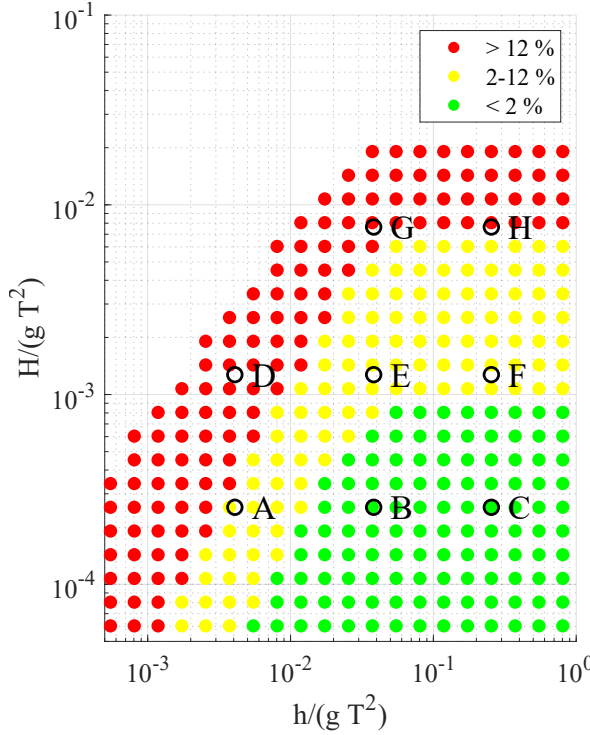


Figure 4.2: Amount of second order energy out of total energy.

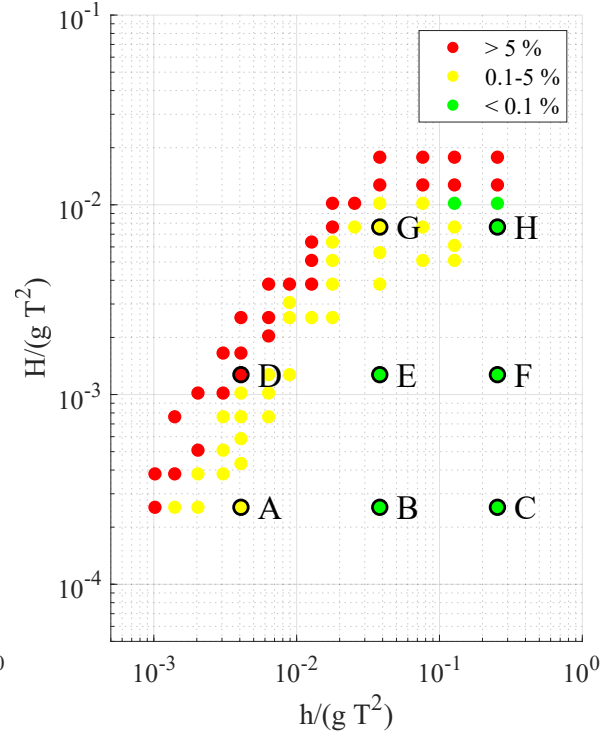


Figure 4.3: Difference in wave celerity based on stream function theory compared to linear wave theory.

Although Case H is placed outside the area in the Diagram of Le MeHauté where the linear wavelength is valid, it does not have any error on the wavelength compared to stream function theory, which might be because it is placed in deep water.

The specific results for the cases appear from Table 4.3. The difference in wave celerity is determined such that for Case D, it means that the wavelength, and thereby the wave celerity, is 6.12 % larger than predicted by linear wave theory. The cases with a difference in wave celerity are Case A, D and G.

Table 4.3: Nonlinear effects for the test cases.

| Case | Amount of second order energy | Difference in wave celerity |
|------|----------------------------------|--------------------------------|
| A | 10.2 % | 0.3 % |
| B | 0.7 % | 0.0 % |
| C | 0.5 % | 0.0 % |
| D | 38.6 % | 6.1 % |
| E | 3.2 % | 0.0 % |
| F | 2.5 % | 0.0 % |
| G | 17.2 % | 2.5 % |
| H | 13.5 % | 0.0 % |

For the waves with amplitude dispersion, the synthetic waves are generated based on linear wave theory in which the wavelength is multiplied by a factor to take the differences of wave celerity stated in Table 4.3 into account. The same factor is used for all wave components within the same case.

The cases will be referred to as the given letter, which indicates the given parameters the respective case has. Further, the cases will be given a number which is related to the order of synthetically generated waves. The number 1 indicates that the wave field is based on first order wave theory when generating the synthetic waves, likewise the number 2 denotes a wave field generated based on second order wave theory, while the number 3 indicates the inclusion of amplitude dispersion which includes Case A, D and G.

In the following analyses, the directional wave analysis will be held against the nonlinear effects for determination of the reliability when using methods based on linear wave theory for directional analysis of waves in general. Additionally, other effects will be considered, this being for example noise on the signal, errors related to calibration of the wave gauges, or robustness in relation to the arrangement of gauges used for measurements. All other effects are analysed in relation to the nonlinear effects as well.

II

Nonlinear Effects

| | | |
|------------------|--|-----------|
| Chapter 5 | Method 1: Long-Crested Waves | 26 |
| 5.1 | Analysis of First Order Waves | |
| 5.2 | Analysis of Second Order Waves | |
| 5.3 | Analysis of Waves With Amplitude Dispersion | |
| 5.4 | Summary of Long-Crested Waves - Method 1 | |
| Chapter 6 | Method 2: Long-Crested Waves | 37 |
| 6.1 | Analysis of First Order Waves | |
| 6.2 | Analysis of Second Order Waves | |
| 6.3 | Analysis of Waves With Amplitude Dispersion | |
| 6.4 | Summary of Long-Crested Waves - Method 2 | |
| Chapter 7 | Method 2: Short-Crested Waves | 44 |
| 7.1 | Generation Models of Synthetic Waves | |
| 7.2 | Analysis of First Order Waves | |
| 7.3 | Analysis of Second Order Waves | |
| 7.4 | Analysis of Waves With Amplitude Dispersion | |
| 7.5 | Summary of Short-Crested Waves | |
| Chapter 8 | Evaluation of Methods and Nonlinear Effects | 58 |

5 | Method 1: Long-Crested Waves

In this chapter, long-crested, oblique waves are considered. The directional analysis of the long-crested waves is based on the phase difference between signals of surface elevations in different gauge positions when using Method 1 as elaborated in section 3.1. For irregular, long-crested waves, a frequency domain analysis is performed assuming that an irregular wave is described by a sum of random phase processes. For each of the frequency components, the procedure is then similar to the procedure for a regular wave, for which the mathematical procedure was described in section 3.1. Since the direction is determined based on the phase difference and wavelength of the regular wave or wave component, the analysis will detect only one direction at each frequency component.

The analysis of the wave direction is based on synthetically generated wave fields of first order waves compared to second order waves and lastly, waves with amplitude dispersion. The eight test cases presented in chapter 4 are used to calculate the possible deviation from a target direction and study what influence is experienced for cases, that do not fulfill the assumptions of linear wave theory according to the respective relative water depth and relative wave steepness. For analyses in this chapter, the angle of a single gauge pair is considered, as the third gauge position only determines whether the wave travels in either of two possible directions. This does therefore not provide the most accurate result, as the mean of the gauge pair combinations could be used. In the present thesis, the inclusion of statistics is however first included in Method 2 used in the next chapter.

The synthetically generated wave fields, which are analysed in this chapter, are given as irregular wave fields represented by the frequency distribution based on a JONSWAP spectrum with significant wave height, H_{m0} , peak frequency, f_p , and water depth, h , corresponding to the values of the wave height, H , wave period, T , and water depth, h , of the eight cases of regular waves presented in chapter 4. The samples are furthermore generated with sample frequency $f_s = 5$ Hz, and $N = 2^9$ number of frequency components.

For the following analyses, the results from the analysis of the first order waves will be used as benchmark for inclusion of second order wave theory in the synthetic data and inclusion of amplitude dispersion according to stream function theory as described in chapter 2.

5.1 Analysis of First Order Waves

When analysing a wave field, it is most often of interest to determine the significant wave height, the peak period and the direction of the waves. In this thesis, the direction of the waves is of greatest interest. In order to determine weighted values of the direction, the spectral density of the wave field is used, which in this thesis is determined from a frequency domain analysis. The spectral density of an irregular wave based on first order waves is shown in Figure 5.1 with an example for Case D1 as the analysed spectrum. This case is placed in shallow water depth with a relatively high steepness.

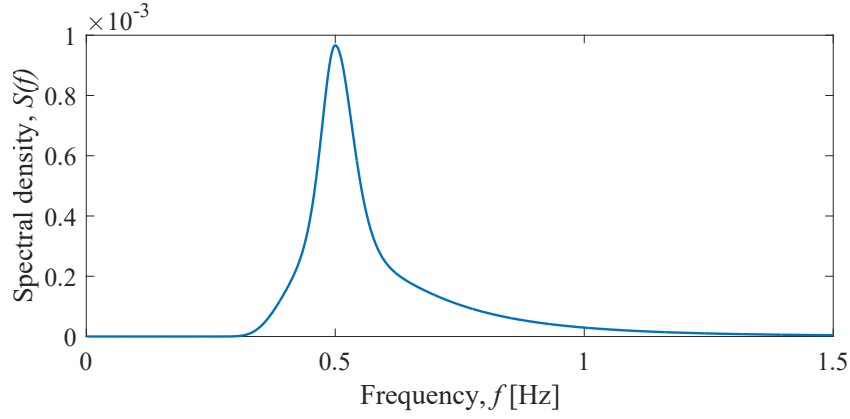


Figure 5.1: Spectral density for Case D1.

The estimated direction of each wave component is calculated using Equation (3.6) for each frequency component. The results of the directional components appear from Figure 5.2, where a wave field has been generated with a target direction of 30° for Case D1.

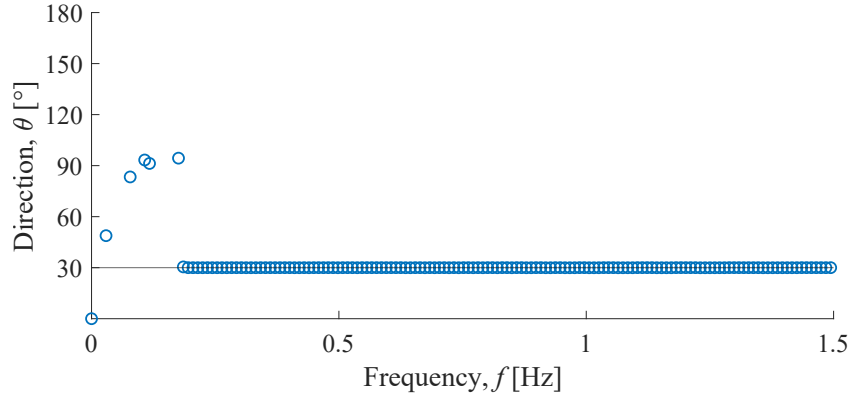
Figure 5.2: Estimated direction for components in the wave field with target direction of 30° , Case D1.

Figure 5.2 shows that for a main part of the frequency components, the estimated direction is close to the horizontal line representing the target direction, which is the value used for the generation. But at the lowest frequencies, the method cannot accurately estimate a proper direction. Since the components of low frequency have a large wavelength, the difference in the surface elevation between the two gauges becomes negligible, which leads to inaccuracies in the phase difference. This yields an estimated distance between the two gauges which is larger than the physical distance, wherefore the direction cannot be determined.

All directions in the range of 360° in intervals of 10° are investigated in Appendix C. From this a tendency is found, which is shown in Figure 5.3, in relation to whether the weighted direction is over- or underestimated. This might be due to inaccuracies in the estimation of the phase difference or wavelength. Therefore, the investigation will continue using a single quadrant, here the first quadrant with the directions from 0 to 90° is chosen.

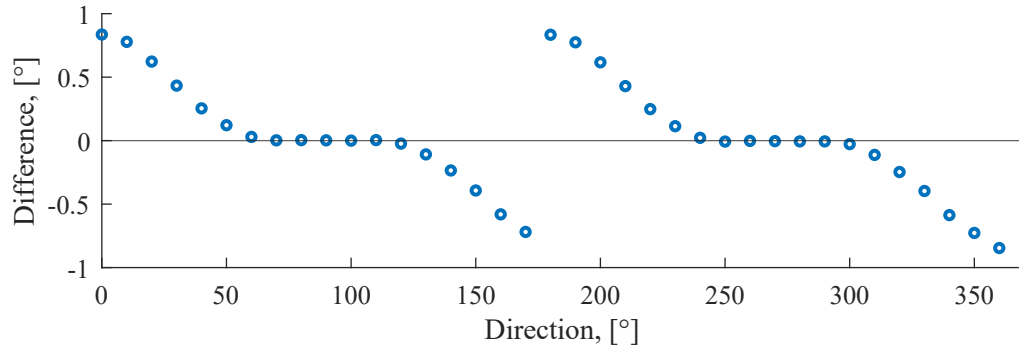


Figure 5.3: Difference of weighted estimated directions for 360°

Figures with results for Case A to H with target directions from 0° to 90° are plotted in Appendix AA. The weighted value of the direction, θ , is calculated based on the spectral density of the components, that the analysis was able to determine the direction of. The weighted direction for the example case is estimated to 30.44° which correspond to an error of 0.44° compared to the target direction. The results of the analysed directions from 0° to 90° for all the cases appear from Table 5.1.

Table 5.1: Target and estimated values of the wave direction.

| Analysed direction, θ , [°] | Generated direction, θ , [°] | | | | | | | | | | |
|------------------------------------|-------------------------------------|------|-------|-------|-------|-------|-------|-------|-------|-------|-------|
| | | 0 | 10 | 20 | 30 | 40 | 50 | 60 | 70 | 80 | 90 |
| Case A1 | | 0.84 | 10.78 | 20.62 | 30.43 | 40.25 | 50.12 | 60.03 | 70.00 | 80.00 | 90.00 |
| Case B1 | | 0.71 | 10.66 | 20.53 | 30.38 | 40.24 | 50.11 | 60.03 | 70.00 | 80.00 | 90.00 |
| Case C1 | | 0.71 | 10.66 | 20.53 | 30.38 | 40.24 | 50.12 | 60.03 | 70.00 | 80.00 | 90.00 |
| Case D1 | | 0.84 | 10.78 | 20.62 | 30.44 | 40.26 | 50.12 | 60.04 | 70.01 | 80.01 | 90.00 |
| Case E1 | | 0.71 | 10.66 | 20.53 | 30.38 | 40.24 | 50.12 | 60.03 | 70.00 | 80.00 | 90.00 |
| Case F1 | | 0.71 | 10.66 | 20.53 | 30.38 | 40.24 | 50.12 | 60.03 | 70.00 | 80.00 | 90.00 |
| Case G1 | | 0.71 | 10.66 | 20.53 | 30.38 | 40.24 | 50.12 | 60.03 | 70.00 | 80.00 | 90.00 |
| Case H1 | | 0.71 | 10.66 | 20.53 | 30.38 | 40.24 | 50.11 | 60.03 | 70.00 | 80.00 | 90.00 |

The differences between the weighted directions obtained from the analyses and the target values are illustrated in Figure 5.4.

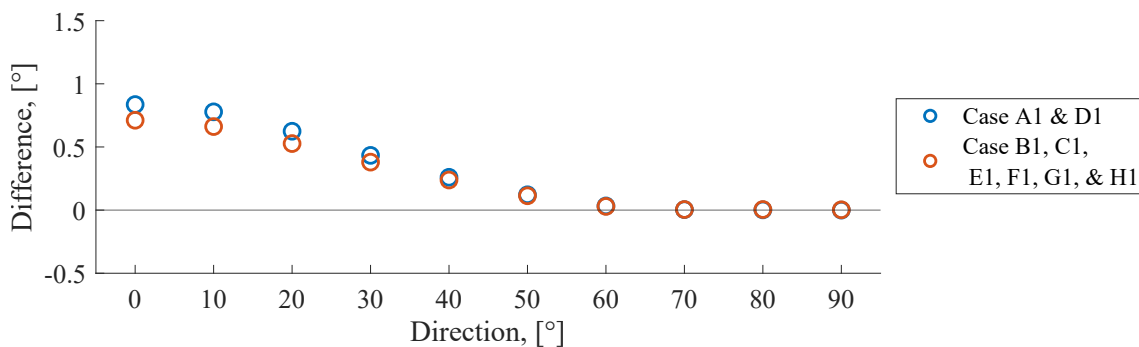


Figure 5.4: Difference in estimated direction from target value for first order waves without truncation of spectrum.

The results of the analysed directions show that the greatest deviation between the target and the estimated direction is 0.84° for Case A1 and D1 for the target direction of 0°. Case A1 and D1 are placed in shallow water which might have an influence on the calculated wavelength

and thereby the estimated wave direction. Further, the results from Table 5.1 show that the angle between the wave propagation direction and gauge pair has an influence on the estimated direction, since the estimated direction becomes more accurate when moving from left to right in the figure. The explanation to this can be, that the geometry of the gauge pair plays an important role. For waves travelling perpendicular towards the gauge pair, there will be no phase difference between the two signals to measure, wherefore the direction can be estimated with high accuracy. For waves travelling almost in line with the gauge pair, a small inaccuracy in the phase difference between the two signals will result in larger influence on the estimated direction due to the geometry.

Figure 5.2 shows that the estimated directions based on the very small frequencies have the largest deviation. This error can be solved by truncating the auto-spectrum, and estimating the direction from only the frequencies with the most energy. The truncated auto-spectrum is shown in Figure 5.5. The truncated auto-spectrum used for the analysis discards all the frequencies placed outside the range of $f_p/2.5$ to $f_p \cdot 2.5$.

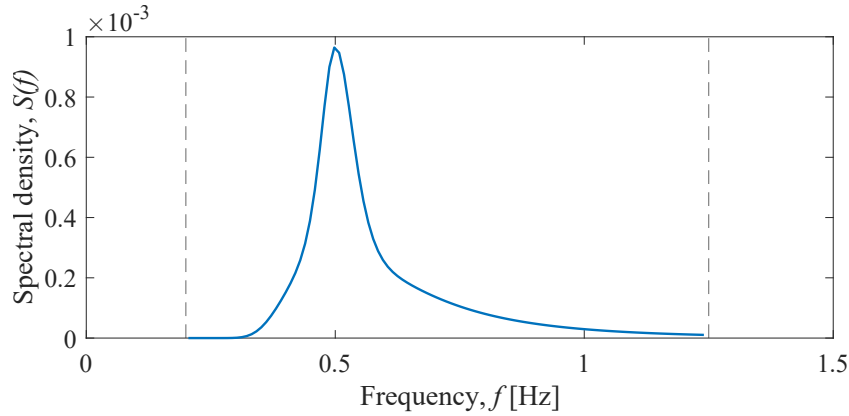


Figure 5.5: Truncated spectral density for Case D1.

The estimated directions for the wave components from the truncated auto-spectrum appear from Figure 5.6, where waves have been generated with a target direction of 30° for Case D1.

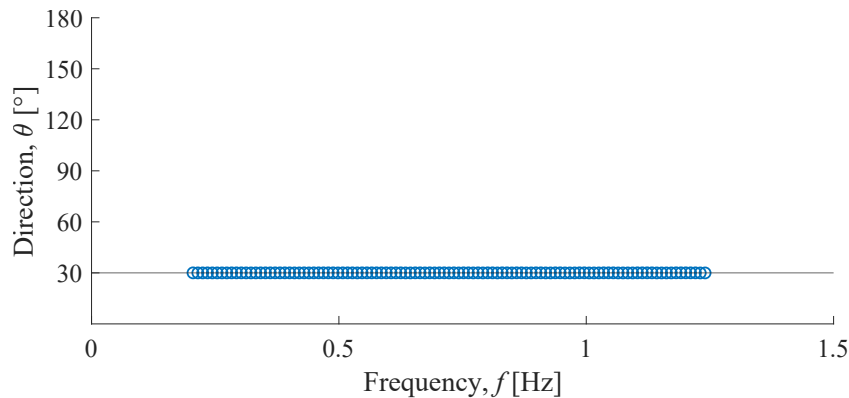


Figure 5.6: Estimated direction for components in the wave field with target direction of 30° , Case D1.

As seen in Figure 5.6, all of the analysed frequency components now have an estimated direction close to the target value, and the weighted deviation for the components of the direction is estimated to 0.00° for all cases. The weighted deviation describes how much the direction of the individual frequency components deviate from the weighted direction and is weighted in

relation to the amount of energy of the relevant frequency component. The weighted direction is estimated to 30.00° which correspond to no error compared to the target direction, which is a great reduction of the error compared to the same case analysed with full spectrum. The analysed directions for all the cases appear from Table 5.2.

Table 5.2: Target and estimated values of the wave direction including a truncated auto-spectrum.

| | Generated direction, θ , [°] | | | | | | | | | | |
|------------------------------------|-------------------------------------|------|-------|-------|-------|-------|-------|-------|-------|-------|-------|
| Analysed direction, θ , [°] | | 0 | 10 | 20 | 30 | 40 | 50 | 60 | 70 | 80 | 90 |
| | Case A1 | 0.00 | 10.00 | 20.00 | 30.00 | 40.00 | 50.00 | 60.00 | 70.00 | 80.00 | 90.00 |
| | Case B1 | 0.00 | 10.00 | 20.00 | 30.00 | 40.00 | 50.00 | 60.00 | 70.00 | 80.00 | 90.00 |
| | Case C1 | 0.00 | 10.00 | 20.00 | 30.00 | 40.00 | 50.00 | 60.00 | 70.00 | 80.00 | 90.00 |
| | Case D1 | 0.00 | 10.00 | 20.00 | 30.00 | 40.00 | 50.00 | 60.00 | 70.00 | 80.00 | 90.00 |
| | Case E1 | 0.00 | 10.00 | 20.00 | 30.00 | 40.00 | 50.00 | 60.00 | 70.00 | 80.00 | 90.00 |
| | Case F1 | 0.00 | 10.00 | 20.00 | 30.00 | 40.00 | 50.00 | 60.00 | 70.00 | 80.00 | 90.00 |
| | Case G1 | 0.00 | 10.00 | 20.00 | 30.00 | 40.00 | 50.00 | 60.00 | 70.00 | 80.00 | 90.00 |
| | Case H1 | 0.00 | 10.00 | 20.00 | 30.00 | 40.00 | 50.00 | 60.00 | 70.00 | 80.00 | 90.00 |

If Table 5.1 and Table 5.2 are compared, it shows that the truncated spectrum, without including the energy at the very small and high frequency components, yield a bit more accurately estimated directions than when including the entire spectrum. Similarly, the difference between the estimated directions and the target values are illustrated in Figure 5.7.

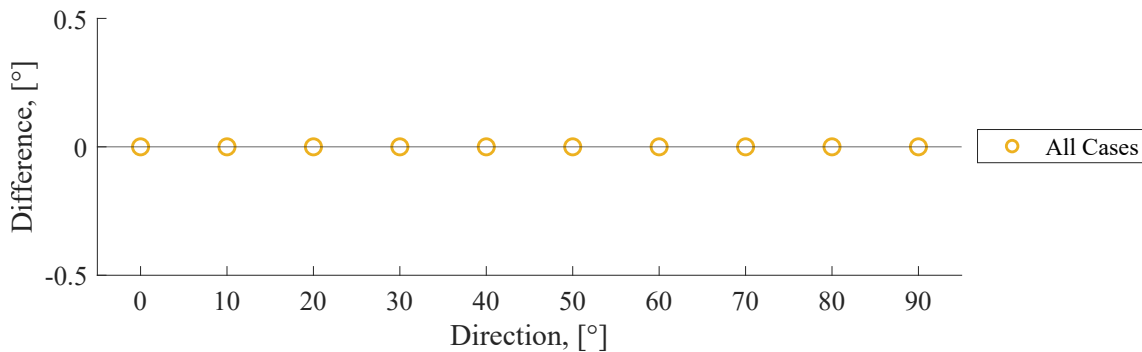


Figure 5.7: Difference in estimated direction from target value for first order waves with truncation of spectrum.

5.2 Analysis of Second Order Waves

In this section, the direction and the deviation in relation to the results of the first order waves are estimated by using the simple analysis on synthetic data generated based on second order wave theory as described in section 2.2. The analysis of the direction is performed similar to the analysis of the first order waves, where the components inside the truncated spectrum are determined from a frequency domain analysis of the synthetic surface elevation signals. The approach using Method 1 for a bichromatic wave field is expounded in Appendix D, to show the principle. Further, the approach for a second order wave field with the non-truncated spectrum is stated in Appendix D, which is used to compare with the second order wave field with the truncated spectrum.

In the following, the analysis of a second order wave field generated from the truncated auto-spectrum is shown, which is compared to the analysis of the first order waves. The auto-spectrum of the wave field is illustrated in Figure 5.8 for Case D2 as an example. For Case D2 the amount of second order energy represents more than 12 % of the total energy, cf. Figure 4.2.

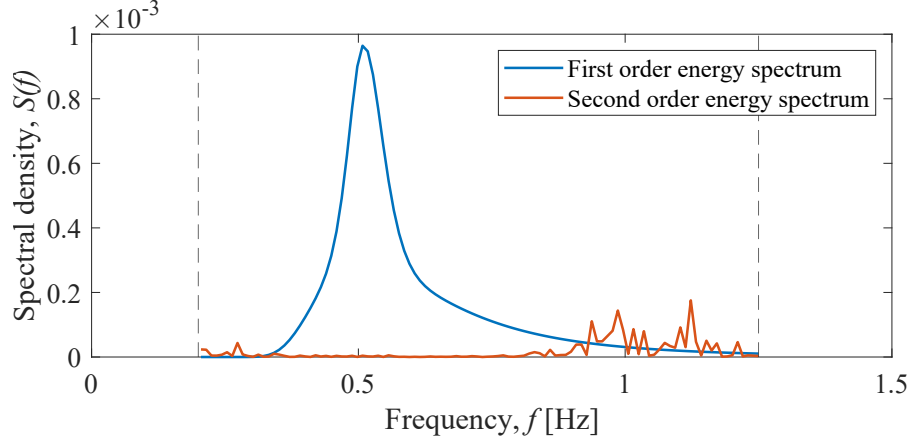


Figure 5.8: Truncated spectral density for Case D2.

As the auto-spectrum in Figure 5.8 shows, the energy is distributed over a frequency range as the theoretical empirical spectrum with the energy redistribution from first order spectral density now including second order components. As shown in section 2.2.1, the second order components are concentrated at lower and higher frequencies than the peak frequency for the first order components, wherefore the truncation of the spectrum might influence the results. The directions are analysed for the same eight cases with a truncated auto-spectrum, considering only the frequency components in the interval of $\frac{f_p}{2.5} < f < 2.5 \cdot f_p$ which might reduce the second order effects by removing the energy at the very low and high frequencies. The estimated direction for all the wave components appears from Figure 5.9, where waves have been generated with a target direction of 30° for Case D2.

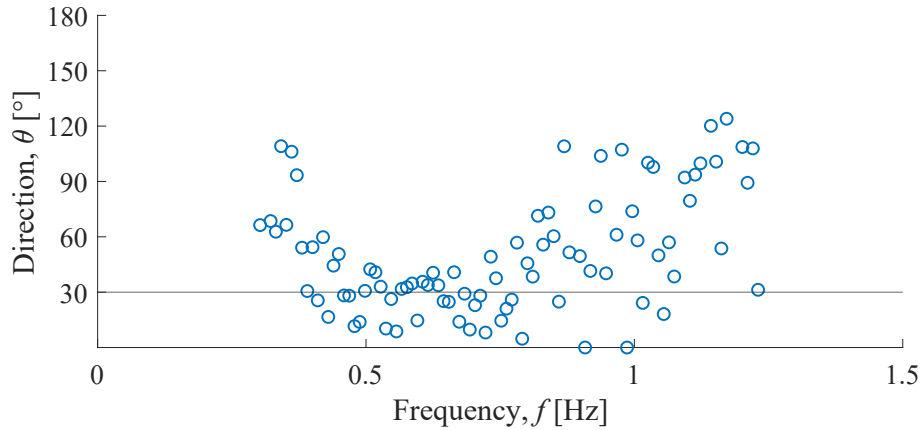


Figure 5.9: Estimated direction for components in the wave field with target direction of 30° .

For the given case, a weighted direction of 41.67° with a weighted deviation of 39.68° is calculated for the truncated auto-spectrum. The weighted direction as well as the weighted deviation show significant increase. The weighted directions for all the cases appear from Table 5.3, while the appurtenant weighted deviations are stated in Table 5.4.

The results of the analyses show how the second order energy components affect the deviation of the estimated direction components which induce a more imprecise weighted direction. The deviations and directions are though improved compared to the analysis of the full spectrum of second order waves. The differences between the weighted directions from Table 5.3 and the weighted directions for the first order waves from Table 5.2 appear from Figure 5.10.

Table 5.3: Target and estimated values of the wave directions for a truncated auto-spectrum.

| | Generated direction, θ , [°] | | | | | | | | | | |
|------------------------------------|-------------------------------------|-------|-------|-------|-------|-------|-------|-------|-------|-------|-------|
| Analysed direction, θ , [°] | | 0 | 10 | 20 | 30 | 40 | 50 | 60 | 70 | 80 | 90 |
| | Case A2 | 12.71 | 12.19 | 20.25 | 30.38 | 39.93 | 49.68 | 60.24 | 70.12 | 80.08 | 90.00 |
| | Case B2 | 3.79 | 9.77 | 20.02 | 29.96 | 39.99 | 50.01 | 59.99 | 70.00 | 80.00 | 90.00 |
| | Case C2 | 3.49 | 10.02 | 20.03 | 30.05 | 39.96 | 50.06 | 60.00 | 70.00 | 80.00 | 90.00 |
| | Case D2 | 41.06 | 42.01 | 45.19 | 41.67 | 53.98 | 61.37 | 64.80 | 74.89 | 82.70 | 90.00 |
| | Case E2 | 7.63 | 10.10 | 20.84 | 29.79 | 39.86 | 49.92 | 59.79 | 69.99 | 80.02 | 90.00 |
| | Case F2 | 8.28 | 9.71 | 19.51 | 30.20 | 40.14 | 49.71 | 59.82 | 70.06 | 80.02 | 90.00 |
| | Case G2 | 20.97 | 19.78 | 22.27 | 33.39 | 39.14 | 49.35 | 59.78 | 69.90 | 80.06 | 90.00 |
| | Case H2 | 20.60 | 17.56 | 21.85 | 29.50 | 40.78 | 50.59 | 59.47 | 70.08 | 80.42 | 90.00 |

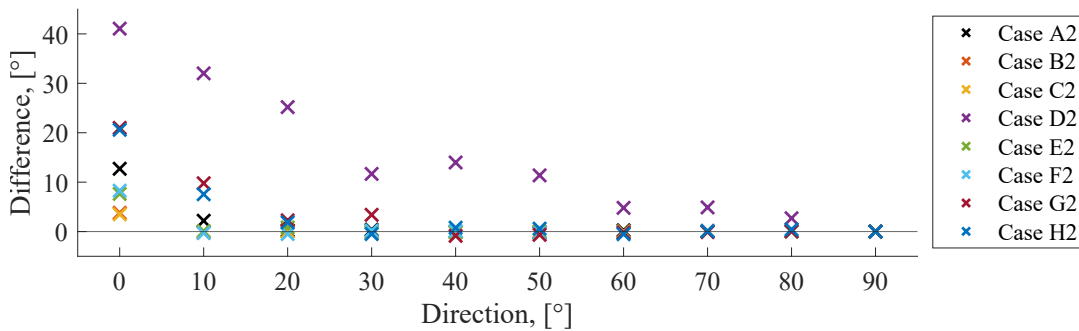


Figure 5.10: Difference in mean direction compared to value determined based on first order wave theory.

Table 5.4: Weighted deviations of the wave directions.

| | Generated direction, θ , [°] | | | | | | | | | | |
|-------------------------|-------------------------------------|-------|-------|-------|-------|-------|-------|-------|-------|------|------|
| Weighted Deviation, [°] | | 0 | 10 | 20 | 30 | 40 | 50 | 60 | 70 | 80 | 90 |
| | Case A2 | 9.75 | 9.10 | 7.27 | 4.92 | 5.23 | 4.65 | 3.02 | 3.84 | 1.42 | 0.00 |
| | Case B2 | 1.43 | 1.16 | 0.51 | 0.36 | 0.28 | 0.19 | 0.15 | 0.09 | 0.06 | 0.00 |
| | Case C2 | 1.82 | 0.95 | 0.44 | 0.34 | 0.25 | 0.20 | 0.14 | 0.10 | 0.06 | 0.00 |
| | Case D2 | 53.38 | 47.27 | 49.95 | 39.68 | 38.01 | 27.44 | 19.37 | 15.63 | 7.91 | 0.00 |
| | Case E2 | 3.88 | 4.66 | 2.83 | 2.05 | 1.35 | 0.86 | 0.64 | 0.49 | 0.34 | 0.00 |
| | Case F2 | 3.09 | 3.83 | 2.31 | 1.73 | 1.56 | 0.91 | 0.69 | 0.39 | 0.27 | 0.00 |
| | Case G2 | 8.88 | 10.10 | 8.71 | 9.52 | 8.40 | 6.24 | 4.47 | 2.90 | 2.23 | 0.00 |
| | Case H2 | 9.24 | 9.16 | 9.37 | 9.05 | 7.24 | 5.34 | 3.81 | 2.99 | 1.57 | 0.00 |

The results from the analyses show an error of 41.06° for Case D2. It is difficult for Method 1 to estimate the results for the target direction of 0°, when including second order energy for the cases, which have a high amount of second order energy i.e. Case D2, G2 and H2. The target direction of 0° has an acute angle in relation to the two wave gauges in Figure 3.4, which have an

influence when estimating the weighted direction. The present analyses have shown to depend on the direction of the waves relative to the orientation of the gauge pair. It is assumed that the same pattern is seen for the remaining three quadrants of the coordinate system, wherefore the directions that are possible to determine within an accuracy of $\pm 5^\circ$ are marked with green in Figure 5.11 for each of the investigated cases of second order waves, and directions that are not are marked with red.

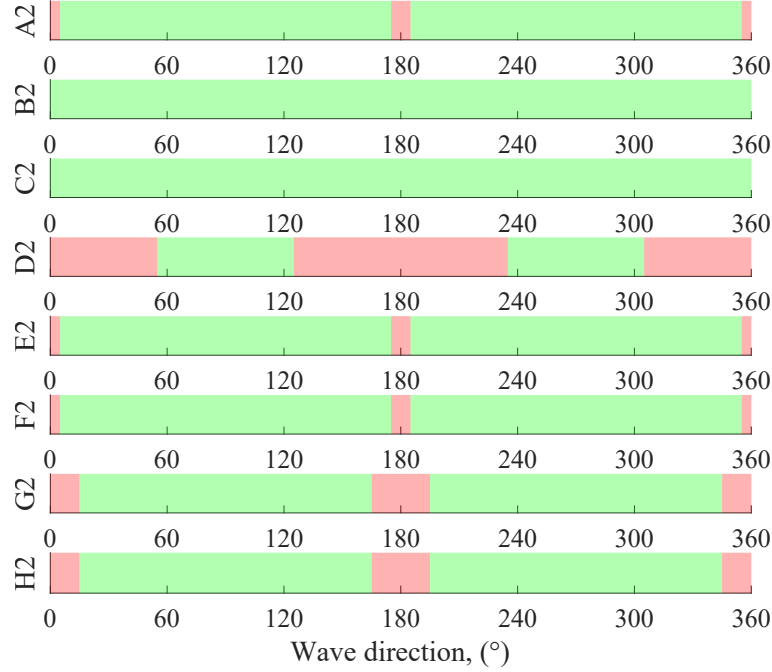


Figure 5.11: Possible directions to determine within $\pm 5^\circ$ for second order waves.

5.3 Analysis of Waves With Amplitude Dispersion

In this section, waves with amplitude dispersion are considered, which means that waves are generated based on first order theory with a factor adjusting the wavelength to include the simplified amplitude dispersion as stated in Table 4.2. The spectrum of the analysis is truncated as done in the previous section at $\frac{f_p}{2.5} < f < 2.5 \cdot f_p$.

In the following, the error of the direction is determined depending on the error on the wavelength, which for Case B, C, E, F and H is smaller than the precision used for determination of the wavelengths. The error on the wavelength for Case A is small, being on the third decimal, in opposition to the errors related to Case D and G, which have a greater influence. Furthermore, the orientation of the gauge pair that is used for the determination of the direction is also taken into account, which is still as given in Figure 3.4. The analysis is performed in the same way as for the first and second order waves. Since the data is generated based on first order theory, the same tendency is seen in Figure 5.12 as an example, that for a truncated auto-spectrum, the method predicts the same direction for all frequency components. In this case where the wave celerity is adjusted according to stream function theory, the estimated direction is however not as exact as for first order waves.

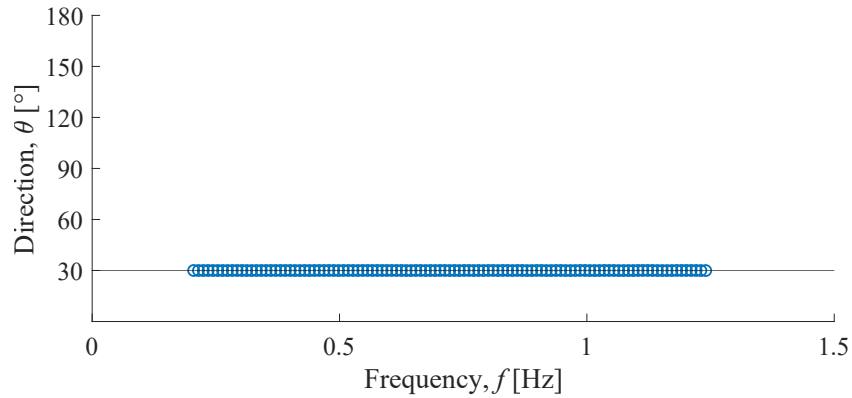


Figure 5.12: Estimated direction for irregular waves with amplitude dispersion, Case D3, with a target direction of 30° .

The example in Figure 5.12 is shown for just a single direction. To consider the effect in relation to the direction of the gauge pair, as the direction of the waves is determined solely based on the wavelength and the phase difference between signals, the generation of the long-crested waves and analysis hereof is repeated for directions evenly distributed between 0° and 360° . The error in relation to each of the target directions is then found. Results for all test cases appear from Appendix AA and are summed up in Figure 5.13 and Table 5.5.

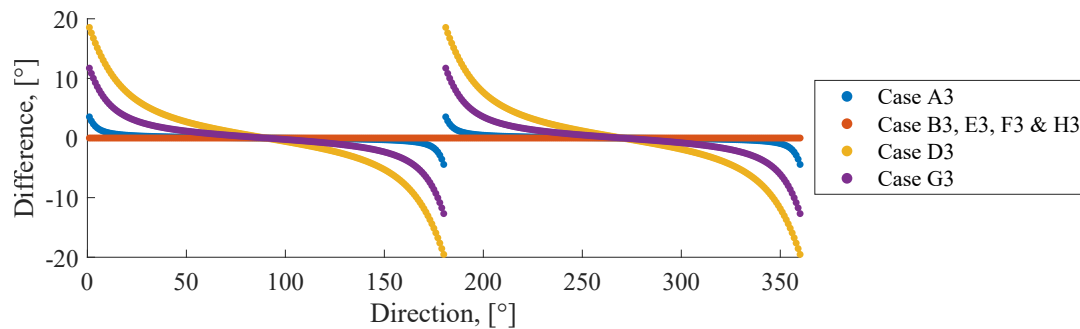


Figure 5.13: Difference in mean direction compared to target value.

Table 5.5: Maximum absolute error of direction for each test case.

| Case | A3 | B3 | C3 | D3 | E3 | F3 | G3 | H3 |
|---------------|-------|------|------|-------|------|------|-------|------|
| Maximum error | 4.43° | 0.0° | 0.0° | 19.5° | 0.0° | 0.0° | 12.7° | 0.0° |

It appears from Figure 5.13, that the reliability of the estimated direction is highly dependent on the direction of the wave, θ , in relation to the orientation of the gauge pair. The smallest error on the direction is experienced for waves travelling almost perpendicular towards the gauge pair, for reasons as mentioned earlier. In the worst case, which is for waves travelling in the same or opposite direction parallel to the direction of the gauge pair, the direction is however misjudged by 19.5° for an error on the wavelength of 6.1 % relative to linear wave theory for Case D. For cases A3, D3 and G3, it can be concluded, that the error on the direction is less influenced by the wavelength, when the direction of the waves is almost perpendicular to the orientation of the gauge pair that is used for measuring. The accuracy level of each test is indicated by the maximum error of the estimated direction relative to the target value, which is given for all cases in Table 5.5. The target value is here used as benchmark, as the analysis of first order waves did not cover as many wave directions as the present analysis.

To obtain an accuracy of $\pm 5^\circ$ on the estimated direction, only certain directions can be determined accurately depending on the case, that is considered. Cases A, B, C, E, F and H are all within the present accuracy, wherefore only case D and G are here considered. Figure 5.14 illustrates whether a certain direction is possible to determine within $\pm 5^\circ$ accuracy for a gauge pair orientation of 0° . Green intervals are within the given accuracy, red areas are outside.

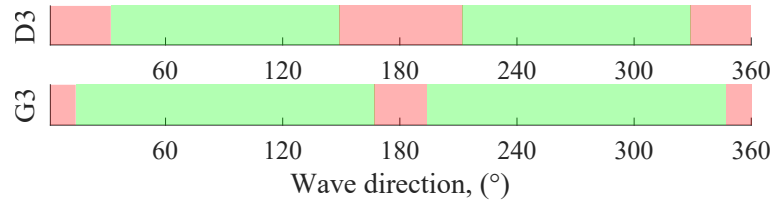


Figure 5.14: Possible directions to determine within $\pm 5^\circ$ for a gauge pair with 0° orientation as illustrated in Figure 3.4 for case D3 and G3.

The present analysis shows that the amplitude dispersion of the waves is of significant influence when performing the directional analysis based on linear wave theory. For the relevant cases, A, D and G, where a difference in wavelengths were discovered, Case A with difference in wavelengths of 0.3 %, gave an estimated direction within $\pm 5^\circ$ of the target direction, whereas the Case D and G showed maximum deviations of 19.5° and 12.7° from the target values.

Furthermore, the results indicate that the orientation of the different gauge pairs is relevant to consider in further analyses, as it for some directions was still possible to determine the direction reasonably correct despite a higher difference in wavelength from linear wave theory. Based on the present analysis, it seems possible to estimate a critical wave steepness, $H/L = 0.05$, and relative wave height, $H/h > 0.06$ based on Case D and G with parameters at stated in Table 4.3. For wave fields with characteristics below these values, it is possible to determine the direction of the waves with an accuracy of $\pm 5^\circ$ using Method 1 when including amplitude dispersion, which means that the amount of amplitude dispersion is very low.

5.4 Summary of Long-Crested Waves - Method 1

For directional analysis of long-crested wave fields, the present analyses performed by Method 1 have shown an overestimation of the direction for wave with a propagation direction in the first quadrant from 0 til 90° . Further, the analysis of the first order waves showed that the energy components which appear at the low frequencies are difficult to estimate the directions from. The standard deviation of the estimated directions distributed over a certain number of frequency components became less when truncating the auto-spectrum to only analyse the frequency components inside the range of $f_p/2.5$ and $2.5f_p$.

This was followed by an analysis of a second order wave field, which showed that the estimated direction of the individual frequency components was less accurate, which also influenced the weighted direction and was seen as an increase in the weighted standard deviation hereof. From the results of the estimated direction, it is shown that when including second order energy in the spectral density, the deviation of the estimated direction increases, for the cases with the most significant influence of the second order energy and when the waves propagate parallel to the gauge pair. Figure 5.15 illustrates with what accuracy the present method determines the direction of the long-crested waves of second order theory. Regarding influence from amplitude dispersion for the three cases, A3, D3 and G3, where this was relevant, the error on the estimated

direction was shown to be worst at the angles of the wave propagation direction parallel to the wave gauges. The accuracy is similarly illustrated in Figure 5.16.

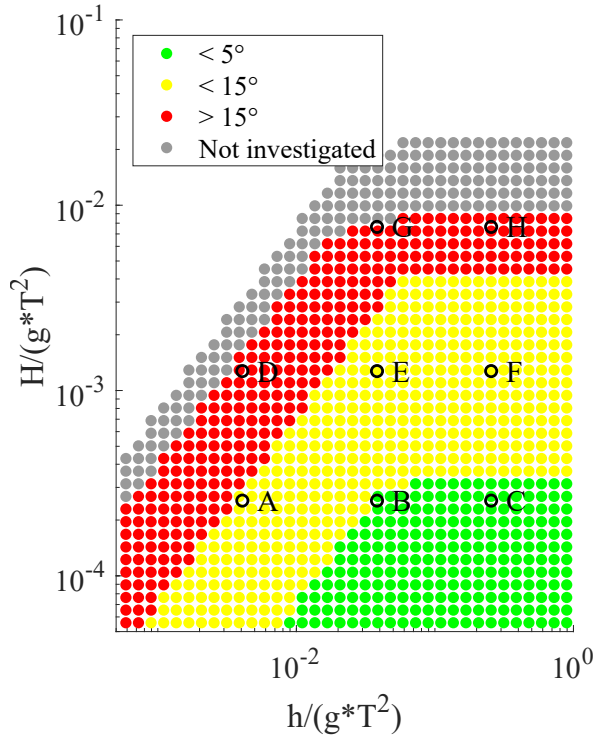


Figure 5.15: Accuracy of estimated direction for second order waves.

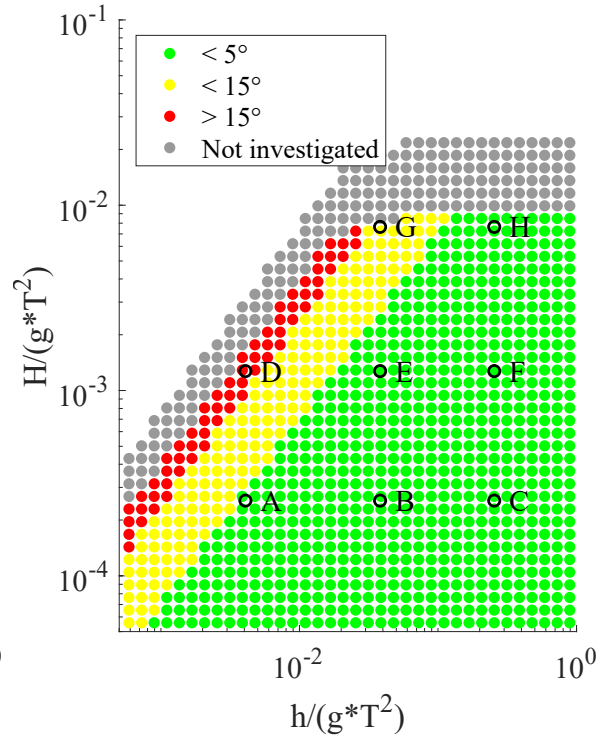


Figure 5.16: Accuracy of estimated direction for waves with amplitude dispersion.

A possibility of this method is to include the third gauge in the determination of the propagation angle, this is however not done in the present thesis. To increase the reliability of the directional analysis, an increase in number of gauge pair will be considered when using Method 2 in the next analyses of this paper, where a statistical fitting is performed.

6 | Method 2: Long-Crested Waves

In this chapter, long-crested, oblique waves are considered as in chapter 5. The determination of the direction of the long-crested waves in this chapter is based on a stochastic analysis method as elaborated in section 3.2 when using Method 2. The direction is here determined based on the method *Maximum Likelihood Estimation of Directional Spectrum in Standard Form*, where the parameters of the mean wave direction, θ_0 , and the spreading parameter, s , are fitted to the cosine power function given in Equation (3.10) in section 3.2. When dealing with long-crested waves only a single direction is considered, wherefore a relatively high value of the spreading parameter, s , is expected, corresponding to a narrow directional spreading of the waves, when fitting to the Mitsuyasu-type directional spreading function.

The chapter is similarly based on the analysis of the direction of synthetic waves generated by first order wave theory for the eight different sea states, A to H , as described in chapter 4, and then compared to waves generated by second order wave theory and lastly for waves with amplitude dispersion. The synthetically generated waves in this chapter are given as irregular wave fields represented by the frequency distribution of a JONSWAP spectrum with significant wave height, H_{m0} , peak frequency, f_p , and water depth, h , corresponding to the values of the wave height, H , wave period, T , and water depth, h , of the eight cases of regular waves presented in chapter 4. The samples are furthermore generated with sample frequency $f_s = 5$ Hz, and $N = 2^{14}$ number of frequency components, which results in 512 components as applied in Method 1, when using $J = 30$ subseries in the analysis. The synthetic waves are generated in six wave gauge positions arranged as CERC 6 as shown in Figure 3.6, which results in 15 cross-spectra to use in the directional analysis. The analysis using Method 2 is performed within a truncation of the auto-spectrum, considering only the frequencies from $f_p/2.5$ to $2.5 \cdot f_p$, as it was found that the deviation of the components of the estimated directions became less.

6.1 Analysis of First Order Waves

In this section, the mean direction of propagation of the wave is determined for waves based on first order wave theory as described in section 2.1. In Figure 6.1, Case D1 is shown as an example with the estimated mean direction and spreading for target value $\theta_0 = 30^\circ$ for the frequency components within the truncation, and without a target value for σ , because long-crested waves are analysed.

The figure shows an estimated spreading of approximately 9° , which is the same value determined for all cases and directions, which seems to be the lowest spreading of the waves, the method can determine. The optimisation is though limited to a certain number of iterations, wherefore lower values maybe could have been experienced. The figure shows further that the estimated mean direction is difficult to estimate with a certain accuracy for the components at the lowest frequencies, which was also experienced when using Method 1. The weighted mean direction is though estimated to 30.01° with a weighted standard deviation of 0.09° , which illustrates that the analysis estimates the mean direction rather well for most of the frequency components.

Figures with results for Case A to H with target directions from 0° to 90° are plotted in Appendix AB.

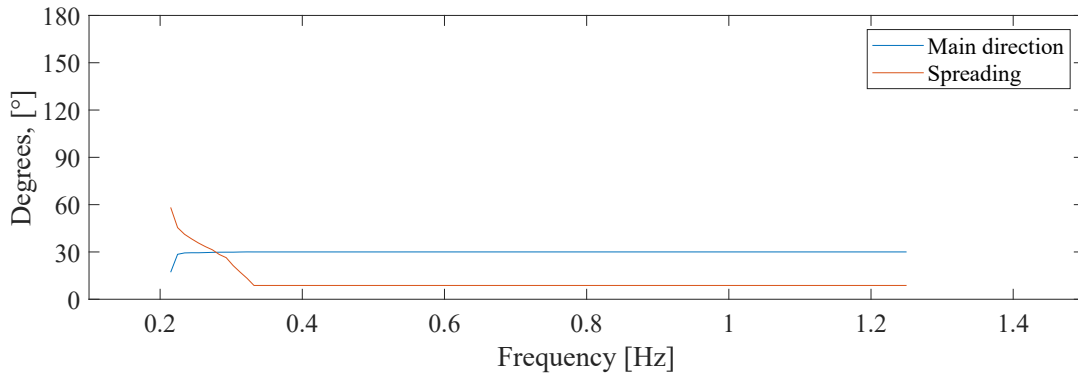


Figure 6.1: Estimated mean direction and spreading for components in the wave field with target direction of 30°, Case D1.

The results for the weighted estimated mean wave direction appear from Table 6.1.

Table 6.1: Estimated values of the wave direction for first order waves.

| | Generated direction, θ , [°] | | | | | | | | | | |
|--------------------------------------|-------------------------------------|------|-------|-------|-------|-------|-------|-------|-------|-------|-------|
| Analysed direction, θ_0 , [°] | | 0 | 10 | 20 | 30 | 40 | 50 | 60 | 70 | 80 | 90 |
| | Case A1 | 0.00 | 10.07 | 20.03 | 30.12 | 40.04 | 50.07 | 60.02 | 70.00 | 80.07 | 90.04 |
| | Case B1 | 0.00 | 10.02 | 20.08 | 30.00 | 40.01 | 50.01 | 60.00 | 70.00 | 80.02 | 90.01 |
| | Case C1 | 0.00 | 10.02 | 20.01 | 30.00 | 40.01 | 50.01 | 60.00 | 70.00 | 80.02 | 90.01 |
| | Case D1 | 0.00 | 10.07 | 20.03 | 30.01 | 40.05 | 50.07 | 60.03 | 70.00 | 80.07 | 90.05 |
| | Case E1 | 0.00 | 10.02 | 20.01 | 30.00 | 40.01 | 50.01 | 60.01 | 70.00 | 80.02 | 90.01 |
| | Case F1 | 0.00 | 10.02 | 20.01 | 30.00 | 40.01 | 50.02 | 60.00 | 70.00 | 80.02 | 90.01 |
| | Case G1 | 0.00 | 10.02 | 20.01 | 30.00 | 40.01 | 50.02 | 60.00 | 70.00 | 80.02 | 90.01 |
| | Case H1 | 0.00 | 10.02 | 20.01 | 30.00 | 40.01 | 50.02 | 60.00 | 70.00 | 80.02 | 90.01 |

Method 2 does not show a tendency to become more accurate when going from waves from 0° to 90°, as the method includes 6 gauge positions instead of a single gauge pair.

6.2 Analysis of Second Order Waves

In this section, the directional analysis of second order waves is performed. Synthetic data generated from second order wave theory is used. Case D2 is shown as example in this section, as the amount of second order energy represents more than 12% of the total energy found in section 2.3. The spectrum for Case D2 is shown in Figure 6.2 to illustrate the contribution from the second order energy.

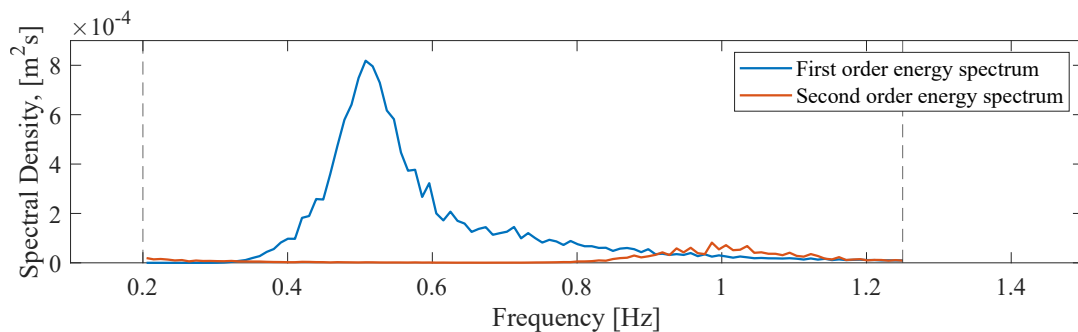


Figure 6.2: Truncated Auto-Spectrum for Case D2.

Figure 6.3 shows the results of the directional analysis of the estimated mean direction and the spreading for a target direction of 30° for Case D2 as an example being representative for all directions.

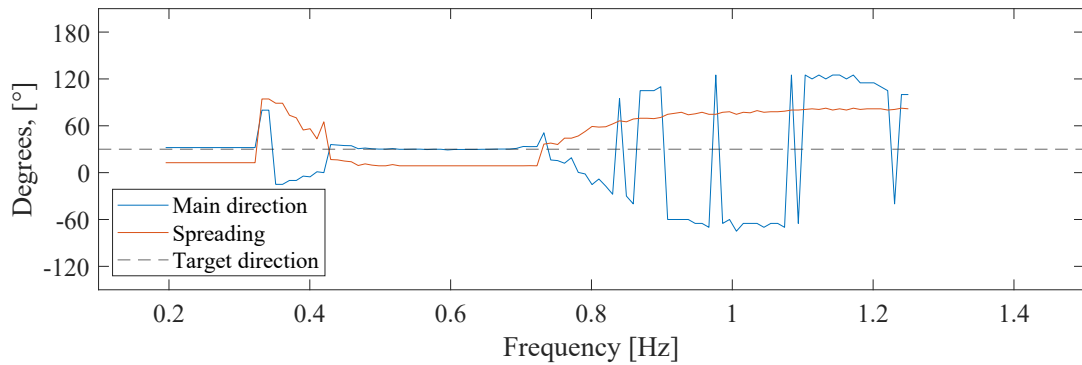


Figure 6.3: Estimated direction for components in the wave field with target direction of 30° , Case D2.

The figure shows an estimated mean wave direction, that deviates significantly more compared to the estimated mean direction in Figure 6.1, which shows an approximately straight line. From Figure 6.3 it is noticed that in the range from approximately 0.4 to 0.7 Hz close to the peak frequency $f_p = 0.5$ Hz, where most of the first order energy is represented, the estimated mean direction and spreading are more or less constant over the frequency components at values equal to those for the analysis of the first order wave field. The frequencies below 0.4 Hz and above 0.7 Hz are in the range where the second order energy components have the greatest influence from the second order energy, which appears from Figure 6.2. In these ranges, the total energy of the second order waves deviates the most from the first order energy. The behaviour of the components with a large amount of second order energy will be discussed further in chapter 13.

For Case D2, the spreading increases from 8.8° to approximately 26° for all of the investigated directions, and similarly less for the remaining affected cases. These results appear from Appendix AB. The result of weighted estimated mean direction in Figure 6.3 is 22.96° with a weighted standard deviation of 37.42° . The increase in standard deviation from the weighted mean direction compared to the first order waves illustrates that the estimated mean directions of the individual wave components deviate more from the target value, and for those deviating the most, the spreading seem to increase significantly as well. The results of the weighted estimated mean wave direction for all cases and directions appear from Table 6.2.

Table 6.2: Estimated values of the wave direction for second order waves.

| Analysed direction, θ_0 , $^\circ$ | Generated direction, θ , $^\circ$ | | | | | | | | | |
|---|--|-------|-------|-------|-------|-------|-------|-------|-------|-------|
| | 0 | 10 | 20 | 30 | 40 | 50 | 60 | 70 | 80 | 90 |
| Case A2 | -0.96 | 10.26 | 19.99 | 30.08 | 39.39 | 50.18 | 60.09 | 69.97 | 79.80 | 90.16 |
| Case B2 | 0.00 | 10.03 | 20.03 | 30.01 | 40.02 | 50.02 | 60.02 | 70.00 | 80.02 | 90.02 |
| Case C2 | 0.00 | 10.03 | 20.02 | 30.00 | 40.01 | 50.03 | 60.02 | 70.00 | 80.03 | 90.02 |
| Case D2 | 1.33 | 17.64 | 17.74 | 22.96 | 49.42 | 60.64 | 59.76 | 64.40 | 86.51 | 88.94 |
| Case E2 | 0.01 | 10.03 | 20.14 | 30.15 | 40.01 | 50.04 | 60.15 | 70.07 | 79.99 | 90.06 |
| Case F2 | 0.00 | 10.09 | 20.10 | 30.12 | 40.02 | 50.03 | 60.13 | 70.05 | 80.01 | 90.12 |
| Case G2 | -3.44 | 11.25 | 19.12 | 30.89 | 38.64 | 50.35 | 59.82 | 72.13 | 81.95 | 89.73 |
| Case H2 | 0.38 | 11.98 | 20.31 | 29.10 | 39.32 | 50.97 | 61.41 | 70.92 | 79.32 | 88.97 |

The results of the estimated values of the weighted wave direction for second order waves from Table 6.2 are compared to the estimated values of the wave direction for first order waves from Table 6.1. The difference in the estimated mean direction introduced by inclusion of second order energy results appear from Figure 6.4.

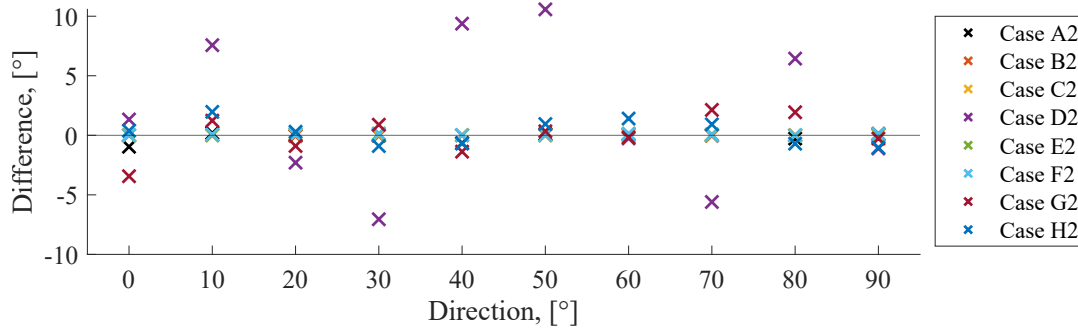


Figure 6.4: Difference in mean direction of second order waves compared to value determined based on the waves of first order wave theory.

As it appears from Figure 6.4, the results for Case D2 deviates significantly more than the rest of the cases, with a maximum deviation of 10.57° . For better illustration of the remaining cases, Figure 6.5 shows a zoom of the results where the error introduced by the second order energy is close to 0° .

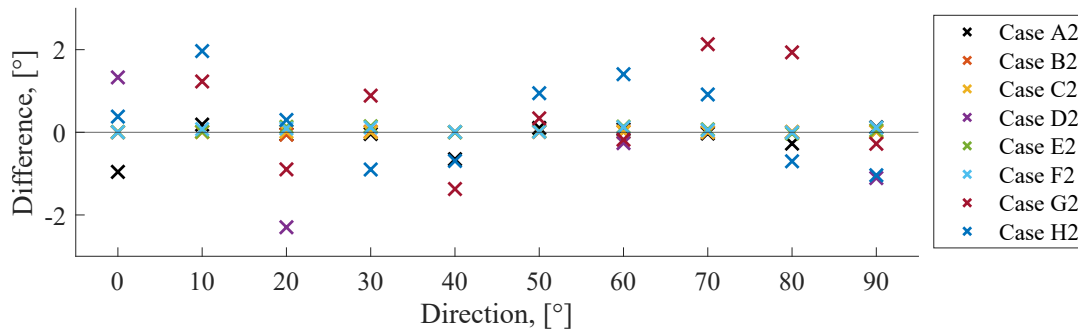


Figure 6.5: Difference in mean direction compared to value determined based on first order wave theory, zoomed.

For Case B2 and C2, for which linear wave theory is valid, the weighted estimated mean directions almost do not deviate from the value determined based on first order theory. Case A2, E2 and F2, for which second order wave theory is valid, show weighted mean directions that deviate with up to 1° . Lastly Case G2 and H2 show deviations of up to 3.44° .

Compared to the results found by use of Method 1, the present results show no dependency in relation to the investigated direction and less influence of the second order energy in general.

6.3 Analysis of Waves With Amplitude Dispersion

As for the analysis using Method 1, the following part will analyse synthetic waves that are generated based on first order theory, but with a wavelength, that has been adjusted according to stream function theory as determined in chapter 4. Only the cases where the difference in wavelength is notable, Case A3, D3 and G3, are here considered, as the remaining cases correspond to the analysis of first order waves in section 6.1, since no amplitude dispersion is included.

Figure 6.6 is here shown as example for Case D3, where the amplitude dispersion results in a 6.1 % difference in wavelengths. The results for the remaining directions and cases are found in Appendix AB.

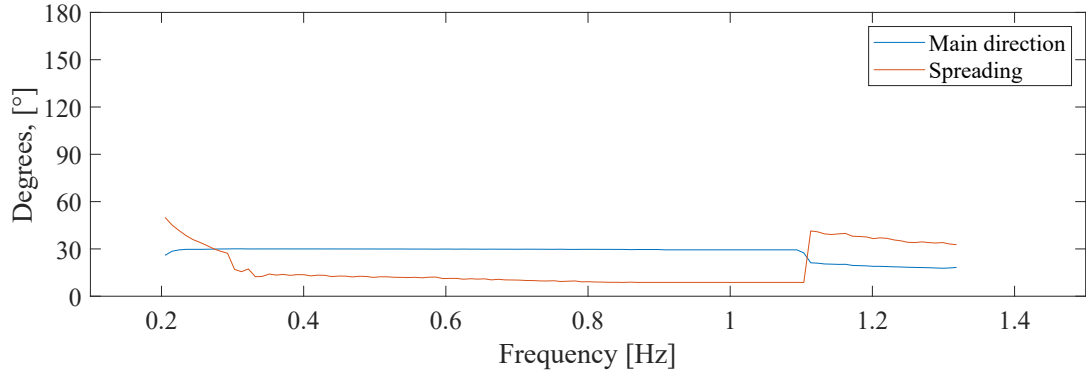


Figure 6.6: Estimated direction for components in the wave field with a target direction of $\theta_0 = 30^\circ$, Case D3.

As was seen for the analysis of first order waves, the present method estimates almost all frequency components to have the same mean direction and spreading. For the results given in Figure 6.6, the weighted mean direction is 29.73° with a weighted standard deviation of 0.14° . Deviations are only seen for very low and high frequencies, which can explain the uncertainties, as the parameters are determined based on a very low spectral density and for the low frequencies with very large wavelengths. Here it is also noticed that the spreading increases. The tendencies are the same as for the analysis of first order waves, which is also expected, since no higher order energy is introduced in the present analysis but only adjustment of the wavelength.

The estimated mean direction, θ_0 , appears for the relevant cases and directions in Table 6.3.

Table 6.3: Estimated values of the wave direction and spreading parameter for waves with amplitude dispersion.

| | | Generated direction, θ , [$^\circ$] | | | | | | | | | |
|---------------------------|---------|--|-------|-------|-------|-------|-------|-------|-------|-------|-------|
| | | 0 | 10 | 20 | 30 | 40 | 50 | 60 | 70 | 80 | 90 |
| θ_0 , [$^\circ$] | Case A3 | 0.00 | 10.48 | 20.45 | 30.42 | 40.05 | 50.15 | 60.12 | 70.04 | 80.15 | 90.14 |
| | Case D3 | 0.00 | 10.23 | 19.95 | 29.73 | 40.35 | 50.16 | 59.90 | 69.88 | 80.29 | 90.03 |
| | Case G3 | 0.00 | 10.02 | 20.00 | 30.07 | 40.07 | 50.03 | 60.04 | 70.33 | 80.11 | 90.01 |

The estimated mean direction for the different cases and target directions is compared to the value determined based on waves of first order theory. The error on the mean direction introduced by inclusion of amplitude dispersion appears from Figure 6.7.

In opposition to the results using Method 1, the present analysis shows very little influence from the amplitude dispersion in relation to the weighted value of the mean wave direction. When considering long-crested waves, the influence of the amplitude dispersion in relation to the reliability of the estimated direction of the waves is highly dependent on the choice of method, because several gauge pairs are used for the estimation of the directional parameters in Method 2. For the use of Method 2, the amplitude dispersion only seems to influence the spreading of the wave direction, that increases for Case D3 from approximately 9° to almost 11.5° in all directions and also slightly for Case G3.

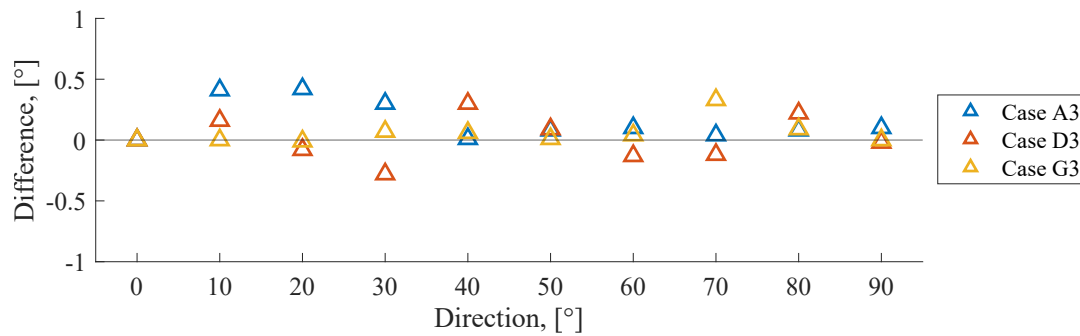


Figure 6.7: Difference in mean direction compared to value determined based on first order wave theory.

6.4 Summary of Long-Crested Waves - Method 2

The present chapter have evaluated the effect related to inclusion of nonlinear effects in the long-crested wave fields when performing the directional analysis based on linear wave theory using Method 2.

The analysis of second order waves showed a maximum error on the mean direction of 10.57° , with a corresponding increase in spreading from 9° to 26° compared to the analysis of the first order waves for a wave field of wave steepness $H/L = 0.02$ and relative wave height $H/h = 0.31$. This case was also the case with the highest amount of second order energy. For the remaining investigated cases, the maximum error on the mean direction due to the inclusion of second order energy became 3.44° .

When considering the amplitude dispersion by including the differences of the wavelength, the estimated mean wave direction changed with less than 0.5° , while the spreading of the waves increased with up to 3.5° . Based on the present analyses, the inclusion of amplitude dispersion is therefore concluded to be of insignificant influence when using Method 2 for measurements of long-crested waves from 6 gauge positions arranged as CERC6. It can therefore be concluded, that the use of statistical fitting is very beneficial for obtaining higher reliability of the estimated direction of the waves with amplitude dispersion.

Based on the present analyses, the accuracy of directional analysis is though mainly influenced by contributions from second order energy. It should though be noted, that not all type of waves have been considered. The accuracy of the estimated mean wave direction in relation to inclusion of nonlinear effects appear from Figure 6.8 and 6.9.

Further, the method used to determine the spreading function from Equation (3.9) uses the cross-spectra between each gauge pair to estimate the directional wave parameters. In this project the gauge array, CERC6, is chosen which results in 15 unique cross-spectra. The number hereof has an influence of the reliability because the spectrum in two positions of measurement theoretically should be identical, but in reality they will vary, which form the basis of a more correct average of the cross-spectra for more gauge pairs.

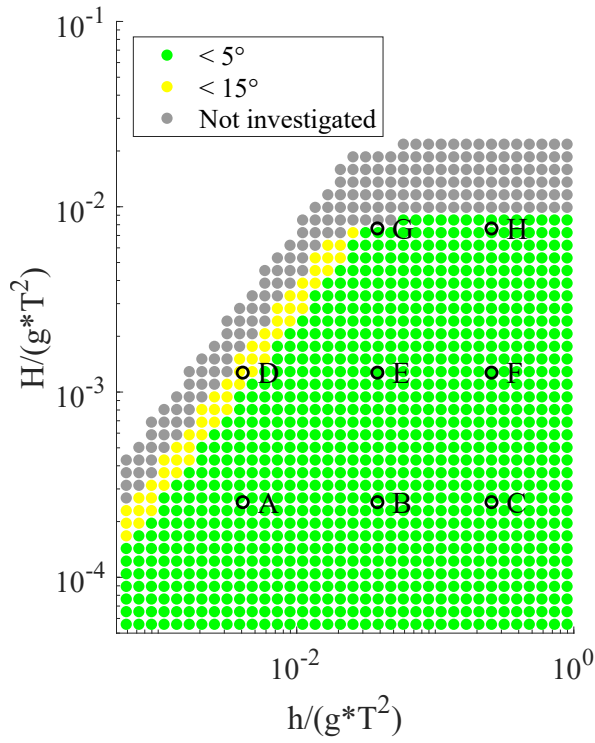


Figure 6.8: Accuracy of estimated mean wave direction for second order waves.

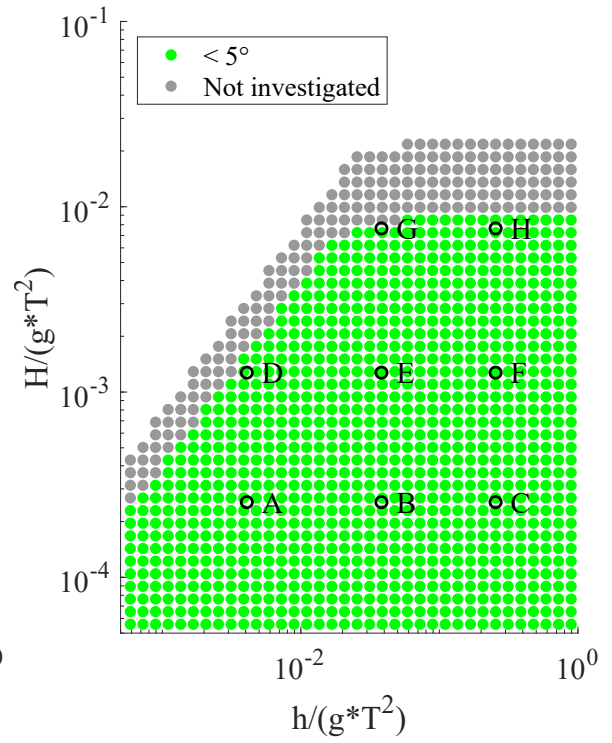


Figure 6.9: Accuracy of estimated mean wave direction for waves with amplitude dispersion.

7 | Method 2: Short-Crested Waves

As next step in the investigation of the nonlinear effects in the directional wave analysis, wave fields consisting of short-crested waves are considered. The analysis of the short-crested waves is performed as a stochastic analysis by use of Method 2, as elaborated in section 3.2. First, the directional parameters for short-crested waves are determined based on analyses using Method 2 for waves generated based on first order wave theory, which means that the analysed data corresponds with the theory the method is based upon. The results from the analysis of the first order waves will then be used as benchmark for inclusion of second order wave theory in the synthetic data and inclusion of simplified amplitude dispersion according to stream function theory.

The wave field is considered to be described by a Mitsuyasu-type directional spreading function, which describes the wave field in terms of a mean wave direction, θ_0 , and a spreading parameter, s . Examples of a distribution of the spreading function are shown in Figure 7.1.

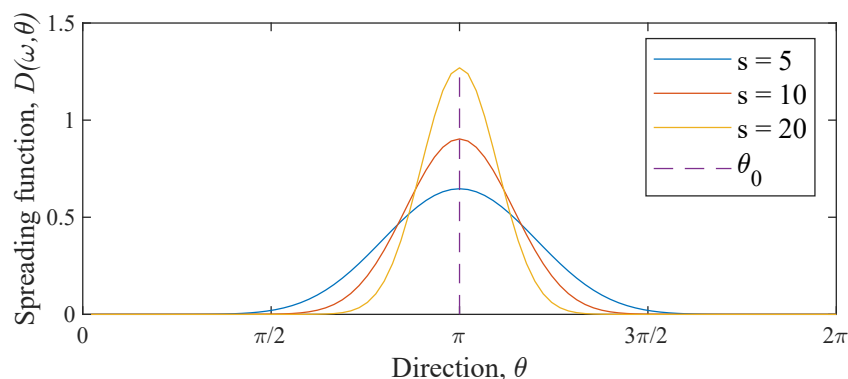


Figure 7.1: Mitsuyasu-type directional spectrum with mean direction $\theta_0 = \pi$ and different spreading parameters, s .

In the present thesis, a value of $s = 5$ is chosen as the spreading parameter. This is chosen on the basis of Y. and Suzuki (1975) which proposed a spreading parameter for the purpose of engineering. The suggestion was to fix values of s for wind waves and swell based on the frequencies. The maximum spreading parameter of the wind generated waves was proposed to 10, wherefore it is chosen to a value below to be sure that the present thesis only deal with wind generated waves.

Common for all analyses is that the data is generated based on a JONSWAP spectrum with significant wave height, H_{m0} , peak frequency, f_p , and water depth, h , corresponding to the values of the wave height, H , wave period, T , and water depth, h , of the eight cases of regular waves presented in chapter 4. Furthermore, the analysis is performed for a truncated auto-spectrum. Waves generated based on the two different generation models mentioned in section 2.1.2; single summation and double summation, will be analysed in the following.

As chapter 6 found that for Method 2, all directions are determined with the same level of accuracy, the present analysis will consider a single direction of 30° as illustrated in Figure 7.2

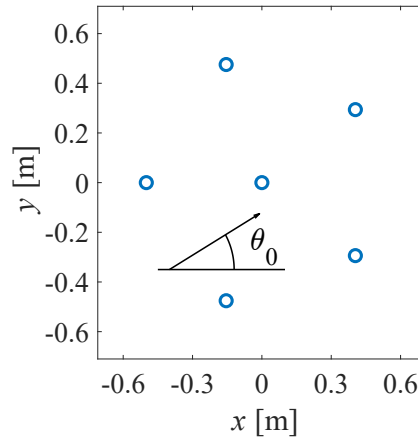


Figure 7.2: Investigated target mean wave direction, $\theta_0 = 30^\circ$.

7.1 Generation Models of Synthetic Waves

The generation of synthetic waves should be considered relative to the context. Both of the generation models used for generation of short-crested synthetic data for the present thesis represent a way to describe the wave field in different levels of complexity. It is out of the scope of this thesis to evaluate how well the different models describe mother nature. Furthermore, the choice of model should be considered in relation to the application. In this thesis, the generation is performed solely with the purpose of numerical analysis.

In relation to the computational performance, the single summation model requires inverse Fourier transforms of a significant amount of Fourier coefficients in order to obtain sufficient variability in the directional spreading, which is chosen based on a random probability of the probability density function of $D(\omega, \theta)$. When analysed, it is therefore similarly required that a larger $\Delta\omega$ is used than for generation in order to detect the correct directional spreading. For the double summation model, each of the Fourier components contain a defined number of directions, which leads to shorter array for the inverse Fourier transform. The generated time-series are therefore also limited to a shorter duration, which yields limited possibilities of separation in subseries in the analysis.

For the generation of second order contributions, all first order directional components of the double summation model interact, wherefore the computational capacity hereof is significantly larger than for a single summation model with equal amount of frequency components and thereby duration. The frequency resolution is found from the convergence study in Appendix E for the single summation model as well the double summation model.

The frequency resolution of the single summation model have $N = 2^{14}$ components and a directional resolution with $M = 1$ components, which is characteristic for this model. While the double summation model has a frequency resolution with $N = 2^{10}$ components and a directional resolution with $M = 30$ components. These magnitudes of resolutions are chosen such that the frequency resolution in the analyses have the same number of components, $N = 2^9$, which become valid when the number of subseries are chosen to $J = 30$ for single summation model and $J = 2$ for the double summation model. For the generation of waves in this thesis, the resolution of the directional spreading has been prioritised higher than the number of subseries.

As described in chapter 2, the direction components of short-crested waves based on the single summation model are chosen from the distribution function of the cosine power distribution, where a random number between 0 and 1 is used for each wave component. The directional components of short-crested waves based on the double summation model are chosen equally distributed from 0 to 2π . Therefore, the generated directional components based on a single summation model is used as benchmark for the directional analysis of the first order waves, as the generated mean direction does not necessarily equal the target direction. All directional components for an arbitrary case and target direction are plotted in Figure 7.3 for the wave field generated based on the single summation model. In the figure, Case D1 is shown with a target direction of 30° and with a target spreading of $\sigma = 34.5^\circ$.

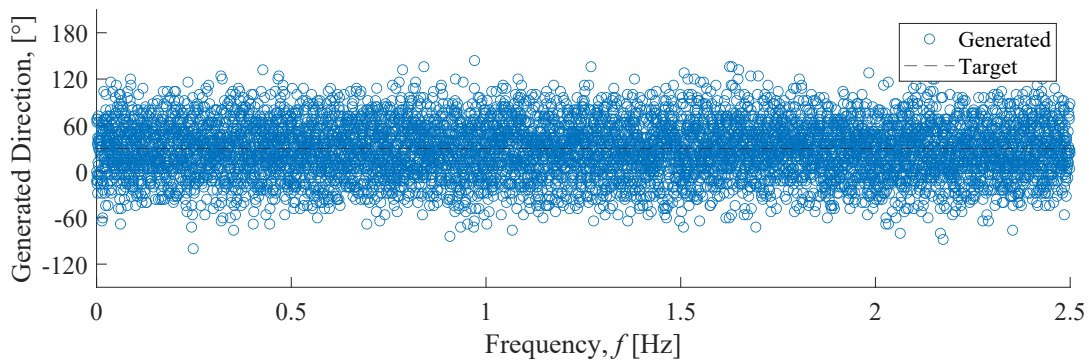


Figure 7.3: Generated directional components from a single summation model with the target values $\theta = 30^\circ$ and $\sigma = 34.5^\circ$.

During the analysis, the sample is divided into 30 subseries, which yields a mean direction for each of the analysed frequency components as shown in Figure 7.4, where the number of components are reduced from $N = 2^{14}$ to $N = 2^9$.

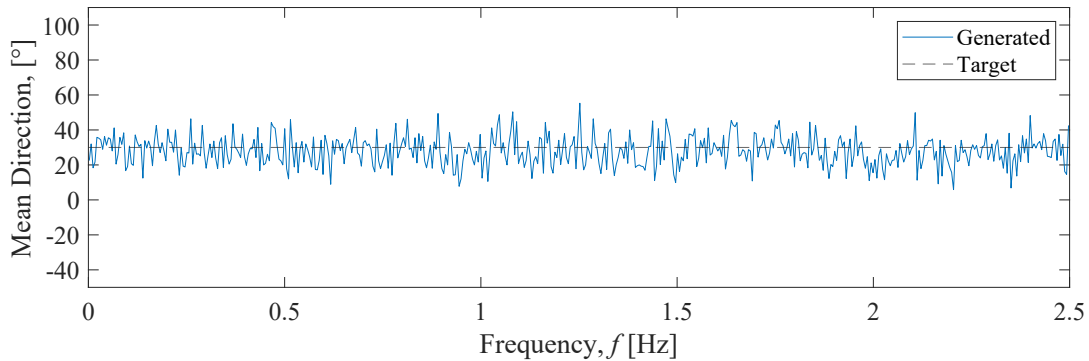


Figure 7.4: Generated directional components from a single summation model with the target direction of $\theta = 30^\circ$ divided into subseries.

A weighted direction for each of the eight cases A1 to H1 is determined from the amount of energy from the spectral density at a given frequency component related to a given directional component. The weighted mean wave directions are stated in Table 7.1, where the values have a systematic deviation of a smaller value compared to the target direction. This is due to the choice of numerical integration of the left hand rule in the generation model which leads to the approximation.

Table 7.1: Weighted wave directions of the 8 test cases generated from a single summation model.

| Case | A1 | B1 | C1 | D1 | E1 | F1 | G1 | H1 |
|--------------|--------|--------|--------|--------|--------|--------|--------|--------|
| θ [°] | 26.56° | 29.04° | 29.28° | 27.79° | 29.06° | 27.57° | 26.52° | 28.03° |
| σ [°] | 34.51° | 33.75° | 32.73° | 34.44° | 34.80° | 34.22° | 33.71° | 33.68° |

A possible problem with the double summation model is phase locking, where wave components with equal frequencies but different propagation directions and phase differences occur in the cross spectra. A solution to this problem has been suggested by Takayama et al. (1989) that the influence of phase locking in the double summation model can be eliminated by a larger number of components.

A selection of results will be shown in the following for Case D, as this is the case with the highest amount of second order energy and the largest difference in wavelength due to amplitude dispersion as determined in chapter 4. Results for the remaining of the eight cases are found in Appendix AC.

7.2 Analysis of First Order Waves

The data used for the following analysis is generated synthetically based on linear wave theory. First, the synthetic data generated from the single summation model is analysed, which is followed by the synthetic data generated from the double summation model. For each case, the parameters of the directional spreading function is determined for each frequency component.

7.2.1 Single Summation Model

The generated direction appear from Figure 7.5 as earlier described. The figure shows only the generated directions which are analysed in the directional analysis, these includes the frequencies within the truncation.

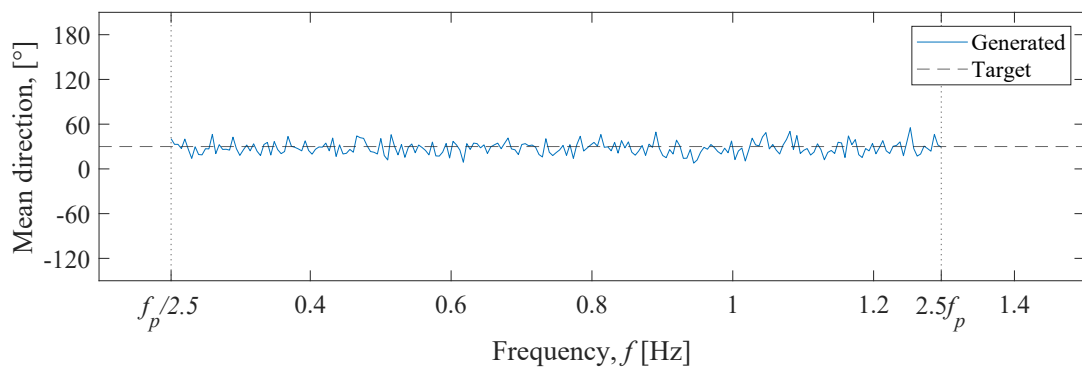


Figure 7.5: Generated directional components from a single summation model with the target direction of $\theta = 30^\circ$ divided into subseries, which are used in the analysis.

For Case D1, the results of the estimated mean direction of the waves and the spreading appear from Figure 7.6.

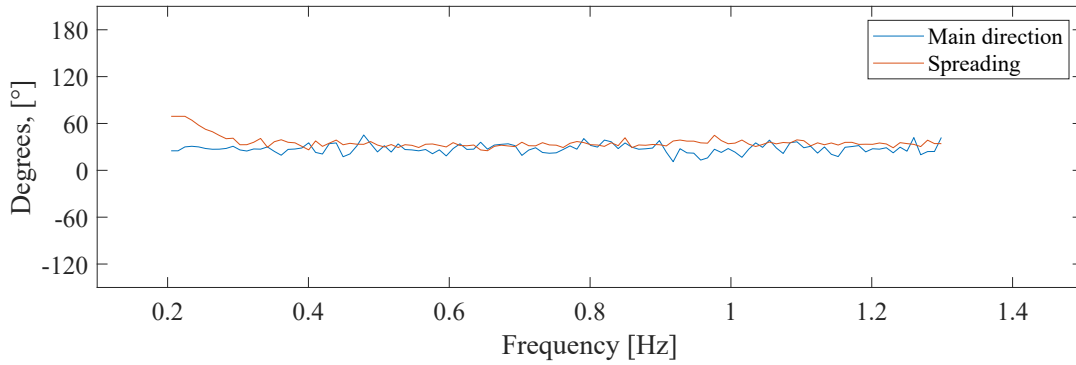


Figure 7.6: Estimated direction for components in the wave field with a target direction $\theta_0 = 30^\circ$ and $\sigma = 34.5^\circ$, Case D1, first order waves generated from single summation.

A weighted value of the two parameters is determined based on the variance spectrum of the measurements, assuming that the estimate of the direction is more accurate for wave components containing most energy. The weighted mean direction was for the case shown above estimated to 28.46° . The weighted values for all eight cases appear from Table 7.2.

Table 7.2: Results of MLM estimation of directional spreading of short-crested waves based on linear wave theory with target values $\theta_0 = 30^\circ$ and $\sigma = 34.5^\circ$.

| Single Summation | | | Deviation from generated parameters | | |
|------------------|---------------------------------------|---------------------------|-------------------------------------|---------------------------------------|---------------------------|
| Case | Mean wave direction θ_0 [°] | Spreading σ [°] | Case | Mean wave direction θ_0 [°] | Spreading σ [°] |
| A1 | 26.56° | 32.23° | A1 | 0.00° | -2.28° |
| B1 | 29.59° | 32.13° | B1 | 0.55° | -1.62° |
| C1 | 29.12° | 31.14° | C1 | -0.16° | -1.59° |
| D1 | 28.46° | 32.59° | D1 | 0.67° | -1.86° |
| E1 | 29.07° | 32.08° | E1 | 0.01° | -2.72° |
| F1 | 27.34° | 33.28° | F1 | -0.23° | -0.94° |
| G1 | 25.38° | 32.33° | G1 | -1.14° | -1.48° |
| H1 | 27.60° | 32.44° | H1 | -0.43° | -1.23° |

As seen in Table 7.2, the largest deviation compared to the generated direction is experienced for Case G1 with a deviation of 1.14° . The differences from the generated parameters does not show any specific tendency, wherefore it is assumed that the difference is caused by statistical uncertainty related to the fitting in Method 2. In the following, waves generated based on the double summation model are also investigated.

7.2.2 Double Summation Model

Due to the limited amount of data points for each data set, the number of subseries in the analysis of the waves based on the double summation model is therefore also limited to 2, which yields a possibility for a high level of variability. This should be taken into account in relation to the reliability of the performed analyses. The analysis is thereby performed for the same resolution of frequency components as the single summation model.

Figure 7.7 shows the results for Case D1 with short-crested waves based on the double summation model, similar to the results shown in Figure 7.6 for waves based on the single summation model.

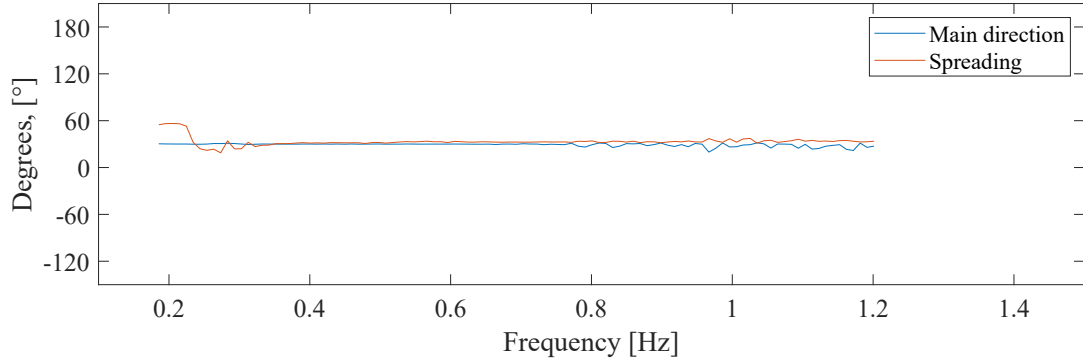


Figure 7.7: Estimated direction for components in the wave field with a target direction $\theta_0 = 30^\circ$ and $\sigma = 34.5^\circ$, Case D1, first order waves generated from double summation.

As for single summation, a weighted value of the two parameters is determined based on the variance spectrum of the measurements, assuming that the estimate of the direction is more accurate for wave components containing most energy. The weighted values for all eight cases appear from Table 7.3.

Table 7.3: Results of MLM estimation of directional spreading of short-crested waves based on linear wave theory with target values $\theta_0 = 30^\circ$ and $\sigma = 34.5^\circ$.

| Double summation | | | Deviation from target direction | | |
|------------------|---------------------------------------|---------------------------|---------------------------------|---------------------------------------|------------------|
| Case | Mean wave direction θ_0 [°] | Spreading σ [°] | Case | Mean wave direction θ_0 [°] | Spreading [°] |
| A1 | 29.91° | 32.20° | A1 | -0.09° | -2.31° |
| B1 | 29.95° | 30.70° | B1 | -0.05° | -3.80° |
| C1 | 29.94° | 30.96° | C1 | -0.06° | -3.54° |
| D1 | 29.91° | 32.30° | D1 | -0.09° | -2.31° |
| E1 | 29.97° | 30.71° | E1 | -0.03° | -3.79° |
| F1 | 29.94° | 31.00° | F1 | -0.06° | -3.51° |
| G1 | 29.93° | 30.73° | G1 | -0.07° | -3.77° |
| H1 | 29.98° | 30.94° | H1 | -0.02° | -3.57° |

From Table 7.2 and Table 7.3, it appears that the accuracy of the estimated mean wave direction for each case depends on the choice of generation model as explained earlier. For data based on the double summation model, the analysis estimates the correct direction within an accuracy of 0.09° , and within 1.14° for data based on the single summation model for the given cases. The use of the different models for generation will be discussed further in chapter 8.

7.3 Analysis of Second Order Waves

In the following, the inclusion of second order energy in the wave field will be evaluated based on both models of generation.

7.3.1 Single Summation Model

Synthetic data is generated based on second order wave theory, all other input parameters are equal to the ones used in the previous section for linear waves. For the present analysis, the single summation model is used for generation of synthetic data.

The spectral density of the first and second order theory respectively is shown in Figure 7.8, in which the vertical axis is shown in logarithmic scale for a better illustration of where the energy from the second order contribution is placed.

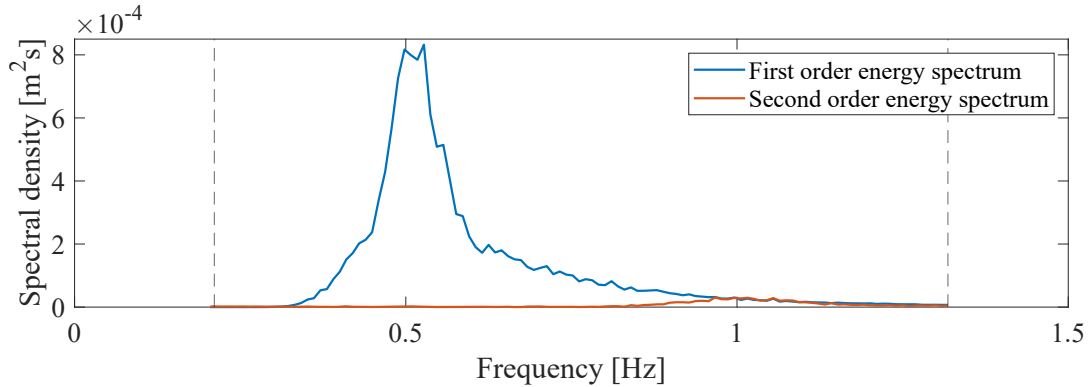


Figure 7.8: Spectral density of first and second order contributions, Case D2, $\theta_0 = 30^\circ$, $\sigma = 34.5^\circ$, generated from single summation.

The results for Case D2 is shown here in Figure 7.9 for illustration as the case with the highest amount of second order energy.

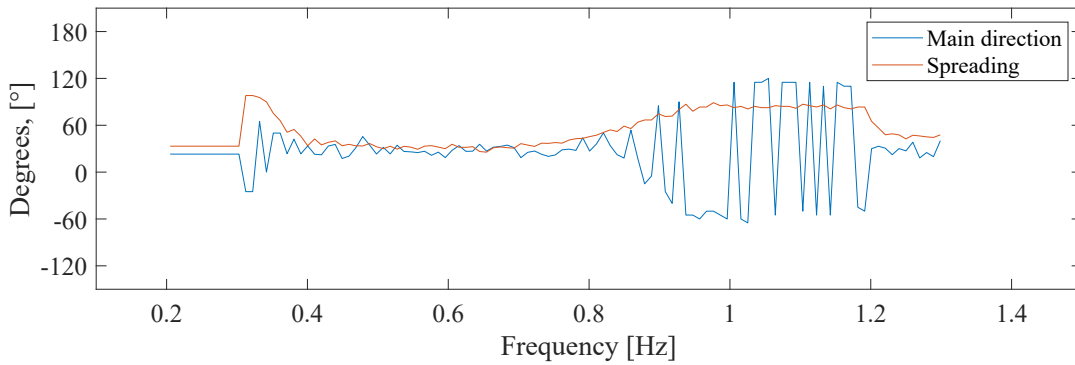


Figure 7.9: Estimated direction for components in the wave field with a target direction $\theta_0 = 30^\circ$ and $\sigma = 34.5^\circ$, Case D2, second order waves generated from single summation.

From Figure 7.9, it seems that the analysis determines the direction reasonably well in a limited region for frequencies close to the peak frequency, $f_p = 0.5$ Hz, and slightly above. The weighted mean direction is determined to be 27.27° with a weighted standard deviation of 24.89° . The significant increase in weighted standard deviation indicates that the estimated direction is less reliable compared to the analysis of first order waves. Although a truncation of the spectrum is already made, it seems to be necessary with a further truncation in order to give more reliable results that matches the ones from the analysis of the first order waves in the previous section. The frequency components that contain second order energy according to Figure 7.8 seems to correspond well with the components, where the estimation of the mean wave direction is very inaccurate according to Figure 7.9. The estimated mean direction of the individual frequencies

seem to split in two directions with random variation between the two over the frequencies with the highest amount of second order energy. The weighted mean direction of the wave field is therefore also expected to be able to vary for other samples than the example of Case D2 shown here.

As for the waves based on linear theory in the previous section, weighted values of the directional spreading function parameters are determined based on the spectral density of each of the frequency components. The results are here as well presented for all eight cases in Table 7.4.

Table 7.4: Results of MLM estimation of directional spreading of short-crested waves based on second order wave theory with target values $\theta_0 = 30^\circ$ and $\sigma = 34.5^\circ$.

| Single Summation | | | Deviation from first order theory. | | |
|------------------|---------------------------------------|---------------------------|------------------------------------|---------------------------------------|---------------------------|
| Case | Mean wave direction θ_0 [°] | Spreading σ [°] | Case | Mean wave direction θ_0 [°] | Spreading σ [°] |
| A2 | 26.49° | 32.82° | A2 | -0.06° | 0.59° |
| B2 | 29.59° | 32.14° | B2 | 0.00° | 0.01° |
| C2 | 29.12° | 31.14° | C2 | 0.00° | 0.00° |
| D2 | 27.27° | 38.91° | D2 | -1.19° | 6.32° |
| E2 | 29.04° | 32.14° | E2 | -0.03° | 0.06° |
| F2 | 27.36° | 33.31° | F2 | 0.02° | 0.03° |
| G2 | 25.53° | 34.09° | G2 | 0.15° | 1.86° |
| H2 | 27.62° | 33.84° | H2 | -0.02° | 1.40° |

From the results in Table 7.4 it appears that the case with the most significant influence from the second order energy is Case D2, which agrees well with the findings in chapter 4. This yields a difference in the estimated mean direction of 1.19° compared to the waves of first order theory. The estimation of the mean wave direction is less than 0.15° different from the analysis of first order waves for all other cases. The spreading of the waves increase for higher amount of second order energy.

7.3.2 Double Summation Model

The results for Case D2 of the estimated mean wave direction and spreading are shown in Figure 7.10, again for illustration as the case with the highest amount of second order energy.

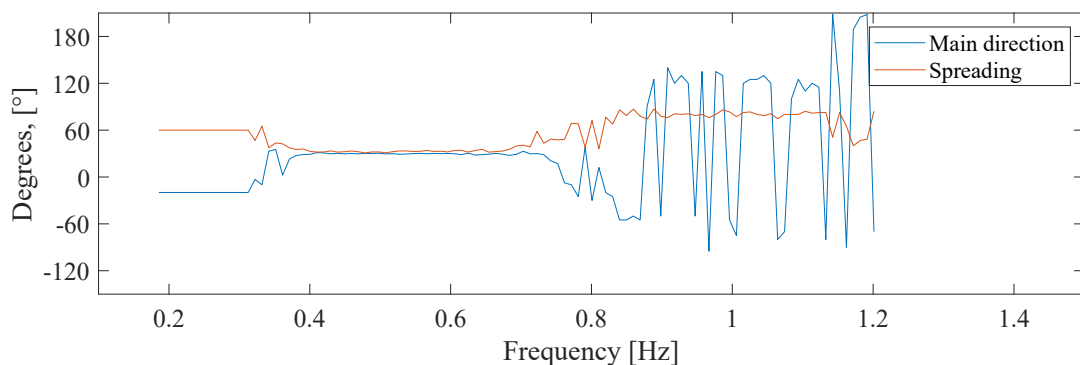


Figure 7.10: Estimated direction for components in the wave field with a target direction $\theta_0 = 30^\circ$ and $\sigma = 34.5^\circ$, Case D2, second order waves generated from double summation.

The results of the weighted estimated wave directions and spreading parameters are stated in Table 7.5 including the difference from the analysis of the first order wave theory.

Table 7.5: Results of MLM estimation of directional spreading of short-crested waves based on second order wave theory with target values $\theta_0 = 30^\circ$ and $\sigma = 34.5^\circ$.

| Double Summation | | | Deviation from first order theory. | | |
|------------------|---------------------------------------|---------------------------|------------------------------------|---------------------------------------|---------------------------|
| Case | Mean wave direction θ_0 [°] | Spreading σ [°] | Case | Mean wave direction θ_0 [°] | Spreading σ [°] |
| A2 | 29.36° | 33.32° | A2 | -0.55° | 1.12° |
| B2 | 29.95° | 30.70° | B2 | 0.00° | 0.00° |
| C2 | 29.96° | 30.96° | C2 | 0.02° | 0.00° |
| D2 | 32.68° | 39.89° | D2 | 2.77° | 7.69° |
| E2 | 30.01° | 30.71° | E2 | 0.05° | 0.00° |
| F2 | 29.95° | 31.00° | F2 | 0.00° | 0.00° |
| G2 | 29.71° | 31.37° | G2 | -0.22° | 0.63° |
| H2 | 29.74° | 31.27° | H2 | -0.24° | 0.33° |

The results of the estimated weighted mean wave directions show the largest deviation compared to the analysis of the first order waves for the cases A2, D2, G2 and H2, which contain a larger amount of second order energy. Case D2 is the case containing most second order energy according to the position of the case in the Diagram of Le Mehaute. The estimated mean direction deviates with 2.77° compared to the analysis of the first order waves for this case. The cases A2, G2 and H2 have a minor deviation, while the cases B2, C2, E2 and F2 shows only insignificant differences compared to the results based on first order waves.

Overall, the analysis of the waves generated based on the single and double summation show the same tendency in relation to the frequency components with a high level of second order energy as seen in Figure 7.9 and 7.10. And in general, the second order effects do not influence the estimation of the weighted mean direction significantly.

7.4 Analysis of Waves With Amplitude Dispersion

The analysis of waves with amplitude dispersion is also performed on data generated based on the single summation model as well as double summation model. The relevant cases in relation to amplitude dispersion are stated in Table 4.3, as the remaining cases had no significant difference in wavelengths, meaning that the results correspond to the analysis of the first order waves.

As explained in section 5.3, the amplitude dispersion is included by multiplying the wavelengths with a factor taking the difference stated in Table 4.3 into account. The same factor is used for all frequency components.

7.4.1 Single Summation Model

In the following, the results from the analysis of synthetic waves generated based on the single summation model will be presented. Figure 7.11 illustrates an example of how well the method estimates the mean wave direction and spreading of each frequency component within the truncation compared to the analysis of waves of first order wave theory.

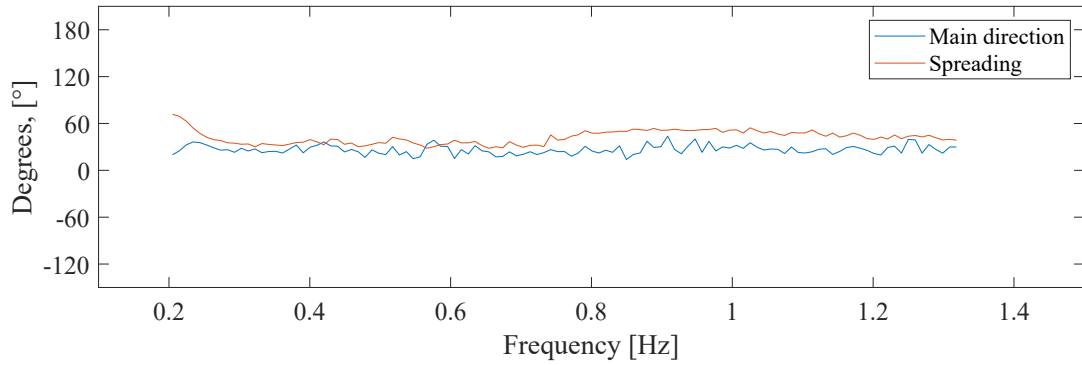


Figure 7.11: Estimated direction for components in the wave field with a target direction $\theta_0 = 30^\circ$ and $\sigma = 34.5^\circ$, Case D3, waves with amplitude dispersion generated from single summation.

From Figure 7.11, it appears as for the analysis of the first order waves, that the estimation of the mean direction differs with different intensity from the target value across the frequency components. The weighted value of the mean direction and spreading of the waves is determined taking the spectral density distribution into account. For Case D3 the weighted mean direction is 24.62° . The results for the relevant cases appear from Table 7.6 including the deviation from the generated values, as the waves with amplitude dispersion are based on a different data set than the first and second order waves. The generated values appear from Appendix AC.

Table 7.6: Results of MLM estimation of directional spreading of short-crested waves with amplitude dispersion with target values $\theta_0 = 30^\circ$ and $\sigma = 34.5^\circ$.

| Single Summation | | | Deviation from generated value | | |
|------------------|---------------------------------------|---------------------------|--------------------------------|---------------------------------------|---------------------------|
| Case | Mean wave direction θ_0 [°] | Spreading σ [°] | Case | Mean wave direction θ_0 [°] | Spreading σ [°] |
| A3 | 27.13° | 34.34° | A3 | -0.41° | 2.11° |
| D3 | 24.62° | 36.72° | D3 | -1.69° | 4.13° |
| G3 | 27.69° | 32.89° | G3 | -0.70° | 0.66° |

Based on the results in Table 7.6, the estimated direction for Case D3 is the one most influenced by the inclusion of amplitude dispersion, with a difference of 1.69° compared to the analysis of the first order waves. Based on the present analysis the error on the direction seem to increase with increasing amount of amplitude dispersion.

7.4.2 Double Summation Model

Next, the results based on the analysis of synthetic data generated based on the double summation model is presented. Figure 7.12 shows a case with similar input parameters as the example in the previous section.

On the higher frequencies the results seem to deviate more from the target value. The weighted mean direction is here determined to 28.80° .

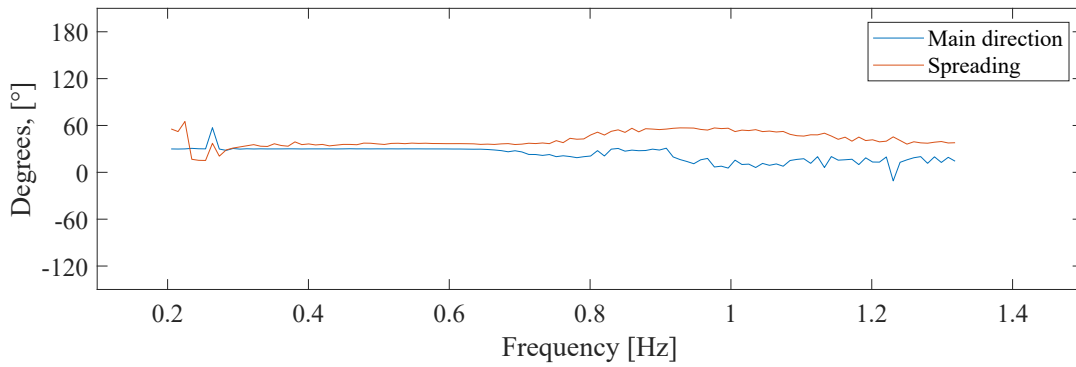


Figure 7.12: Estimated direction for components in the wave field with a target direction $\theta_0 = 30^\circ$ and $\sigma = 34.5^\circ$, Case D3, waves with amplitude dispersion, double summation.

The weighted values of the parameters for the relevant cases are stated in Table 7.7 including the difference from first order theory.

Table 7.7: Results of MLM estimation of directional spreading of short-crested waves with amplitude dispersion with target values $\theta_0 = 30^\circ$ and $s = 5$.

| Double Summation | | | Deviation from first order theory | | |
|------------------|---------------------------------------|------------------|-----------------------------------|---------------------------------------|------------------|
| Case | Mean wave direction θ_0 [°] | Spreading [°] | Case | Mean wave direction θ_0 [°] | Spreading [°] |
| A3 | 29.81° | 32.41° | A3 | -0.10° | 0.21° |
| D3 | 28.80° | 37.62° | D3 | -1.11° | 5.42° |
| G3 | 29.87° | 32.16° | G3 | -0.06° | 1.42° |

From the weighted values of the mean wave direction in Table 7.7, the deviation in relation to first order theory is largest for Case D3, which was also seen for the single summation model. Here, the amplitude dispersion though only results in a change in the estimated direction of 1.11° .

Based on the present analysis of the data from the double summation model, it is possible to determine the mean wave direction within a reliability of $\pm 1.5^\circ$ when using the CERC6 gauge arrangement for all investigated levels of wave steepness and relative wave height, which corresponds to up to at least 6.1 % difference in wavelength compared to the value based on linear wave theory.

Three other directions are examined to base the conclusion of the deviation of the results upon more generated data sets than one. These results are used to evaluate the reliability of the size of the deviation of the results in the report, which is used to validate the method. The results used for comparison are stated in Appendix F. As for the previous chapters, the analysis is performed for increasing level of wave theory starting with first order theory in order to determine the accuracy of the method itself for analysis of a short-crested wave field.

7.5 Summary of Short-Crested Waves

Within generation of short-crested waves it should be considered, whether the data is generated based on the single or double summation model. The differences in resolution of frequency components for the generation versus the analysis is therefore also of significant influence in relation to the reliability of the synthetic waves. On the other hand, the generation based on the double summation model requires a large amount of components in the generation in order to fulfill the assumptions made for the wave field, wherefore variations can be expected. The inaccuracies can also be related to the statistical uncertainty related to the procedure in Method 2.

Figure 7.13 and 7.14 sum up the results of the analyses of short-crested waves generated using the single summation model. For the first order waves, the generated values are used as benchmark, for the second order waves and waves with amplitude dispersion, the results based on the first order waves are used as benchmark.

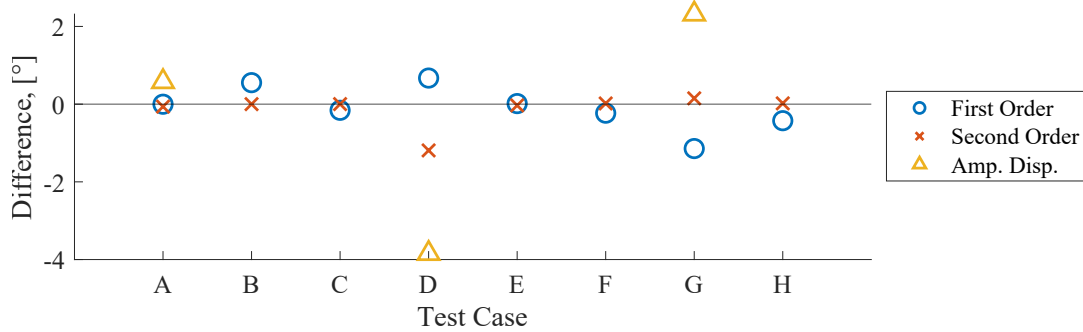


Figure 7.13: Difference in estimated mean directions compared to the generated values for first order, and compared to first order for inclusion of nonlinear effects, single summation models.

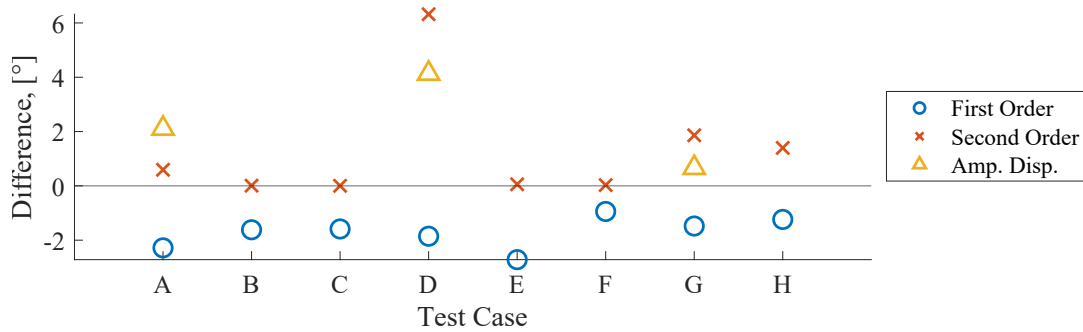


Figure 7.14: Difference in estimated directional spreading of waves compared to the generated values for first order, and compared to first order for inclusion of nonlinear effects, single summation models.

In relation to the second order energy for the waves generated based on the single summation model, all investigated cases showed an error on the direction of less than 1.2° compared to analysis of waves of first order theory, and the spreading of the waves did not show any significant influence either. In relation to the inclusion of amplitude dispersion, the present analyses show that the error on the mean direction became up to 1.69° for a wave field with wave steepness $H/L = 0.02$ and relative wave height $H/h = 0.31$. The nonlinear effects made the spreading of the waves increase, though only with few degrees.

For the analyses of the waves generated based on the double summation model, the results showed an opposite tendency in relation to whether the second order energy or amplitude dispersion is of larger influence on the estimated mean direction. The results are summed in Figure 7.15 and 7.16.

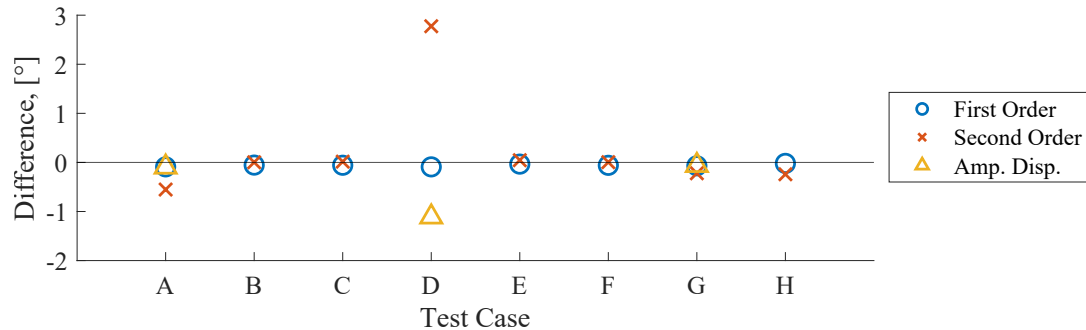


Figure 7.15: Difference in estimated mean directions compared to the generated values for first order, and compared to first order for inclusion of nonlinear effects, double summation models.

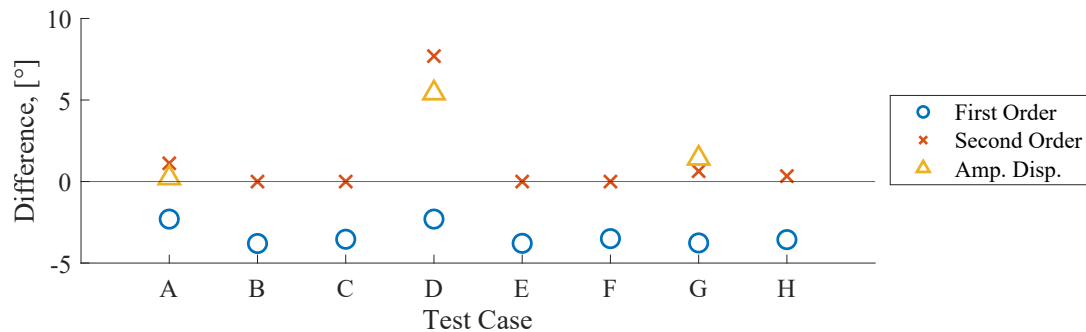


Figure 7.16: Difference in estimated directional spreading of waves compared to the generated values for first order, and compared to first order for inclusion of nonlinear effects, double summation models.

Based on the present analyses of short-crested waves generated from the single as well as double summation model, none of the results give rise to further improvements of the method used for the directional analysis, wherefore the accuracy of the estimated mean wave direction is as illustrated in Figure 7.17.

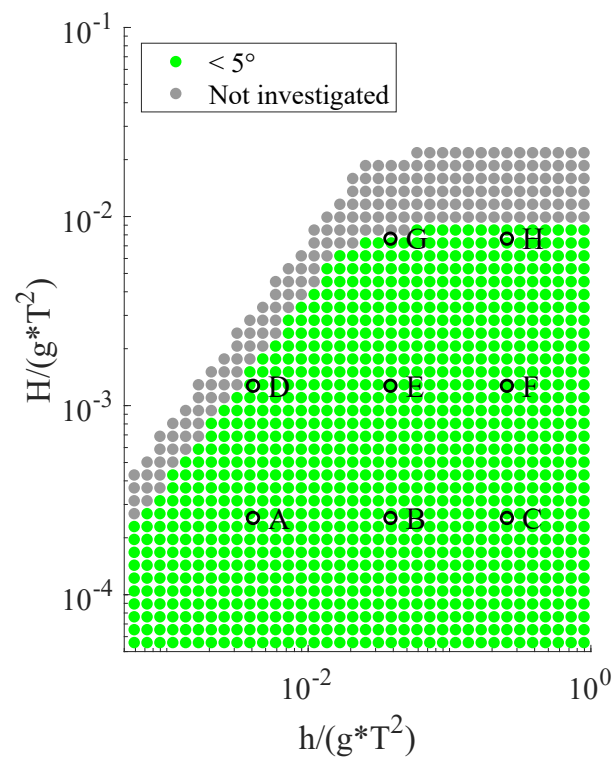


Figure 7.17: Accuracy of estimated mean wave direction for short-crested waves.

8 | Evaluation of Methods and Nonlinear Effects

In the following, the two different methods used for the analyses will be evaluated based on the results in the previous chapters. All analyses so far have been performed on idealised data containing solely nonlinear effects, wherefore it has been possible to determine the effects hereof.

Accuracy of Methods - Linear Wave Theory

To conclude on the nonlinear effects, the different methods used for analysis and models used for generation are first considered in order to verify the reliability of those before adding nonlinear effects. For the short-crested waves, a single sample is considered for each case, as only a single direction is considered. For the long-crested waves a range of target directions are considered, though here also only one sample per target direction. It is assumed, that the duration of each sample is sufficient in order to determine the reliability of the two methods. Method 1 does however only use a single subseries for the analysis, wherefore the results can be associated with significant variability. Figure 8.1 illustrates how much the estimated mean wave direction deviates from the target mean wave direction for each of the analyses and generation models used in the previous parts of this paper. The error on the mean direction is shown in absolute values. For the analyses of long-crested waves, the maximum error from the investigated directions is representative for each case.

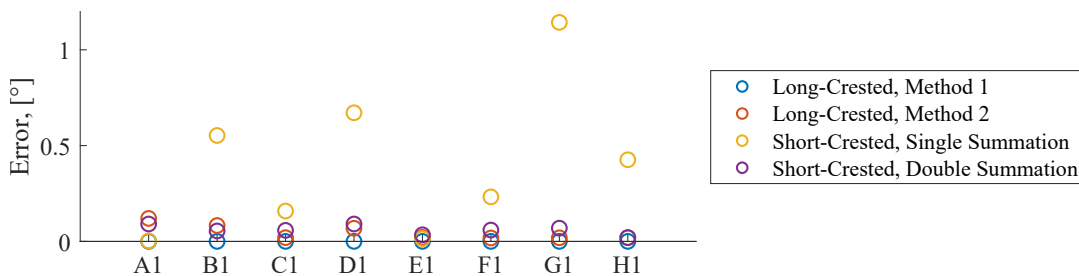


Figure 8.1: Maximum absolute errors on mean wave direction for the investigated cases in relation to the target value for synthetic waves generated based on linear wave theory.

Based on the analysis of long-crested waves using the full spectral density, Method 1 showed a tendency to become more accurate for wave directions close to 90° and 270° relative to the gauge pair. And similarly less accurate for waves travelling at 0° and 180° from the gauge pair. When truncating the spectrum, all estimated directions were determined accurately. For analysis of short-crested waves, only Method 2 was applicable. From Figure 8.1 it appears that the analysis of the data generated based on the double summation model was more accurate than the analysis of data generated based on the single summation model. Since the analyses of the short-crested waves is similar for the generation based on both models, it is more likely that the uncertainties are related to the generation of the waves.

Although Method 1 has a very limited area of application, as it is only applicable for analysis of long-crested waves, it has turned out to be a useful tool for determination of more specific

tendencies especially in relation to reliability of estimated directions relative to the orientation of gauge pairs. However, Method 1 is not usable in practice as Method 2. When using Method 2, the data was fitted to the Mitsuyasu-type directional spreading function, wherefore a spreading of the long-crested waves was also determined. The value was approximately 85, which corresponds to a spreading of approximately 9° , which based on the present analyses seems to be the smallest spreading, that the method can detect. Figure 8.2 illustrates the directional spreading for certain values of s .

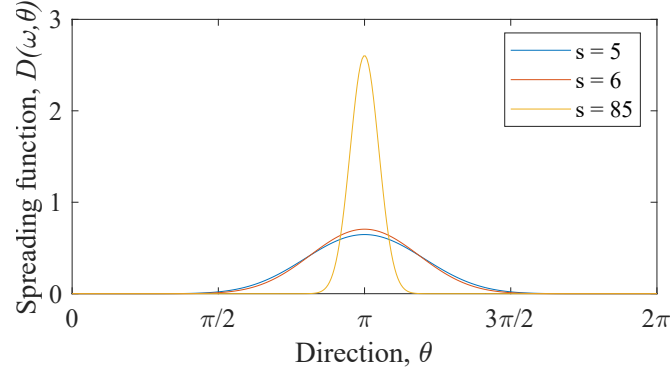


Figure 8.2: Mitsuyasu-type directional spectrum with mean direction $\theta_0 = \pi$ and different spreading parameters s .

Figure 8.2 furthermore illustrates the target value used for the short-crested waves, $s = 5$. The results based on the first order waves though showed estimates of approximately $s = 6$, meaning that the methods estimated a smaller spreading of the waves than expected. It is unknown whether the difference in spreading of the first order waves compared to the target value is due to the generation of the waves or caused by the analysis. As seen from the figure, the difference is though of very small influence.

Sensitivity Towards Nonlinear Effects

Furthermore, it has been investigated how the two different methods of analyses handle the nonlinear effects included as second order energy and amplitude dispersion, respectively. The effects were investigated based on long-crested as well as short-crested wave fields, which yielded the results shown in Figure 8.3 and 8.5. The figures show the maximum absolute error relative to the estimated mean direction of the waves generated based on linear wave theory.

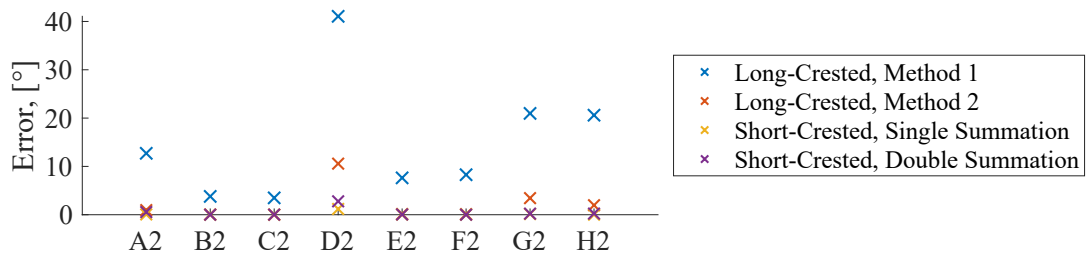


Figure 8.3: Maximum errors on mean wave direction for the investigated cases for synthetic, long- and short-crested waves generated based on second order wave theory in relation to results for waves of linear wave theory.

As it appears from Figure 8.3, the different analyses show different sensitivity towards the inclusion of second order energy, which was seen from Figure 4.2. Especially for analyses of Method 1, a higher amount of second order energy seems to be associated with a larger error on

the estimated direction. The estimate seems to be improved for all cases, when using Method 2. For the analysis of the long-crested waves by use of Method 2, Case D2 was the only case, where the mean direction could not be determined within $\pm 5^\circ$, with deviations of more than 10° . For the analysis of the short-crested waves, the influence from the second order energy is insignificant for all cases. As mentioned earlier, the deviation of the results for the double summation model is though associated with a large variability due to the limited number of subseries used in the analysis.

For the directional analysis of long-crested as well as short-crested second order waves, the frequency components with a high amount of second order energy showed a general tendency to have other mean directions than the components with a low amount of second order energy. An example is given in Figure 8.4 for the analysis of the short-crested waves with target direction 30° and target spreading of 34.5° .

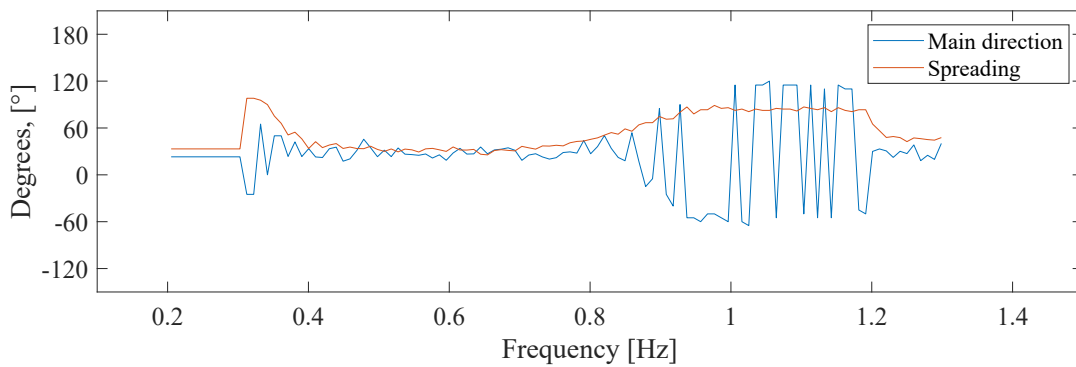


Figure 8.4: Estimated direction for components in the short-crested wave field generated based on the single summation model with target values $\theta_0 = 30^\circ$ and $\sigma = 34.5^\circ$, Case D2.

The analysis tool seems to find two separate patterns that goes towards $\pm 90^\circ$ of the target direction for a range where the superharmonic components are present, and it seems to be random which one of them is estimated as the best fit, wherefore the estimated mean wave direction differs in smaller or larger extent from the target value. The second order contribution is generated based on the interactions between the first order components. The bound sub- and superharmonics will therefore have different directions, which do not contribute to the same directional spreading function as the primary components. Sand (1979) found that the bound subharmonics have a larger spreading than the first order contribution, which is also experienced in the present analysis to some extent. For the very low frequencies it should though be noted, that for the example given in Figure 8.4, the analysis tool is quite sensitive towards the initial guesses used for the optimisation as described in section 3.2.2. In the present case, the initial guesses from the peak frequency is used, when it is no longer possible to determine a unique best fit from a range of different values of the mean direction and spreading. Based on the investigations of the present thesis, the spreading of the superharmonics similarly seems to be larger, wherefore the mean direction may become more difficult to determine when a high amount of second order energy is present in the wave field.

The influence from inclusion of amplitude dispersion according to stream function theory appears from Figure 8.5. Based on the influence from amplitude dispersion, Method 2 reduces the nonlinear effects significantly for analysis of long-crested waves, since the analyses showed almost no sensitivity towards amplitude dispersion. The increase in accuracy can be related to the

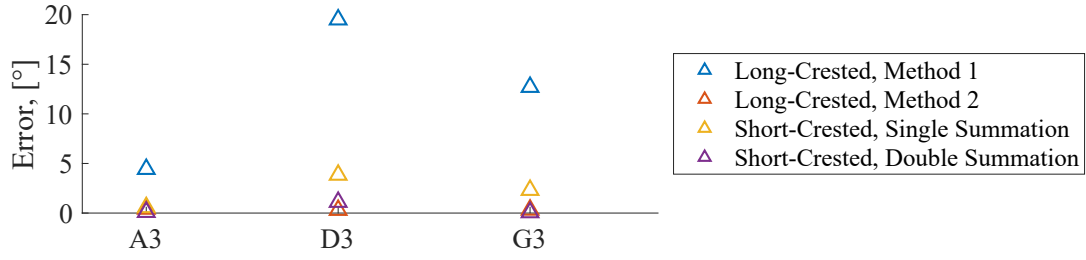


Figure 8.5: Maximum errors on mean wave direction for the investigated cases for synthetic, long- and short-crested waves with amplitude dispersion in relation to results for waves of linear wave theory.

statistical fitting in relation to the number of subseries used for the analysis as well as the number of gauges used for measurements. From the analyses using Method 1, it became evident that the angle of the wave in relation to the angle of a gauge pair is of significant influence when determining the reliability of the estimated mean direction. For waves with amplitude dispersion, Method 1 showed to provide errors up to almost 20° on the mean direction. The analyses furthermore demonstrated the strengths of the geometry and number of gauges in the CERC6 array, since all evaluated directions showed the same level of accuracy. These results give rise to an investigation of the influence of having a symmetrical wave gauge arrangement, which is performed in chapter 11.

As the directional analyses of the present thesis are based on idealised data generated based on either first or second order wave theory, the effects from amplitude dispersion have been included in a simplified way by multiplying the wavelengths of the different components of the irregular waves of first order wave theory with the same factor. The nonlinear effects of the waves containing amplitude dispersion should therefore also be considered in relation to this. For more accurate generation, this factor could have been adjusted for the individual frequency components, which could possibly influence the order of magnitude of the effects, as some components would have larger or smaller influence from amplitude dispersion than indicated by the factor.

In relation to the spreading of the short-crested waves, most of the investigations showed a small increase in spreading due to the nonlinear effects, though not higher than a deviation of 5° . For a target value of the spreading parameter $s = 5$, the estimated value seemed to change with approximately 1, which is illustrated in Figure 8.6 for the directional spreading function, and corresponds to an increase in the spreading of approximately 3° .

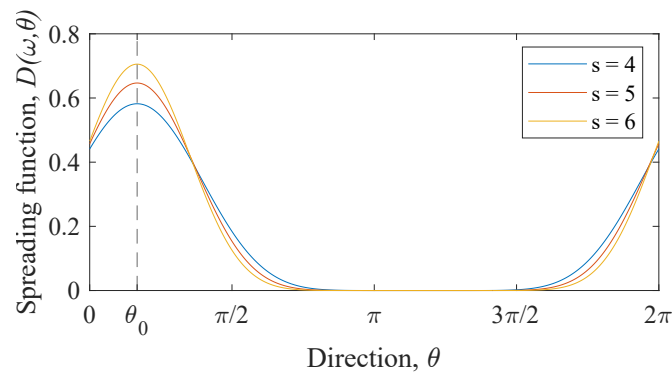


Figure 8.6: Mitsuyasu-type directional spectrum with mean direction $\theta_0 = 30^\circ$ and different spreading parameters s .

Statistical Choice

In the present thesis, the long-crested waves were all generated with ten target directions of the eight test cases, which produces eighty representative data sets each with $N = 512$ frequency components. These different target directions are determined to have an influence on the analysed direction in Method 1, where the errors are varying along the varying direction because of the gauge array. This gives a random sample for each test case for each direction, from which the limitation diagram is illustrated. This sample size is chosen to be representative for the investigation of Method 1. Method 2 have an array with more gauges, which makes the error from the target direction due to the varying directions less influenced compared to Method 1 as determined from the analysis of long-crested waves, wherefore only a single direction is considered for short-crested waves. Furthermore, the generated long-crested wave fields used in Method 2 are all generated with $N = 16,384$ frequency components separated into 30 subseries in the analysis to obtain the 512 wave components in this analysis. The number of the 30 subseries is chosen from a compromise between reliability and resolution, where the resolution is kept the same size as for the analysis using Method 1. From the assumption that the spectral density is the sum of the squares of two Fourier coefficients which are assumed to be Gaussian, random, independent variables, the distribution of the spectral density becomes χ^2 -distributed, which yields that the relative error of the reliability is 18% when using 30 subseries for Method 2 and 100% for Method 1 which has only one subseries. If the analysis should have been more reliable, a higher number of subseries would have decreased the relative error of the reliability. This has been studied in Appendix G for the analysis of waves based on the double summation model. The resolution of each subseries would have become more coarse, which seems to increase the estimated directional spreading. Further, the relatively low number of frequency components $N = 1,024$ in the double summation generation model was chosen due to the generation of the second order components. Each of the directional and frequency components interact, which results in a larger number of wave components for the second order contribution. Thus, the quality of the data was affected, which means that the data does not fulfill the requirement of being homogeneous and ergodic. This is illustrated in Figure 8.7. The figure shows how the spectra determined from different gauge positions deviate from each other, even though they theoretically should be equal to each other. In the analysis, the mean value of the spectral density is used for estimation of the mean wave direction and spreading, which might be far from the actual energy measured by each of the gauges.

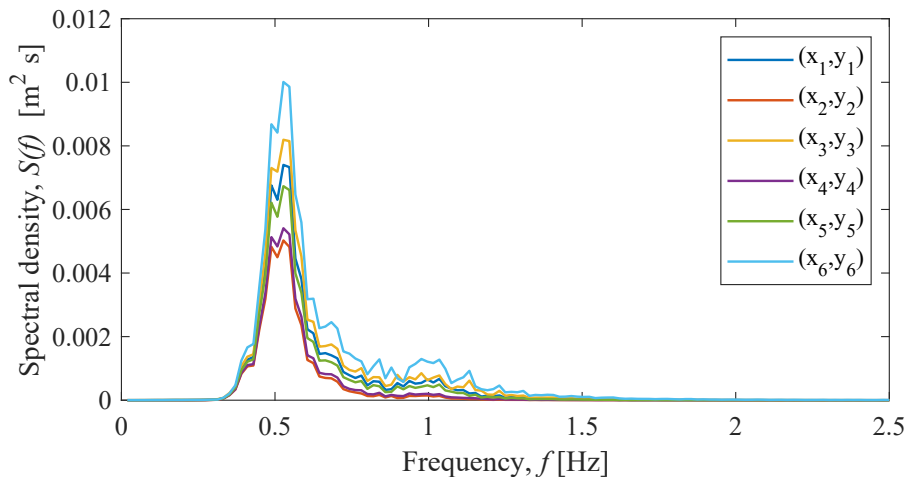


Figure 8.7: Spectral density based on a double summation model.

Limitations of Application

Based on the investigations of the present thesis, the results does not show an unambiguous tendency in relation to whether second order energy or amplitude dispersion is of most significant influence in relation to the directional analysis. For analysis of long-crested waves, the present analyses indicate that the inclusion of second order energy affects the estimation of the mean direction the most. For analysis of short-crested waves, the analyses indicate that the inclusion of amplitude dispersion affects the mean direction the most. Common for all analyses is though that the influence seems to depend on the level on nonlinearity of the specific wave field. The accuracy of the estimated mean wave direction based on the analyses of the present thesis is illustrated in Figure 8.8 for Method 1 and in Figure 8.9 for Method 2.

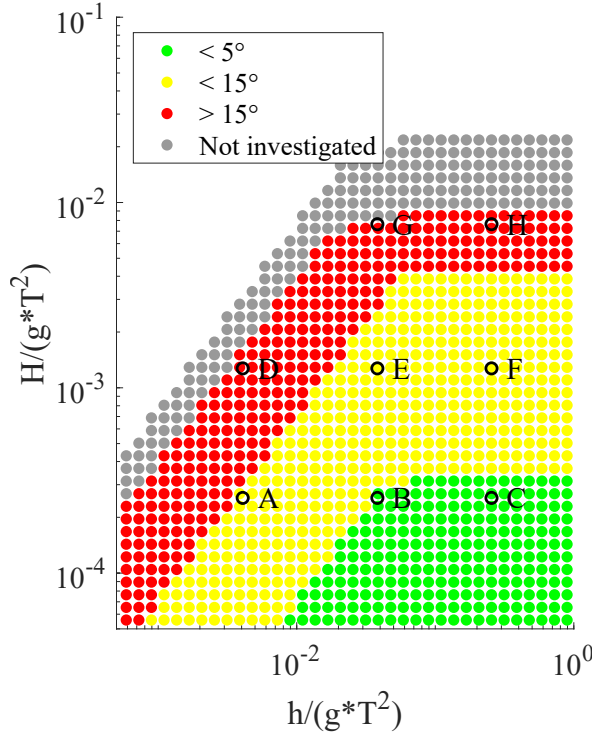


Figure 8.8: Accuracy of estimated mean wave direction using Method 1.

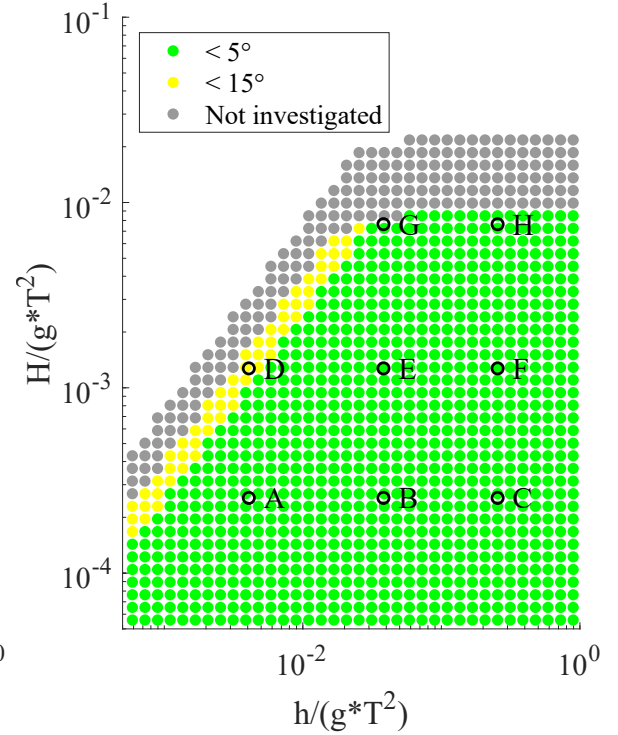


Figure 8.9: Accuracy of estimated mean wave direction using Method 2.

In Part III of this paper, the influence of the nonlinear effects will be considered in relation to other effects in the performance and reliability of the directional analysis based on linear wave theory.

III

Other Effects

| | | |
|-------------------|--|-----------|
| Chapter 9 | Noise | 65 |
| 9.1 | Long-Crested Waves | |
| 9.2 | Short-Crested Waves | |
| 9.3 | Summary of Noise Error | |
| Chapter 10 | Errors Related to Calibration | 72 |
| 10.1 | Long-Crested Waves | |
| 10.2 | Short-Crested Waves | |
| 10.3 | Limitation of Application | |
| Chapter 11 | Wave Gauge Arrangement | 77 |
| Chapter 12 | Analysis of Laboratory Tests | 81 |

9 | Noise

An effect which might have an influence on the surface elevation signal and thereby the estimated directional parameters is for example noise. This is investigated in the following to test the robustness to possible errors by using Method 2. All analyses in this chapter are performed in the same manner as in the previous part. For that reason the approach and sub-results are stated in Appendix H, while the figures of the results are mainly shown in Appendix AD for long-crested waves and in Appendix AE for short-crested waves. The deviations from each benchmark for the different wave fields are illustrated to outline the effect the noise has in this chapter. The results without noise from Part II are used as benchmark to isolate the effect from noise.

To study how robust the present analysis is, white Gaussian noise is added to the signal of surface elevation for each gauge by using the incorporated tool in MatLab, *awgn*. This analysis is performed for different magnitude of noise and for the synthetic first order waves as well as the second order waves and waves with amplitude dispersion. The signal to noise ratio (*snr*) is determined for the different cases as shown in Table 9.1, where the values are resolved based on the change in spectral density when including noise on the signal. In the generation, the signal to noise ratio is set equal to the table value, such that the noise consist of approximately 2 % of the spectral density. The similar amount of white Gaussian noise is added to all wave fields to study affect the noise of the directional analysis.

Table 9.1: Magnitude of signal to noise ratio in proportion to the spectral density.

| Case | A | B | C | D | E | F | G | H |
|----------------|------|------|------|------|------|------|------|------|
| H [m] | 0.01 | 0.01 | 0.01 | 0.05 | 0.05 | 0.05 | 0.30 | 0.30 |
| <i>snr</i> [-] | 70 | 70 | 70 | 55 | 55 | 55 | 40 | 40 |

9.1 Long-Crested Waves

The effect from noise in the analysis of long-crested waves is determined based on the same data of synthetic generated waves as chapter 6, though here with noise included. Figure 9.1 represents the signal of Case D1 with white Gaussian noise added.

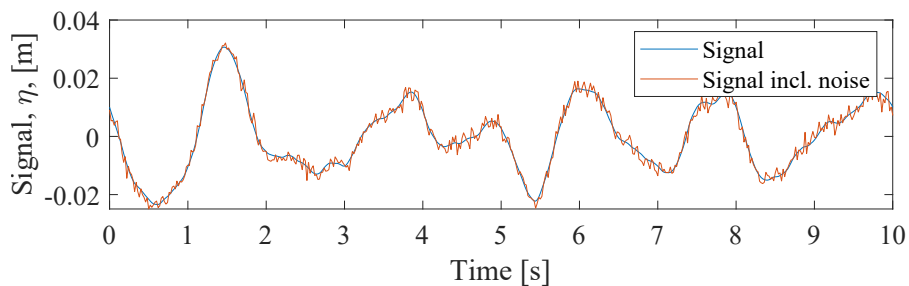


Figure 9.1: Surface elevation signal for Case D1 including white Gaussian noise.

The signals with white Gaussian noise added are analysed using Method 2 to obtain an estimated direction and the spreading which are comparable to the results without noise to investigate how sensitive the analysis is.

Errors at Estimated Mean Wave Direction

The estimated mean wave directions of the wave field with noise are compared to the results from the analysis of waves without noise included. The deviations for all the cases appear from Figure 9.2, 9.3 and 9.4 for the directions from 0° to 90° for the first and second order signal and the signal with amplitude dispersion, respectively.

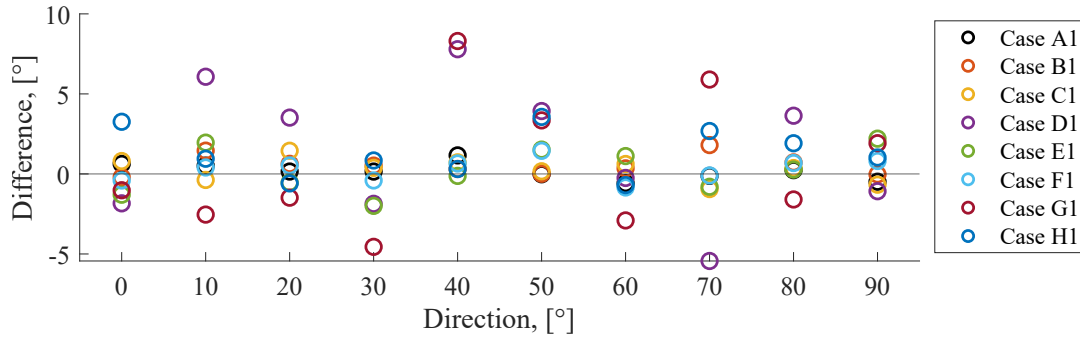


Figure 9.2: Difference in mean direction compared to value determined based on first order wave theory without noise.

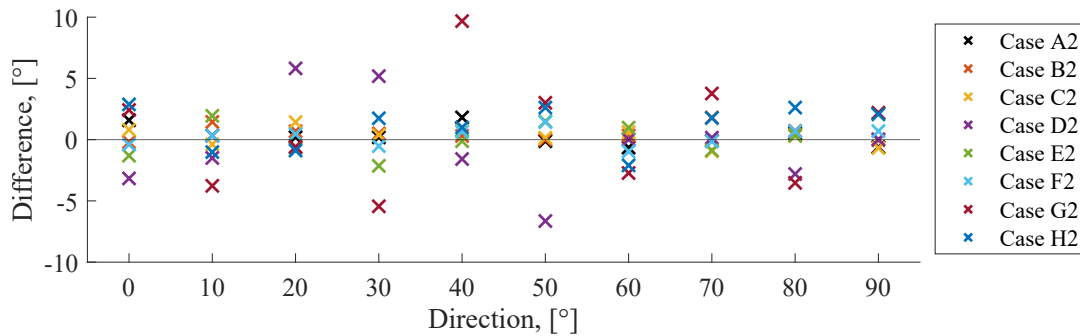


Figure 9.3: Difference in mean direction compared to value determined based on second order wave theory without noise.

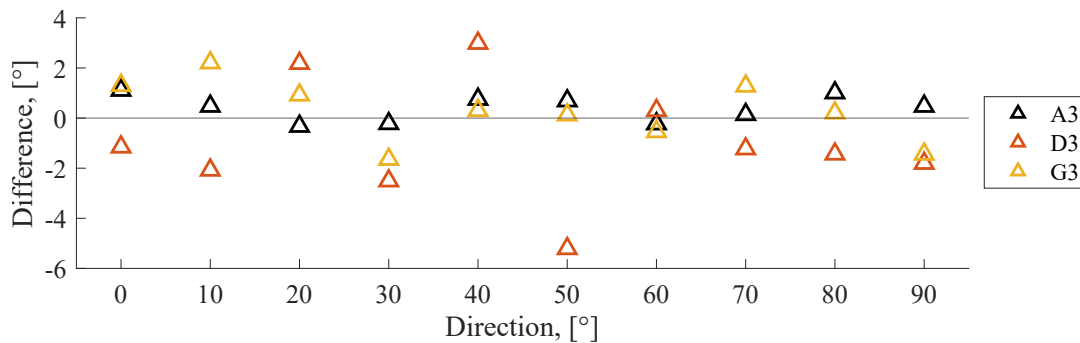


Figure 9.4: Difference in mean direction compared to value determined based on waves with amplitude dispersion without noise.

As it appears from Figure 9.2, the results of the estimated directions are within an accuracy of $\pm 8.30^\circ$ compared to the first order waves without any noise. However, all cases seem to be affected quite randomly by the noise.

Figure 9.3 shows that for the cases containing the largest amount of second order energy, the estimated mean wave directions are affected to a greater extent by the noise than for the first order waves. The results of the estimated directions are within an accuracy of $\pm 9.7^\circ$ compared

to the second order waves without any noise. The magnitudes of errors related to noise for the estimated mean wave directions are in the same range as between the first order waves with and without noise for Case A2, B2, C2, E2 and F2. But especially Case D2, G2 and H2 are affected by the noise, when estimating the mean wave direction. This indicates that the second order effects and noise will worsen each other according to the analysis of the mean wave direction.

From Figure 9.4 the largest deviation for waves with amplitude dispersion including noise is shown to be for Case D3 with an error of -5.2° and it seems like Case D3 in general has the largest deviations. The results look as if they are random as for the different cases and directions. Apart from the largest deviation, the other errors are within a deviation of $\pm 5^\circ$. The deviations are shown to be larger for the directions analysed from second order waves compared to waves with amplitude dispersion.

Errors at Estimated Spreading

The influence on the estimated spreading of the waves appears from Figure 9.5 for first order waves, Figure 9.6 for second order waves and Figure 9.7 for waves with amplitude dispersion, where the differences in spreading compared to the value determined based on signals without noise are plotted.

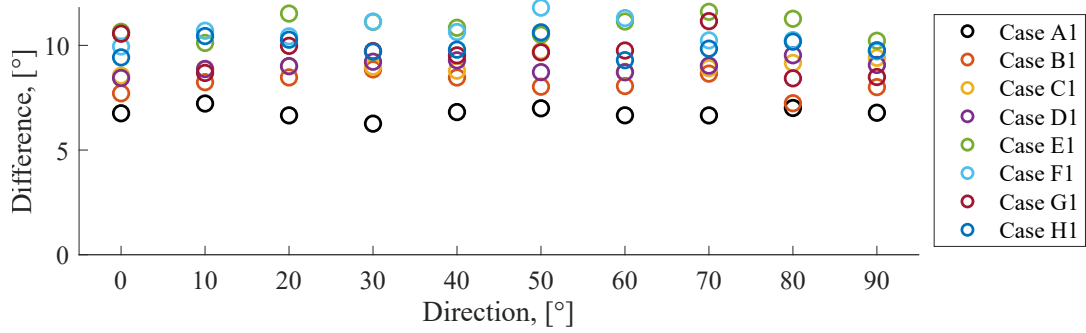


Figure 9.5: Difference in spreading of long-crested first order waves compared to value determined based on waves without noise.

From Figure 9.5 the deviations seem to depend on which case, and is in the range of 6° to 14° .

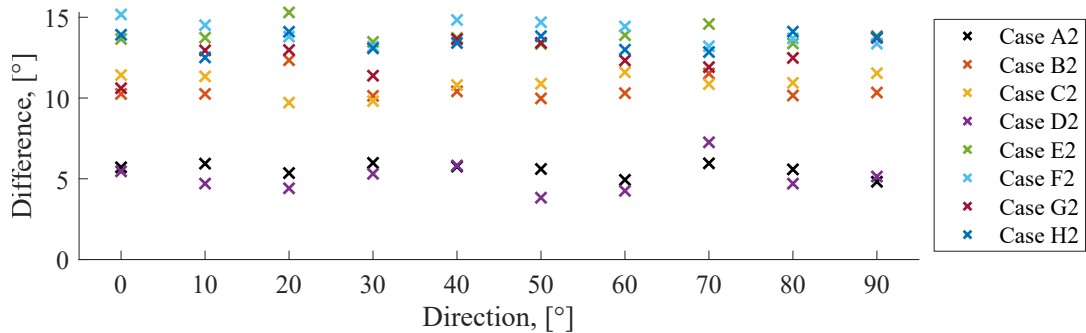


Figure 9.6: Difference in spreading of long-crested second order waves compared to value determined based on waves without noise.

The deviations from Figure 9.6 more or less in the same range as the noise affected first order wave around 4° to 15° , but Case D2 are one of the lowest deviating cases. This is contrary to in Figure 9.7, where Case D3 has the highest deviation. This might indicate a worse impact of the

spreading of the waves when introducing noise in combination with large amplitude dispersion compared to a large amount of second order energy.

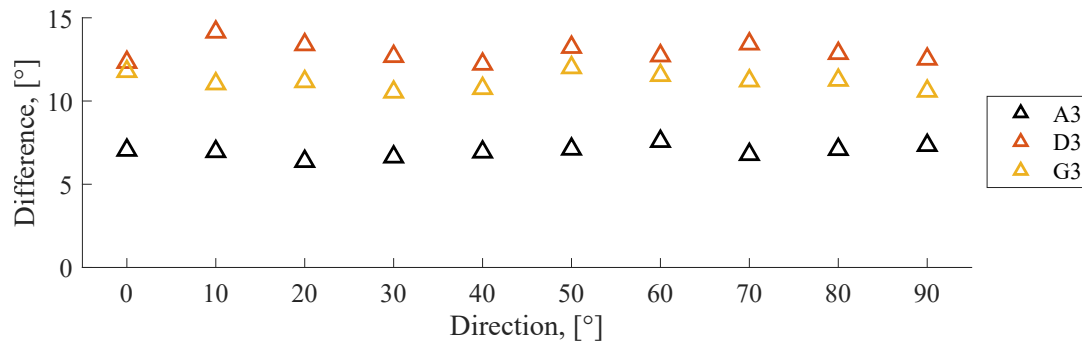


Figure 9.7: Difference in spreading of long-crested waves with amplitude dispersion compared to value determined based on waves without noise.

As seen from all three figures, the inclusion of noise on the signal makes the estimated directional spreading of the waves increase with 6° to 14°. The increase seem to depend on the relative wave steepness and water depth, since the values decreases when the relative wave steepness and water depth increases.

An overall tendency of the long-crested waves affected by noise is found from figures of the estimated directions and the spreading through this chapter and in Appendix H. It is illustrated that the noise which is added has the greatest influences at the frequencies where only a little amount of energy was already represented. This means that the most inaccurate results of the estimated mean wave directions and the components which have the highest spreading, that are the components with lowest energy. The estimated components near the peak frequency containing most energy are closer to the target direction and have the smallest spreading closest to the target value. When combining the noise with the second order energy, the range of the more accurately estimated mean wave directions gets smaller and the estimated mean wave direction of the other components deviate more depending on the amount of second order energy.

9.2 Short-Crested Waves

The effect of noise in the directional analysis of short-crested waves is performed based on the same data as analysed in chapter 7, though here with white Gaussian noise included. The analysis is performed of the synthetic waves generated from the single and double summation models. The estimated mean wave directions and spreading parameters from the analysis of the short-crested wave fields without noise are used as benchmark for the analysis.

Errors at Estimated Mean Wave Direction

In Figure 9.8, 9.9 and 9.10 the results of the estimated mean wave direction for waves with noise added to the signal are plotted to show the differences compared to the directional analyses of waves without noise included. From Figure 9.8, minor differences between the results with and without noise included are shown. The deviations are in same range as the similar results of the long-crested first order waves.

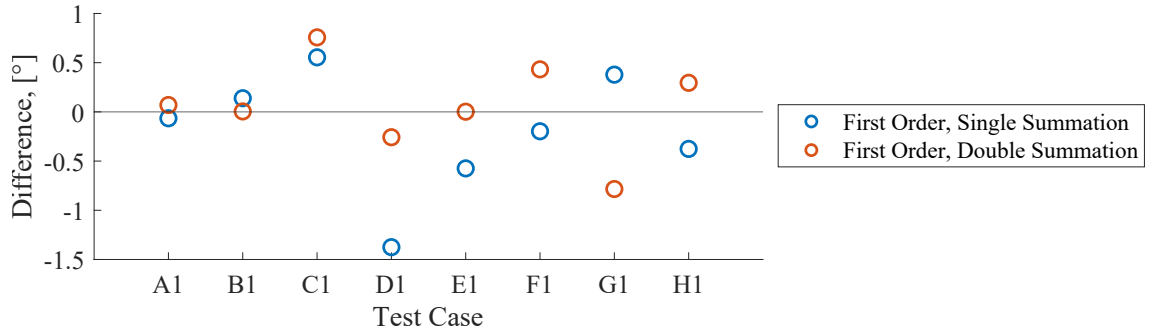


Figure 9.8: Difference in mean direction compared to value determined based on waves of first order wave theory without noise.

For the model based on single summation generation, the weighted estimated mean wave directions are deviating in the range of $\pm 1.34^\circ$, while the model based on a double summation generation, the weighted estimated mean wave directions are deviating with up to $\pm 0.78^\circ$.

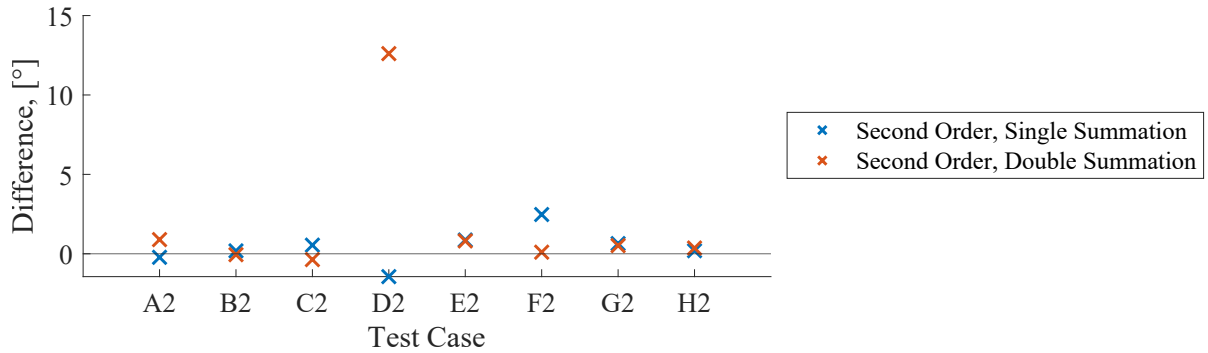


Figure 9.9: Difference in mean direction compared to value determined based on second order wave theory without noise.

From Figure 9.9, the most inaccurate weighted estimated mean wave direction is the result of Case D2 generated by the double summation model. The deviation reach 12.6° , while the other cases are only deviating with up to $\pm 1.5^\circ$.

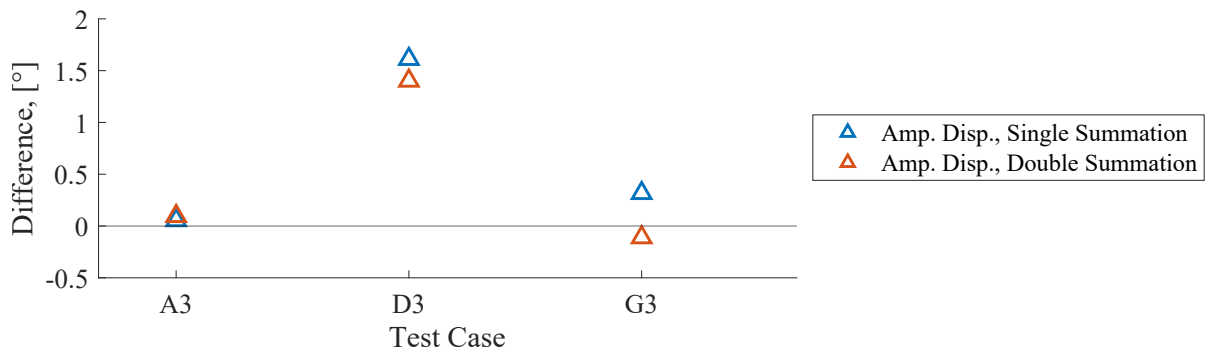


Figure 9.10: Difference in mean direction compared to value determined based on waves with amplitude dispersion without noise.

The largest deviation of the weighted estimated mean wave direction, which is noticed from Figure 9.10, is for Case D3 of 1.6° . Based on these results, the deviations do seem to be correlated with the amount of amplitude dispersion.

Errors at Estimated Spreading Parameter

In relation to the influence on the spreading of the waves, the effect of inclusion of noise on the signal is illustrated in Figure 9.11, where the differences compared to the similar analysis of data without noise is shown.

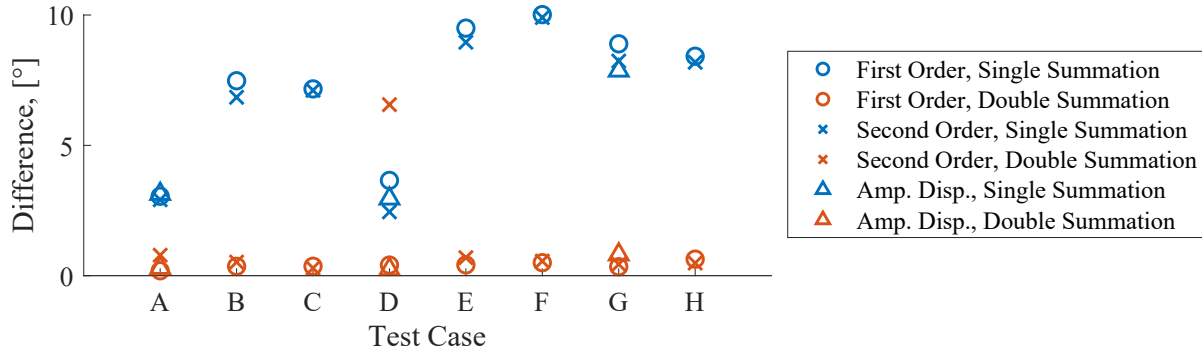


Figure 9.11: Difference in spreading of short-crested waves compared to value determined based on waves without noise.

As seen from Figure 9.11, the inclusion of noise does not seem to influence the analysis of waves generated based on the double summation model particularly, on the other hand the waves generated based on the single summation model show an increase in spreading when noise is included. The differences in the spreading does not seem to depend on amount of second order energy and amplitude dispersion.

9.3 Summary of Noise Error

The effect of including noise on the signal according to the directional analysis seems to have the largest influence in the combination with second order energy. It is discovered that the deviation of the weighted estimated mean wave direction will worsen if the error related to noise and second order energy is introduced simultaneously.

Long-crested waves are investigated where the noise seems to affect the estimations of the mean wave directions for both the case where second order energy is introduced and the amplitude dispersion but to a smaller extent for the waves with amplitude dispersion. The accuracy of the estimated mean wave direction is plotted for both second order waves in Figure 9.12 and waves with amplitude dispersion in Figure 9.13, respectively. Short-crested waves are investigated by the use of different generation models, single and double summation models. The noise seems to affect the estimations of the mean wave directions to a smaller extent than the long-crested waves, but based on the figures it seems like the noise affects the estimation evenly distributed over the most of the frequency range. The accuracy of the estimated mean wave direction is plotted for both second order waves in Figure 9.14 and waves with amplitude dispersion in Figure 9.15, respectively.

From the four figures, it is simple to read off that the combination of noise and second energy are worse than if combining noise and amplitude dispersion.

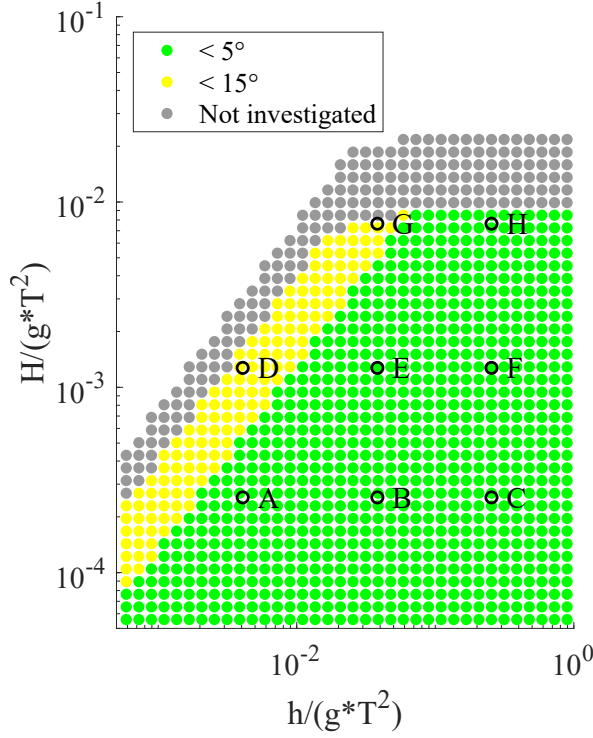


Figure 9.12: Accuracy of estimated mean wave direction for long-crested second order waves.

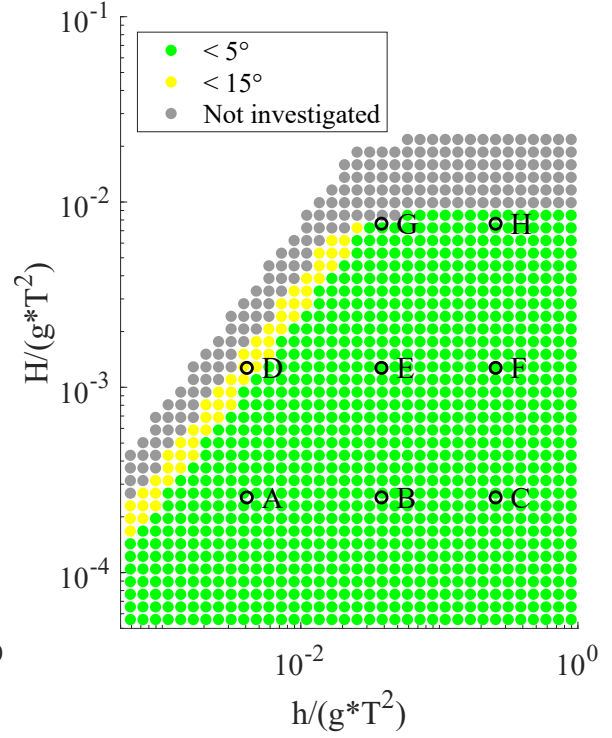


Figure 9.13: Accuracy of estimated mean wave direction for long-crested waves with amplitude dispersion.

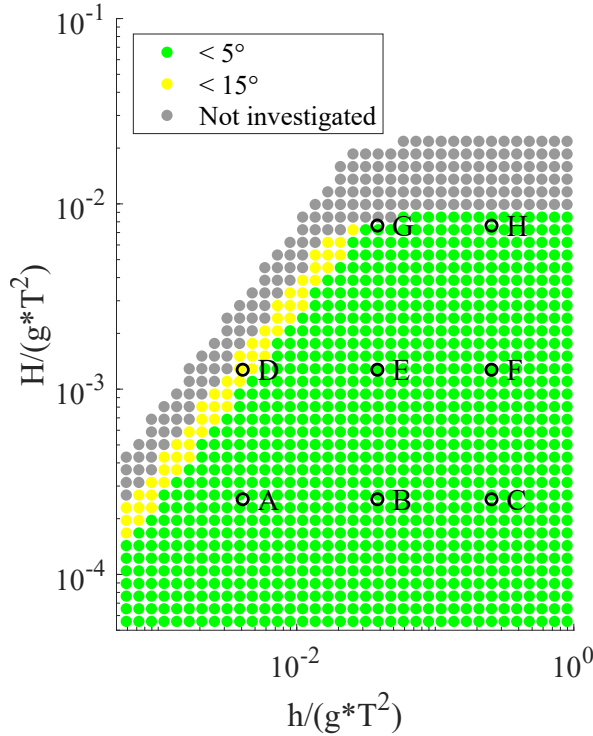


Figure 9.14: Accuracy of estimated mean wave direction for short-crested second order waves.

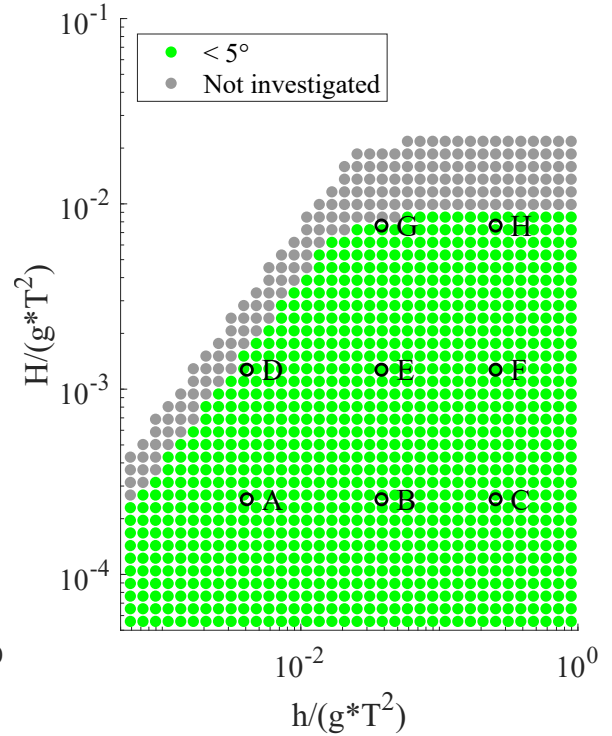


Figure 9.15: Accuracy of estimated mean wave direction for long-crested waves with amplitude dispersion.

10 | Errors Related to Calibration

Another effect which might have an influence on the surface elevation signal is errors related to calibration of the wave gauges. The robustness of Method 2 is investigated in relation to such errors in the following. In this chapter, all calibration errors have a magnitude of 5% of the surface elevation signal. Three different scenarios are investigated; calibration error on either one gauge in position (x_1, y_1) , two gauges next to each other in position (x_1, y_1) and (x_2, y_2) , or two gauges in position (x_1, y_1) and (x_4, y_4) as illustrated in Figure 10.1.

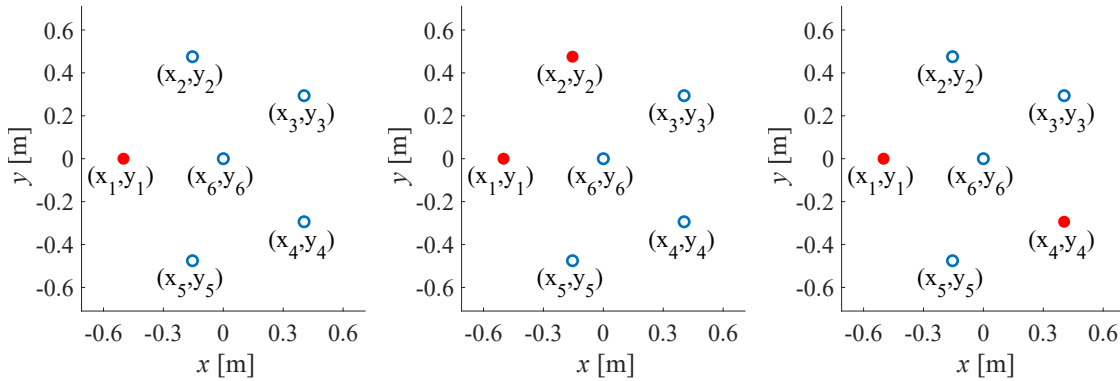


Figure 10.1: Scenarios of affected gauges in investigation of errors related to calibration.

The analyses are performed as in chapter 6 and 7 and consist of a part where long-crested waves are studied, which is followed by a part where short-crested waves are studied. Both parts contain first order waves, second order waves and waves with amplitude dispersion. The results are then compared to the results from the directional analysis without calibration error. The analyses are elaborated in Appendix I and merely the results used are stated in Appendix AF and AG. In the following, the findings of chapter I will be presented.

10.1 Long-Crested Waves

The study of error related to calibration performed for long-crested waves showed an overall tendency of an error relative to the weighted mean wave direction. The study showed how the pattern of errors between the analysed mean wave directions of first order wave theory with and without calibration errors changed almost systematically across the investigated directions when changing which of the three scenarios where different gauges were affected by the calibration error. Overall, the scenario that lead to the largest deviations of the directional parameters, was when including calibration error on two gauges, that are not placed next to each other.

For each of the three scenarios, the pattern is similar for all cases of the first order waves. The level of difference seems to depend on the relative water depth of the different cases, as Case A1 and D1 are the ones with the highest influence. The tendencies for the three scenarios are illustrated for a single case in Figure 10.2. The inclusion of calibration error does not influence the estimated spreading of the first order waves.

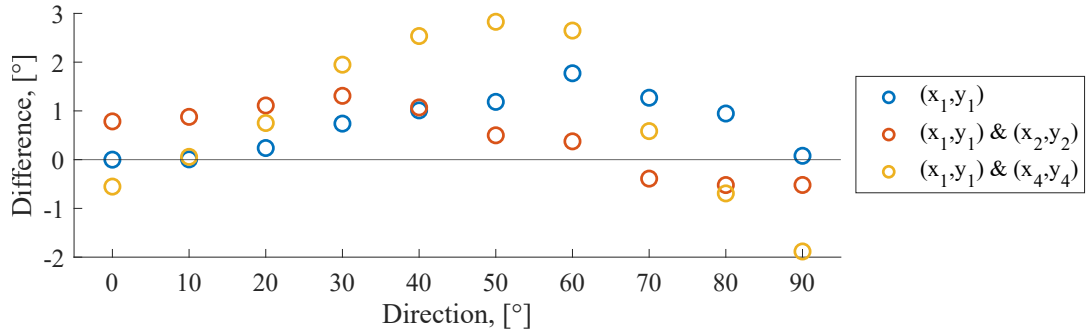


Figure 10.2: Difference in estimated mean direction of long-crested first order waves with calibration error on gauges as stated in the legend compared to value determined based on data without calibration error, Case D1.

For analysis of second order waves, the inclusion of calibration error seems to amplify the effect of the second order energy. The relative error on the mean wave direction therefore depends on the amount of second order energy in the wave field. Furthermore, the inclusion of calibration errors results in a small increase of the spreading of the waves, which on the other hand does not depend on the amount of second energy. The cases with low amount of second order energy show the same behaviour of the estimated mean directions as shown in Figure 10.2. For Case D2, which contains a higher amount of second order energy, the difference in the estimated mean directions for the present analyses compared to the analysis without calibration error appear from Figure 10.3, which is the case that is most affected by the inclusion of calibration error.

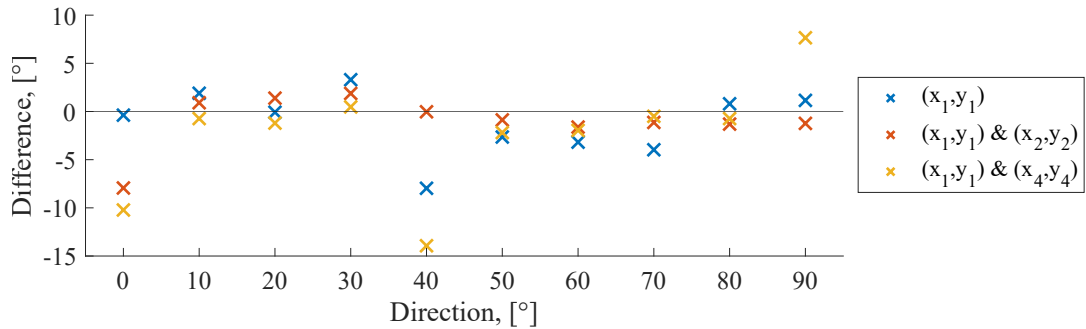


Figure 10.3: Difference in estimated mean direction of long-crested second order waves with calibration error on gauges as stated in the legend compared to value determined based on data without calibration error, Case D2.

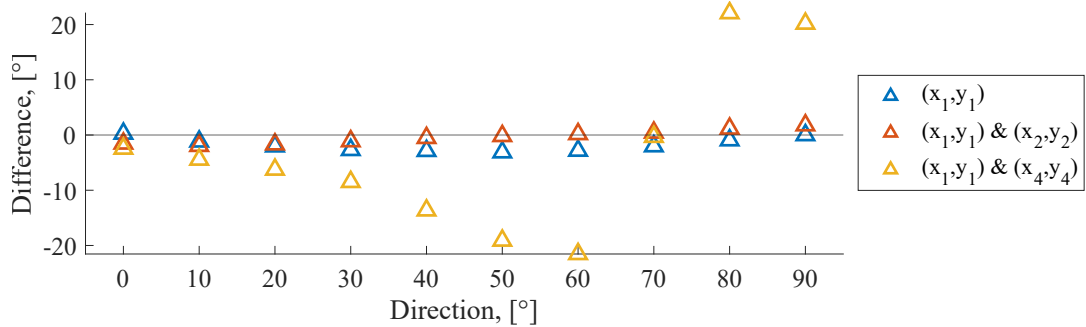


Figure 10.4: Difference in estimated mean direction of long-crested waves with amplitude dispersion with calibration error on gauges as stated in the legend compared to value determined based on data without calibration error, Case D3.

For the waves with amplitude dispersion, the inclusion of calibration similarly seems to increase the nonlinear effects yielding larger errors on the estimated mean direction of the waves. As seen for the first and second order waves, the worst scenario is with amplitude dispersion on two gauges, that are not placed next to each other. The spreading increases for the cases most affected by the inclusion of calibration errors. Figure 10.4 shows the difference of the estimated mean directions for waves with amplitude dispersion with and without calibration error for Case D3, which is also the case with the largest amount of amplitude dispersion.

Overall, the study of calibration errors in analysis of long-crested waves for the three different scenarios showed that the worst deviations were found for calibration error on two gauges not placed next to each other. The maximum absolute error on the estimated mean direction of each case due to inclusion of calibration errors are illustrated in Figure 10.5, and the maximum errors on the estimated spreading of the waves are illustrated in Figure 10.6.

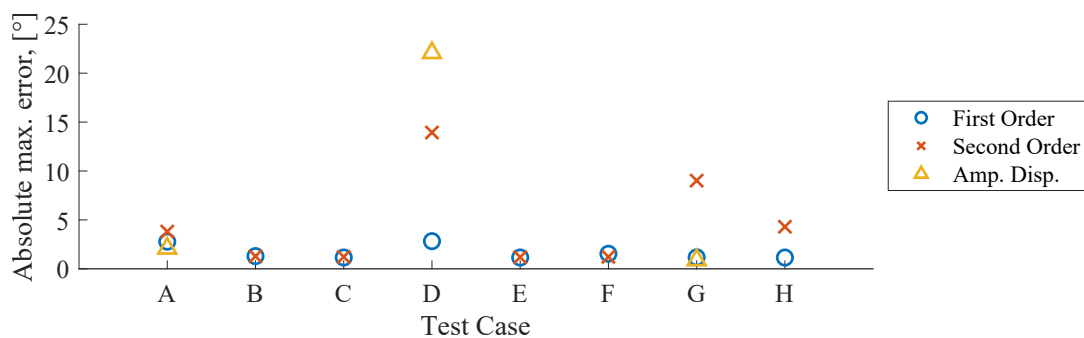


Figure 10.5: Maximum absolute error of mean direction over all investigated directions compared to value determined based on data without calibration error, long-crested waves.

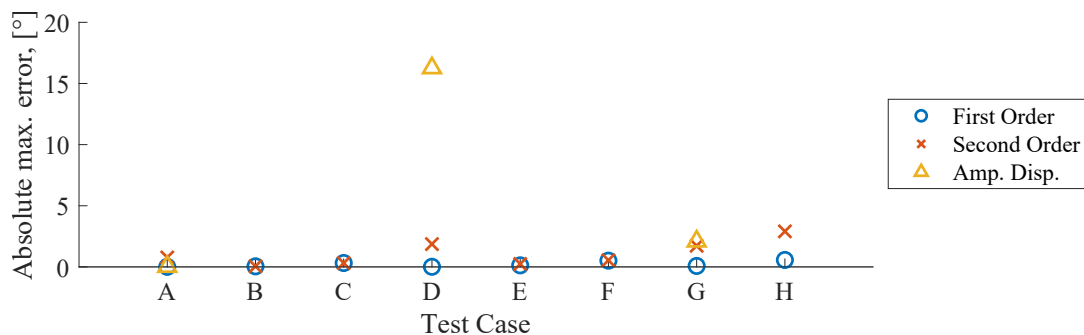


Figure 10.6: Maximum absolute error of spreading over all investigated directions compared to value determined based on data without calibration error, long-crested waves.

From 10.5 and 10.6, it is possible to draw the conclusion, that for the long-crested waves, Case D produce the absolute largest errors when introducing calibration errors. The situation with the largest error of the mean direction for the long-crested waves is when analysing waves with amplitude dispersion with calibration error at two gauges, which is not placed next to each other, this case reaches an error of 22.07°. For this case, the errors related to the calibration furthermore seems to be increased by inclusion of nonlinear effects. The estimated spreading of the waves is almost not influenced by the inclusion of calibration error except for Case D3, where the inclusion of calibration error leads to an increase in the estimated spreading of 16.26°.

10.2 Short-Crested Waves

A certain mean wave direction of 30° is investigated in the following as in chapter 7, wherefore the variability of the deviation in relation to the directional analysis of the long-crested waves is not taken into account. This will be a study of calibration error related to a comparison of the two different generation models and a study of the nonlinear effects including calibration error.

For the short-crested waves, the analyses have shown a larger sensitivity towards inclusion of calibration errors than the long-crested waves. Similar to the analysis of long-crested waves, the worst scenario was experienced for calibration errors on two gauges in position (x_1, y_1) and (x_4, y_4) .

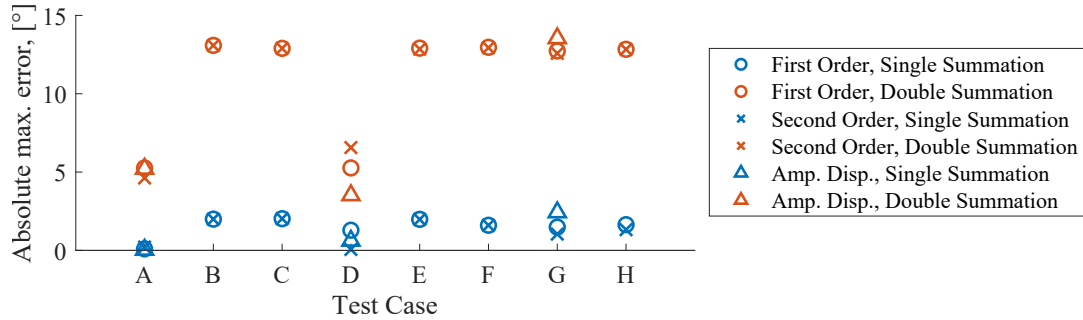


Figure 10.7: Maximum absolute error on mean direction compared to value determined based on data without calibration error, short-crested waves.

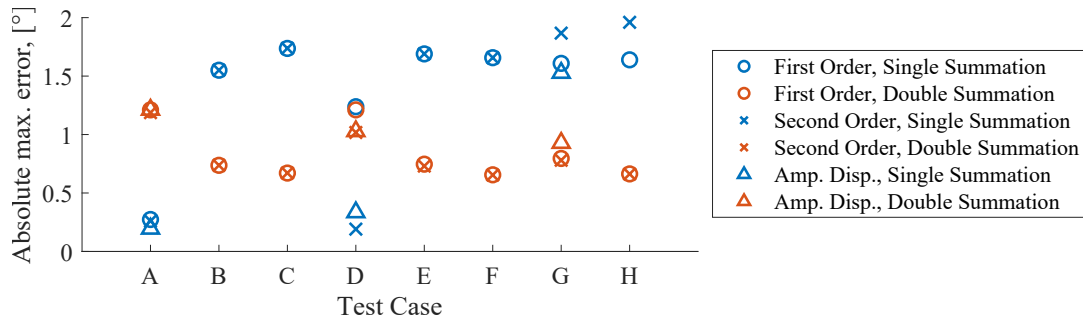


Figure 10.8: Maximum absolute error on spreading of waves compared to value determined based on data without calibration error, short-crested waves.

Contrary to the results based on long-crested waves, the influence on the directional parameters do not seem to depend on the level of nonlinearity of the short-crested wave field for neither second order energy or amplitude dispersion. The absolute errors of the mean direction and spreading introduced by inclusion of calibration errors appear from Figure 10.7 and 10.8 respectively. As seen from Figure 10.8, the effect on the estimated spreading of the short-crested waves is limited to less than 2° for all investigated cases.

For the waves generated from the single summation model, the errors are more or less in the same magnitude as the errors from the analysis of the long-crested. The errors of the mean wave directions analysed from the data based of the double summation model are in general the largest of all situations, therefore the accuracy of the estimate differs for the two generation models. All cases are within an accuracy of 2.02° of the mean direction for the waves generated based on the single summation model, while all cases are within an accuracy of 13.09° of the mean direction for waves generated based on the double summation model.

10.3 Limitation of Application

The most sensitive scenario based on the investigated cases of the present thesis is found to be when introducing a calibration error of 5 % of the surface elevation at the gauges in position (x_1, y_1) and (x_4, y_4) combined with nonlinear effects. These results lead to the figures of the accuracy of the estimated mean wave direction for long- and short-crested waves in Figure 10.9 and Figure 10.10, respectively, where the long-crested wave analysis showed a correlation between the combination of nonlinear effects and calibration error, while the short-crested wave analysis showed large deviations with and without inclusion of nonlinear effects.

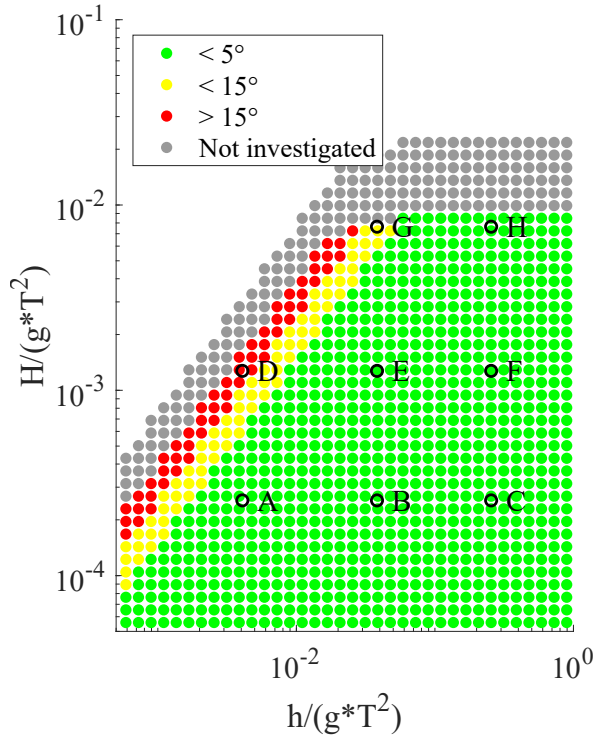


Figure 10.9: Accuracy of mean wave direction for long-crested waves.

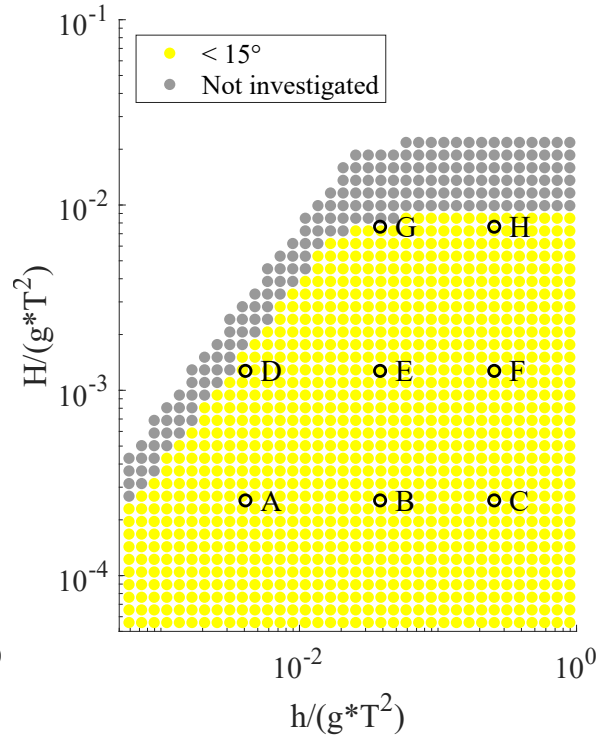


Figure 10.10: Accuracy of mean wave direction for short-crested waves.

11 | Wave Gauge Arrangement

Since the statistical fitting seemed to be of great influence in relation to the directional analysis of long-crested waves in chapter 5 and 6, the importance of the number of gauges used for measurements will therefore be investigated further in the following.

The CERC6 array, which have been used for the data sets for Method 2 of the present thesis, is arranged symmetrically as shown in Figure 11.1, such that the angles between the different gauges are evenly distributed as illustrated in Figure 11.2.

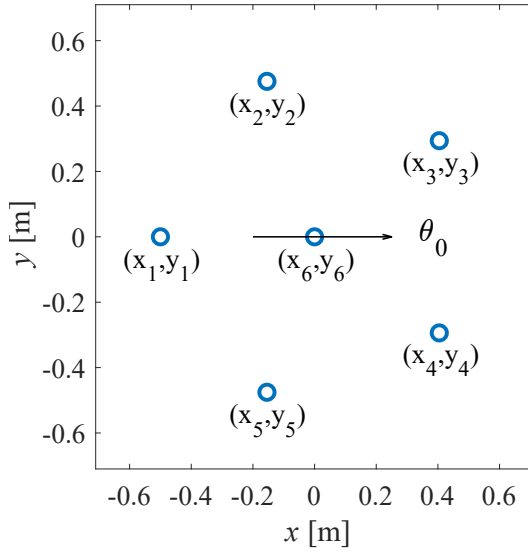


Figure 11.1: CERC6 Wave Gauge Arrangement

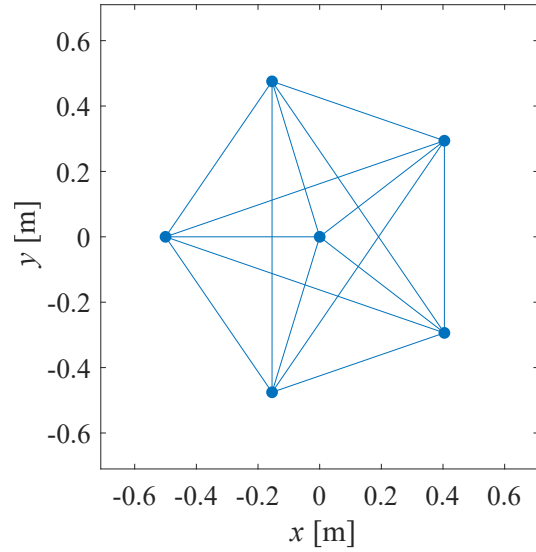


Figure 11.2: Direction of all possible gauge pairs in CERC6 arrangement.

Due to the number of gauges, the uncertainties related to the direction of the wave in relation to the direction of the gauge pair, as chapter 5 illustrated especially for inclusion of amplitude dispersion, are less significant. Method 2 is based on the statistical analysis of solving Equation (3.9) including the auto- and cross-spectra for each gauge pair. When one gauge is removed, the number of cross-spectra used in the analysis is decreased from 15 to 10 when decreasing the number of gauges in the array from 6 to 5. This will affect the statistical reliability of the analysis. For the present analysis it is therefore investigated how much it affects the results if one of the gauges is missing, which means that that geometry and thereby symmetry of the gauge array is changed.

The analysis are performed based on synthetic long-crested waves similar to those of chapter 6, which means the same data sets are used, but only with 5 of the gauge positions used for the analysis. Similar to the previous parts of the present thesis, the removal of a gauge position is investigated for first order waves, second order waves and for waves with amplitude dispersion. The data sets of the present analyses have a target mean direction of 0° , which becomes relevant when an asymmetric wave gauge arrangement is considered. The arrangement therefore also corresponds to the CERC5 array for the specific wave direction, if all other cases than the one in position (x_6, y_6) is removed.

The removal of a single gauge have been investigated for all six gauge positions, with results as stated in Appendix AH and illustrated in Figure 11.3 and 11.4 for Case D, which is the case with the highest relative amount of second order energy and amplitude dispersion. The lines in the figure indicate the weighted mean wave directions determined based on the CERC6 arrangement for waves of first and second order theory respectively in chapter 7. The symbols illustrate the results of the analyses with removal of a single gauge position.

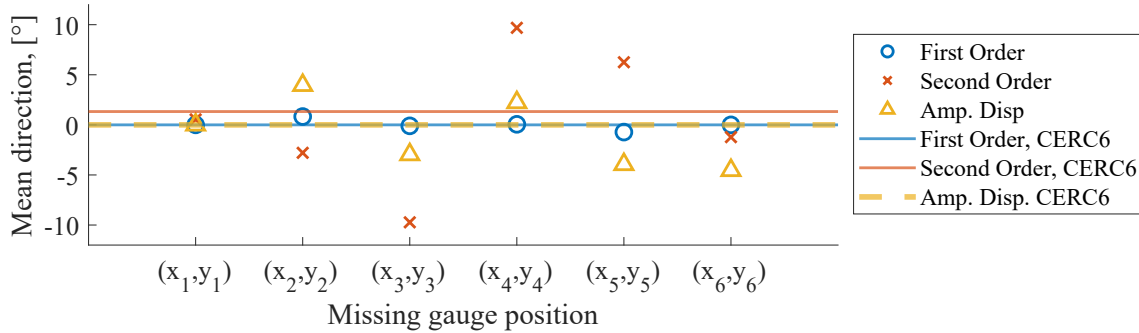


Figure 11.3: Case D, weighted mean direction of propagation for analysis with removal of gauge in given positions according to the CERC6 array.

When considering the estimated mean wave directions from Figure 11.3, it appears that the removal of the gauge in position (x_1, y_1) does not have influence on the accuracy of the estimated direction, which can be explained by the beneficial geometry relative to the target direction of the wave field. Since removal of the other gauges leads to larger deviations, it becomes clear that the geometry of the array is of higher importance than the number of gauges. For analyses of waves generated based on first order wave theory, the removal of measurements from a single gauge lead to a maximum difference in the estimated mean direction of 0.83° for removal of an arbitrary gauge.

The removal of the gauges in position (x_2, y_2) and (x_5, y_5) yield differences in the estimated mean directions of the same size but with opposite signs for inclusion of second order energy as well as amplitude dispersion. The same thing accounts for removal of the gauges in position (x_3, y_3) and (x_4, y_4) . Based on the present analyses, the second order energy seem to have a larger influence on the accuracy of the directional analysis than the inclusion of amplitude dispersion. For the second order waves, the maximum deviation caused by removal of a gauge position was 9.73° for the gauge in position (x_3, y_3) . For the waves with amplitude dispersion, the maximum deviation was 4.55° for the gauge in position (x_6, y_6) .

The influence on the spreading of the waves appear from Figure 11.4, which shows that based on the analysis of first order waves, the spreading is unaffected by the removal of a gauge. For inclusion of second order energy, the spreading increases with up to 3.81° for removal of the gauge in position (x_3, y_3) . For inclusion of amplitude dispersion, the spreading increases with up to 9.08° for removal of the gauge in position (x_6, y_6) .

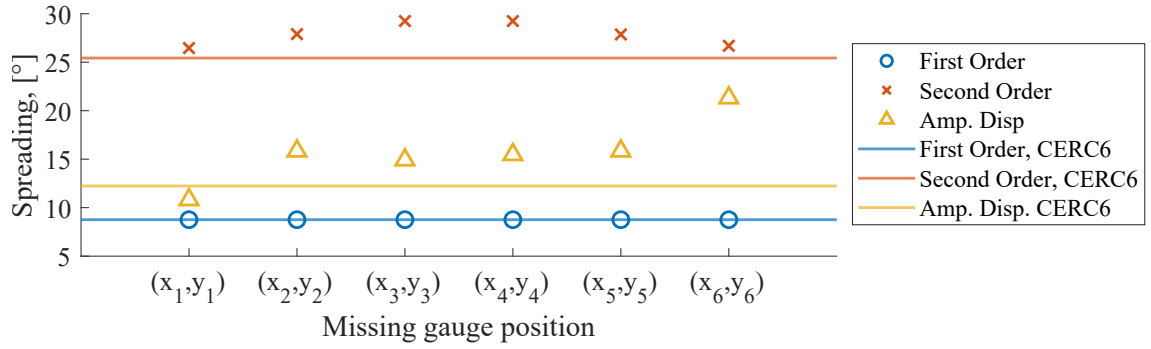


Figure 11.4: Case D, weighted spreading of waves for analysis with removal of gauge in given positions according to the CERC6 array.

The analyses of the nonlinear effects show that for waves propagation with a direction of 0° , the most significant influence is experienced for removal of the gauge in position (x_3, y_3) or (x_4, y_4) due to symmetry and is caused by inclusion of second order energy. With removal of the wave gauge in position (x_3, y_3) , the arrangement of the remaining gauges leads to the combination of gauge pairs with orientations as stated in Figure 11.5, wherefore it is clear, that the wave gauge arrangement is no longer symmetrical in relation to the wave direction of 0° .

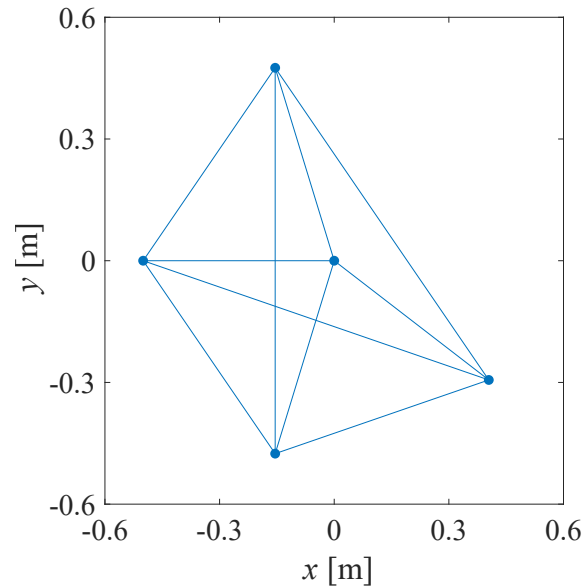


Figure 11.5: Direction of all possible gauge pairs in CERC6 arrangement without gauge in position (x_3, y_3) .

From Figure 11.5 it is clear that the orientations of the individual gauge pairs is no longer uniformly distributed over all directions, wherefore the direction of the waves is dependent hereof as was also seen for all analysis in Figure 11.3. The maximum deviations based on the two cases with the highest amount of second order energy as well as amplitude dispersion, Case D and G, are summarised in Table 11.1.

Table 11.1: Maximum absolute deviations from weighted mean direction determined from waves generated based on first order theory with use of CERC6 array.

| Case | Max. deviation | Case | Max. deviation |
|------|----------------|------|----------------|
| D2 | 9.73° | D3 | 4.55° |
| G2 | 3.17° | G3 | 0.27° |

Based on the present analysis, it can be concluded, that the influence of including second order energy and amplitude dispersion becomes more significant in combination with the asymmetrical wave gauge arrangement. Compared to the analysis of Case G as shown in Appendix AH, which is the case with the second highest amount of second order energy and amplitude dispersion, the influence of the asymmetrical gauge arrangements seem to be correlated with the amount of nonlinear effects, as the deviations are similarly smaller.

To determine the direction within $\pm 5^\circ$, the present analyses show that the wave field can have relative wave height of up to $H/h = 0.2$, which in combination with a wave steepness of $H/L = 0.05$ corresponds to Case G, which is illustrated in Figure 11.6. Of the investigated cases, Case D with a relative wave height of $H/h = 0.31$ yields the largest influence of asymmetrical wave gauge arrangements.

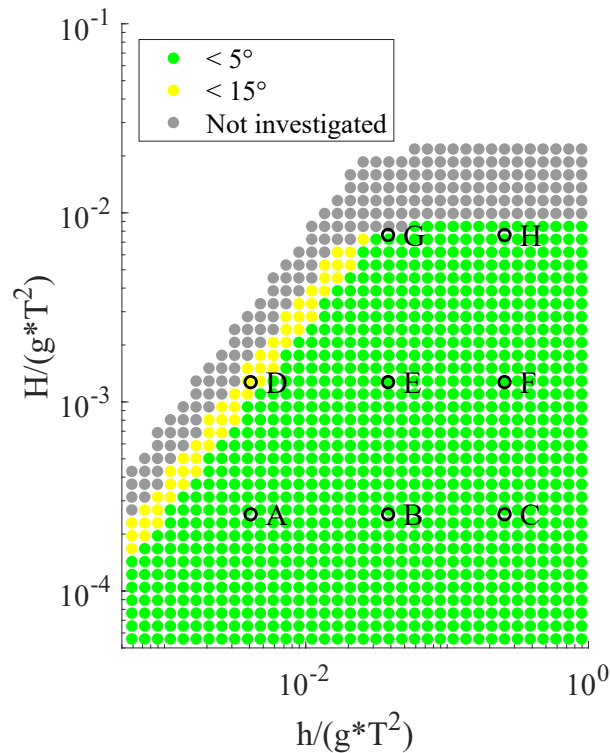


Figure 11.6: Accuracy of estimated mean wave direction.

To reduce the influence caused by inexpedient wave gauge arrangements for critical sea states according to the present analyses, it could be considered to weight the gauge pairs with high reliability. Based on the findings in chapter 5, the direction is most accurate when the angle between the gauge pair is perpendicular to the direction of wave propagation. The gauge pairs measuring directions of approximately perpendicular directions could therefore be of higher weighting in such analyses, under the assumption that these estimates are more reliable than estimates of oblique wave directions. This is however not investigated further in the present thesis. Based on the present analyses with removal of gauge positions, it furthermore becomes clear, that the CERC5 array can be orientated in a more favorable direction when the direction of the waves is already known.

12 | Analysis of Laboratory Tests

The data sets from the wave laboratory are surface elevation measurements from IAHR Seminar, Multidirectional Waves and their Interaction with Structures Hawkes et al. (1997). The surface elevations are measured in the same wave gauge array, a CERC6, and consists of a JONSWAP spectrum with a significant wave height of H_s , a peak period of T_p and a peak enhancement factor of $\gamma = 3.3$. A test case is analysed, which contain the wave parameters stated in Table 12.1, which place the laboratory case in the Diagram of Le Mehaute as shown in Figure 12.1.

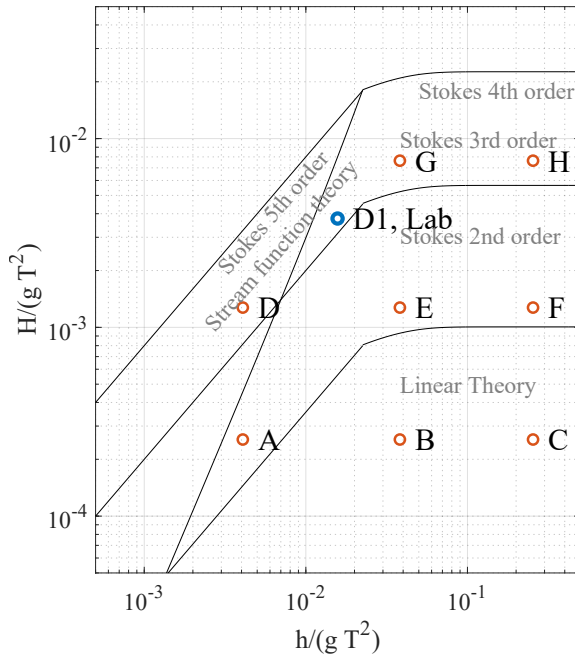


Table 12.1: Parameters for laboratory test case.

| Wave Parameter | | |
|----------------------|-----------|--------------|
| H_{m0} [m] | T_p [s] | h [m] |
| 0.12 | 1.8 | 0.5 |
| Targets | | |
| θ_0 [°] | s [-] | σ [°] |
| 30° | 6 | 31.75° |
| Actual Targets | | |
| θ_0 [°] | s [-] | σ [°] |
| 27.96° | 6.9 | 29.72° |
| Directional Analysis | | |
| θ_0 [°] | s [-] | σ [°] |
| 28.58° | 4.4 | 39.90° |

Figure 12.1: Laboratory test in Diagram of Le Mehaute.

The actually target direction produced in the laboratory was 27.96° with the target spreading of 29.72° for D1, Lab. The estimated direction for components of Case D1, Lab is plotted in Figure 12.2. From Table 12.1 the weighted results of the mean wave direction and spreading parameter determined from the laboratory test appear, which spreading parameter have a higher estimation compared to the actual target, while the estimated mean wave direction deviates with less than 1°.

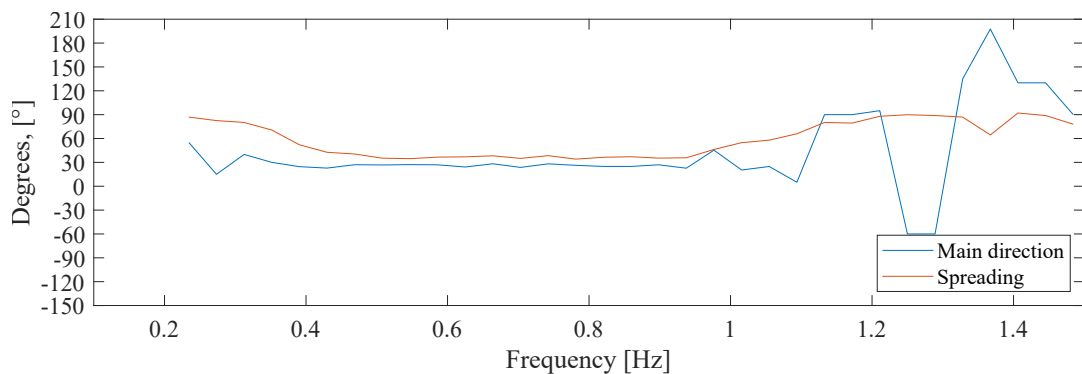


Figure 12.2: Estimated direction for components in the wave field of Case D1, Lab.

IV

Evaluation

| | |
|---|-----------|
| Chapter 13 Discussion | 83 |
| 13.1 Nonlinearity Including Other Effects | |
| 13.2 Application of Data | |
| 13.3 Further Investigation | |
| Chapter 14 Conclusion | 87 |
| Chapter 15 References | 89 |

13 | Discussion

In this chapter, the relevant choices, methods and results of the present thesis will be discussed. Lastly, ideas for further investigations in relation to the results of the present thesis will be presented.

13.1 Nonlinearity Including Other Effects

As shown through the thesis, Method 1 is a simple method used to study the consequence of nonlinear effects. The method is not used in practice, wherefore only Method 2 is considered when including other effects in the data sets.

In the present thesis, all the data used in the directional analyses are numerical, synthetic, generated waves, and is therefore a hypothetical perception of reality compared to laboratory data or measurements from the real sea. Other effects are therefore included in the investigation of whether it is reliable to use linear wave theory in directional wave analysis of nonlinear waves. Each data set of the eight test cases is reused from the previous directional analysis of first order waves, second order waves and waves with amplitude dispersion, respectively, to analyse the deviation from just that certain modification in Part III. Even though these effects are added to the synthetic generation of the wave field, noise, calibration error or reducing number of gauges, the effects are just an estimate of the real occurrence.

As described in chapter 9, the noise was chosen on the basis of the proportion to the spectral density being approximately 2 %. This was showing a quite random tendency of the errors of the estimated mean wave directions. Whether the size is realistic is unknown, but a larger value of the signal to noise ratio might have caused larger error, and the deviations caused by the noise would still be random and unpredictable. The results of the analysis of long-crested waves with calibration error from chapter 10 established, by contrast, a correlation of the errors and the affected gauges. Except for Case D2 and D3, the errors of the estimated mean wave directions were shown having a pattern related to the direction of propagation and a magnitude of errors related to which and the number of affected gauges with added calibration errors. The error of Case D2 and D3 showed on the other hand, that calibration error affects the errors to a greater extent, when including enough second order energy or a large enough error on the wavelength due to amplitude dispersion. The results from chapter 11 showed that it would yield more accurate results if leaving one gauge out than estimating the mean wave direction from a gauge arrangement with two gauges with 5% calibration error added.

The study of the errors related to calibration showed that calibration error on two gauges could lead to large deviates of the mean direction of the analysed wave field. The first step towards avoiding errors like this could be to detect the possibility of calibration errors, which have been investigated further for the data of the present thesis in Appendix J. The study showed that if the frequency domain analysis determines differences in the zero moment of the spectral density, m_0 , of more than 10 % of the values determined based on each gauge position, caution should be made. The difference can be caused by calibration errors for short-crested data based on the single summation model or long-crested wave data. On the other hand, the difference can also be caused by poor quality of data for short-crested wave data generated based on the double

summation model, or by refraction or reflection in the wave field, in which case the calibration errors cannot be detected.

Further, from a single laboratory test in chapter 12, the directional analysis showed an estimated mean wave direction which was quite close to the actual target for the frequencies around the peak frequency of $f_p = 0.56$ Hz, as found for the numerical generated data through this thesis. Further the estimated mean wave direction showed some variation at the lowest and highest frequencies, which might indicate that some second or higher order wave energy is present. Likewise, the estimated spreading seems to reach the actual target at the same frequencies as the estimated mean wave direction and increases at the lowest and highest frequencies.

13.2 Application of Data

All data in the present thesis is numerically generated to control the output and with it study the analysis method and the sensitivity towards nonlinear effects. Moreover, the chosen test cases, A to H, were selected based on different wave characteristics as the wave height and wave period, which were substituted into the empirical wave spectrum of a JONSWAP spectrum. This is the ocean-wave spectrum derived from a project collecting wave data from the North Sea. The chosen sea states related to the cases are investigated to determine if they are realistic. From measured wave data from a buoy near the Port of Hanstholm, which is placed by the North Sea, appearing sea states based on the wave parameters of the significant wave height and the peak period are plotted in Figure 13.1 to examine the occurrence of the chosen cases.

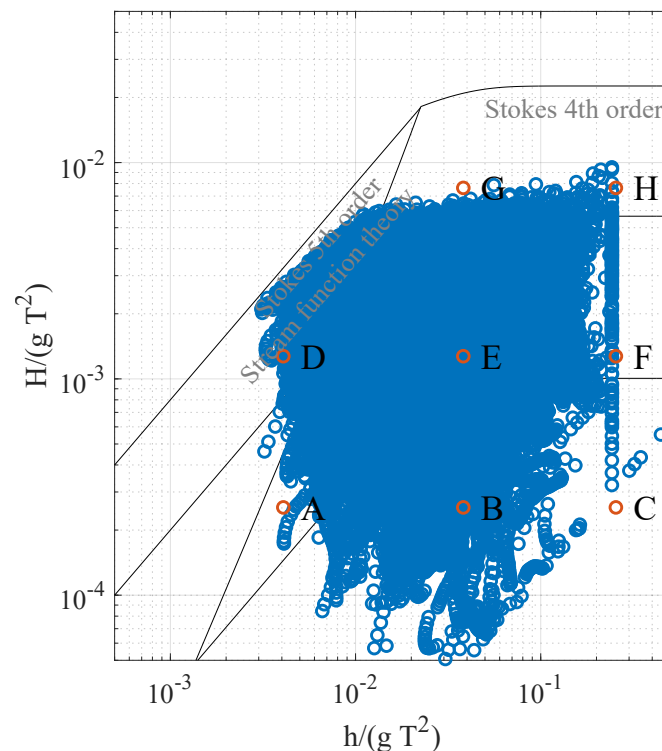


Figure 13.1: Measurements from Hanstholm, Denmark.

As seen in the figure, the occurrence of the chosen test cases seems to exist, wherefore all cases in the present thesis seem relevant to have studied.

The results in the present thesis are presented in figures as limitations of application for an accuracy of $\pm 5^\circ$ to create an overview of the precision of the methods and the sensitivity towards nonlinear effects, when introducing other effects as noise, calibration errors and less wave gauges in the wave data. An applicable tool to employ, when dealing with three-dimensional waves, is a wave rose. A wave rose visualises the directions from where the wave comes and how often the wave appear from that direction. A wave rose is divided into intervals of a certain span of degrees in a range of 360° . That spans are varying from sizes of 6 to 22.5° according to the requested number of wave sectors. The Danish Coastal Authority use the span of 15° at their web page Department of the Environment, The Danish Coastal Authority (2022) , which makes results with the accuracy of $\pm 5^\circ$ possible to place in the wave rose of that precision. Case D2 is shown as an example in Figure 13.2 where spans of 15° are illustrated.

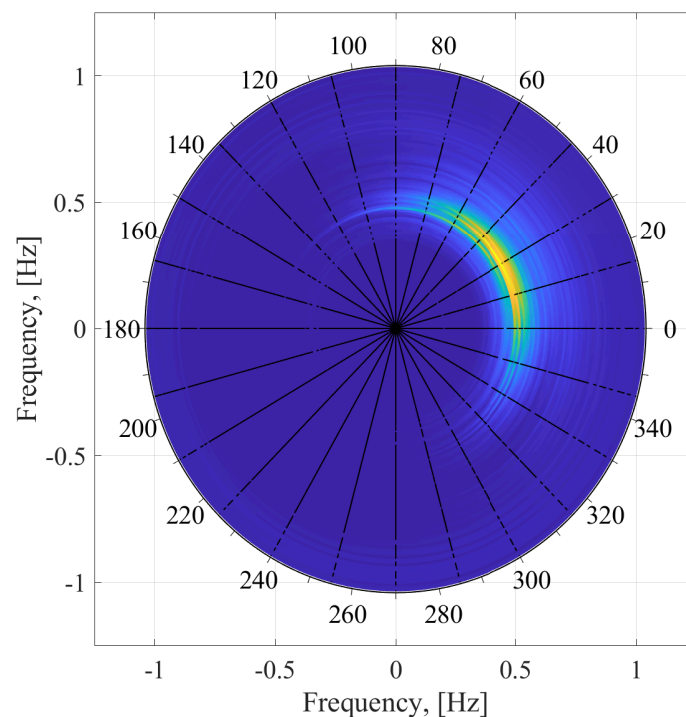


Figure 13.2: Polar plot of Case D2 with a target direction of 30° and a spreading in degrees of 34.5° .

13.3 Further Investigation

Based on the analyses of the present thesis, it can be concluded, that as long as disturbances in the surface elevation signal from for instance noise and calibration can be avoided, and a sufficient amount of wave components, subseries and wave gauges are used for the analysis, Method 2 estimates the mean direction of the wave field with reasonable accuracy. It has yet to be investigated how the combination of second order energy and amplitude dispersion would influence the results of the directional analysis performed based on linear wave theory, which might give rise to further improvements of the method.

Furthermore, only wave fields with Mitsuyasu-type directional spreading function with a single mean wave direction have been investigated in the present thesis. For further analysis, reflection could be included in the wave fields. Then the directional spreading function might look as

Figure 13.3 including two peaks. Based on the analyses of the second order waves, challenges with reflected components could be expected, as the incident sub- and superharmonics have different directions than the primary components, wherefore the analysis cannot necessarily differentiate between reflected primary components or incident second order components.

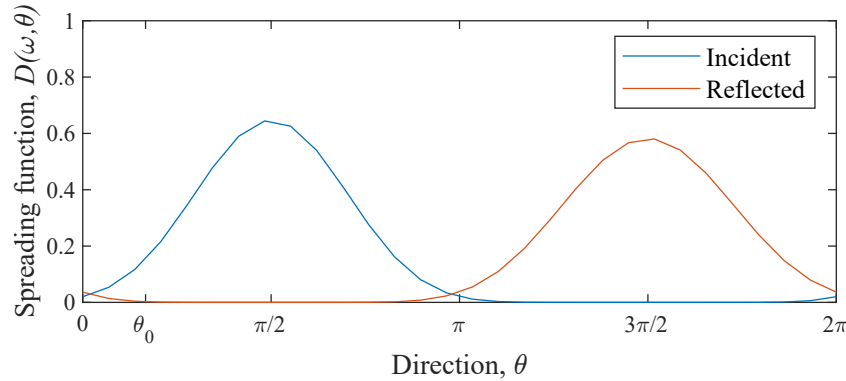


Figure 13.3: Sketch of incident and reflected plotted as a directional spreading function.

In addition to the choice of the directional spreading function, other spreading functions could similarly be investigated. The cosine 2l-power spreading function was the earliest directional spreading function and suggest by Pierson et al. (1955), but the wave direction has a limited range of $-\pi/2$ to $\pi/2$. The Half-cosine 2s-power type initiated by M.S. et al. (1963) applies for the half plane of $|\theta| \leq \pi/2$ from the cosine 2l-power type spreading function. When the value of the spreading parameter, s , in directional spreading function becomes dependent on the frequency, it becomes the Mitsuyasu-type directional spreading function. In the present thesis, this could mainly have been relevant for the analysis of long-crested waves, such that a spreading function distributed over a single frequency more similar to what was generated was used in the directional analysis. The synthetic short-crested wave fields were all generated based on the Mitsuyasu-type directional spreading function, which was the same as the one used for the present analyses. Additionally, other methods that do not fit to a certain directional spreading function could be used.

The present thesis exclusively uses surface elevation measurements for estimation of the directional parameters. For future analysis, it could furthermore be of interest to see if data from other types of measurements, e.g. buoy type measurements of heave, pitch and roll motions, show the same sensitivity towards nonlinear effects in the analyses.

14 | Conclusion

The aim of the present thesis is to investigate the reliability of using linear wave theory in directional wave analysis of nonlinear waves. The nonlinear waves in this thesis are divided into two overall cases of waves generated from second order wave theory and waves which were adjusted for amplitude dispersion by a factor on the wavelength. The synthetic waves were generated from a tool developed for the purpose of this thesis.

The analyses have been carried out by use of numerical tools similarly programmed for the purpose of this thesis. The investigation of the nonlinear waves was limited by the use of two different methods, whereof Method 1 only managed to analyse long-crested waves. Method 1 represents a simple method to perform directional analysis, wherefore it does not require more than measurements from 3 wave gauges. The method therefore also showed the largest sensitivity towards second order energy and amplitude dispersion. Due to the maximum likelihood fitting in Method 2, a larger number of measurements was required, which also showed a positive effect in relation to uncertainties. It is concluded that both methods were able to determine the mean wave direction for the relevant wave fields of first order theory, wherefore the methods were also used for inclusion of nonlinear effects. Method 2 was chosen to fit to a cosine power function for the directional distribution, where from the spreading of short-crested waves was determined. As the long-crested waves only have one propagation direction, the cosine power function is an unsuitable estimate hereof.

For the analysis of second order waves, the present thesis showed a correlation between the amount of second order energy and the errors on the estimated directions by use of both methods. The influence was most significant in the analysis of the long-crested waves, for which Method 1 was concluded to be most sensitive, particularly for waves travelling parallel to a gauge pair. The influence was significantly lower for analysis of short-crested waves using Method 2, for which the generation was based on the same directional spreading function as the one that was fitted to in the analysis. It can furthermore be concluded that the estimated spreading of the waves, determined when using Method 2, increases for increasing amount of second order energy.

Based on the analyses of waves with amplitude dispersion, Method 2 is concluded to be less sensitive towards inclusion hereof due to the statistical fitting and use of a larger number of gauges. Based on Method 1, it can be concluded that the orientation of the gauge pairs relative to the direction of the waves was of significant influence also when including amplitude dispersion, wherefore the direction could still be estimated correct for waves travelling perpendicular towards a gauge pair, as the inaccurate calculation of the wavelength in such cases do not have influence on the estimated direction. In relation to the spreading of the waves determined by Method 2, the inclusion of amplitude dispersion furthermore seems to increase the estimated spreading, but to a smaller extent than the inclusion of second order energy.

It can be concluded that disturbances on the surface elevation signal caused by for instance noise or errors related to calibration should be avoided as that tends to influence the reliability of the results significantly independent of the level of nonlinearity. Especially errors related to calibration yields large deviations on the estimated mean direction of the waves. The present thesis furthermore showed, that for use of inexpedient wave gauge arrays investigated by removal

of a single gauge in the CERC6 array, the influence of the nonlinear effects in the directional analysis is amplified.

Overall, Method 1 showed an accuracy of the direction of propagation of $\pm 5^\circ$ for wave fields containing less than 2% second order energy and for wave fields having a difference in wave celerity below 0.1% estimated from linear wave theory compared to stream function theory. For the wave fields that contain less than 12% second order energy and do not reach a difference in wave celerity of 5%, the analysis showed an accuracy of the estimated mean wave direction within $\pm 15^\circ$. This is illustrated in Figure 14.1. While using Method 2, it was possible to estimate the mean wave direction within an accuracy of $\pm 5^\circ$ when analysing wave fields having a difference in wave celerity below 5% and an amount of less than 12% second order energy, as illustrated in Figure 14.2.

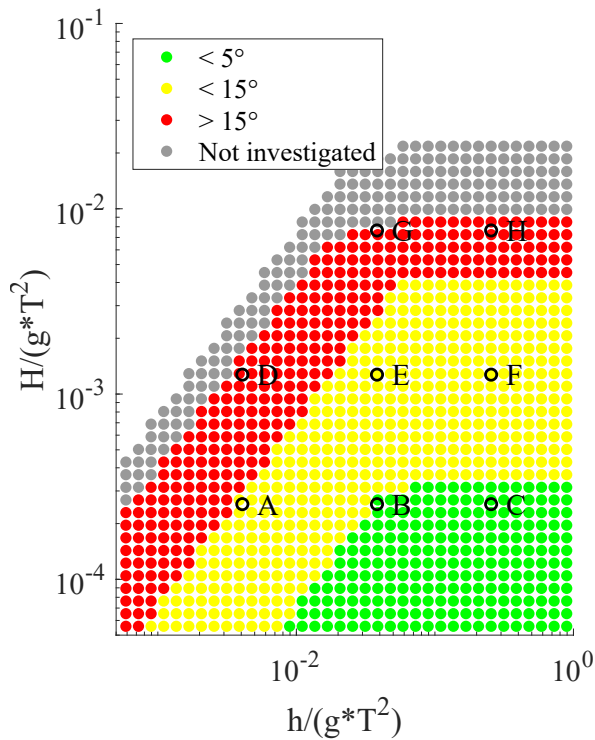


Figure 14.1: Accuracy of estimated mean wave direction using Method 1.

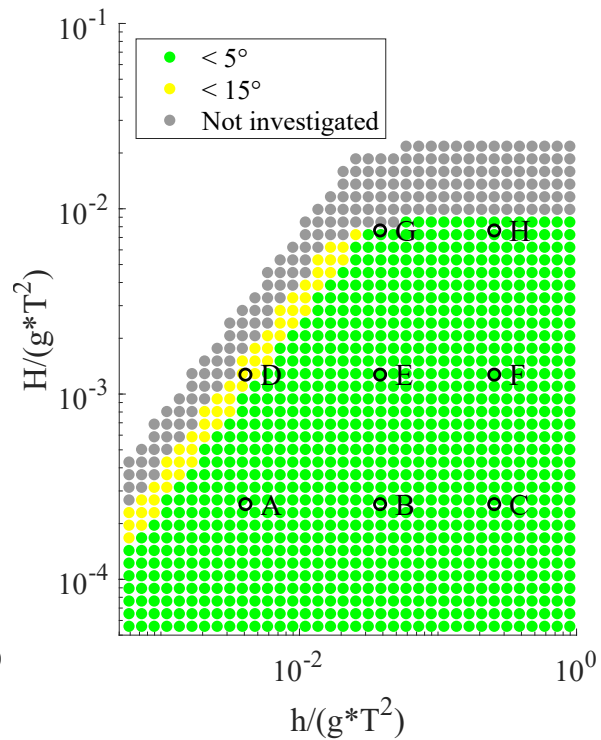


Figure 14.2: Accuracy of estimated mean wave direction using Method 2.

15 | References

- Aalborg University, 2022. Aalborg University. *WaveLab*.
<https://www.hydrosoft.civil.aau.dk/wavelab/>, 2022. Visited: 11/04/2022.
- Andersen and Eldrup, 2019. Thomas Lykke Andersen and Mads Røge Eldrup.
Estimation of Incident and Reflected Wave Trains in Highly Nonlinear Two-Dimensional Irregular Waves. *Journal of Waterway, Port, Coastal and Ocean Engineering*, 145(1), 2019.
- Andersen et al., 2017. Thomas Lykke Andersen, Mads Røge Eldrup and Peter Frigaard. *Estimation of incident and reflected components in highly nonlinear regular waves*. *Coastal Engineering* 119, 51-64, 2017.
- Bendat and Piersol, 2010. Julius S. Bendat and Allan G. Piersol. *Random Data: Analysis and Measurement Procedures, Fourth Edition*. John Wiley & Sons, Inc., 2010.
- Benoit et al., 1997. Michel Benoit, Peter Frigaard and Hemming A. Schäffer.
IAHR Seminar Multidirectional Waves and their Interaction with Structures: Analysing Multi-directional Wave Spectra: A Tentative Classification of Available Methods. XXVII IAHR Congress, 1997.
- Christensen and Sørensen, 1994. Morten Christensen and Niels Bo Sørensen.
Maximum Likelihood Estimation of Directional Spectrum Expressed in Standard Form. *Hydraulics & Coastal Engineering Laboratory, Aalborg University*, 1994.
- Department of the Environment, The Danish Coastal Authority, 2022.
Department of the Environment, The Danish Coastal Authority. *Kystdirektoratets Kystatlas*. <https://kyst.dk/kyster-og-klima/vaerktoejer/kystatlas/>, 2022. Visited: 20/05/2022.
- Eriksson, 1998. Anders I. Eriksson. *Analysis Methods for Multi-Spacecraft Data, Spectral Analysis*. ISSI Scientific Report SR-001 (Electronic edition 1.1), 1998.
- Frigaard and Andersen, 2014. Peter Frigaard and Thomas Lykke Andersen.
Analysis of Waves, Technical documentation for WaveLab 3. Aalborg University, Department of Civil Engineering, 2014.
- Hasselmann et al., 1973. K. Hasselmann, T.P. Barnett, E. Bouws, H. Carlson, D.E. Cartwright, K. Enke, J.A. Ewing, H. Gienapp, D.E. Hasselmann, P. Kruseman, A. Meerburg, P. Müller, D.J. Olbers, K. Richter, W. Sell and H. Walden. *Measurements of Wind-Wave Growth and Swell Decay during the Joint North Sea Wave Project (JONSWAP)*. Deutsches Hydrographisches Institut, Hamburg, 1973.
- Hawkes et al., 1997. P J Hawkes, J A Ewing, C M Harford, G Klopman, C T Stansberg, Michel Benoit, M J Briggs, Peter Frigaard, T Hiraishi, M Miles, J Santas and Hemming A. Schäffer. *IAHR Seminar Multidirectional Waves and their Interaction with Structures: Comparative Analysis of Multidirectional Wave Basin Data*. XXVII IAHR Congress, 1997.

- Isobe, 1990. Masahiko Isobe.** *Estimation of Directional Spectrum Expressed in Standard Form. Proc. 22nd Int. Conf. on Coastal Engineering*, pp.647-660, 1990.
- Isobe and Kondo, 1984. Masahiko Isobe and Kosuke Kondo.** *Method for Estimating Directional Wave Spectrum in Incident and Reflected Wave Field. Proc. Coastal Engineering Conf., vol. I*, pp. 467-483, 1984.
- Le MéHauté, 1976. Bernard Le MéHauté.** *An Introduction to Hydrodynamics and Water Waves. Springer*, 1976.
- Lin and Huang, 2004. Chun-Yuan Lin and Ching-Jer Huang.** *Decomposition of incident and reflected higher harmonic waves using four wave gauges. Coastal Engineering* 51, 395-406, 2004.
- Lin, 2008. Pengzhi Lin.** *Numerical Modeling of Water Waves. Taylor and Francis*, 2008.
- Liu and Frigaard, 2001. Zhou Liu and Peter Frigaard.** *Generation and Analysis of Random Waves. Aalborg University, Department of Civil Engineering*, 2001.
- Mitsuyasu et al., 1975. Hisashi Mitsuyasu, Fukuzo Tasai, Toshiko Suhara, Shinjiro Mizuno, Makoto Ohkusu, Tadao Honda and Kunio Rikiishi.** *Observations of the directional spectrum of ocean waves using a cloverleaf buoy. Journal of Physical Oceanography, Vol. I*, pp. 750-760, 1975.
- M.S. et al., 1963. Longuet-Higgins M.S., D.E. Cartwright and N.D. Smith.** *Observation of the directional spectrum of sea waves using the motions of a floating buoy, Oc. Wave Spectra. Prentice Hall, Inc., 1963.*
- Nelder and Mead, 1965. J. A. Nelder and R. Mead.** *A simplex method for function minimization. Computer Journal*, vol. 7, p. 308, 1965.
- Pierson et al., 1955. W.J. Pierson, G. Neumann and R.W. James.** *Practical Methods for Observing and Forecasting Ocean Waves by Means of Wave Spectra and Statistics. US Navy Hydrographic Office*, 1955.
- Sand, 1979. Stig Erik Sand.** *Three-dimensional Deterministic Structure of Ocean Waves. Institute of Hydrodynamics and Hydraulic Engineering, Technical University of Denmark*, 1979.
- Schäffer and Steenberg, 2002. H.A. Schäffer and C.M. Steenberg.** *Second-order wavemaker theory for multidirectional waves. DHI Water and Environment*, 2002.
- Svendsen and Jonsson, 1980. Ib A. Svendsen and Ivar G. Jonsson.** *Hydrodynamics of Coastal Regions. Den Private Ingeniørfond, Technical University of Denmark*, 1980.
- Takayama et al., 1989. T. Takayama, T. Hiraishi and Y. Goda.** *Comparison of Single and Double Summation Models for Multi-Directional Wave Generation. Proc. International Association for Hydraulic Research XXIII Congress, Ottawa, Canada, August 21-25, 1989.*
- Tanaka, 2019. Mitsuhiro Tanaka.** *Physics of Nonlinear Waves. Morgan and Claypool Publishers*, 2019.
- Tuah and Hudspeth, 1982. H. Tuah and R. T. Hudspeth.** *Comparison of Numerical Random Sea Simulations. Journal of the Water-way, Port, Coastal and Ocean Division*, 1982.

Y. and Suzuki, 1975. Goda Y. and Y. Suzuki. *Computation of refraction and diffraction of sea waves with Mitsuyasu's directional spectrum. Technical Note, Port and Harbor Research Institute, 230, 1975.*



Appendix I

| | | |
|-------------------|--|------------|
| Appendix A | Generation of Synthetic Waves | 94 |
| A.1 | Long-Crested Waves | |
| A.2 | Nonlinear Wave | |
| A.3 | Short-crested Waves | |
| Appendix B | Fourier Analysis | 111 |
| B.1 | Cosine Taper Data Window | |
| Appendix C | Directions | 113 |
| C.1 | Method 1 | |
| C.2 | Method 2 | |
| Appendix D | Second Order Wave Field | 115 |
| D.1 | Bichromatic Wave Field | |
| D.2 | Irregular Wave Field | |
| Appendix E | Convergence Study | 119 |
| E.1 | Single Summation Model | |
| E.2 | Double Summation Model | |
| Appendix F | Short-Crested Waves in More Directions | 124 |
| F.1 | First Order Waves | |
| F.2 | Second Order Waves | |
| F.3 | Waves with Amplitude Dispersion | |
| Appendix G | Variability due to Number of Subseries | 128 |
| Appendix H | Analysis of Signal with Noise Added | 132 |
| H.1 | Long-Crested Waves | |
| H.2 | Short-Crested Waves | |
| Appendix I | Errors Related to Calibration | 141 |
| I.1 | Long-Crested Waves | |
| I.2 | Short-Crested Waves | |
| Appendix J | Improvements Related to Calibration Error | 169 |
| J.1 | Detection of Calibration Error | |

Appendix A | Generation of Synthetic Waves

The synthetic waves are generated in the programming and numeric computing platform MatLab as a tool, which makes it possible to analyse different circumstances with different methods.

The generation of waves is based on the generation technique of Random Phase Method, which is an Inverse Fourier Transform method. This method is a deterministic technique which generates random waves in frequency domain and uses an Inverse Fast Fourier Transform (IFFT) to obtain the surface elevation in time domain. The deterministic technique of generating waves will generate a wave train of finite duration with an energy spectrum which corresponds to the chosen target wave spectrum. The corresponding time series are obtained by Inverse Fourier Transformation of the complex Fourier coefficients. The input used to generate synthetic waves are the following.

| | |
|----------|---|
| H_{m0} | Significant wave height [m] |
| h | Water depth [m] |
| f_p | Peak frequency, $f_p = f _{S_\eta(f)=max}$ [Hz] |
| f_s | Sample frequency [Hz] |
| N | Resolution of spectrum/Number of frequency components [-] |
| S_η | Spectrum [Hz] |
| γ | Peak enhancement factor, $\gamma = 3.3$ in average in the North Sea [-] |
| g | Gravitational acceleration, $g = 9.82$ [m/s ²] |
| (x,y) | Gauge positions [m] |
| θ | Wave propagation angle [rad] |

A.1 Long-Crested Waves

The most simple wave existing is a linear regular wave, and since an irregular wave consists of several linear waves, before generating an irregular wave, the generating procedure is shown for just a regular wave.

A.1.1 Linear Regular Wave

The surface elevation of a linear regular wave is described in the frequency-domain by Equation (A.1), where the energy distributed over one frequency.

$$\eta(t) = a \cdot \cos(\omega \cdot t - k \cdot x \cdot \cos(\theta) - k \cdot y \cdot \sin(\theta) + \phi) \quad (\text{A.1})$$

where

| | |
|----------|---|
| t | Time, [s] |
| a | Amplitude [m] |
| ω | Angular frequency, $\omega = \frac{2\pi}{T}$ [rad s ⁻¹] |
| T | Wave period [s] |
| k | Wave number, $k = \frac{2\pi}{L}$ |
| L | Wavelength [m] |
| ϕ | Initial phase [rad] |
| x,y | Position of wave gauge [m] |
| θ | Wave propagation angle between 0 and 2π [rad] |

The wavelength is determined from the dispersion relation using an iterative process for solving Equation (A.2).

$$L = \frac{gT^2}{2\pi} \tanh\left(\frac{2\pi h}{L}\right) \quad (\text{A.2})$$

An example of a linear regular surface elevation is shown in Figure A.1 showing Equation (A.1) plotted.

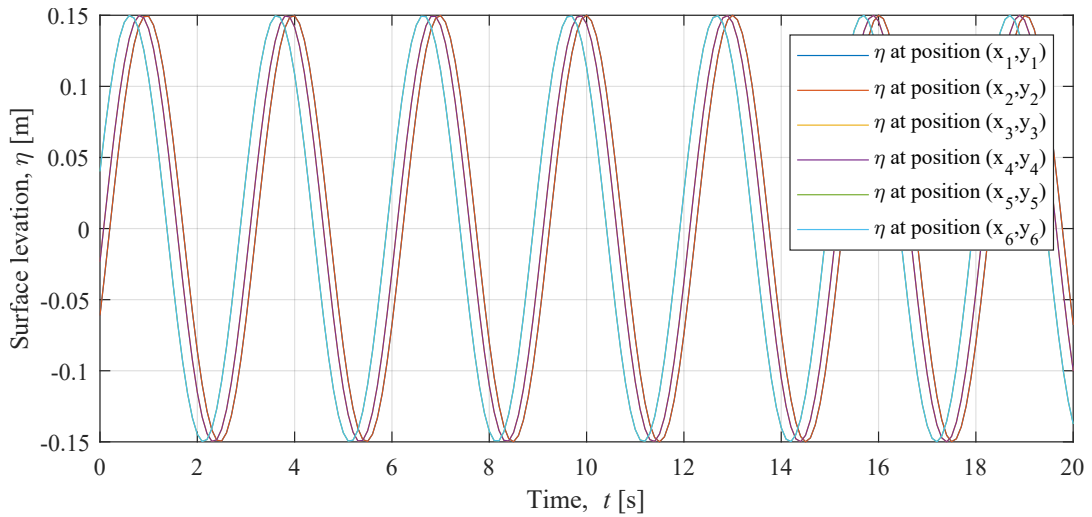


Figure A.1: Surface elevation for a regular wave measure at 6 different positions. Input: $H_{m0} = 0.3$ m, $T = 3$ s, $f_s = 10$ Hz and $N = 1024$.

The generation of the wave is performed using the random phase method, where the surface elevation is generated based on the energy calculated from the amplitude, a , which can be described as the variance. The variance of the surface elevation describes how much the stochastic variable of the surface elevation in average deviate from the mean value of the surface elevation. The input of the significant wave height, H_{m0} , determines the amplitude which is used to calculate the variance, σ_η^2 for the surface elevation, this is shown in Equation (A.3).

$$\sigma_\eta^2 = \frac{1}{2}a^2 \quad (\text{A.3})$$

The variance which is based on the energy of the spectrum and is used to calculate the variance

spectral density for a linear regular wave in Equation (A.4), which appears from Figure A.2.

$$S_\eta = \frac{\sigma_\eta^2}{\Delta f} \quad \text{where} \quad \Delta f = \frac{f_s}{N} \quad (\text{A.4})$$

Figure A.2 shows the frequencies below the Nyquist frequency which is $f_{N/2} = f_s/2$. The frequency, f , where the energy is represented is calculated from the period, $f = 1/T$.

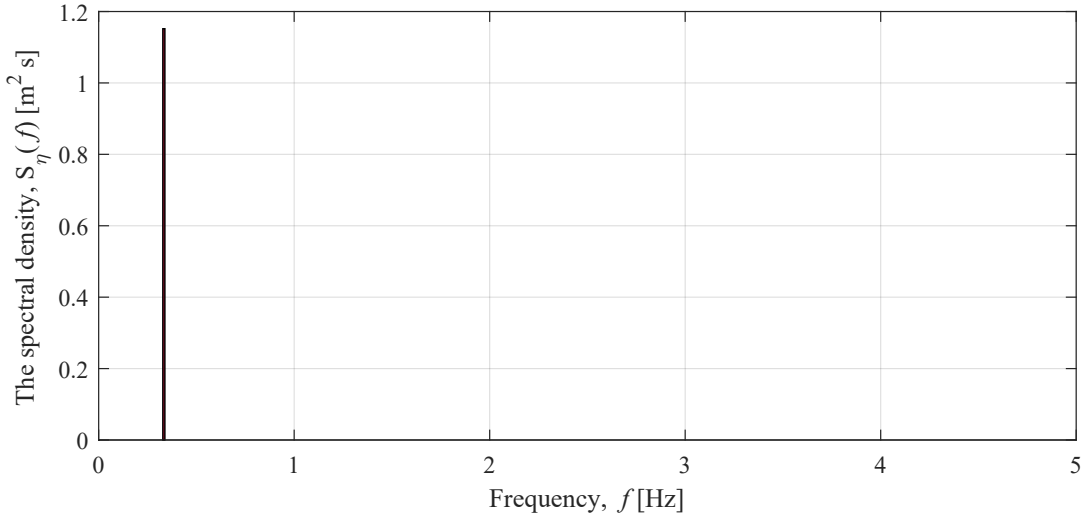


Figure A.2: Variance Spectrum for a linear regular wave. Input: $H_{m0} = 0.3$ m, $T = 3$ s, $f_s = 10$ Hz and $N = 1024$.

As shown in the figure, the energy for a regular wave is distributed over only one frequency. The simple relation is that the magnitude of energy depends on the wave height and the frequency depends on the period in case the duration consists of a total amount of wave periods. If the wave spectrum is distributed over more frequencies the phenomenon irregular wave is obtained. To obtain the specific position in the energy vector where the energy peak occur, the resolution of the spectrum, N , is used to calculate the position of the specific frequency. The other values in the energy vector are zero.

The sample duration is calculated from the resolution number, N , and the sample frequency, f_s in Equation (A.5).

$$T_0 = \frac{N - 1}{f_s} \quad (\text{A.5})$$

The relation between the sample duration, T_0 , and the period of the wave, T , which is shown in Equation (A.6), results in the position of the energy when it is rounded off and added with one because MatLab counts from zero.

$$N_f = \frac{T_0}{T} + 1 \quad (\text{A.6})$$

The relation between the amplitude and the energy was shown in Equation (A.3), this is used to calculate the Fourier coefficients, from which the surface elevation can be obtained by inverse

Fast Fourier Transforms. This approach is convenient to use when generating an irregular wave. First, the amplitude is isolated which is solved in Equation (A.7).

$$a = \sqrt{2 \cdot \sigma_\eta^2} \quad (\text{A.7})$$

Then the amplitude is stated as the Fourier coefficients, A and B , where $C = a$

$$C = \sqrt{A^2 + B^2} \quad \Longleftrightarrow \quad C = \sqrt{2 \cdot \sigma_\eta^2} \quad (\text{A.8})$$

The Fourier coefficient A is related to the cosine part of the amplitude while the Fourier coefficient B is related to the sine part of the amplitude. When generating the surface elevation from the Fourier coefficients, it is performed by generating a random phase, ϕ , between 0 and 2π for frequencies below the Nyquist frequency. The random phase is used to determine the Fourier coefficients which are calculated as shown in Equation (A.9) and (A.10).

$$A = \cos(\phi - k \cdot x \cdot \cos(\theta) - k \cdot y \cdot \sin(\theta)) \cdot \sqrt{\sigma_\eta(f)^2 / \sqrt{2}} \quad \text{for } N_f \quad (\text{A.9})$$

$$B = \sin(\phi - k \cdot x \cdot \cos(\theta) - k \cdot y \cdot \sin(\theta)) \cdot \sqrt{\sigma_\eta(f)^2 / \sqrt{2}} \quad \text{for } N_f \quad (\text{A.10})$$

In MatLab the counting starts from 0 to $N/2 - 1$ when calculating the Fourier coefficients. These Fourier coefficients are mirrored similar to the method which MatLab uses to mirror Fourier coefficients. This is shown in Equation (A.11) and Equation (A.12), where MatLab as standard procedure mirrors around component number $\frac{N}{2} + 1$. The number at that place is overwritten by the first component for A_i , where $A(N/2 + 1) = A(1)$ and by zero for B_i , where $B(N/2 + 1) = 0$ before mirroring.

$$A(N_f) = A(N - N_f) \quad (\text{A.11})$$

and

$$B(N_f) = B(N - N_f) \quad (\text{A.12})$$

The Fourier coefficients are further used in the Inverse Fourier Transform (IFFT) to obtain the corresponding surface elevation η as a time series. When performing a IFFT, the number of data points must be an integer power of two ($N = 2^M$) according to Eriksson (1998). It is shown in Equation (A.13), where the Fourier coefficients are used in complex form.

$$\eta(t) = \text{ifft}(A + i \cdot B) \quad (\text{A.13})$$

The result of the surface elevation is shown in Figure A.3 which is equal to the plot of the cosine wave in Figure A.1 just for one wave gauge measurement point.

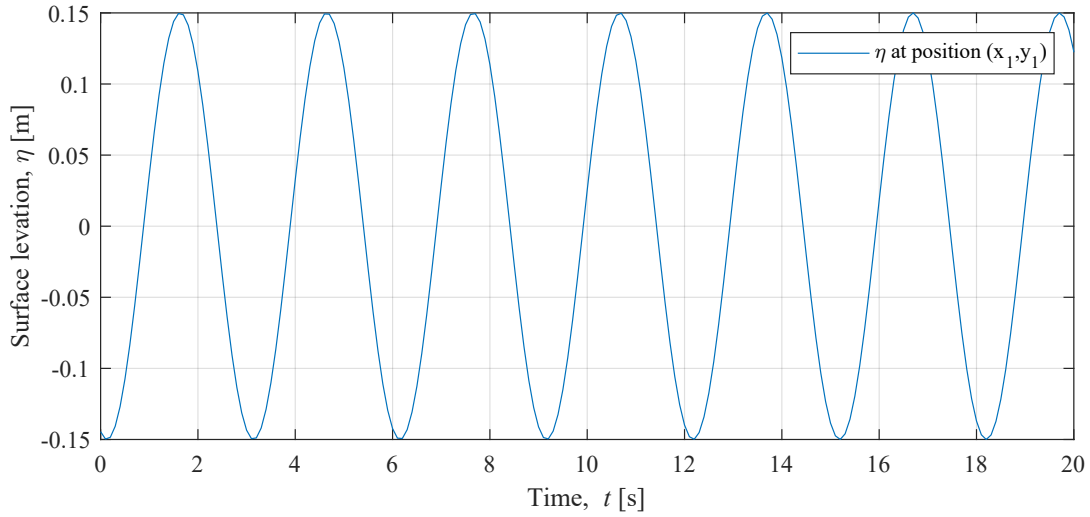


Figure A.3: Surface elevation for a regular wave measure at one position. Input: $H_{m0} = 0.3$ m, $T = 3$ s, $f_s = 10$ Hz and $N = 1024$.

This approach is also used to generate an irregular wave.

A.1.2 Linear Irregular Wave

Empirical Spectrum

The random waves are generated based on a target wave energy density spectrum of the empirical spectrum; JONSWAP spectrum suggested by Hasselmann et al. (1973) with the frequency, f as variable, where the spectral density, S_η is given in Equation (A.14). The JONSWAP spectrum is an extension of the Pierson Moskowitz spectrum, where the JONSWAP spectrum has a peak enhancement factor, γ , included.

$$S_\eta(f) = \alpha \cdot H_{m0}^2 \cdot f_p^{-5} \cdot \gamma^\beta \cdot \exp\left(-\frac{5}{4} \left(\frac{f_p}{f}\right)^4\right) \quad (\text{A.14})$$

where

f | Frequency [Hz]

$$\alpha = \frac{0.0624}{0.230 + 0.0336\gamma - \frac{0.185}{1.9+\gamma}} \quad (\text{A.15})$$

$$\beta = \exp\left(-\frac{(f - f_p)^2}{2\sigma_f^2 f_p^2}\right) \quad (\text{A.16})$$

$$\sigma_f = \begin{cases} 0.07 & \text{for } f \leq f_p \\ 0.09 & \text{for } f > f_p \end{cases} \quad (\text{A.17})$$

The JONSWAP spectrum is derived during the Joint North Sea Wave Project, from here the name JONSWAP origins. The energy spectrum is obtained from the steady easterly wind, and is often used for projects in the North Sea. In Figure A.4, the energy distribution over frequencies of the JONSWAP spectrum is shown. Liu and Frigaard (2001)

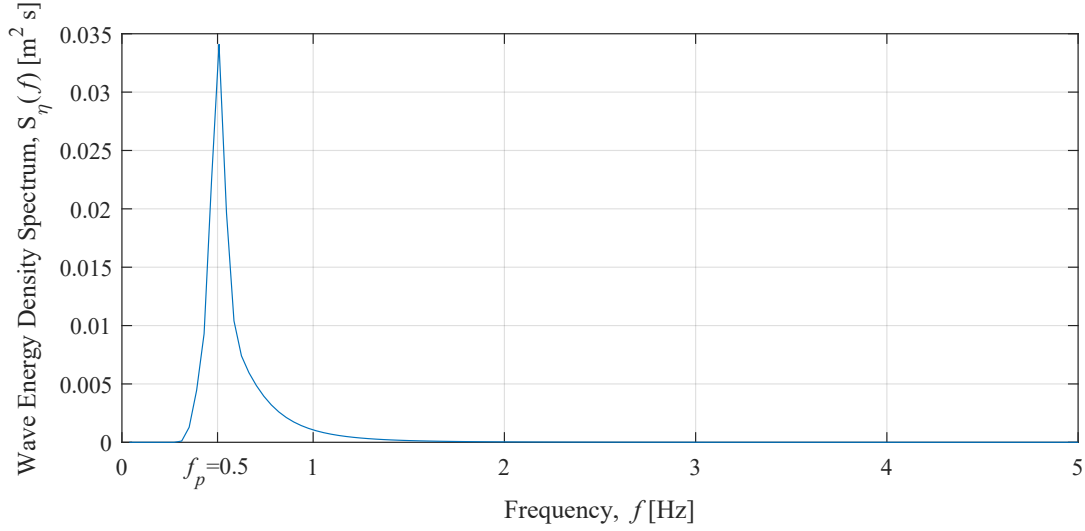


Figure A.4: JONSWAP spectrum with the input parameters: $H_{m0} = 0.3$ m, $f_s = 10$ Hz, $h = 0.7$ m, $f_p = 0.5$ Hz and $N = 1024$.

The spectrum is multiplied with the frequency band width, Δf to obtain the discrete amplitude wave spectrum, $\sigma_\eta^2(f)$ which is shown in Equation (A.18). This corresponds to the variance of the spectrum.

$$\sigma_\eta^2(f) = S_\eta(f) \cdot \Delta f \quad \text{where} \quad \Delta f = f_s/N \quad (\text{A.18})$$

Generation of Surface Elevation

In this section, linear wave theory is assumed, which means that governing equation and boundary conditions are linear when assuming small amplitude wave theory. When linear wave theory is applied, superposition of a number of linear waves with different wave heights and wave periods will generate a linear irregular wave.

$$\eta(t) = \sum_{i=1}^N a_i \cdot \cos(\omega_i \cdot t - k_i \cdot x \cdot \cos(\theta) - k_i \cdot y \cdot \sin(\theta) + \phi_i) \quad (\text{A.19})$$

Equation (A.19) is rewritten using Fourier coefficients which are related to the amplitude $a_i = \sqrt{A_i^2 + B_i^2}$, this is stated in Equation (A.20) where $\eta(t)$ can be expanded as a Fourier series.

$$\begin{aligned} \eta(t) = \sum_{i=1}^N & A_i \cdot \cos(\omega_i \cdot t - k_i \cdot x \cdot \cos(\theta) - k_i \cdot y \cdot \sin(\theta)) \\ & + B_i \cdot \sin(\omega_i \cdot t - k_i \cdot x \cdot \cos(\theta) - k_i \cdot y \cdot \sin(\theta)) \end{aligned} \quad (\text{A.20})$$

To obtain the energy at the different frequencies in the energy spectrum, an irregular wave of the JONSWAP spectrum is generated as described in section A.1.2. It is performed by generating random phases, ϕ_i , uniformly distributed between 0 and 2π for frequencies below the Nyquist frequency, $f_n = f_s/2$. The random phases are used to determine the Fourier coefficients which

are calculated as shown in Equation (A.21) and (A.22).

$$A_i = \cos(\phi_i - k \cdot x \cdot \cos(\theta) - k \cdot y \cdot \sin(\theta)) \cdot \sqrt{\sigma_\eta(f_i)^2 / \sqrt{2}} \quad \text{for } i = 1 \dots N/2 + 1 \quad (\text{A.21})$$

$$B_i = \sin(\phi_i - k \cdot x \cdot \cos(\theta) - k \cdot y \cdot \sin(\theta)) \cdot \sqrt{\sigma_\eta(f_i)^2 / \sqrt{2}} \quad \text{for } i = 1 \dots N/2 + 1 \quad (\text{A.22})$$

where

| | |
|----------|---|
| k_i | Wave number [-] |
| x, y | Position of wave gauge [m] |
| θ | Wave propagation angle between 0 and 2π [rad] |

As for the regular wave, these Fourier coefficients are mirrored similar to the method which MatLab uses to mirror Fourier coefficients. This is shown in Equation (A.23) and Equation (A.24).

$$A_i \left(\frac{N}{2} + i + 1 \right) = A_i \left(\frac{N}{2} - i + 1 \right) \quad \text{for } i = 1, 2, \dots, N/2 \quad (\text{A.23})$$

and

$$B_i \left(\frac{N}{2} + i + 1 \right) = -B_i \left(\frac{N}{2} - i + 1 \right) \quad \text{for } i = 1, 2, \dots, N/2 \quad (\text{A.24})$$

The Fourier coefficients are further used in the Inverse Fourier Transform (IFFT) to obtain the corresponding surface elevation η as a time series. It is shown in Equation (A.25), where the Fourier coefficients are used in complex form.

$$\eta(t) = \text{ifft}(A_i + i \cdot B_i) \quad (\text{A.25})$$

In Figure A.5, the irregular surface elevation is plotted for a random situation to show the principle.

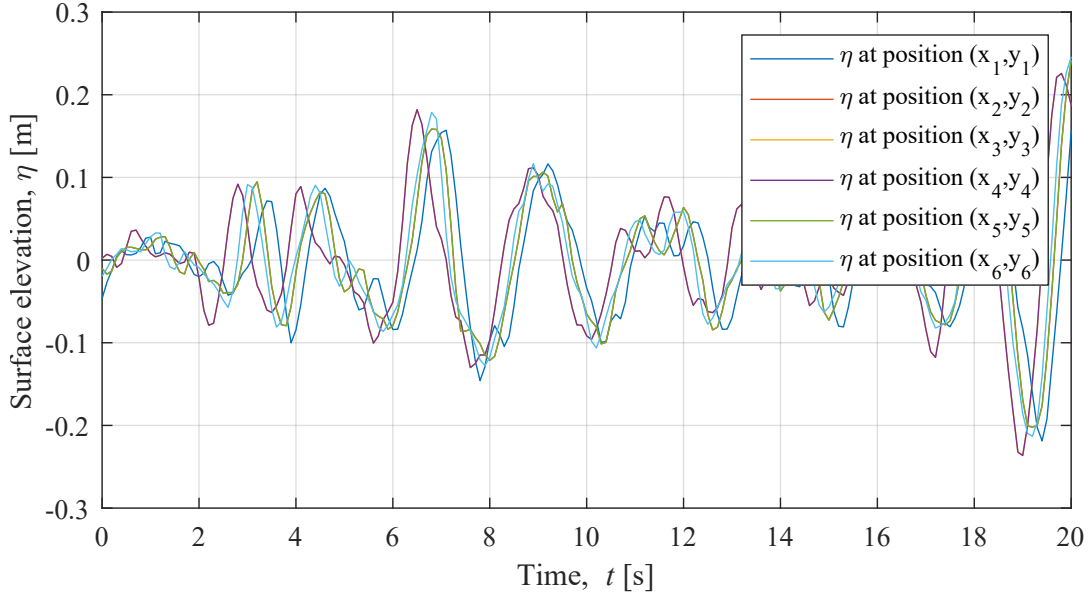


Figure A.5: Surface elevation for a regular wave measure at 6 different positions. Input: $H_{m0} = 0.3$ m, $f_s = 10$ Hz, $h = 0.7$ m, $f_p = 0.5$ Hz and $N = 1024$.

The energy spectrum is derived from more amplitudes, which results in a wave energy spectrum which is distributed over more frequencies.

A.2 Nonlinear Wave

The surface elevation of a nonlinear wave can be described by a series expansion when using Stokes higher order wave theory. In Equation (A.26), Stokes second order wave theory is shown, which is the sum of the first and second order wave.

$$\eta(t) = \underbrace{\eta^{(1)}(t)}_{\text{First order}} + \underbrace{\eta^{(2)}(t)}_{\text{Second order}} \quad (\text{A.26})$$

where

$$\begin{array}{l|l} \eta^{(1)}(t) & \text{Surface elevation for a first order wave stated in Equation (2.1).} \\ \eta^{(2)}(t) & \text{Second order contribution.} \end{array}$$

The second order contribution of the surface elevation is derived by Stokes second order theory in Equation (A.27) where the amplitude, a_2 , is different from first order theory and the cyclic frequency, ω , is doubled which means that the second order term is oscillating twice as fast as the first order term does.

$$\eta^{(2)}(t) = a_2 \cdot \cos 2(\omega \cdot t - k \cdot x \cdot \cos(\theta) - k \cdot y \cdot \sin(\theta)) \quad (\text{A.27})$$

The amplitude of the second order term of a wave, a_2 , is expressed in Equation (A.28).

$$a_2 = \frac{1}{16} k \cdot H_{m0}^2 (3 \cdot \coth(kh)^3 - \coth(kh)) \quad (\text{A.28})$$

The surface elevations of a wave of first and second order term from Stoke's theory are plotted in Figure A.6 along with the total surface elevation.

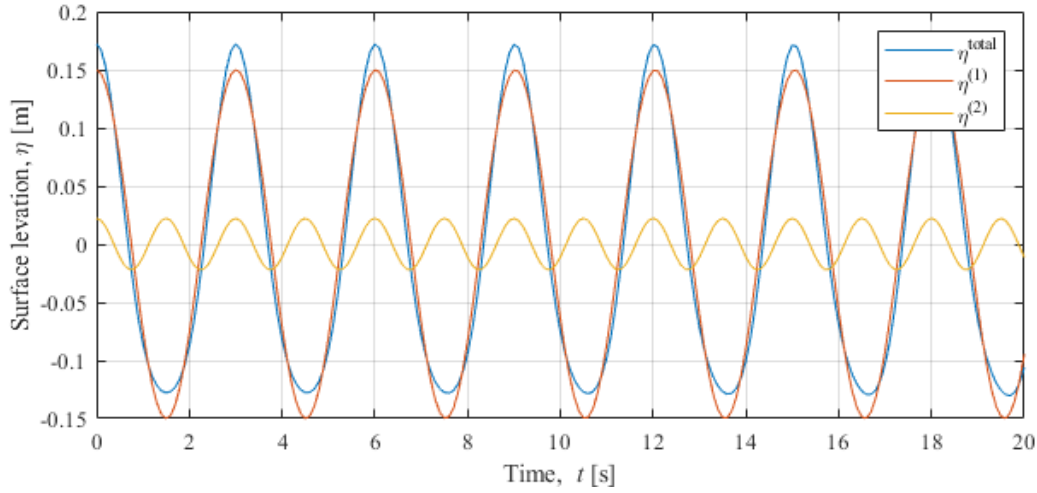


Figure A.6: Surface elevation of a regular first and second order term and the total surface elevation using Stoke's second order wave theory. Input: $H_{m0} = 0.3$ m, $T = 3$ s, $f_s = 10$ Hz and $N = 1024$.

As the theory describes, the total surface elevation gets a shorter and steeper crest and a longer and more plane trough, which is closer to the waves experienced in a real sea. This theory can be used when it is a single monochromatic wavetrain in first order.

The nonlinear process occurs from interaction between two linear components, η_n and η_m , with different angular frequencies, ω_m and ω_n , and directions, θ_n and θ_m , generally. For long-crested waves, the directions of the components are equal, $\theta_n = \theta_m$. These constitute the second order spectrum, which is solved by a bichromatic analysis in the frequency domain as given by Schäffer and Steenberg (2002). For convenience, the first order solution is rewritten to the complex solution, which is stated in Equation (A.29).

$$\eta^{(1)}(t) = \begin{cases} \eta_n = \frac{1}{2} \left(A_n e^{i(\omega_n t - \vec{k}_n \vec{x})} + c.c \right) \\ \eta_m = \frac{1}{2} \left(A_m e^{i(\omega_m t - \vec{k}_m \vec{x})} + c.c \right) \end{cases} \quad (\text{A.29})$$

where

| | |
|-----------|---|
| A | Amplitude |
| ω | Angular frequency |
| \vec{k} | Wave number vector, $\vec{k} = k(\cos \theta, \sin \theta)$ |
| θ | Wave propagation direction |
| $c.c.$ | Complex conjugate of the preceding term |

The surface elevation for the bound second order contribution is given by Equation (A.30) where the n 'th and the m 'th wave interact with each other.

$$\eta^{(2)}(t) = \eta_{nm}^{\pm} = \frac{1}{2} \left(G_{nm}^{\pm} A_n A_m^{-*} e^{i(\Theta_n \pm \Theta_m^{-*})} + c.c. \right) \quad (\text{A.30})$$

where

| | |
|----------------|--|
| n | n'th wave |
| m | m'th wave |
| G_{nm}^{\pm} | 2 nd Order Surface Elevation Transfer Function |
| $A_n A_m$ | Amplitudes [m] |
| Θ | $\begin{cases} \Theta_n = \omega_n t - \vec{k}_n \cdot \vec{x} \\ \Theta_m = \omega_m t - \vec{k}_m \cdot \vec{x} \end{cases}$ |

This will give following combinations of the second order component. Tanaka (2019)

$$\eta^{(2)}(t) = \begin{cases} A_n^2 e^{2i\Theta_n} + c.c. \\ A_m^2 e^{2i\Theta_m} + c.c. \\ A_n A_m e^{i(\Theta_n + \Theta_m)} + c.c. \\ A_n A_m * e^{i(\Theta_n - \Theta_m)} + c.c. \end{cases} \quad (\text{A.31})$$

The symbol $- : *$ denote the meaning of a value which has to be calculated as its own value for superharmonics while it has to be calculated as its complex conjugated for subharmonics.

$$A_m^{-:*} = \begin{cases} A_m & \text{for superharmonics} \\ A_m * = \text{conj}(A_m) & \text{for subharmonics} \end{cases}$$

This is rewritten from complex form to the trigonometric equation stated in Equation (A.32).

$$\begin{aligned} \eta_{nm}^{\pm} = & G_{nm}^{\pm} \left[(a_n a_m \mp b_n b_m) \cos \left((\omega_n \pm \omega_m)t - (\vec{k}_n \pm \vec{k}_m) \cdot \vec{x} \right) \right] \\ & + G_{nm}^{\pm} \left[(a_m b_n \pm a_n b_m) \sin \left((\omega_n \pm \omega_m)t - (\vec{k}_n \pm \vec{k}_m) \cdot \vec{x} \right) \right] \end{aligned} \quad (\text{A.32})$$

where

| | |
|-------------------------|---|
| a | Cosine part of amplitude |
| b | Sine part of amplitude |
| $\omega_m \pm \omega_n$ | Angular frequency at sub- and superharmonics [rad s ⁻¹] |
| \vec{k} | Wave number vector, $\vec{k} = (k \cos \theta, k \sin \theta)$ |
| \vec{x} | Horizontal position vector, $\vec{x} = (x, y)$ |

The second order contribution will as described previously in the report consist of the number of the first order components squared. As described in the introduction, if the model consists of two wave components, n and m , with each a frequency, ω_n and ω_m , the second order contribution will be $2^2 = 4$ components. If there are N wave components, the number of second order contribution will be N^2 components as long the model generates long-crested waves.

The second order surface elevation transfer function, G_{nm}^{\pm} , is calculated in Equation (A.33) where the \pm symbolize the super- and subharmonics.

$$G_{nm}^{\pm} = \frac{\delta_{nm}}{g} \left((\omega_m \pm \omega_n) \cdot \frac{H_{nm}^{\pm}}{D_{nm}^{\pm}} - L_{nm}^{\pm} \right) \quad (\text{A.33})$$

where

$$\left. \begin{array}{l} \delta_{nm} \\ g \end{array} \right| \begin{array}{l} \text{where } \delta_{nm} = \begin{cases} \frac{1}{2}, & \text{for } \omega_n = \omega_m \\ 1, & \text{otherwise} \end{cases} \\ \text{Gravity acceleration, } g = 9.82 \text{ m/s}^2 \end{array}$$

Furthermore, the other parameters H_{nm}^{\pm} , D_{nm}^{\pm} and L_{nm}^{\pm} are given by the following equations.

$$H_{nm}^{\pm} = (\omega_n \pm \omega_m) \left(\pm \omega_n \omega_m - \frac{g^2 \vec{k}_n \cdot \vec{k}_m^{-*}}{\omega_n \omega_m} \right) + \frac{\omega_n^3 + \omega_m^3}{2} - \frac{g^2}{2} \left(\frac{k_n^2}{\omega_n} \pm \frac{k_m^2}{\omega_m} \right) \quad (\text{A.34})$$

$$D_{nm}^{\pm} = g k_{nm}^{\pm} \tanh(k_{nm}^{\pm} h) - (\omega_n \pm \omega_m)^2 \quad (\text{A.35})$$

$$L_{nm}^{\pm} = \frac{1}{2} \left(\frac{g^2 \vec{k}_n \cdot \vec{k}_m^{-*}}{\omega_n \omega_m} \pm \omega_n \omega_m - (\omega_n^2 + \omega_m^2) \right) \quad (\text{A.36})$$

Where the wave number k_{nm}^{\pm} is given by Equation (A.37).

$$k_{nm}^{\pm} = \sqrt{(k_{xn} \pm k_{xm}^{-*})^2 + (k_{yn} + k_{ym})^2} \quad (\text{A.37})$$

The total second order contribution is the sum of the super- and subharmonics, η_{nm}^{\pm} , calculated from Equation (A.32). The surface elevation of the second order contribution from Equation (A.30) is plotted in Figure A.7 and A.8. And the sum of these the total contribution is plotted in Figure A.9.

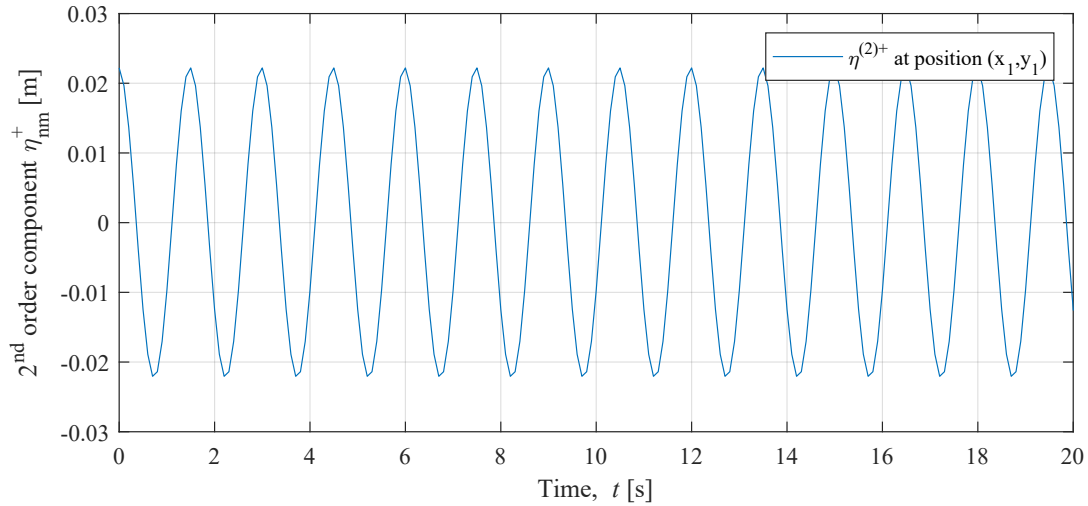
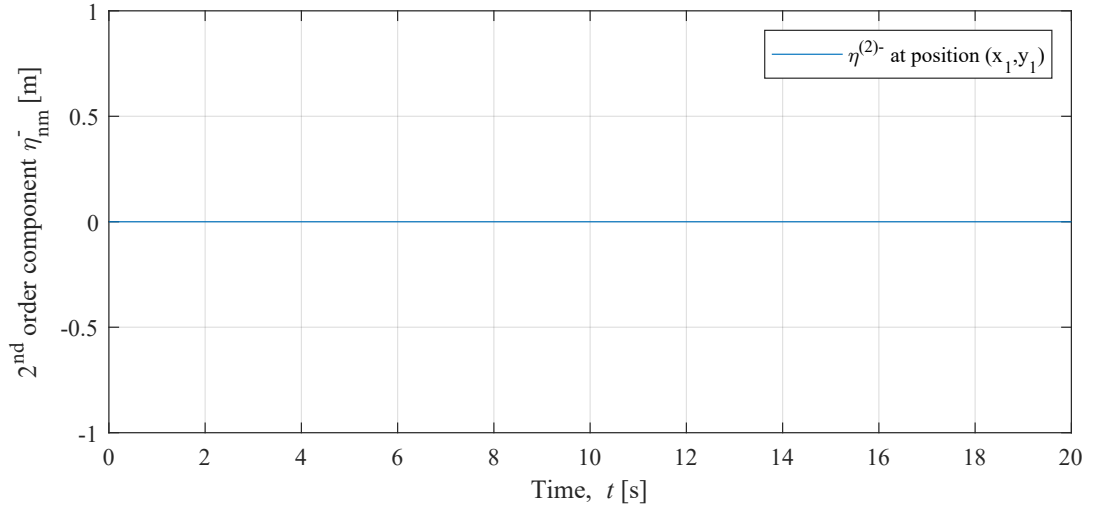
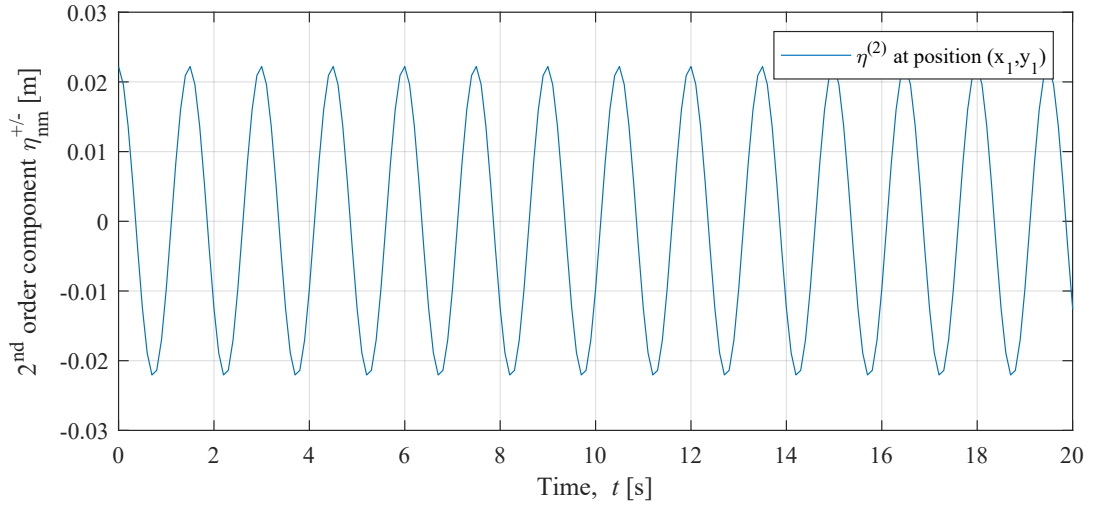
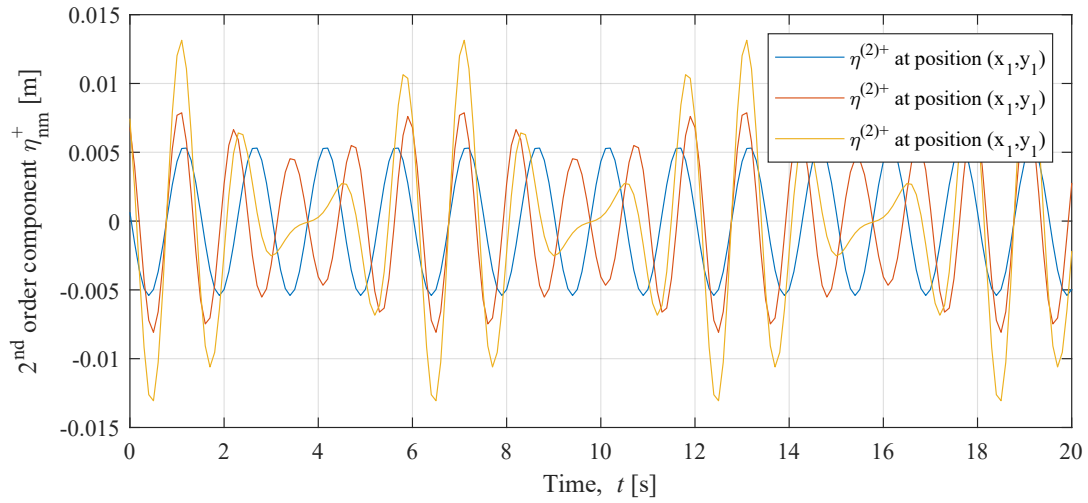


Figure A.7: Super harmonic 2nd order contribution.

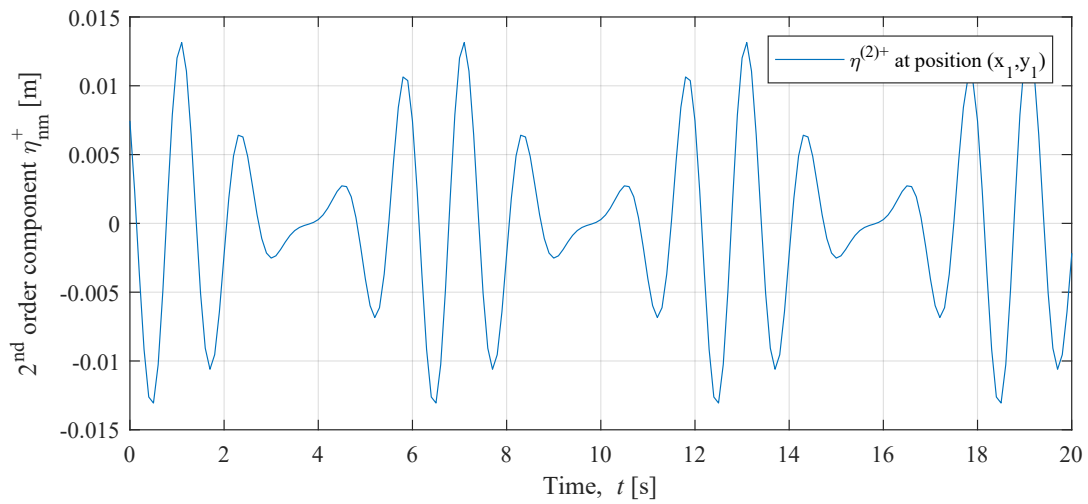
Figure A.8: Sub harmonic 2nd order contribution.Figure A.9: Surface elevation of the second order contribution using Schäffer and Steenberg (2002) second order solution. Input: $H_{m0} = 0.3$ m and $T = 3$ s.

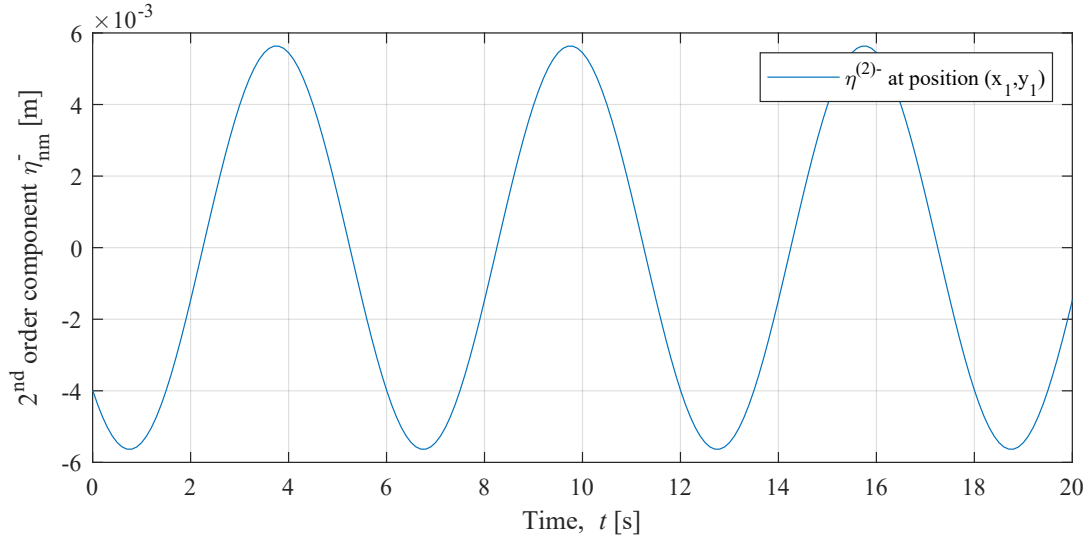
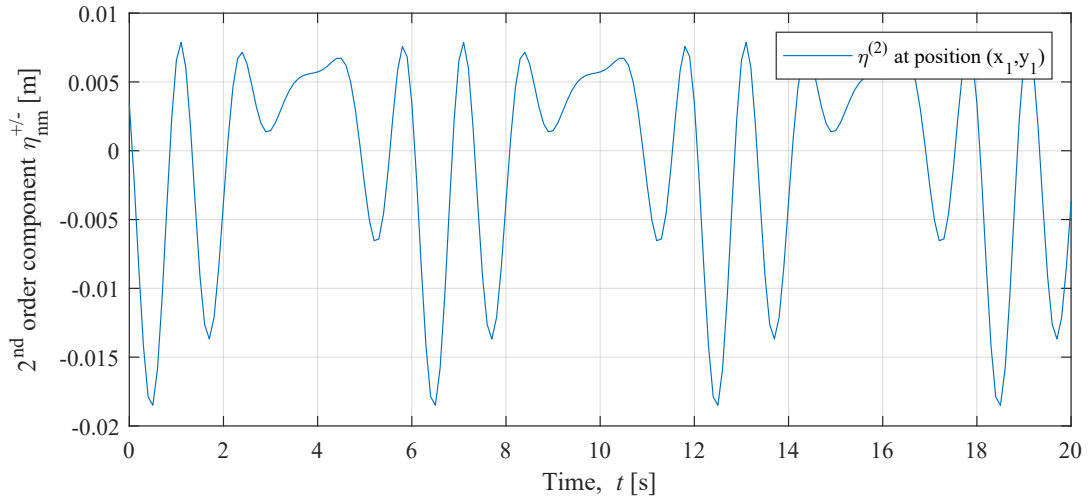
When a wave interact with it self, it will become equal to Stoke's second order wave from Equation (A.27) as shown in Figure A.9 which is equal to the second order wave, $\eta^{(2)}$, in Figure A.6.

Now two different wave components, η_n and η_m are shown as example to visualize the second order contribution. First, the superharmonics are plotted in Figure A.10 to show the different components.

Figure A.10: Super harmonic 2^{nd} order contribution.

The surface elevations of the second order contribution are plotted as the sum of the superharmonics in Figure A.11, the the subharmonic in Figure A.12 and the total sum in Figure A.13.

Figure A.11: Superharmonic 2^{nd} order contribution.

Figure A.12: Subharmonic 2nd order contribution.Figure A.13: Surface elevation of the second order contribution using Schäffer and Steenberg (2002) second order solution. Input: $H_{m0} = 0.3$ m and $T = 3$ s together with $H_{m0} = 0.2$ m and $T = 3$ s.

A.3 Short-crested Waves

So far, the synthetically generated waves have been long-crested waves, which were generated based on the variance spectrum, $S_\eta(\omega)$. When including more directions the waves become short-crested, and the directional spectrum, $D(\omega, \theta)$, is introduced.

A.3.1 Generated Directional Wave Spectrum

The directional wave spectrum is generated by the auto-spectrum and the directional spreading function as shown in Equation (A.38).

$$S(\omega, \theta) = S(\omega) \cdot D(\omega, \theta) \quad (\text{A.38})$$

where

$D(\theta)$ | Directional spreading function [rad]

The directional spreading function shown in Equation (A.39) is used to generate the distribution of the directions.

$$D(\omega, \theta) = \frac{2^{2s-1} \Gamma^2(s+1)}{\pi \Gamma(2s+1)} \left[\cos \left(\frac{\theta - \theta_0}{2} \right) \right]^{2s} \quad (\text{A.39})$$

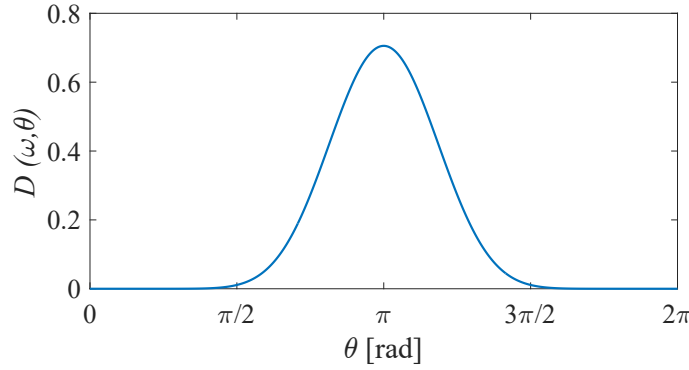


Figure A.14: Cosine distribution of directional spreading function, $D(\omega, \theta)$.

The distribution of the directional spreading function, $D(\omega, \theta)$ is a cosine distribution. This distribution is obtained by calculating the directional spreading function from Equation (A.39) and doing a numerical integration of the distribution to obtain the cumulative distribution, $F(\theta)$, which is shown in Equation (A.40).

$$F(\theta) = \sum_{\theta=0}^M D(\omega, \theta) \cdot \frac{2\pi}{M} \quad (\text{A.40})$$

The cumulative distribution is shown in Figure A.15.

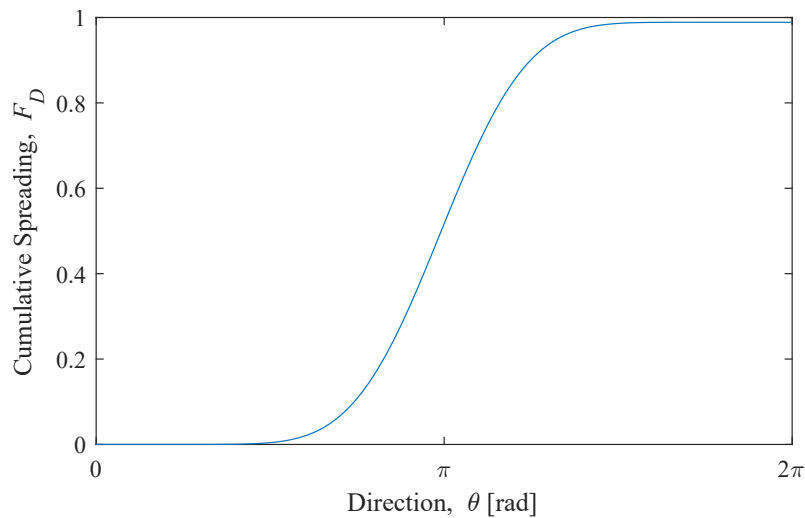


Figure A.15: Cumulative distribution of the directional spreading function.

The cumulative distribution of the probability density function equal to directional spreading function is used for picking a direction, θ_i , as a random number when using the model of single

summation, where the surface elevation is given as in Equation (A.41).

$$\eta(\vec{x}, t) = \sum_{i=1}^{N \cdot M} a_i \cos(k_i \cdot (x \cos(\theta_i) + y \sin(\theta_i)) - \omega_i t + \phi_i) \quad (\text{A.41})$$

To obtain the surface elevation, the random phase method is used again to determine the Fourier coefficients, A_i and B_i , where the direction θ_i is determined based on the cumulative distribution, $F(\theta_i)$.

$$A_i = \cos(\phi_i - k_i \cdot x \cdot \cos(\theta_i) - k_i \cdot y \cdot \sin(\theta_i)) \cdot \sqrt{\sigma_\eta(f_i, \theta_i)^2 / \sqrt{2}} \quad \text{for } i = 1 \dots N/2 + 1 \quad (\text{A.42})$$

$$B_i = \sin(\phi_i - k_i \cdot x \cdot \cos(\theta_i) - k_i \cdot y \cdot \sin(\theta_i)) \cdot \sqrt{\sigma_\eta(f_i, \theta_i)^2 / \sqrt{2}} \quad \text{for } i = 1 \dots N/2 + 1 \quad (\text{A.43})$$

The coefficients from Equation (A.42) and (A.43) are mirrored likewise the long-crested waves, and further is a Inverse Fourier Transform performed to obtain the generated surface elevation, η .

The energy spectrum of a wave field based in the single summation model is shown in Figure A.16, where a single direction is assigned to each frequency component.

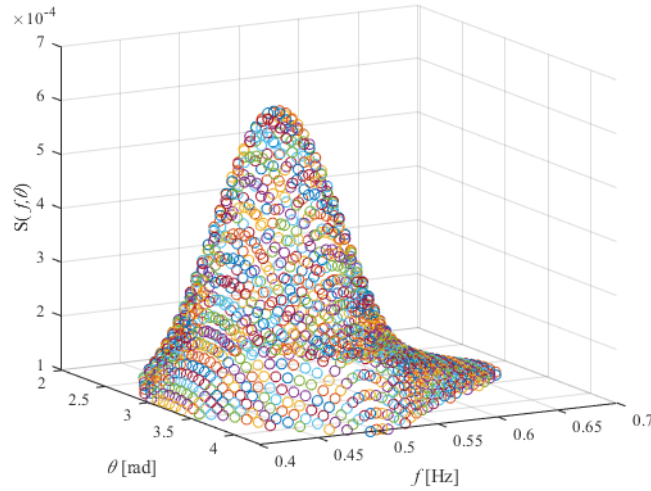


Figure A.16: Single summation energy spectrum.

When using the double summation model, multiple directions are assigned to each frequency component. Therefore, the direction, θ is chosen equally distributed from 0 to 2π , which is used when determining the Fourier coefficients which are done in Equation (A.44) and (A.45).

$$A_{ij} = \cos(\phi_i - k_i \cdot x \cdot \cos(\theta_j) - k_i \cdot y \cdot \sin(\theta_j)) \cdot \sqrt{\sigma_\eta(f_i, \theta_j)^2 / \sqrt{2}} \quad (\text{A.44})$$

for $i = 1 \dots N/2 + 1$ and $j = 1 \dots M$

$$B_{ij} = \sin(\phi_i - k_i \cdot x \cdot \cos(\theta_j) - k_i \cdot y \cdot \sin(\theta_j)) \cdot \sqrt{\sigma_\eta(f_i, \theta_j)^2 / \sqrt{2}} \quad (\text{A.45})$$

for $i = 1 \dots N/2 + 1$ and $j = 1 \dots M$

These coefficients are mirrored likewise the others, and a Inverse Fourier Transform is performed to obtain the generated surface elevation.

The energy spectrum is determined from the principle that each frequency has multiple directions, which is shown in Figure A.17.

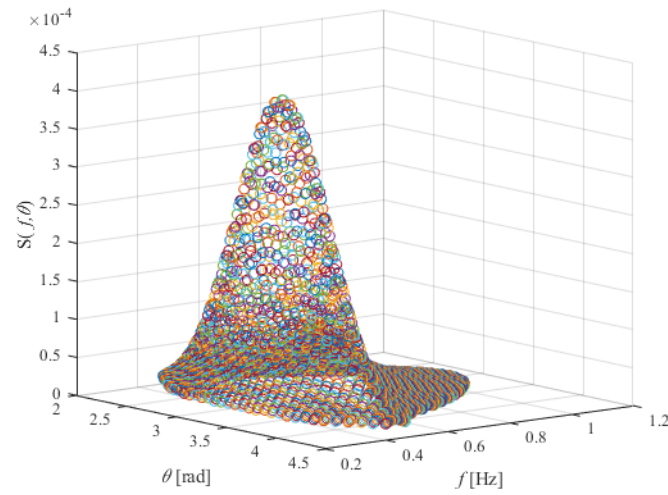


Figure A.17: Double summation energy spectrum.

To include second order energy in the spectrum, the approach from section A.2 is used.

Appendix B | Fourier Analysis

A spectral estimation of the measured time-series are found from Fourier analysis using finite Fourier transforms as given by Bendat and Piersol (2010). From a pair of signals, $\eta_m(t)$ and $\eta_n(t)$, which are assumed to be stationary random processes, the cross-spectral density function is stated in Equation (B.1) as function of the duration of the time-series, T_0 .

$$S_{mn}(\omega, T_0) = \frac{1}{T_0} X^*(\omega, T_0) Y(\omega, T_0) \quad (\text{B.1})$$

where

$$\begin{aligned} X(\omega, T_0) &= \int_0^{T_0} \eta_m(t) \exp(-i\omega t) dt \\ Y(\omega, T_0) &= \int_0^{T_0} \eta_n(t) \exp(-i\omega t) dt \end{aligned} \quad (\text{B.2})$$

The correct cross-spectral density function is found as T_0 tends to infinity, which leads to:

$$S_{mn}(\omega) = \lim_{T_0 \rightarrow \infty} E[S_{mn}(\omega, T_0)] \quad (\text{B.3})$$

The discrete Fourier transform of Equation (B.2) is stated in Equation (B.4).

$$X(\omega, T_0) = \sum_t^{T_0} \eta_m(t) \exp(-i\omega t) \Delta t \quad (\text{B.4})$$

The cross-spectrum, $S_{mn}(\omega)$ can be expressed as a complex function as stated in Equation (B.5) with the coincident spectral density function, C_{mn} , as the real part and the quadrature spectral density function, Q_{mn} , as the imaginary part. As negative frequencies are of no physical meaning in this context, the one-sided spectrum is used, wherefore C_{mn} and Q_{mn} are multiplied by 2 in Equation B.6.

$$S_{mn}(\omega) = C_{mn} - iQ_{mn} \quad (\text{B.5})$$

where

$$\begin{aligned} C_{mn} &= \frac{2}{T_0} (\mathcal{R}(X)\mathcal{R}(Y) + \mathcal{I}(X)\mathcal{I}(Y)) \\ Q_{mn} &= \frac{2}{T_0} (\mathcal{R}(X)\mathcal{I}(Y) - \mathcal{I}(X)\mathcal{R}(Y)) \end{aligned} \quad (\text{B.6})$$

B.1 Cosine Taper Data Window

For modification of the time-series before the Fourier analysis, the cosine taper data window as stated by Frigaard and Andersen (2014) is used, which is given in Equation (B.7)

$$d(t) = \begin{cases} \frac{1}{2} \left(1 - \cos \left(\frac{10\pi t}{T_0} \right) \right) & 0 \leq t \leq \frac{T_0}{10} \\ 1 & \frac{T_0}{10} \leq t \leq \frac{9T_0}{10} \\ \frac{1}{2} \left(1 + \cos \left(\frac{10\pi \left(t - \frac{9T_0}{10} \right)}{T_0} \right) \right) & \frac{9T_0}{10} \leq t \leq T_0 \end{cases} \quad (\text{B.7})$$

The time-series are then modified by:

$$\eta_{\text{mod}}(t) = \eta(t)d(t) \quad (\text{B.8})$$

Appendix C | Directions

In this appendix Case C1 is chosen to investigate the directions of long-crested waves in 360° in intervals of 10° . The results of each directions are stated in Table C.1 determined from Method 1 and Table C.2 determined from Method 2.

C.1 Method 1

Table C.1: Target and estimated values of the wave direction.

| Analysed direction, θ , $^\circ$ | Case | Generated direction, θ , $^\circ$ | | | | | | | | |
|---|------|--|--------|--------|--------|--------|--------|--------|--------|--------|
| | | 0 | 10 | 20 | 30 | 40 | 50 | 60 | 70 | 80 |
| | C1 | 0.71 | 10.66 | 20.53 | 30.38 | 40.24 | 50.11 | 60.03 | 70.00 | 80.00 |
| | | 90 | 100 | 110 | 120 | 130 | 140 | 150 | 160 | 170 |
| | C1 | 82.16 | 100.00 | 110.00 | 119.98 | 129.89 | 139.78 | 149.65 | 159.51 | 169.39 |
| | | 180 | 190 | 200 | 210 | 220 | 230 | 240 | 250 | 260 |
| | C1 | 179.29 | 189.34 | 199.48 | 209.62 | 219.76 | 229.89 | 239.97 | 250.00 | 260.00 |
| | | 270 | 280 | 290 | 300 | 310 | 320 | 330 | 340 | 350 |
| | C1 | 270.45 | 280.00 | 290.00 | 300.03 | 310.11 | 320.23 | 330.36 | 340.49 | 350.61 |

C.2 Method 2

Table C.2: Target and estimated values of the wave direction.

| Analysed mean direction, θ , $^\circ$ | Case | Generated direction, θ , $^\circ$ | | | | | | | | |
|--|------|--|--------|--------|--------|--------|--------|--------|--------|--------|
| | | 0 | 10 | 20 | 30 | 40 | 50 | 60 | 70 | 80 |
| | C1 | 0.00 | 10.02 | 20.01 | 30.00 | 40.01 | 50.02 | 60.00 | 70.00 | 80.02 |
| | | 90 | 100 | 110 | 120 | 130 | 140 | 150 | 160 | 170 |
| | C1 | 90.01 | 100.00 | 110.01 | 120.02 | 130.01 | 140.00 | 149.93 | 160.00 | 169.85 |
| | | 180 | 190 | 200 | 210 | 220 | 230 | 240 | 250 | 260 |
| | C1 | 180.00 | 190.02 | 200.01 | 210.00 | 220.00 | 230.00 | 239.99 | 250.00 | 260.01 |
| | | 270 | 280 | 290 | 300 | 310 | 320 | 330 | 340 | 350 |
| | C1 | 270.00 | 279.99 | 290.00 | 300.01 | 310.00 | 319.99 | 330.01 | 340.01 | 349.99 |

Table C.3: Target and estimated values of the spreading parameter.

| Analysed spreading parameter, s , [–] | Case | Spreading parameter, s , [–] | | | | | | | | |
|--|------|--------------------------------|-------|-------|-------|-------|-------|--------|-------|-------|
| | C1 | 85.03 | 85.11 | 85.11 | 85.11 | 85.11 | 84.93 | 85.11 | 85.11 | 85.11 |
| | C1 | 85.11 | 85.11 | 84.99 | 85.11 | 85.11 | 85.11 | 85.11 | 85.11 | 84.64 |
| | C1 | 84.95 | 85.11 | 85.02 | 85.11 | 84.83 | 85.11 | 85.11 | 85.11 | 85.11 |
| | C1 | 85.11 | 85.11 | 85.11 | 85.11 | 84.91 | 85.1 | 185.11 | 85.11 | 85.11 |

Appendix D | Second Order Wave Field

D.1 Bichromatic Wave Field

In this analysis, a simple bichromatic wave field is considered. The bichromatic wave field consists of the two wave components with the wave parameters stated in Table D.1. The waves are generated at a water depth of $h = 1.5$ m at sample frequency $f_s = 5$ Hz.

Table D.1: Regular wave components for bichromatic wave

| Component | Wave Height | Wave Period | Frequency | Direction |
|-----------|-------------|-------------|-----------|-----------|
| η_m | 0.3 m | 3 s | 0.3 Hz | 60° |
| η_n | 0.3 m | 2 s | 0.5 Hz | 30° |

The analysis of the direction is performed for the components that contain energy, which is determined from a frequency domain analysis of the synthetic surface elevation signals. The variance spectrum of the wave field is illustrated in Figure D.1. As the second order energy is much lower than the first order energy, a zoom of the spectrum is illustrated in Figure D.2.

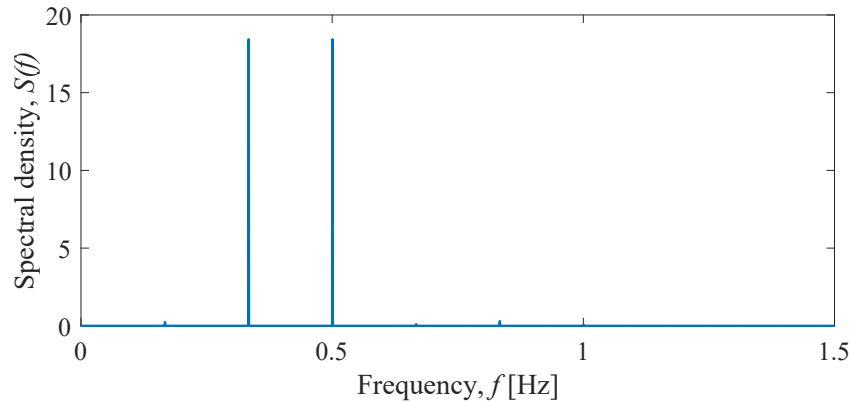


Figure D.1: Spectral density of wave field based on frequency domain analysis.

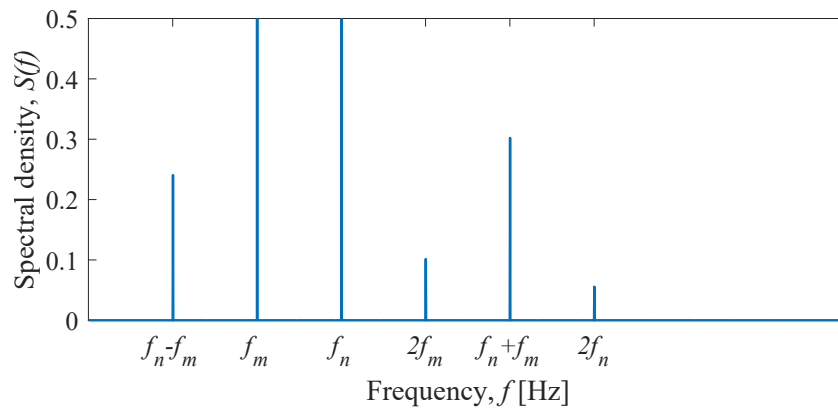


Figure D.2: Spectral density of wave field based on frequency domain analysis, zoomed to make second order energy visible.

The energy of the wave field in Figure D.2 is as expected with first order components at the two primary frequencies $f_m = 0.33$ Hz and $f_n = 0.50$ Hz and at the sub- and superharmonics due to the second order wave theory as elaborated in Section 2.2.1. The directional components of the first order contribution, θ_m and θ_n , similar interacts and generates directional components with other directions for the super- and subharmonics solved from the wave number. The principle is shown in Figure D.3 for the bichromatic wave.

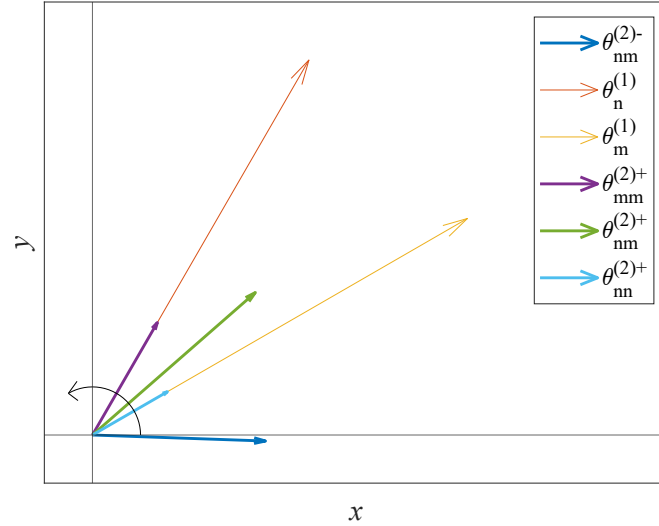


Figure D.3: Second order directional components.

This is not taken into account in the analysis method, because the MLM fitting method is based on linear wave theory of directional spectrum.

Throughout the analysis it is experienced that the direction is not possible to determine for some of the components, as the estimated distance between the two gauges in the direction of the wave, Δx , is too large compared to the distance between the gauges. This might be similar for some of the subharmonics, particular, because they are redistributed to a lower frequency which cause a larger period for that component. The estimated directions for the wave components appear from Figure D.4, where waves have been generated with a target direction of 40° .

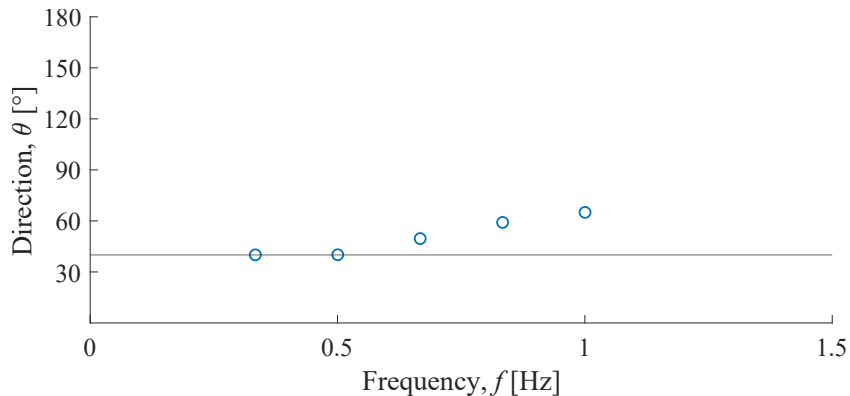


Figure D.4: Estimated direction for components in the wave field with target direction of 40° .

As it appears from Figure D.4, it was not possible to determine the direction of the subharmonic component. Furthermore the analysis shows that the estimated direction of the first order

components is very close to the target value, whereas the estimated direction of the second order components is far from the target value. As the energy of the second order components is low, the weighted value of the direction is calculated based on the spectral density of the components, that the analysis was able to determine the direction of.

The figures for all directions of all components can be found in Appendix AA. In general, the estimated direction of the second order components does not seem reliable. But if a weighted value of the direction is calculated based on the spectral density of each of the components, the estimated direction becomes less than 1° . It though seems that as long as the second order contribution is small, the nonlinearity is of insignificantly influence when determining the direction of a bichromatic wave field from a simple analysis based on the phase difference between the surface elevation signals in three different positions.

D.2 Irregular Wave Field

The irregular wave field is represented by the frequency distribution of a JONSWAP spectrum with the parameters of water depth, h , and a significant wave height, H_{m0} , as the eight cases presented in chapter 4. The spectral density of the case used as an example D2 is shown in Figure D.5, while the belonging estimated directions for all the wave components appear from Figure D.6, where waves have been generated with a target direction of 30° for Case D2.

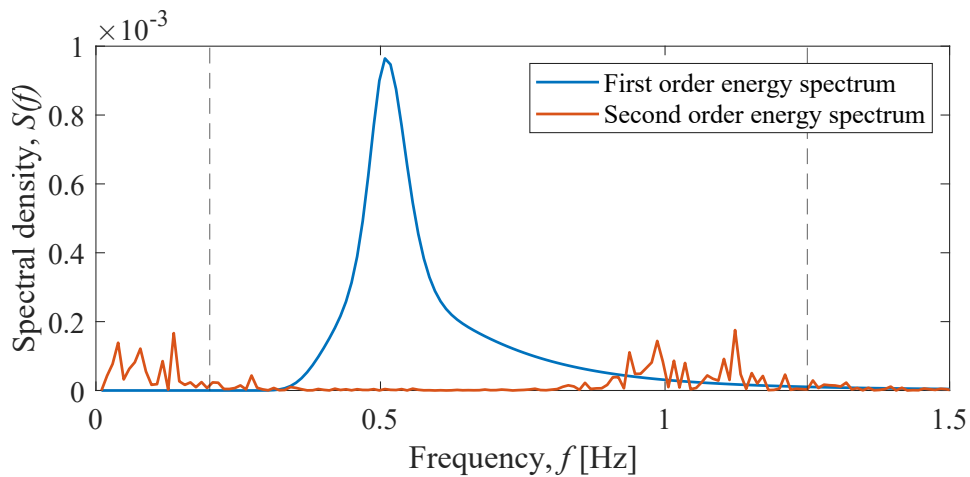


Figure D.5: Spectral density of wave field based on frequency domain analysis for Case D2.

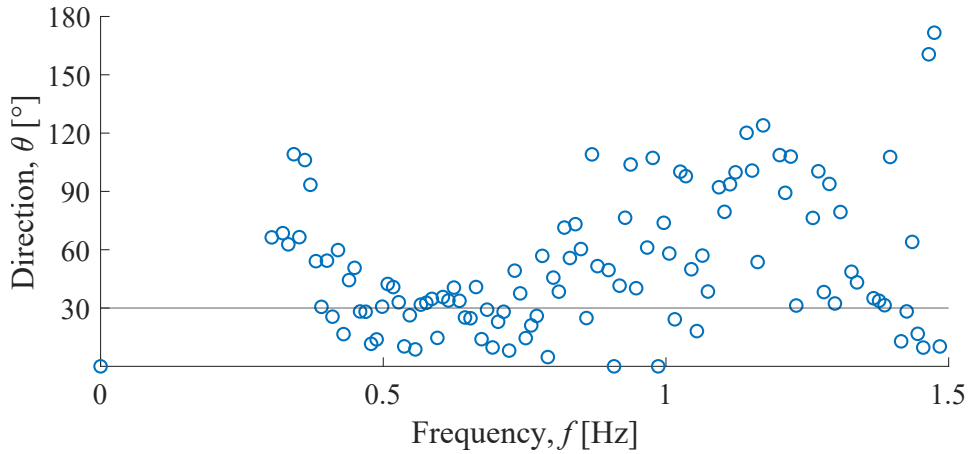


Figure D.6: Estimated direction for components in the wave field with target direction of 30° , Case D2.

It appears from Figure D.6 that the direction components of the different frequencies are placed around the line of target direction. If this is compared to Figure 5.2 the result shows that the estimated directions based on the first and second order components have a greater deviation than the estimated directions based on only the first order components. The weighted direction is then determined to be 44.11° , which is significantly larger compared to the first order direction components.

Waves from different directions in a range of 0° to 90° are investigated. Figures with results for Case A to H with target directions from 0° to 90° are plotted in Appendix AA. The analysed directions for the cases appear from Table D.2.

Table D.2: Target and estimated values of the wave direction.

| | Generated direction, θ , [°] | | | | | | | | | | |
|------------------------------------|-------------------------------------|-------|-------|-------|-------|-------|-------|-------|-------|-------|-------|
| Analysed direction, θ , [°] | | 0 | 10 | 20 | 30 | 40 | 50 | 60 | 70 | 80 | 90 |
| | Case A2 | 13.51 | 13.03 | 20.89 | 30.71 | 40.15 | 49.80 | 60.27 | 70.14 | 80.20 | 90.00 |
| | Case B2 | 4.50 | 10.41 | 20.52 | 30.33 | 40.21 | 50.11 | 60.01 | 70.00 | 80.00 | 90.00 |
| | Case C2 | 4.21 | 10.62 | 20.53 | 30.40 | 40.17 | 50.16 | 60.02 | 70.00 | 80.00 | 90.00 |
| | Case D2 | 43.77 | 43.92 | 47.25 | 44.11 | 55.06 | 62.29 | 65.67 | 75.73 | 85.67 | 90.00 |
| | Case E2 | 8.37 | 10.76 | 21.27 | 30.16 | 40.07 | 50.03 | 59.84 | 70.00 | 80.02 | 90.00 |
| | Case F2 | 8.97 | 10.39 | 20.01 | 30.59 | 40.35 | 49.84 | 59.85 | 70.06 | 80.02 | 90.00 |
| | Case G2 | 22.12 | 20.71 | 23.23 | 34.14 | 39.66 | 49.60 | 59.99 | 70.01 | 80.15 | 90.00 |
| | Case H2 | 21.88 | 18.64 | 22.70 | 30.30 | 41.15 | 50.84 | 60.42 | 70.14 | 80.47 | 90.00 |

The results of the estimated directions from Table D.2 indicate, that the cases D, G and H, which are placed outside the area where first order and second order wave theory are valid with regard to the Diagram of Le Mehaute, are not within a very accurate range, when analysing the direction using this simple method. Especially the estimated directions that are almost parallel to the wave gauges are inaccurate.

Table D.2 is compared to Table 5.1 to study how much the second order energy affects the calculation of the direction according to the weighted direction. It is discovered that the second order energy has an impact on the weighted direction for all cases which become more imprecise.

Appendix E | Convergence Study

In this appendix, a convergence study is performed to investigate the influence of the number of frequencies and the number of directions in the generation models, single and double summation, based on the precision of the results. All wave fields used in this study are synthetically generated first order waves.

Case G is used for the study of convergence for changing parameters which increase the resolution of the frequency and directional spectra. The parameters which are changed are the resolution of the auto spectrum by increasing the number of frequencies and the related number of subseries in the analysis. This is followed by changing the resolution of the directional spectrum where the number of directions is increased.

A synthetic wave field is generated with the different parameters of N and M, which is followed by an analysis, where the number of subseries is changed correspondingly, such that the number of frequencies in the analysis remains 512 for each subseries.

E.1 Single Summation Model

The changes of number of frequencies appear from Table E.1.

Table E.1: Changing resolution of convergence study.

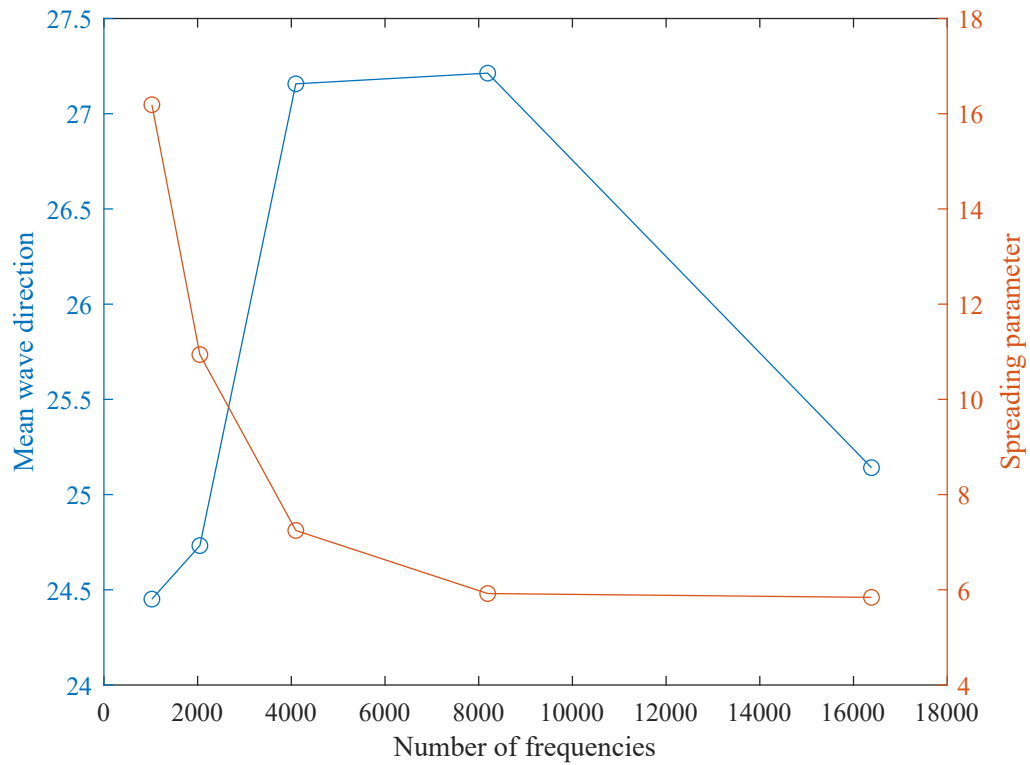
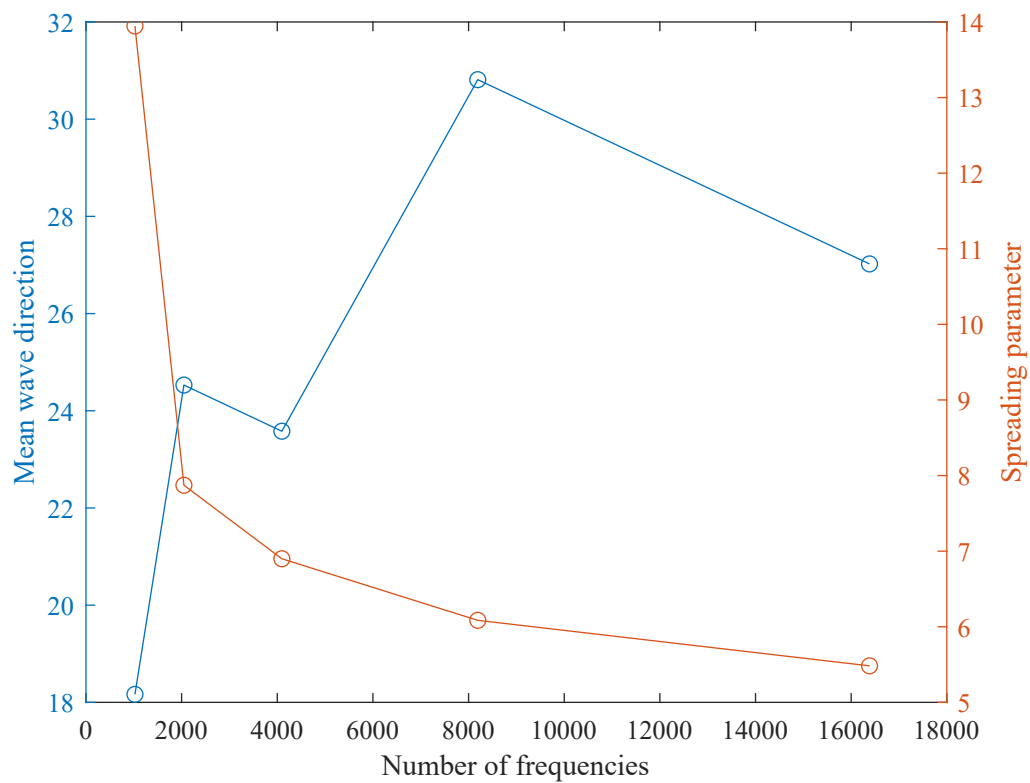
| | Study | | | | |
|--------------------------|-------------|----------|----------|----------|----------|
| Parameter | 1N | 2N | 3N | 4N | 5N |
| Number of frequencies, N | 2^{10} | 2^{11} | 2^{12} | 2^{13} | 2^{14} |
| Number of sub series, J | 2 | 4 | 8 | 16 | 30 |
| Figure | E.1 and E.2 | | | | |

The estimated values of the mean wave direction and directional spreading parameter are stated in Table E.2. Two tests with similar parameters are performed.

Table E.2: Estimated parameters of convergence study.

| Study | θ_0 | s | Study | θ_0 | s |
|-------|------------|-------|-------|------------|-------|
| 1Na | 26.66 | 11.35 | 1Nb | 18.16 | 13.95 |
| 2Na | 21.03 | 12.16 | 2Nb | 24.53 | 7.87 |
| 3Na | 27.16 | 7.25 | 3Nb | 23.58 | 6.90 |
| 4Na | 27.21 | 5.92 | 4Nb | 30.81 | 6.09 |
| 5Na | 25.14 | 5.84 | 5Nb | 27.02 | 5.48 |

In Figure E.1 and Figure E.2 the development of increasing the number of frequencies are shown.

Figure E.1: Case G1, 30° , $s = 5$, single summation a.Figure E.2: Case G1, 30° , $s = 5$, single summation b.

The figures show that the spreading parameter has converged and the mean wave direction has the tendency hereof too.

E.2 Double Summation Model

The double summation model is based on the same settings as the single summation model.

The changes of number of frequencies appear from Table E.3 and changes of number of directions appear from Table E.4.

Table E.3: Changing resolution of convergence study.

| | Study | | | | | | | | | |
|--------------------------|----------|----------|----------|----------|----------|----------|----------|----------|----------|----------|
| Parameter | 1N | 2N | 3N | 4N | 5N | 6N | 7N | 8N | 9N | 10N |
| Number of frequencies, N | 2^{10} | 2^{11} | 2^{12} | 2^{13} | 2^{14} | 2^{10} | 2^{11} | 2^{12} | 2^{13} | 2^{14} |
| Number of sub series, J | 2 | 4 | 8 | 16 | 30 | 2 | 4 | 8 | 16 | 30 |
| Number of directions, M | 30 | | | | | 90 | | | | |
| Figure | E.3 | | | | | E.4 | | | | |

Table E.4: Changing resolution of convergence study.

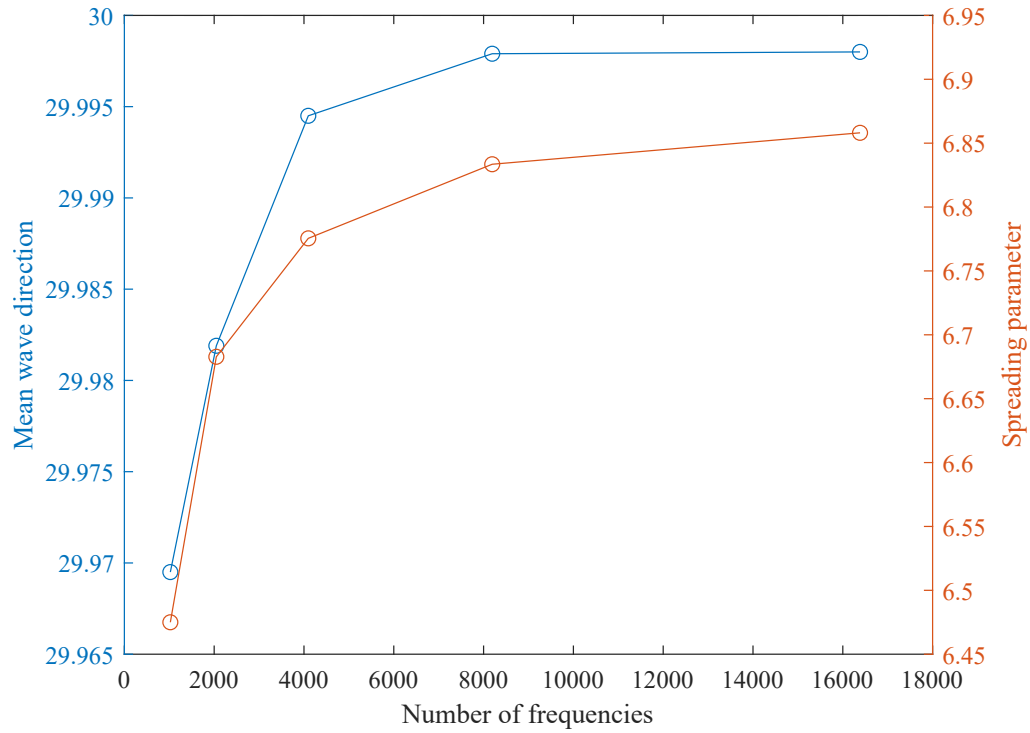
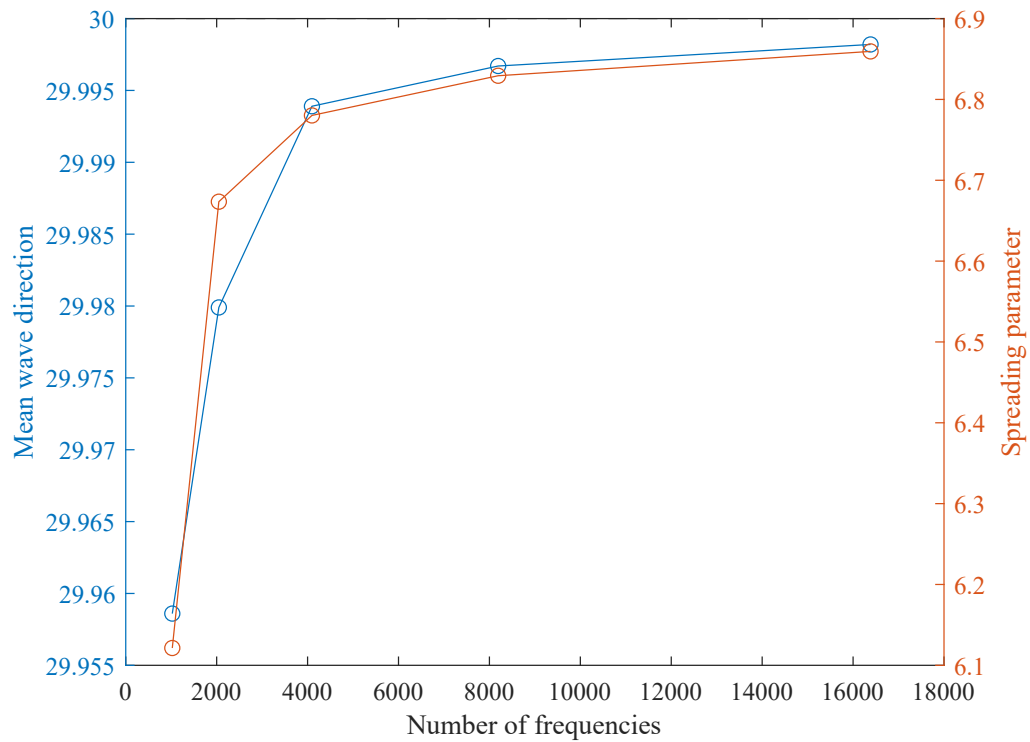
| | Study | | | | | | | | | |
|--------------------------|----------|----|----|----|----|----------|----|----|----|-----|
| Parameter | 1M | 2M | 3M | 4M | 5M | 6M | 7M | 8M | 9M | 10M |
| Number of frequencies, N | 2^{10} | | | | | 2^{14} | | | | |
| Number of sub series, J | 2 | | | | | 30 | | | | |
| Number of directions, M | 30 | 45 | 60 | 75 | 90 | 30 | 45 | 60 | 75 | 90 |
| Figure | E.5 | | | | | E.6 | | | | |

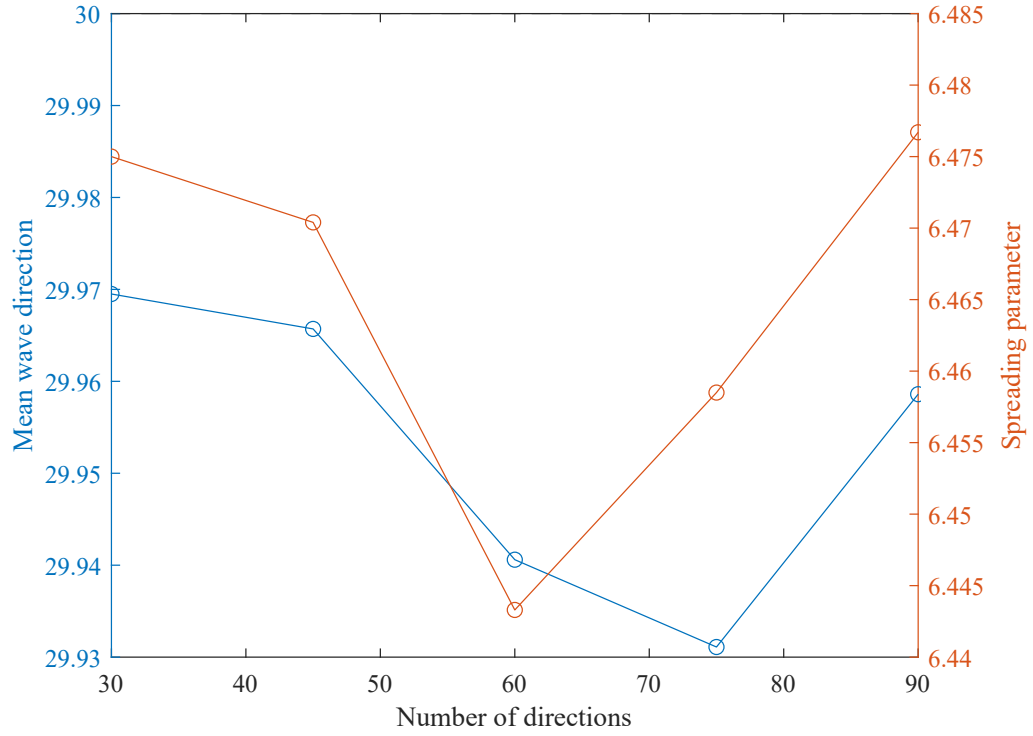
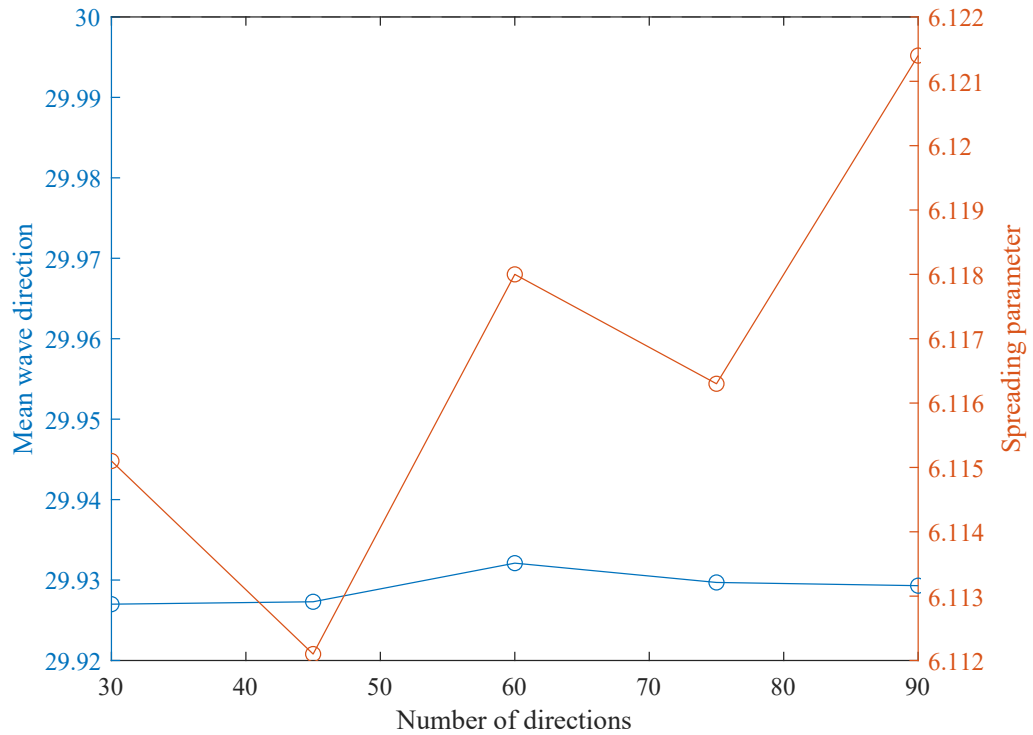
The estimated values of the mean wave direction and directional spreading parameter are stated in Table E.5.

Table E.5: Estimated parameters of convergence study.

| Study | θ_0 | s | Study | θ_0 | s |
|-------|------------|------|-------|------------|------|
| 1N | 29.97 | 6.48 | 1M | 29.97 | 6.48 |
| 2N | 29.98 | 6.68 | 2M | 29.97 | 6.47 |
| 3N | 29.99 | 6.78 | 3M | 29.94 | 6.44 |
| 4N | 30.00 | 6.83 | 4M | 29.93 | 6.46 |
| 5N | 30.00 | 6.86 | 5M | 29.96 | 6.48 |
| 6N | 29.96 | 6.12 | 6M | 29.93 | 6.11 |
| 7N | 29.98 | 6.67 | 7M | 29.93 | 6.12 |
| 8N | 29.99 | 6.78 | 8M | 29.93 | 6.12 |
| 9N | 30.00 | 6.83 | 9M | 29.93 | 6.12 |
| 10N | 30.00 | 6.86 | 10M | 29.96 | 6.48 |

In Figure E.3 and Figure E.4 the development of increasing the number of frequencies are shown, while Figure E.5 and Figure E.6 the development of increasing the number of directions are shown.

Figure E.3: Case G1, 30° , $s = 5$, double summation. $M=30$.Figure E.4: Case G1, 30° , $s = 5$, double summation. $M=90$.

Figure E.5: Case G1, 30° , $s = 5$, double summation. $N=2^{10}$ Figure E.6: Case G1, 30° , $s = 5$, double summation. $N=2^{14}$

Appendix F | Short-Crested Waves in More Directions

In this appendix three other mean wave directions different from the one outlined in the report are analysed. In the report both a single and double summation model are used to generate wave field of first order theory, second order theory and waves with amplitude dispersion for the target mean wave direction of 30° with a spreading parameter of 5. In this appendix, the target wave direction is analysed in three other directions, 60° , 90° and 120° .

First, the weighted results of the mean wave direction and spreading parameter are analysed for the wave field generated from the single summation model for first order waves, which is followed by an analysis of the the wave field generated from the single double model for first order waves. This is followed by an analysis of the second order and amplitude dispersion waves.

The data is generated by the single summation model, which uses $N = 2^{14}$ frequency components, while the double summation model uses $N = 2^{10}$ frequency components and $M = 30$ directional components. This data is analysed by the use of $J = 30$ and $J = 2$ subseries, respectively.

In this appendix, the spreading parameter, s , is not converted to the spreading in degrees, σ .

F.1 First Order Waves

Table F.1: Results of MLM estimation of directional spreading of short-crested waves based on linear wave theory with target values $\theta_0 = 60^\circ$ and $s = 5$.

| Single Summation | | | Double Summation | | |
|------------------|---|-----------------------------------|------------------|---|-----------------------------------|
| Case | Mean wave direction θ_0 [$^\circ$] | Spreading parameter s [-] | Case | Mean wave direction θ_0 [$^\circ$] | Spreading parameter s [-] |
| A1 | 53.00° | 5.88 | A1 | 59.81° | 5.56 |
| B1 | 54.33° | 5.81 | B1 | 59.96° | 6.11 |
| C1 | 56.14° | 6.03 | C1 | 59.96° | 5.96 |
| D1 | 53.26° | 5.68 | D1 | 59.83° | 5.55 |
| E1 | 53.29° | 6.05 | E1 | 59.93° | 6.08 |
| F1 | 56.68° | 6.47 | F1 | 59.96° | 5.96 |
| G1 | 55.08° | 6.06 | G1 | 59.95° | 6.09 |
| H1 | 55.28° | 5.89 | H1 | 59.97° | 5.95 |

Table F.2: Results of MLM estimation of directional spreading of short-crested waves based on linear wave theory with target values $\theta_0 = 90^\circ$ and $s = 5$.

| Single Summation | | | Double Summation | | |
|------------------|---------------------------------------|--------------------------------|------------------|---------------------------------------|--------------------------------|
| Case | Mean wave direction θ_0 [°] | Spreading parameter s [-] | Case | Mean wave direction θ_0 [°] | Spreading parameter s [-] |
| A1 | 82.16° | 5.17 | A1 | 89.95° | 5.57 |
| B1 | 83.16° | 6.40 | B1 | 90.01° | 6.11 |
| C1 | 84.31° | 5.81 | C1 | 90.00° | 5.98 |
| D1 | 85.91° | 5.41 | D1 | 89.92° | 5.56 |
| E1 | 81.48° | 5.91 | E1 | 89.99° | 6.13 |
| F1 | 82.59° | 5.59 | F1 | 89.99° | 5.97 |
| G1 | 82.80° | 5.85 | G1 | 90.01° | 6.08 |
| H1 | 85.17° | 5.91 | H1 | 89.99° | 5.98 |

Table F.3: Results of MLM estimation of directional spreading of short-crested waves based on linear wave theory with target values $\theta_0 = 120^\circ$ and $s = 5$.

| Single Summation | | | Double Summation | | |
|------------------|---------------------------------------|--------------------------------|------------------|---------------------------------------|--------------------------------|
| Case | Mean wave direction θ_0 [°] | Spreading parameter s [-] | Case | Mean wave direction θ_0 [°] | Spreading parameter s [-] |
| A1 | 114.77° | 5.73 | A1 | 120.10° | 5.57 |
| B1 | 115.86° | 5.28 | B1 | 120.036° | 6.10 |
| C1 | 113.23° | 5.28 | C1 | 120.05° | 5.96 |
| D1 | 115.13° | 5.89 | D1 | 120.17° | 5.56 |
| E1 | 115.66° | 6.09 | E1 | 120.04° | 6.10 |
| F1 | 113.60° | 5.54 | F1 | 120.05° | 5.97 |
| G1 | 110.40° | 6.31 | G1 | 120.05° | 6.09 |
| H1 | 113.02° | 5.92 | H1 | 120.08° | 5.96 |

F.2 Second Order Waves

Table F.4: Results of MLM estimation of directional spreading of short-crested waves based on second wave theory with target values $\theta_0 = 60^\circ$ and $s = 5$.

| Single Summation | | | Double Summation | | |
|------------------|---------------------------------------|--------------------------------|------------------|---------------------------------------|--------------------------------|
| Case | Mean wave direction θ_0 [°] | Spreading parameter s [-] | Case | Mean wave direction θ_0 [°] | Spreading parameter s [-] |
| A2 | 52.95° | 5.74 | A2 | 60.00° | 5.44 |
| B2 | 54.32° | 5.81 | B2 | 59.95° | 6.11 |
| C2 | 56.15° | 6.03 | C2 | 59.95° | 5.96 |
| D2 | 52.71° | 5.37 | D2 | 72.55° | 5.17 |
| E2 | 53.29° | 6.04 | E2 | 59.95° | 6.08 |
| F2 | 56.68° | 6.47 | F2 | 60.00° | 5.97 |
| G2 | 55.09° | 5.92 | G2 | 59.43° | 5.92 |
| H2 | 55.29° | 5.81 | H2 | 59.51° | 5.85 |

Table F.5: Results of MLM estimation of directional spreading of short-crested waves based on second wave theory with target values $\theta_0 = 90^\circ$ and $s = 5$.

| Single Summation | | | Double Summation | | |
|------------------|---------------------------------------|--------------------------------|------------------|---------------------------------------|--------------------------------|
| Case | Mean wave direction θ_0 [°] | Spreading parameter s [-] | Case | Mean wave direction θ_0 [°] | Spreading parameter s [-] |
| A2 | 82.19° | 5.03 | A2 | 90.08° | 5.45 |
| B2 | 83.16° | 6.40 | B2 | 90.00° | 6.10 |
| C2 | 84.31° | 5.81 | C2 | 90.00° | 5.98 |
| D2 | 85.39° | 5.17 | D2 | 97.85° | 5.33 |
| E2 | 81.47° | 5.90 | E2 | 89.97° | 6.13 |
| F2 | 82.59° | 5.58 | F2 | 90.05° | 5.97 |
| G2 | 82.84° | 5.68 | G2 | 90.03° | 5.90 |
| H2 | 85.21° | 5.82 | H2 | 90.07° | 5.95 |

Table F.6: Results of MLM estimation of directional spreading of short-crested waves based on second wave theory with target values $\theta_0 = 120^\circ$ and $s = 5$.

| Single Summation | | | Double Summation | | |
|------------------|---------------------------------------|--------------------------------|------------------|---------------------------------------|--------------------------------|
| Case | Mean wave direction θ_0 [°] | Spreading parameter s [-] | Case | Mean wave direction θ_0 [°] | Spreading parameter s [-] |
| A2 | 114.78° | 5.61 | A2 | 120.07° | 5.42 |
| B2 | 115.86° | 5.28 | B2 | 120.03° | 6.11 |
| C2 | 113.23° | 5.28 | C2 | 120.05° | 5.96 |
| D2 | 113.46° | 5.72 | D2 | 126.47° | 5.32 |
| E2 | 115.68° | 6.08 | E2 | 120.04° | 6.10 |
| F2 | 113.60° | 5.54 | F2 | 120.09° | 5.96 |
| G2 | 110.48° | 6.17 | G2 | 120.27° | 5.92 |
| H2 | 113.06° | 5.83 | H2 | 120.19° | 5.94 |

F.3 Waves with Amplitude Dispersion

Table F.7: Results of MLM estimation of directional spreading of short-crested waves based on waves with amplitude dispersion with target values $\theta_0 = 60^\circ$ and $s = 5$.

| Single Summation | | | Double Summation | | |
|------------------|---------------------------------------|--------------------------------|------------------|---------------------------------------|--------------------------------|
| Case | Mean wave direction θ_0 [°] | Spreading parameter s [-] | Case | Mean wave direction θ_0 [°] | Spreading parameter s [-] |
| A3 | 55.87° | 6.08 | A3 | 59.84° | 5.76 |
| D3 | 54.89° | 4.69 | D3 | 59.31° | 4.25 |
| G3 | 53.61° | 5.94 | G3 | 59.95° | 5.89 |

Table F.8: Results of MLM estimation of directional spreading of short-crested waves based on waves with amplitude dispersion with target values $\theta_0 = 90^\circ$ and $s = 5$.

| Single Summation | | | Double Summation | | |
|------------------|---------------------------------------|--------------------------------|------------------|---------------------------------------|--------------------------------|
| Case | Mean wave direction θ_0 [°] | Spreading parameter s [-] | Case | Mean wave direction θ_0 [°] | Spreading parameter s [-] |
| A3 | 83.82° | 4.93 | A3 | 89.98° | 5.75 |
| D3 | 83.07° | 4.62 | D3 | 89.85° | 4.23 |
| G3 | 84.31° | 5.77 | G3 | 89.99° | 5.90 |

Table F.9: Results of MLM estimation of directional spreading of short-crested waves based on waves with amplitude dispersion with target values $\theta_0 = 120^\circ$ and $s = 5$.

| Single Summation | | | Double Summation | | |
|------------------|---------------------------------------|--------------------------------|------------------|---------------------------------------|--------------------------------|
| Case | Mean wave direction θ_0 [°] | Spreading parameter s [-] | Case | Mean wave direction θ_0 [°] | Spreading parameter s [-] |
| A3 | 114.01° | 5.45 | A3 | 120.10° | 5.78 |
| D3 | 113.77° | 4.33 | D3 | 120.54° | 4.26 |
| G3 | 112.89° | 5.82 | G3 | 120.06° | 5.89 |

From these results of the estimated mean wave direction and spreading parameter, it is discovered that the overall deviations are in the same size for the same generation model and the same order. Therefore, a single target direction of 30° is studied and used in the main report.

Appendix G | Variability due to Number of Subseries

In this appendix, the variability due to the limited number of subseries used for the analysis of short-crested waves generated based on the double summation model will be investigated.

Due to the required computational capacity in relation to generation of data based on the double summation model, the influence of the variability is here studied by performing different analyses of the same data set. A single test case and direction is here considered, Case D with target mean direction of 30° and spreading parameter $s = 5$. Data sets of different duration are considered in order to identify the influence of number of subseries versus the resolution of the frequency domain in the analysis. For the generation of the data, $M = 30$ number of directional components and a sample frequency of $f_s = 5$ Hz is used.

Table G.1: Duration and resolution of investigated data sets.

| Duration, T_0 | Number of components in frequency domain, N |
|--------------------|--|
| 204.6 s | 1024 |
| 409.4 s | 2048 |
| 819.0 s | 4096 |

First, the wave field containing solely the first order energy will be analysed with different number of subseries for each analysis. As the duration of each data set remains constant, an increase in number subseries will reduce the number of frequency components. Next, the wave field containing the first order as well as the second order contribution is considered. The different analyses will be evaluated based on the mean direction as well as the spreading of the waves. The results related to the mean direction appear from Figure G.1 to G.3 for the data sets of different duration.

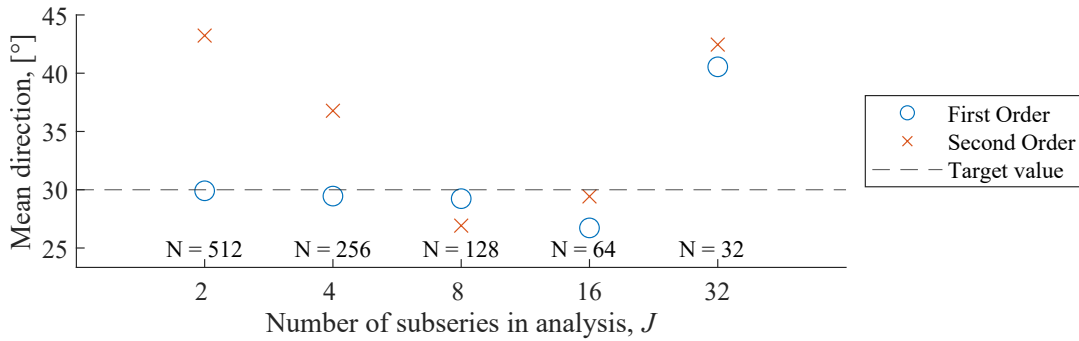


Figure G.1: Estimated mean direction for analysis with different number of subseries for data set with $N = 1024$ used for generation.

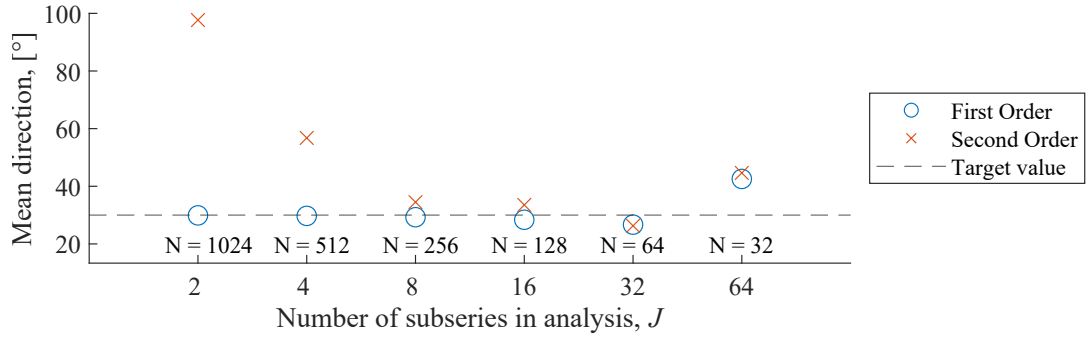


Figure G.2: Estimated mean direction for analysis with different number of subseries for data set with $N = 2048$ used for generation.

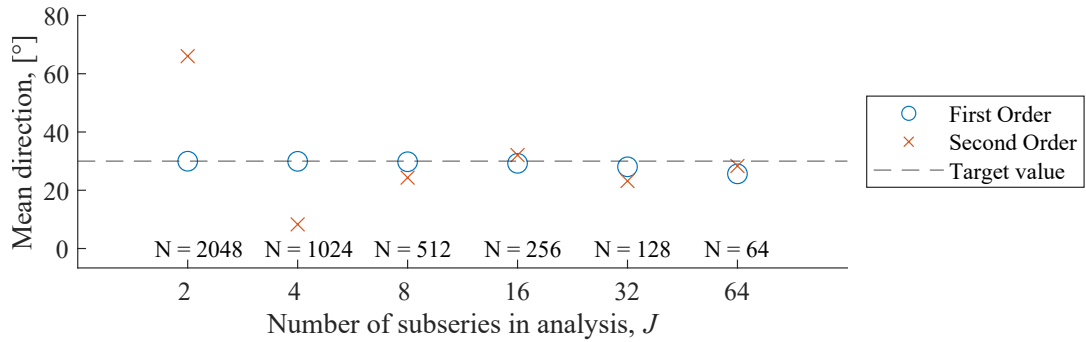


Figure G.3: Estimated mean direction for analysis with different number of subseries for data set with $N = 4096$ used for generation.

Based on the estimated mean wave directions in Figure G.1 to G.3, the estimated mean direction of the first order waves tends to be rather accurate until the number of frequency components reach a critical value of $N = 32$, and thereby less accurate for increasing number of subseries. For the analysis of the second order waves, the influence of the second order contribution seem to decrease with increasing number of subseries. An interesting thing to notice in Figure G.2, is that analyses of the same data set can over- and well as underestimate the mean direction based on the resolution used for the analysis, which emphasizes the studied variability.

For determination of the mean wave direction within an accuracy of $\pm 5^\circ$, the present analyses show that a minimum of 8 should be used for analysis, with no less than $N = 32$ frequency components in the interval $0 \text{ Hz} < f < f_s$ for each subseries, as it will cause a very limited number of components being inside the truncation of the spectrum. Hereby, the nonlinear effects are of insignificant size, although 38.6% of the energy stems from second order contributions for the given test case, which is the highest amount of second order energy investigated in this paper.

Figure G.4 to G.6 illustrate the corresponding spreading of waves in degrees for the performed analyses.

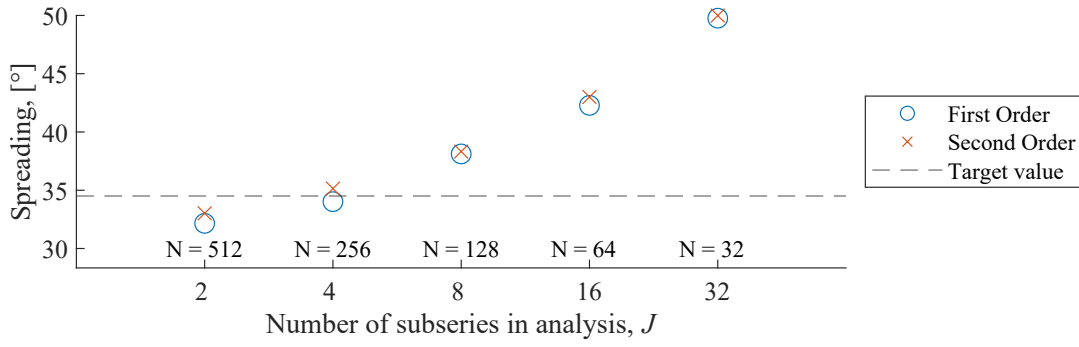


Figure G.4: Estimated spreading of waves for data set with $N = 1024$ used for generation.

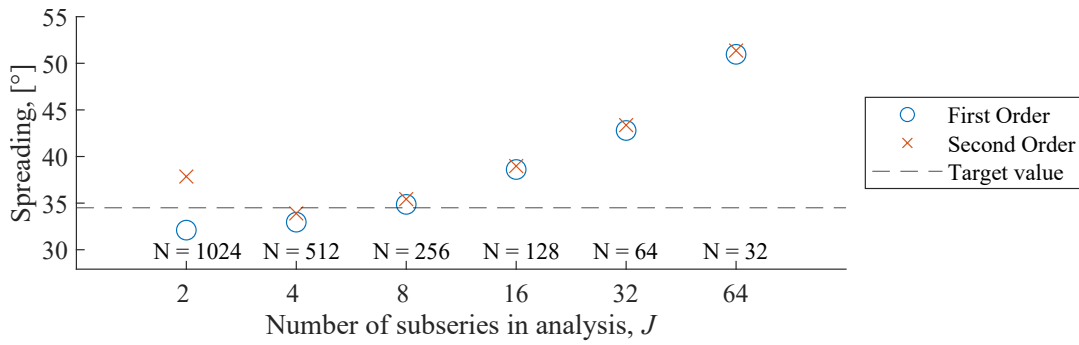


Figure G.5: Estimated spreading of waves for data set with $N = 2048$ used for generation.

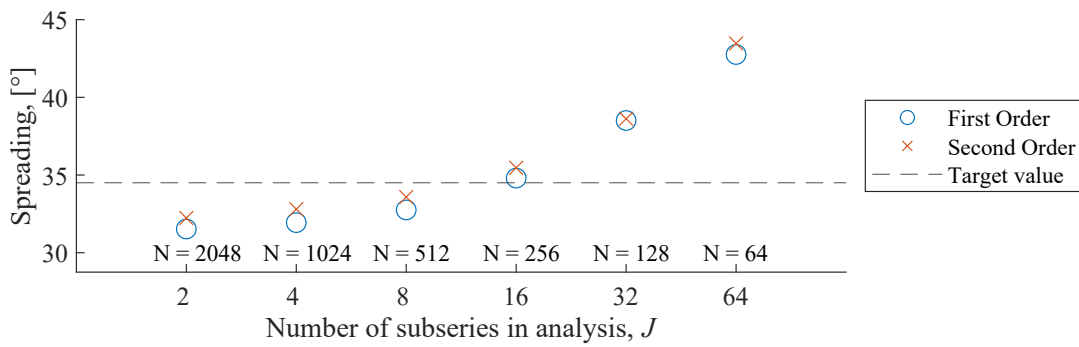


Figure G.6: Estimated spreading of waves for data set with $N = 4096$ used for generation.

As seen from the figures, the spreading seems to increase with increasing number of subseries and thereby also decreasing number of analysed frequency components used in the analysis. In opposition to the mean direction of the waves, the accuracy of the spreading does not seem to depend on the number of subseries, but on the resolution of the frequency domain instead. For all three data sets, the spreading is closest to the target spreading of the waves for analyses performed with $N = 256$ frequency components in the interval $0 \text{ Hz} < f < f_s$.

As this appendix deals with data generated based on the double summation model, the known possible problem related to the large requirement of components in order to generate a certain quality of the wave field. As an example, the analysed spectra for the largest data set for each

of the six wave gauges in the CERC6 array appear from Figure G.7.

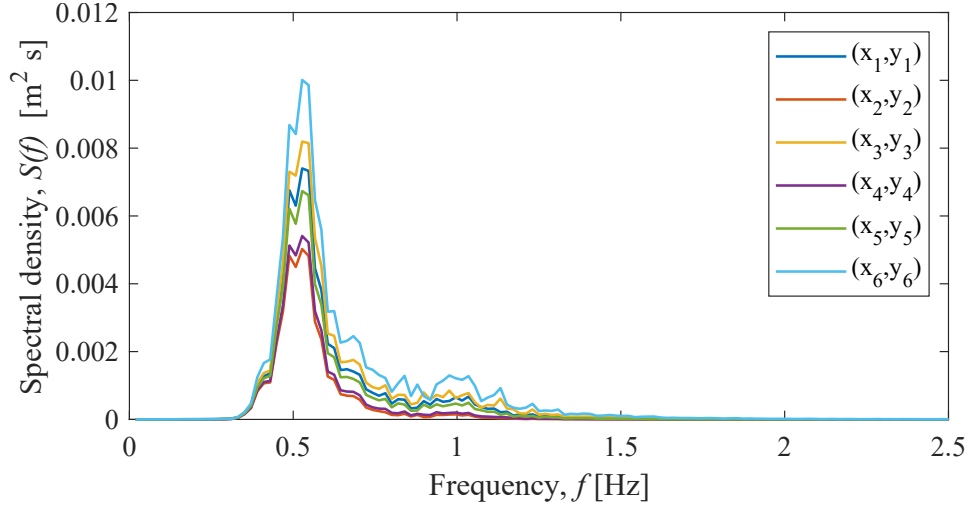


Figure G.7: Spectral density determined based on surface elevation measurements in the six wave gauge positions of the CERC6 array.

As seen in Figure G.7, the data set does not seem to be ergodic, as the analysed spectral density differs for the different wave gauge measurements, which indicate a poor quality of the generated data. Despite the fact that the irregular surface elevation does not fulfill the assumptions of the analysis method, the adjustment of the subseries and number of frequencies still seems to increase the reliability of the directional parameters based on the present analyses. It should be kept in mind that the present analyses only considers a single direction and a single test case, wherefore further studies should be performed in order to state general tendencies covering all wave fields.

Generally, the current study have hereby shown that the choice of number of subseries is a compromise between resolution and reliability of the analysis, and that the reliability of the estimated mean direction and spreading of the waves do not depend on similar parameters.

Appendix H | Analysis of Signal with Noise Added

In this appendix the weighted results of the directional analysis of first and second order waves and waves with amplitude dispersion including noise at the surface elevation signals.

H.1 Long-Crested Waves

H.1.1 Analysis of First Order Waves

In Figure H.1, Case D1 including noise is plotted with the estimated wave direction and the spreading shown with the target direction of 30° .

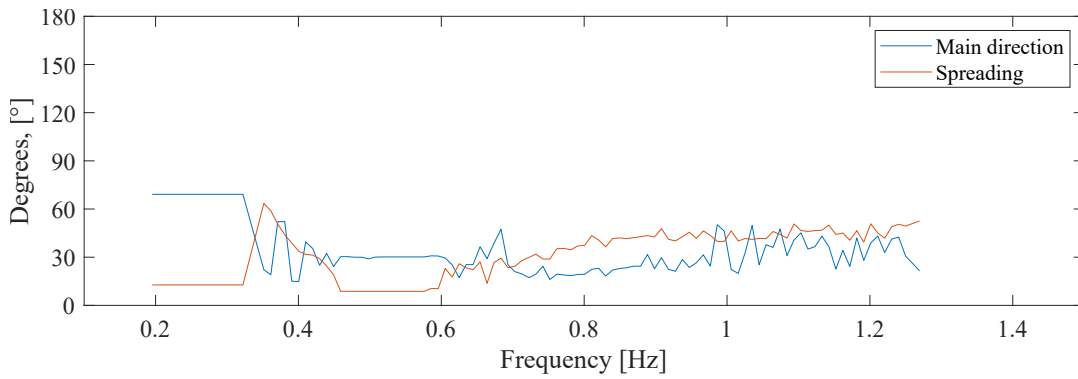


Figure H.1: Estimated direction for components in the wave field with target direction of 30° , Case D1.

The figure shows that the estimated mean direction, θ_0 , become more inaccurate compared to the estimated direction for first order waves without noise. The figure shows that the estimated mean direction is less sensitive in the frequency range with large energy components, i.e. in this case at frequency components of approximately $\pm 0.1f_p$. The weighted estimated directions for all the cases appear from Table H.1 for the directions from 0° to 90° where noise is added to the signal.

Table H.1: Estimated values of the wave direction for first order waves.

| Analysed direction, θ_0 , $^\circ$ | Generated direction, θ , $^\circ$ | | | | | | | | | |
|---|--|-------|-------|-------|-------|-------|-------|-------|-------|-------|
| | 0 | 10 | 20 | 30 | 40 | 50 | 60 | 70 | 80 | 90 |
| Case A1 | -0.77 | 10.75 | 20.51 | 29.86 | 40.79 | 50.17 | 59.65 | 69.67 | 81.54 | 90.62 |
| Case B1 | -0.08 | 10.68 | 20.59 | 30.82 | 39.97 | 49.20 | 58.92 | 69.69 | 80.32 | 90.00 |
| Case C1 | -0.44 | 10.60 | 20.01 | 28.66 | 40.10 | 51.06 | 61.67 | 69.27 | 81.33 | 89.23 |
| Case D1 | -0.48 | 11.30 | 19.77 | 28.97 | 40.19 | 50.09 | 60.91 | 69.70 | 80.95 | 90.40 |
| Case E1 | 0.11 | 11.48 | 18.59 | 30.38 | 40.08 | 50.27 | 59.32 | 69.57 | 79.82 | 89.38 |
| Case F1 | -0.48 | 10.93 | 18.87 | 29.91 | 41.02 | 50.54 | 60.13 | 70.62 | 79.55 | 91.17 |
| Case G1 | -0.92 | 10.16 | 20.38 | 31.04 | 39.75 | 50.05 | 60.93 | 70.29 | 79.95 | 90.86 |
| Case H1 | 0.98 | 11.23 | 20.41 | 30.13 | 39.69 | 50.33 | 59.43 | 70.96 | 80.43 | 91.19 |

The results show that the estimated mean directions, θ_0 , deviates with maximum $\pm 2.34^\circ$ from the target directions, which are generally more imprecise compared to the results stated in Table 6.1, but still in a low magnitude of deviation. The deviation of the weighted estimated directions are stated in Table H.2.

Table H.2: Estimated values of the wave direction for first order waves - Difference to first order estimated values of the wave direction without noise.

| Analysed direction, θ_0 , [°] | Generated direction, θ , [°] | | | | | | | | | |
|--------------------------------------|-------------------------------------|------|-------|-------|-------|-------|-------|-------|-------|-------|
| | 0 | 10 | 20 | 30 | 40 | 50 | 60 | 70 | 80 | 90 |
| Case A1 | -0.77 | 0.68 | 0.48 | -0.26 | 0.75 | 0.10 | 0.37 | -0.33 | 1.47 | 0.58 |
| Case B1 | -0.08 | 0.66 | 0.51 | 0.92 | -0.04 | -0.87 | -1.09 | -0.31 | 0.30 | -0.01 |
| Case C1 | -0.44 | 0.40 | 0.00 | -2.34 | -0.09 | 1.05 | 1.67 | -0.63 | 1.31 | -0.74 |
| Case D1 | -0.48 | 1.28 | -0.20 | -1.04 | 0.14 | 0.02 | 0.88 | -0.30 | 0.88 | 0.35 |
| Case E1 | 0.11 | 1.46 | -1.42 | 0.38 | 0.07 | 0.26 | -0.68 | -0.43 | -0.20 | -0.63 |
| Case F1 | -0.48 | 0.91 | -1.14 | -0.09 | 1.01 | 0.52 | 0.13 | 0.62 | -0.47 | 1.16 |
| Case G1 | -0.92 | 0.14 | 0.37 | 1.04 | -0.26 | 0.03 | 0.93 | 0.29 | -0.07 | 0.85 |
| Case H1 | 0.98 | 1.21 | 0.40 | 0.13 | -0.32 | 0.31 | -0.57 | 0.96 | 0.41 | 1.18 |

H.1.2 Analysis of Second Order Waves

Further, the synthetically generated waves including second order energy and white Gaussian noise are investigated. The signal to noise ratio is equal to the aforementioned. In Figure H.2, Case D2 with the estimated direction and the spreading shown with the target direction of 30° is shown.

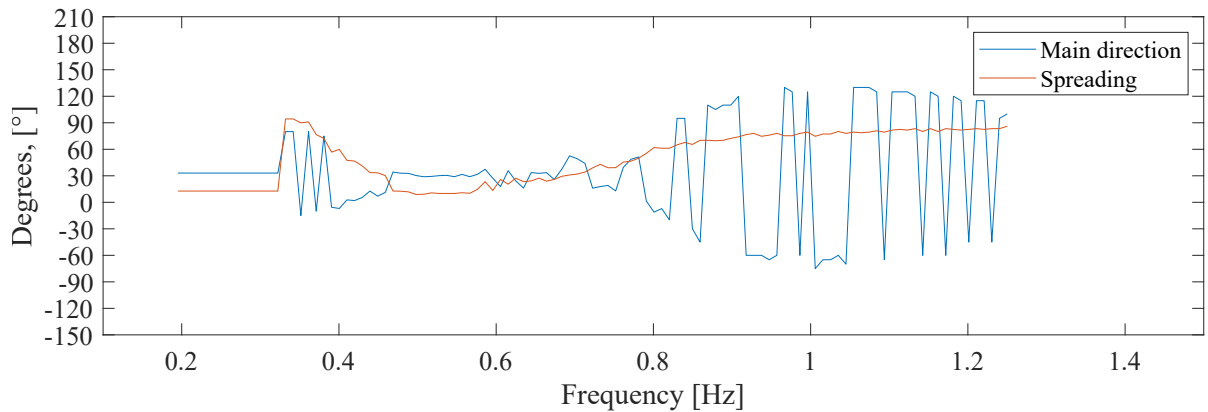


Figure H.2: Estimated direction for components in the wave field with target direction of 30° , Case D2.

The figure shows that the frequency range, where the estimated mean direction is still unaffected by the white Gaussian noise, has become smaller compared to the frequency range in Figure H.1 and the deviations of the estimated mean direction components are larger, generally. The weighted estimated mean directions for all the cases appear from Table H.3 for second order waves for the directions from 0° to 90° where the white Gaussian noise is added to the signal.

Table H.3: Estimated values of the wave direction for second order waves.

| | Generated direction, θ , [°] | | | | | | | | | | |
|--------------------------------------|-------------------------------------|-------|-------|-------|-------|-------|-------|-------|-------|-------|-------|
| Analysed direction, θ_0 , [°] | | 0 | 10 | 20 | 30 | 40 | 50 | 60 | 70 | 80 | 90 |
| | Case A2 | 0.63 | 10.59 | 20.18 | 30.27 | 41.20 | 50.05 | 59.44 | 69.88 | 80.30 | 89.55 |
| | Case B2 | -0.20 | 11.47 | 20.71 | 30.52 | 40.32 | 50.03 | 60.35 | 71.80 | 80.74 | 89.98 |
| | Case C2 | 0.80 | 19.64 | 21.46 | 30.38 | 40.74 | 50.18 | 60.63 | 69.05 | 80.38 | 89.34 |
| | Case D2 | -1.84 | 16.14 | 23.55 | 28.15 | 47.84 | 54.00 | 59.77 | 64.56 | 83.71 | 88.97 |
| | Case E2 | -1.30 | 11.98 | 19.48 | 28.01 | 39.89 | 51.53 | 61.13 | 69.20 | 80.29 | 92.21 |
| | Case F2 | -0.41 | 10.42 | 20.54 | 29.59 | 40.66 | 51.46 | 59.16 | 69.90 | 80.70 | 90.82 |
| | Case G2 | -1.00 | 27.48 | 18.53 | 25.45 | 48.32 | 53.36 | 57.10 | 75.90 | 78.42 | 91.93 |
| | Case H2 | 3.26 | 10.97 | 19.42 | 30.84 | 40.32 | 53.58 | 59.31 | 72.68 | 81.94 | 91.04 |

The difference of the results of the estimated weighted direction compared to the second order waves are stated in Table H.4.

Table H.4: Estimated values of the wave direction for second order waves - Difference to second order estimated values of the wave direction without noise.

| | Generated direction, θ , [°] | | | | | | | | | | |
|--------------------------------------|-------------------------------------|-------|-------|-------|-------|-------|-------|-------|-------|-------|-------|
| Analysed direction, θ_0 , [°] | | 0 | 10 | 20 | 30 | 40 | 50 | 60 | 70 | 80 | 90 |
| | Case A2 | 1.58 | 0.33 | 0.20 | 0.19 | 1.81 | -0.13 | -0.65 | -0.09 | 0.51 | -0.61 |
| | Case B2 | -0.20 | 1.45 | 0.69 | 0.51 | 0.30 | 0.00 | 0.34 | 1.80 | 0.72 | -0.05 |
| | Case C2 | 0.81 | -0.38 | 1.43 | 0.38 | 0.72 | 0.15 | 0.61 | -0.95 | 0.36 | -0.68 |
| | Case D2 | -3.16 | -1.50 | 5.82 | 5.18 | -1.58 | -6.64 | 0.01 | 0.16 | -2.80 | 0.03 |
| | Case E2 | -1.31 | 1.94 | -0.66 | -2.14 | -0.12 | 1.50 | 0.98 | -0.87 | 0.30 | 2.16 |
| | Case F2 | -0.41 | 0.33 | 0.44 | -0.52 | 0.65 | 1.43 | -0.97 | -0.15 | 0.69 | 0.69 |
| | Case G2 | 2.42 | -3.77 | -0.59 | -5.44 | 9.68 | 3.01 | -2.73 | 3.77 | -3.53 | 2.20 |
| | Case H2 | 2.88 | -1.02 | -0.89 | 1.74 | 1.00 | 2.62 | -2.10 | 1.77 | 2.62 | 2.07 |

H.1.3 Analysis Waves with Amplitude Dispersion

Further, the synthetically generated waves including wave with amplitude dispersion and white Gaussian noise are investigated. In Figure H.3, Case D2 with the estimated direction and the spreading shown with the target direction of 30° is shown.

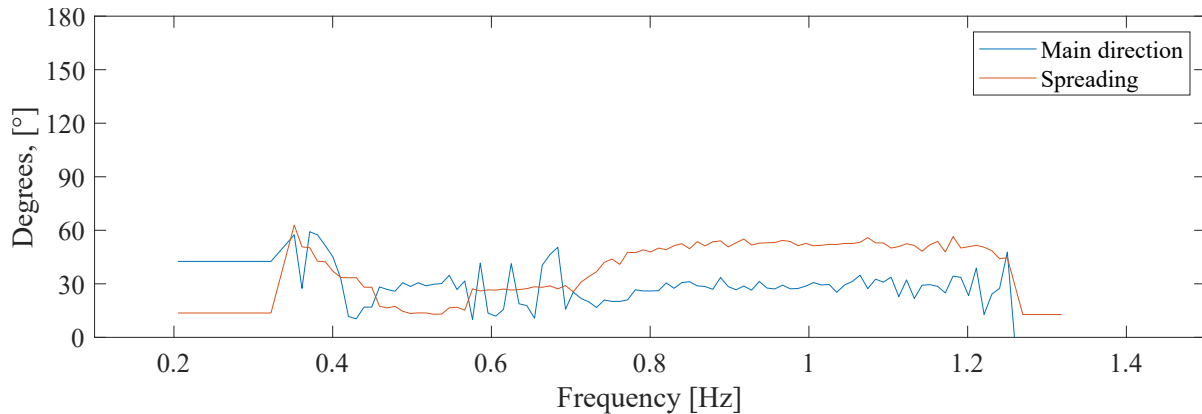


Figure H.3: Estimated direction for components in the wave field with target direction of 30°, Case D3.

The weighted estimated mean directions for all the cases appear from Table H.5 for second order waves for the directions from 0° to 90° where the white Gaussian noise is added to the signal.

Table H.5: Estimated values of the wave direction for waves with amplitude dispersion.

| $\theta_0, [^\circ]$ | Generated direction, $\theta, [^\circ]$ | | | | | | | | | | |
|----------------------|---|-------|-------|-------|-------|-------|-------|-------|-------|-------|-------|
| | | 0 | 10 | 20 | 30 | 40 | 50 | 60 | 70 | 80 | 90 |
| Case A3 | | 1.11 | 10.95 | 20.13 | 30.20 | 40.80 | 50.84 | 59.89 | 70.18 | 81.16 | 90.61 |
| Case D3 | | -1.15 | 8.15 | 22.14 | 27.23 | 43.33 | 44.95 | 60.21 | 68.65 | 78.86 | 88.22 |
| Case G3 | | 1.30 | 12.23 | 20.92 | 28.43 | 40.38 | 50.15 | 59.50 | 71.60 | 80.31 | 88.57 |

The difference of the results of the estimated weighted direction compared to waves with amplitude dispersion are stated in Table H.6.

Table H.6: Estimated values of the wave direction for waves with amplitude dispersion
- Difference to the estimated values of the wave direction without noise.

| $\theta_0, [^\circ]$ | Generated direction, $\theta, [^\circ]$ | | | | | | | | | | |
|----------------------|---|-------|-------|-------|-------|------|-------|-------|-------|-------|-------|
| | | 0 | 10 | 20 | 30 | 40 | 50 | 60 | 70 | 80 | 90 |
| Case A3 | | 1.11 | 0.47 | -0.33 | -0.22 | 0.75 | 0.69 | -0.23 | 0.14 | 1.01 | 0.47 |
| Case D3 | | -1.15 | -2.08 | 2.18 | -2.51 | 2.99 | -5.21 | 0.30 | -1.23 | -1.44 | -1.80 |
| Case G3 | | 1.30 | 2.21 | 0.92 | -1.65 | 0.30 | 0.13 | -0.54 | 1.28 | 0.21 | -1.44 |

H.2 Short-Crested Waves

H.2.1 Analysis of First Order Waves

The results of the directional analysis of first order waves are shown for Case D1 with the estimated direction and the spreading shown with the target direction of 30° . In Figure H.4 the results are based on a single summation model, while in Figure H.5 the results are based on an equivalent double summation model.

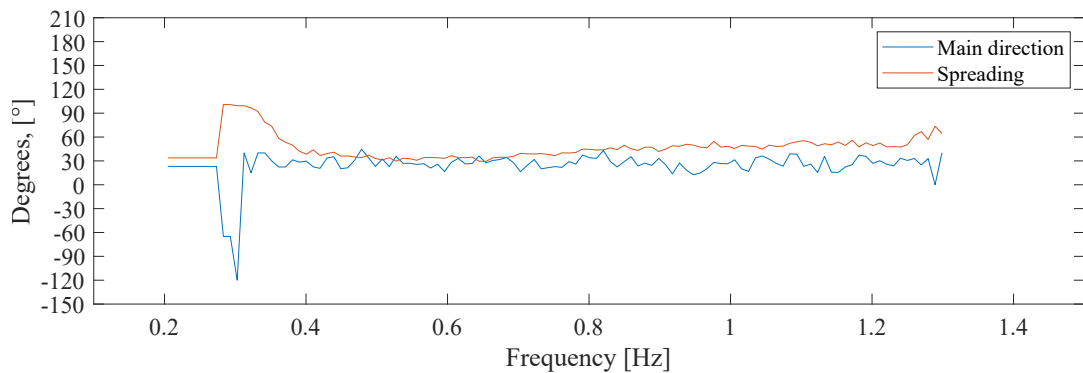


Figure H.4: Estimated direction for components in the wave field with target direction of 30° , Case D1. Generated from single summation model.

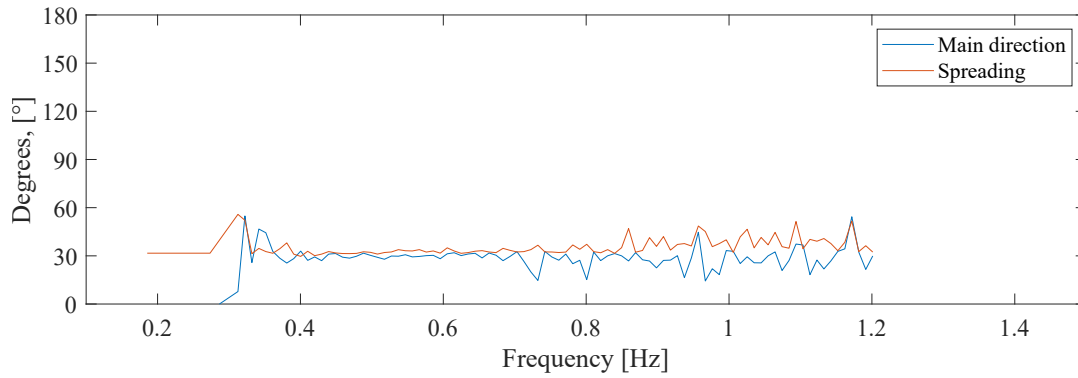


Figure H.5: Estimated direction for components in the wave field with target direction of 30° , Case D1. Generated from double summation model.

The estimated mean wave directions and spreading parameters from first order waves of the short-crested wave field which are analysed in chapter 7 are used as benchmark for the analysis of the same parameters of a signal with noise included. The results are shown in Table H.7 for the short-crested waves modelled by single summation, and results for short-crested waves modelled by double summation are stated in Table H.8. Both tables include the differences to the results analysed without including noise from Table 7.2, and Table 7.3, respectively.

Table H.7: Results of MLM estimation of directional spreading of short-crested waves based on linear wave theory with target values $\theta_0 = 30^\circ$ and $\sigma = 34.5^\circ$.

| Single Summation | | | Deviation from first order theory. | | |
|------------------|--|--------------------------------|------------------------------------|--|--------------------------------|
| Case | Mean wave direction $\theta_0 [^\circ]$ | Spreading $\sigma [^\circ]$ | Case | Mean wave direction $\theta_0 [^\circ]$ | Spreading $\sigma [^\circ]$ |
| A1 | 26.41° | 35.27° | A1 | -0.15° | 3.05° |
| B1 | 30.79° | 39.61° | B1 | 1.20° | 7.48° |
| C1 | 29.00° | 38.31° | C1 | -0.12° | 7.17° |
| D1 | 28.38° | 36.24° | D1 | -0.08° | 3.66° |
| E1 | 31.93° | 41.58° | E1 | 2.86° | 9.50° |
| F1 | 29.63° | 43.29° | F1 | 2.29° | 10.02° |
| G1 | 29.48° | 41.13° | G1 | 4.11° | 8.90° |
| H1 | 28.39° | 40.86° | H1 | 0.78° | 8.42° |

The weighted estimated mean wave directions are deviating in the range of maximum $\pm 2.86^\circ$, while the weighted spreading in degrees deviate with 10.02° compared to the analysis of first order wave without noise included. This means that the results of the analysis of the short-crested waves show that the fitted directional spreading function are distributed over a wider directional span with a minor peak of energy.

In Table H.8 the double summation model is used to generate the wave fields analysed results of the estimated mean wave directions and the spreading. The weighted estimated mean wave directions are deviating with up to $\pm 0.78^\circ$, while the weighted spreading parameters only deviate with 0.50° compared to the analysis of first order wave without noise included. This make a better fit of the weighted spreading parameter, but the model do not improve the result of the weighted estimated mean wave direction.

Table H.8: Results of MLM estimation of directional spreading of short-crested waves based on linear wave theory with target values $\theta_0 = 30^\circ$ and $\sigma = 34.5^\circ$.

| Double Summation | | | Deviation from first order theory. | | |
|------------------|---------------------------------------|---------------------------|------------------------------------|---------------------------------------|---------------------------|
| Case | Mean wave direction θ_0 [°] | Spreading σ [°] | Case | Mean wave direction θ_0 [°] | Spreading σ [°] |
| A1 | 29.98° | 32.38° | A1 | 0.07° | 0.19° |
| B1 | 29.95° | 31.06° | B1 | 0.00° | 0.36° |
| C1 | 30.70° | 31.32° | C1 | 0.76° | 0.36° |
| D1 | 29.65° | 32.60° | D1 | -0.26° | 0.41° |
| E1 | 29.97° | 31.12° | E1 | 0.00° | 0.41° |
| F1 | 30.37° | 31.50° | F1 | 0.43° | 0.50° |
| G1 | 29.15° | 31.08° | G1 | -0.78° | 0.34° |
| H1 | 30.28° | 31.57° | H1 | 0.30° | 0.63° |

H.2.2 Analysis of Second Order Waves

The results of the directional analysis of second order waves are also shown for Case D2 with the estimated direction and the spreading shown with the target direction of 30° . The comparable results are plotted in Figure H.6, where the results are based on the single summation model and in Figure H.7, where the results are based on the double summation model.

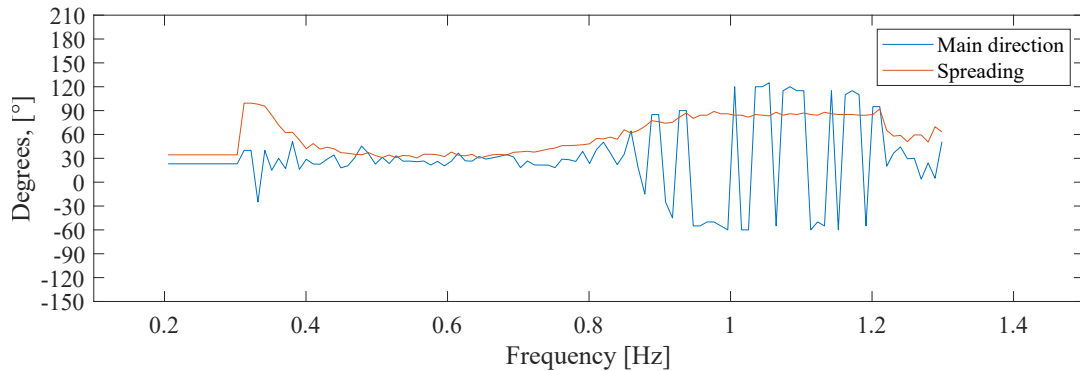


Figure H.6: Estimated direction for components in the wave field with target direction of 30° , Case D2. Generated from single summation model.

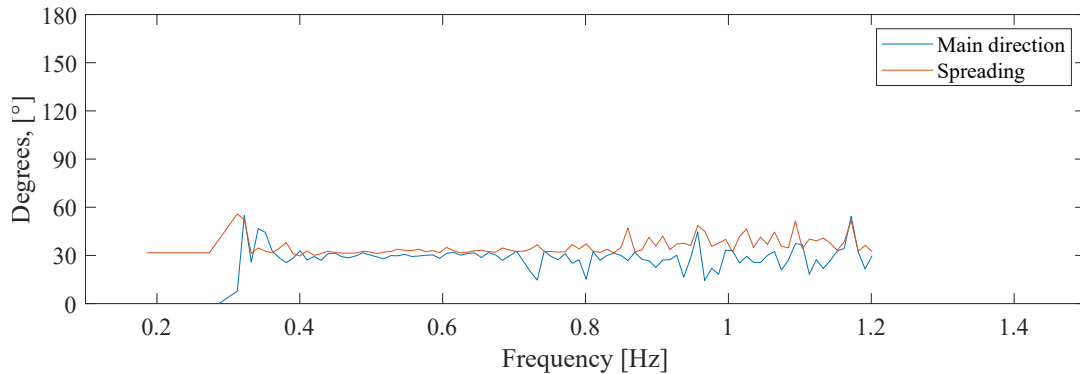


Figure H.7: Estimated direction for components in the wave field with target direction of 30° , Case D2. Generated from double summation model.

Similarly, the estimated mean wave directions and spreading parameters from second order waves

of the short-crested wave field are used as benchmark for the analysis of the same parameters of a signal with noise included. The results are shown in Table H.9 for the short-crested waves modelled by single summation, and results for short-crested waves modelled by double summation are stated in Table H.10. Both tables include the differences to the results analysed without including noise from Table 7.4 and Table 7.5, respectively.

Table H.9: Results of MLM estimation of directional spreading of short-crested waves based on second order wave theory with target values $\theta_0 = 30^\circ$ and $\sigma = 34.5^\circ$.

| Single Summation | | | Deviation from second order theory. | | |
|------------------|--|--------------------------------|-------------------------------------|--|--------------------------------|
| Case | Mean wave direction $\theta_0 [^\circ]$ | Spreading $\sigma [^\circ]$ | Case | Mean wave direction $\theta_0 [^\circ]$ | Spreading $\sigma [^\circ]$ |
| A2 | 26.30° | 35.73° | A2 | -0.22° | 2.91° |
| B2 | 29.78° | 38.99° | B2 | 0.18° | 6.84° |
| C2 | 29.67° | 38.26° | C2 | 0.54° | 7.11° |
| D2 | 46.59° | 41.35° | D2 | -1.44° | 2.45° |
| E2 | 29.91° | 41.10° | E2 | 0.87° | 8.96° |
| F2 | 29.83° | 43.21° | F2 | 2.47° | 9.90° |
| G2 | 26.49° | 42.33° | G2 | 0.64° | 8.23° |
| H2 | 28.10° | 42.03° | H2 | 0.19° | 8.19° |

The weighted estimated mean wave directions are deviating with up to $\pm 2.47^\circ$, while the weighted spreading in degrees for all cases only deviate with 9.90° compared to the analysis of second order wave without noise included.

Table H.10: Results of MLM estimation of directional spreading of short-crested waves based on second order wave theory with target values $\theta_0 = 30^\circ$ and $\sigma = 34.5^\circ$.

| Double Summation | | | Deviation from second order theory. | | |
|------------------|--|--------------------------------|-------------------------------------|--|--------------------------------|
| Case | Mean wave direction $\theta_0 [^\circ]$ | Spreading $\sigma [^\circ]$ | Case | Mean wave direction $\theta_0 [^\circ]$ | Spreading $\sigma [^\circ]$ |
| A2 | 33.00° | 33.52° | A2 | 0.89° | 0.79° |
| B2 | 29.89° | 31.22° | B2 | -0.06° | 0.52° |
| C2 | 29.59° | 31.25° | C2 | -0.37° | 0.29° |
| D2 | 55.83° | 39.96° | D2 | 12.60° | 6.56° |
| E2 | 30.82° | 31.40° | E2 | 0.81° | 0.69° |
| F2 | 30.05° | 31.55° | F2 | 0.10° | 0.56° |
| G2 | 30.22° | 31.80° | G2 | 0.51° | 0.44° |
| H2 | 30.11° | 31.73° | H2 | 0.36° | 0.48° |

The weighted estimated mean wave directions are deviating with up to -12.60° again for Case D2, which show the sensitivity of the determination of the weighted estimated mean wave direction in the analysis tool, when the amount of second energy is large enough. The other cases are deviating with up to $\pm 0.89^\circ$, while the weighted spreading in degrees for all cases only deviate with 0.79° compared to the analysis of second order wave without noise included. This shows that the weighted mean wave direction might be difficult to estimate when including both second order energy even though the generation model is double summation. But the weighted spreading parameters determined from this model deviate with approximately a tenth compared to the spreading parameters analysed based on the single summation model.

H.2.3 Analysis of Waves with Amplitude Dispersion

The results of the directional analysis of higher order waves are shown for Case D3 with the estimated direction and the spreading shown with the target values $\theta_0 = 30^\circ$ and $\sigma = 34.5^\circ$. In Figure H.8 the results are based on the single summation model, while in Figure H.9 shows the results which are based on the double summation model.

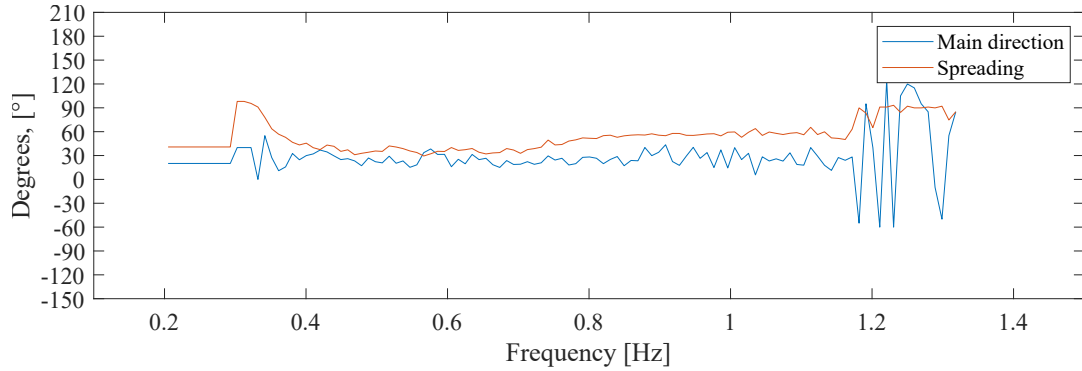


Figure H.8: Estimated direction for components in the wave field with target direction of 30° , Case D3. Single summation model.

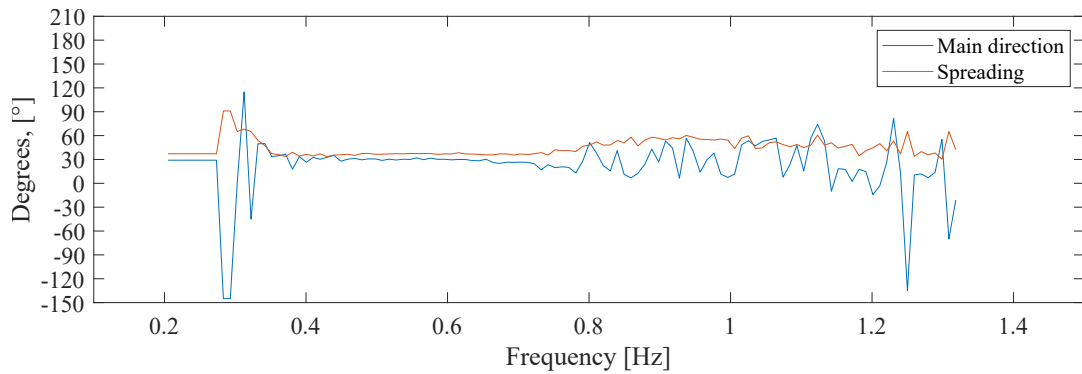


Figure H.9: Estimated direction for components in the wave field with target direction of 30° , Case D3. Double summation model.

The results of the weighted estimated mean wave directions and the spreading parameters and their deviation from the analysed parameters without noise added stated in Table 7.7 appear from Table H.11 based on a single summation model and from Table H.12 based on a double summation model.

Table H.11: Results of MLM estimation of directional spreading of short-crested waves based on amplitude dispersion with target values $\theta_0 = 30^\circ$ and $\sigma = 34.5^\circ$ generated from a single summation model.

| Single Summation | | | Deviation from higher order results. | | |
|------------------|---------------------------------------|---------------------------|--------------------------------------|---------------------------------------|---------------------------|
| Case | Mean wave direction θ_0 [°] | Spreading σ [°] | Case | Mean wave direction θ_0 [°] | Spreading σ [°] |
| A3 | 27.19° | 37.47° | A3 | 0.05° | 3.13° |
| D3 | 26.23° | 39.68° | D3 | 1.61° | 2.96° |
| G3 | 28.01° | 40.76° | G3 | 0.32° | 7.86° |

The deviation of the weighted estimated mean wave directions are up to $\pm 1.61^\circ$, which is in

the same magnitude of deviation as for the the analysis of first order wave field generated by the double summation model with noise included. The weighted spreading in degrees deviates with up to 7.86° , which was in the same order for the analysis of the second order wave field generated by a single summation model.

Table H.12: Results of MLM estimation of directional spreading of short-crested waves based on amplitude dispersion with target values $\theta_0 = 30^\circ$ and $\sigma = 34.5^\circ$ generated from a double summation model.

| Double Summation | | | Deviation from higher order results. | | |
|------------------|--|--------------------------------|--------------------------------------|--|--------------------------------|
| Case | Mean wave direction $\theta_0 [^\circ]$ | Spreading $\sigma [^\circ]$ | Case | Mean wave direction $\theta_0 [^\circ]$ | Spreading $\sigma [^\circ]$ |
| A3 | 29.91° | 32.71° | A3 | 0.10° | 0.30° |
| D3 | 30.20° | 37.87° | D3 | 1.40° | 0.25° |
| G3 | 29.76° | 32.97° | G3 | -0.11° | 0.81° |

The table show that the deviation of the weighted estimated mean wave directions are up to $\pm 1.40^\circ$, which is also in the same magnitude of deviation as for the the analysis of first order wave field generated by the double summation model with noise included. The deviation of the weighted spreading in degrees is with up to 0.81° , which is also in the same order for the analysis of the first order wave field generated by a double summation model. This means that the amplitude dispersion combined with noise yield a more accurate estimate of the weighted spreading parameter compared to the analysis of the second order wave field generated from a double summation model.

Appendix I | Errors Related to Calibration

I.1 Long-Crested Waves

I.1.1 Analysis of First Order Waves

Calibration Error Gauge 1

In this test 5% is added to the first order signal of the surface elevation, where the factor 1.05 is multiplied to the signal at wave gauge in position (x_1, y_1) . The result of the estimated mean direction and the spreading are shown in Figure I.1 for Case D1 with generated first order waves.

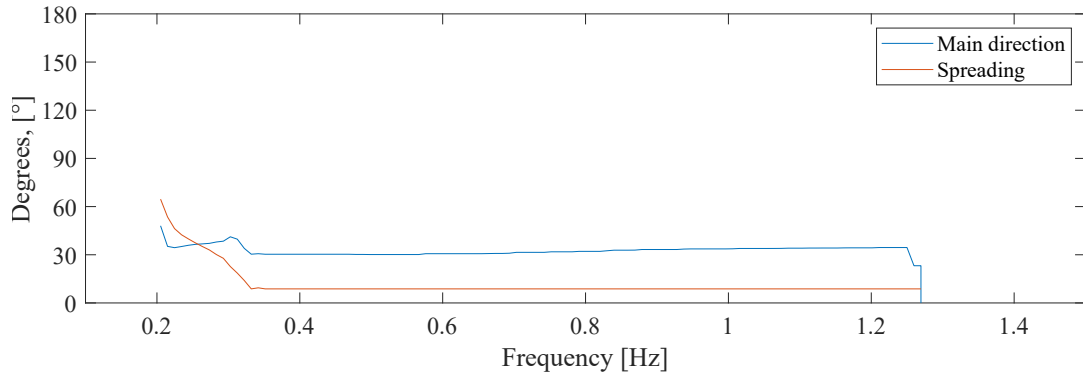


Figure I.1: Estimated direction for components in the wave field with target direction of 30° , Case D1 with error due to calibration added at one wave gauge in position (x_1, y_1) .

This figure is compared to Figure 6.1 where the estimated mean direction components formed a horizontal line from the frequencies above 0.3 Hz. The weighted value appears from Table I.1 where the example of Case D1 for the target direction of 30° is increased from 30.00° to 30.75° . The analysed mean directions and spreading parameters for all the cases appear from Table I.1 for the directions from 0° to 90° .

Table I.1: Estimated values of the wave direction for first order waves with one wave gauge in position (x_1, y_1) with calibration error at 5 %.

| | Generated direction, θ , [°] | | | | | | | | | | |
|--------------------------------------|-------------------------------------|------|-------|-------|-------|-------|-------|-------|-------|-------|-------|
| Analysed direction, θ_0 , [°] | | 0 | 10 | 20 | 30 | 40 | 50 | 60 | 70 | 80 | 90 |
| | Case A1 | 0.00 | 10.84 | 21.17 | 31.43 | 41.80 | 52.03 | 62.11 | 72.13 | 81.15 | 90.58 |
| | Case B1 | 0.00 | 10.07 | 20.27 | 30.75 | 41.06 | 51.25 | 61.80 | 71.27 | 81.01 | 90.13 |
| | Case C1 | 0.00 | 10.09 | 20.21 | 30.34 | 40.50 | 50.57 | 60.54 | 70.53 | 80.44 | 90.21 |
| | Case D1 | 0.00 | 10.07 | 20.27 | 30.75 | 41.06 | 51.25 | 61.80 | 71.27 | 81.01 | 90.13 |
| | Case E1 | 0.00 | 10.09 | 20.21 | 30.40 | 40.44 | 50.63 | 60.60 | 70.48 | 80.44 | 90.46 |
| | Case F1 | 0.00 | 11.56 | 21.48 | 30.70 | 40.68 | 50.76 | 60.78 | 70.74 | 80.65 | 90.41 |
| | Case G1 | 0.00 | 10.09 | 20.23 | 30.41 | 40.58 | 50.61 | 60.88 | 70.61 | 80.61 | 90.14 |
| | Case H1 | 0.00 | 10.08 | 20.23 | 30.36 | 40.49 | 50.58 | 60.56 | 70.51 | 80.45 | 90.23 |

To evaluate on the inclusion of calibration errors, the results are compared to the values determined based on data without calibration error. The differences are illustrated in Figure I.2 and I.3.

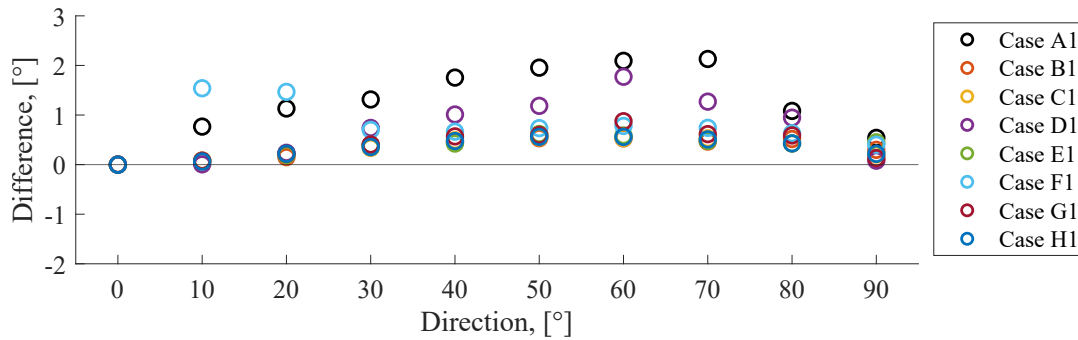


Figure I.2: Difference in estimated mean direction of long-crested first order waves with calibration error on gauge in position (x_1, y_1) compared to value determined based on data without calibration error.

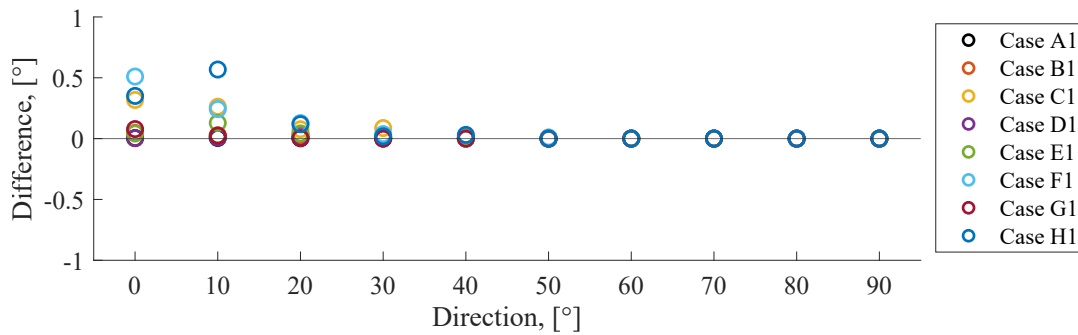


Figure I.3: Difference in estimated spreading of long-crested first order waves with calibration error on gauge in position (x_1, y_1) compared to value determined based on data without calibration error.

As seen from Figure I.2, the errors of the weighted estimated directions are in general increased all in the same positive direction compared to the results of the weighted estimated directions analysed from unaffected first order waves. Especially, Case A1, D1 and F1 have the largest deviation from the estimated mean direction analysed from first order waves with up to 2.09° . Furthermore, all the cases except Case F1, follows the same pattern, which peak around the direction of 60 to 70° . This indicates a tendency, which might be related to specific affected gauge.

In relation to the difference in the spreading of the waves in Figure I.3, it appears that the inclusion of calibration errors on the gauge in position (x_1, y_1) does not have any influence on the spreading of waves of first order wave theory.

Calibration Error Gauge 1 and 2

For this test 5% is again added to the first order signal of the surface elevation, but added to two of the measured signals to investigate how the errors accelerate according to calibration errors added to more wave gauges. The two wave gauges are placed in the position of (x_1, y_1) and (x_2, y_2) . The result of the estimated mean direction and the spreading are shown in Figure I.4 for Case G with generated first order waves.

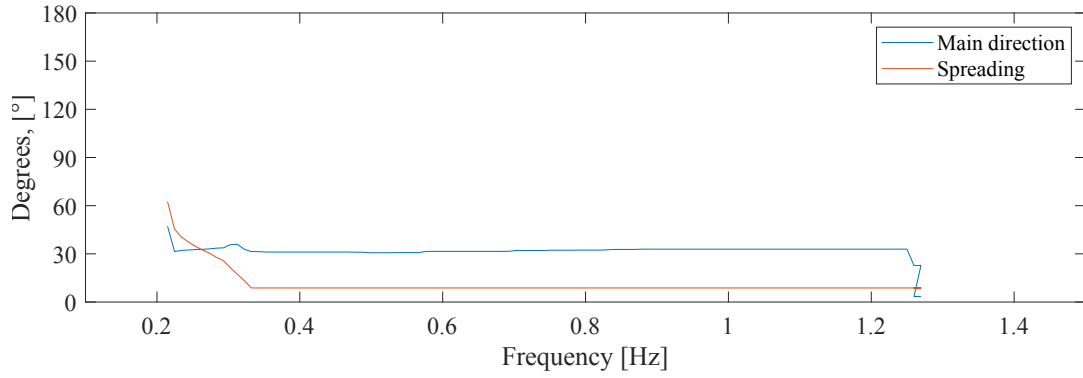


Figure I.4: Estimated direction for components in the wave field with target direction of 30° , Case D with error due to calibration added to two wave gauges in position (x_1, y_1) and (x_2, y_2) .

The figure shows not any mainly difference from Figure I.1 with only error related to calibration added at one gauge. The deviation for the specific case and direction is 1.32° . The analysed directions for all the cases appear from Table I.2 for the directions from 0° to 90° .

Table I.2: Estimated values of the wave direction for first order waves with two wave gauge in position (x_1, y_1) and (x_2, y_2) with calibration error.

| Analysed direction, θ_0 , $^\circ$ | Generated direction, θ , $^\circ$ | | | | | | | | | | |
|---|--|------|-------|-------|-------|-------|-------|-------|-------|-------|-------|
| | | 0 | 10 | 20 | 30 | 40 | 50 | 60 | 70 | 80 | 90 |
| Case A1 | | 0.55 | 10.95 | 21.45 | 31.29 | 41.13 | 50.60 | 59.94 | 69.71 | 79.53 | 89.56 |
| Case B1 | | 1.07 | 11.31 | 21.16 | 31.04 | 40.73 | 50.37 | 59.94 | 69.59 | 79.54 | 89.33 |
| Case C1 | | 0.93 | 11.11 | 21.17 | 30.99 | 40.78 | 50.48 | 60.06 | 69.75 | 79.57 | 89.39 |
| Case D1 | | 0.78 | 10.95 | 21.15 | 31.32 | 41.12 | 50.57 | 60.40 | 69.61 | 79.55 | 89.53 |
| Case E1 | | 0.00 | 11.18 | 21.11 | 31.05 | 40.80 | 50.45 | 60.05 | 69.61 | 79.47 | 89.42 |
| Case F1 | | 0.90 | 11.16 | 21.29 | 31.05 | 40.81 | 50.46 | 60.01 | 69.81 | 79.53 | 89.38 |
| Case G1 | | 0.96 | 11.19 | 21.16 | 30.98 | 40.84 | 50.44 | 60.23 | 69.72 | 79.60 | 89.22 |
| Case H1 | | 0.86 | 11.11 | 21.16 | 30.99 | 40.77 | 50.46 | 60.01 | 69.68 | 79.47 | 89.20 |

The errors of the weighted estimated directions are in general further increased compared to the results of the weighted estimated directions for first order waves with calibration error added to one wave gauge. If the errors are compared to the first order waves without any added calibration error, which is stated in Table 6.1 the largest deviations are 1.42° . The error seems to be shared among all cases. The calibration error is added to two wave gauges placed next to each other, this might explain why the error decrease compared to the error for the case with only one wave gauge with calibration error added.

Further, it is shown from the results, that the error changes from a overestimation of the direction to a underestimation when the directions passes from 0 towards 90° . This might be because of the two gauges position in relation the target wave direction.

The differences of the directional spreading parameters compared to the analyses without calibration error are illustrated in Figure I.5 and I.6.

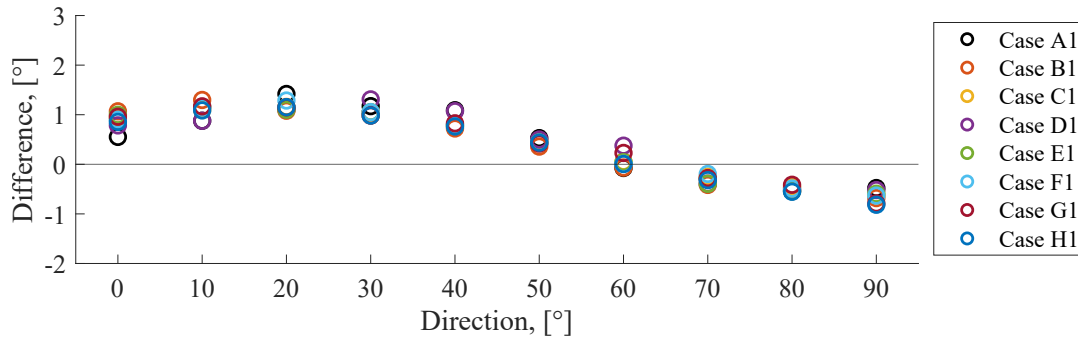


Figure I.5: Difference in mean direction of long-crested first order waves compared to value determined based on data without calibration error.

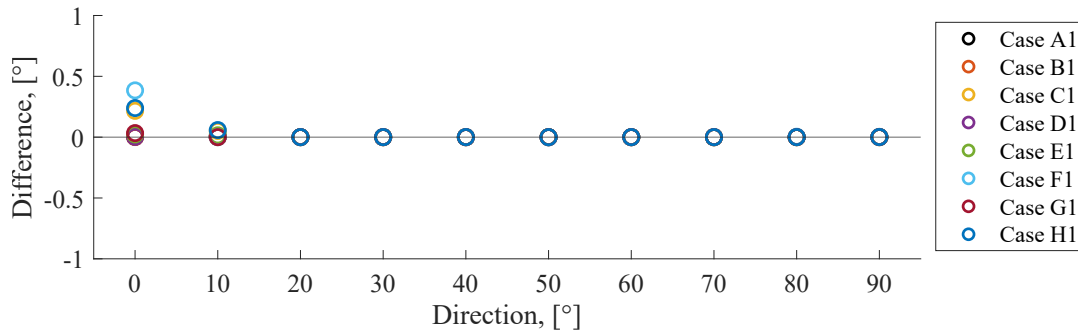


Figure I.6: Difference in estimated spreading of long-crested first order waves compared to value determined based on data without calibration error.

In Figure I.5, the errors of the weighted estimated directions are in general same size compared to the results of the weighted estimated directions for first order waves with calibration error added to one wave gauge. The errors are compared to the first order waves without any added calibration error, where the largest deviation is 1.42° . The error seems to be shared among all cases. The calibration error is added to two wave gauges placed next to each other, this might explain why the error has not increased compared to the error for the case with only one wave gauge with calibration error added. However, the pattern of the errors in relation the directions are very clear in the figure, where the peak is placed around 20° for this combination of gauges affected by calibration error. Further, it is shown from the results, that the error changes from a overestimation of the direction to a underestimation when the directions passes from 0 towards 90° . This might be because of the two gauges position in relation the target wave direction. The estimated spreading of the waves is not influenced by the inclusion of calibration error for the given scenario.

Calibration Error Gauge 1 and 4

For this test 5% is again added to the first order signal of the surface elevation at two measured signals which are not placed next to each other. The two wave gauges are placed in the position of (x_1, y_1) and (x_4, y_4) . The result of the estimated mean direction and the spreading are shown in Figure I.7 for Case D1 with generated first order waves.

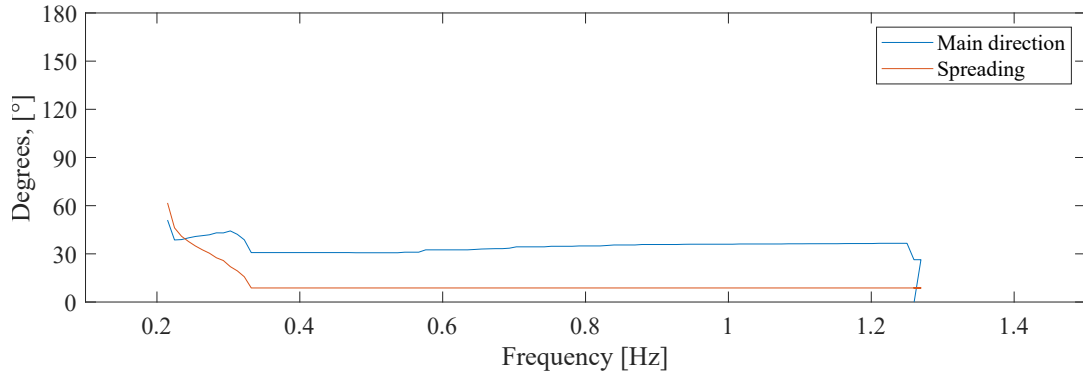


Figure I.7: Estimated direction for components in the wave field with target direction of 40° , Case D with error due to calibration added to two wave gauges in position (x_1, y_1) and (x_4, y_4) .

The figure shown an estimated mean direction with a bit larger slope compared to Figure I.1 and Figure I.4. The might result in the increased deviation of the weighted estimated mean wave direction of this specific case, which is increased with 1.96° . The analysed directions for all the cases appear from Table I.3 for the directions from 0° to 90° .

Table I.3: Estimated values of the wave direction for first order waves with one wave gauge in position (x_1, y_1) with calibration error.

| Analysed direction, θ_0 , $^\circ$ | Generated direction, θ , $^\circ$ | | | | | | | | | | |
|---|--|-------|-------|-------|-------|-------|-------|-------|-------|-------|----|
| | | 0 | 10 | 20 | 30 | 40 | 50 | 60 | 70 | 80 | 90 |
| Case A1 | -0.60 | 10.13 | 21.00 | 31.74 | 42.61 | 52.85 | 62.34 | 70.73 | 79.25 | 88.21 | |
| Case B1 | -0.23 | 9.85 | 19.91 | 30.03 | 40.15 | 50.27 | 60.22 | 70.05 | 79.98 | 89.95 | |
| Case C1 | -0.23 | 10.34 | 20.07 | 30.23 | 40.39 | 50.29 | 60.24 | 70.18 | 80.24 | 90.17 | |
| Case D1 | -0.55 | 10.12 | 20.79 | 31.96 | 42.58 | 52.90 | 62.67 | 70.59 | 79.38 | 88.17 | |
| Case E1 | -0.29 | 9.82 | 19.94 | 30.04 | 40.21 | 50.32 | 60.29 | 70.11 | 80.13 | 90.00 | |
| Case F1 | -0.32 | 9.84 | 19.90 | 30.07 | 40.17 | 50.22 | 60.22 | 70.05 | 80.01 | 90.01 | |
| Case G1 | -0.22 | 9.88 | 19.91 | 30.03 | 40.20 | 50.28 | 60.23 | 70.05 | 80.06 | 90.03 | |
| Case H1 | -0.24 | 9.78 | 19.91 | 30.06 | 40.19 | 50.26 | 60.22 | 70.06 | 80.07 | 90.02 | |

The errors of the weighted estimated directions are in general increased compared to the results of the weighted estimated directions for first order waves stated in Table 6.1. The largest deviation from the target direction with up to 2.83° . This shows that the case is worsened compared to the case where the error was added to two gauges new to each other. The deviations compared to the analysis without calibration error appear from Figure I.8 and I.9.

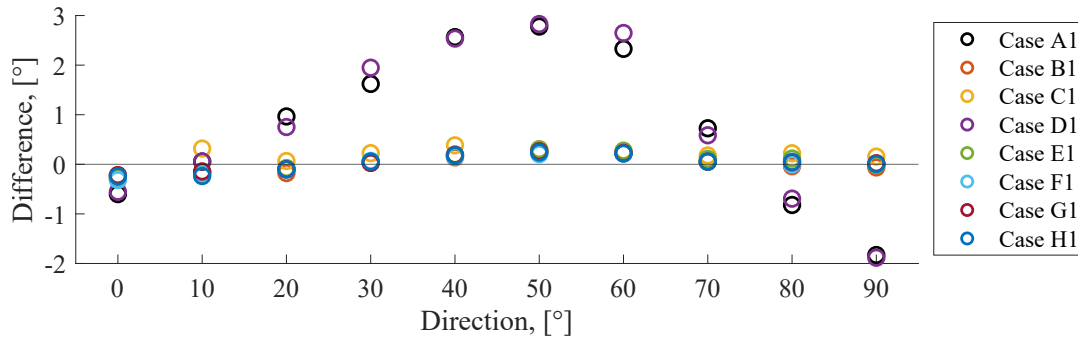


Figure I.8: Difference in mean direction of long-crested first order waves compared to value determined based on data without calibration error.

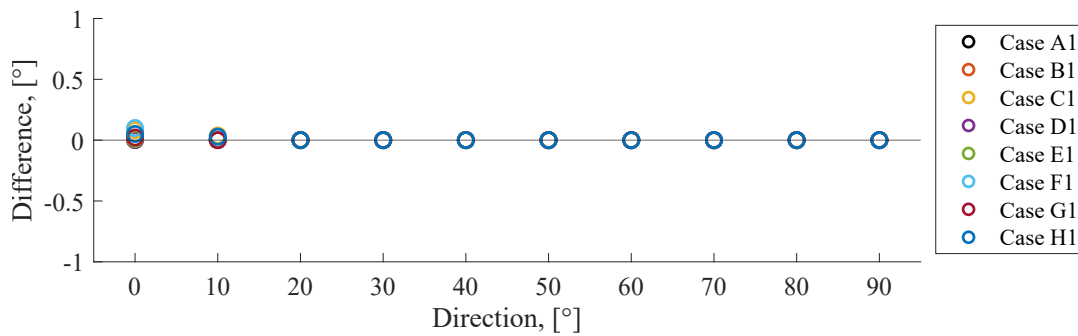


Figure I.9: Difference in estimated spreading of long-crested first order waves compared to value determined based on data without calibration error.

From Figure I.8, it appears that the errors of the weighted estimated directions are in general increased compared to the results of the weighted estimated directions for first order waves including calibration errors. The largest deviation from the target direction with up to 2.83° . This shows that the case is worsened compared to the case where the error was added to two gauges next to each other. The pattern of the errors related to calibration error is shaped alike for Case A1 and D1, which are the cases with shallow water depth. They have a peak at about 50° , whereas the remaining cases shape a pattern closer to the zero line, and are thus not as affected by the calibration errors. The spreading parameters are all more or less unchanged from the investigation with one wave gauges affected by calibration error to both analysis of the signal where two wave gauges were affected by the same amount of calibration error. For the present scenario as well, the spreading of the waves it not affected by inclusion of calibration errors.

I.1.2 Analysis of Second Order Waves

The errors related to calibration are further investigated for the second order waves.

Calibration Error Gauge 1

Again 5% is added to the signal of the surface elevation, where the factor 1.05 is multiplied to the signal at wave gauge in position (x_1, y_1) , the same as the first analysis in the previous analyses. The result of the estimated mean direction, θ_0 , and the spreading are shown in Figure I.10 for Case D2 with generated second order waves.

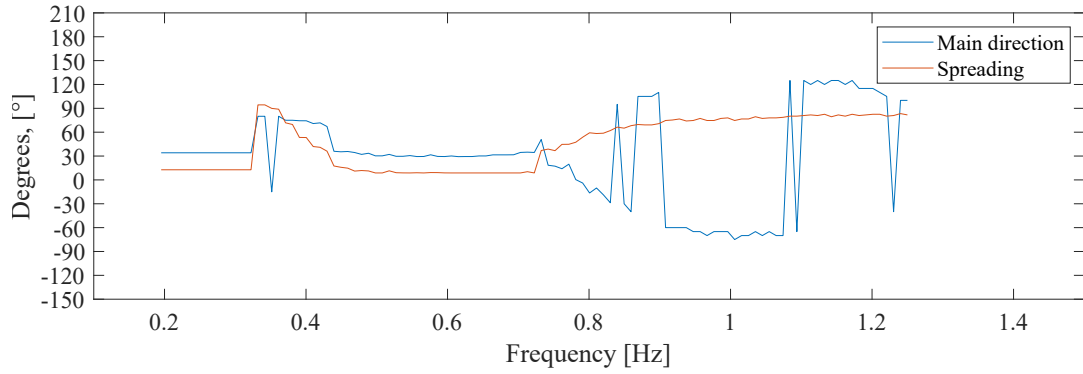


Figure I.10: Estimated direction for components in the wave field with target direction of 30° , Case D2 with error due to calibration added to one wave gauge in position (x_1, y_1) .

The results of the estimated mean wave direction at the figure deviates from the comparable Figure 6.3 at the smallest frequencies below 0.4 Hz and at the highest frequencies above 0.8 Hz, represented by the mess. All the other components seem to be similar and unaffected by the calibration error.

The analysed directions for all the cases appear from Table I.4 for the directions from 0° to 90° .

Table I.4: Estimated values of the wave direction for second order waves with one wave gauge in position (x_1, y_1) with calibration error.

| | Generated direction, θ , [°] | | | | | | | | | | |
|--------------------------------------|-------------------------------------|-------|-------|-------|-------|-------|-------|-------|-------|-------|-------|
| Analysed direction, θ_0 , [°] | | 0 | 10 | 20 | 30 | 40 | 50 | 60 | 70 | 80 | 90 |
| | Case A2 | -0.28 | 9.80 | 20.04 | 30.40 | 41.58 | 51.54 | 61.22 | 71.29 | 80.58 | 90.27 |
| | Case B2 | 0.00 | 10.10 | 20.23 | 30.38 | 40.47 | 50.54 | 60.54 | 70.46 | 80.41 | 90.14 |
| | Case C2 | 0.00 | 10.09 | 20.21 | 30.34 | 40.49 | 50.57 | 60.55 | 70.46 | 80.33 | 90.14 |
| | Case D2 | 0.95 | 19.53 | 17.66 | 26.26 | 41.45 | 57.99 | 56.58 | 60.43 | 87.31 | 90.10 |
| | Case E2 | -0.02 | 10.12 | 20.27 | 30.47 | 40.43 | 50.62 | 60.64 | 70.53 | 80.29 | 90.13 |
| | Case F2 | 0.00 | 10.14 | 20.28 | 30.40 | 40.54 | 50.51 | 60.61 | 70.52 | 80.26 | 90.25 |
| | Case G2 | 2.15 | 12.69 | 22.88 | 32.99 | 45.01 | 53.19 | 62.05 | 72.67 | 82.55 | 88.97 |
| | Case H2 | 1.58 | 12.11 | 23.01 | 33.15 | 43.21 | 53.17 | 63.16 | 72.53 | 81.96 | 90.33 |

This is compared with Table 6.2 with only second order waves. The errors according to the estimated mean directions are in general given a higher value of the angle. The largest deviation from the estimated direction found from the analysis of second waves with up to 13.06° .

The difference in the estimated directional parameters compared to the analysis of second order waves without calibration error appear from Figure I.11 and I.12

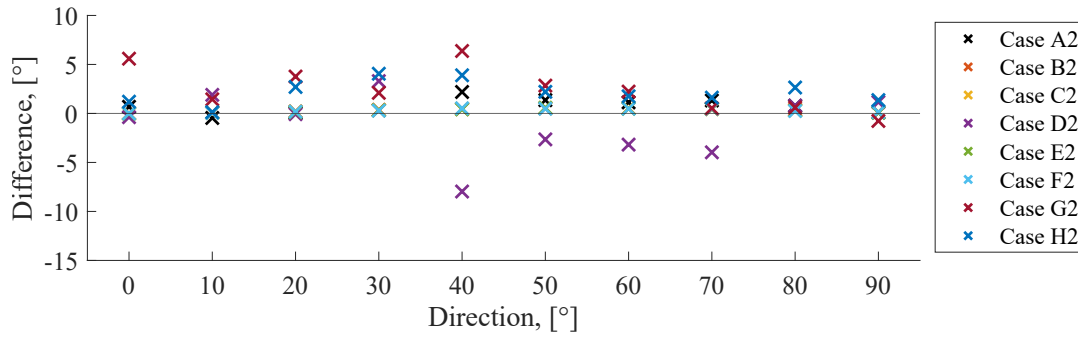


Figure I.11: Difference in mean direction of long-crested second order waves with calibration error on gauge in position (x_1, y_1) compared to value determined based on data without calibration error.

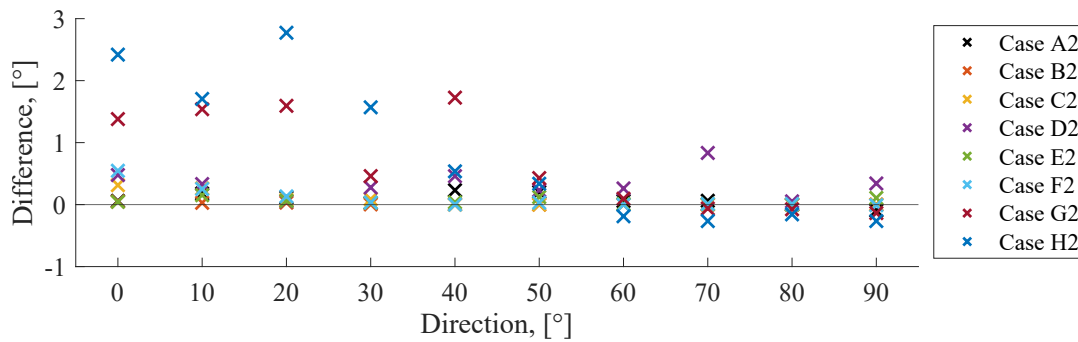


Figure I.12: Difference in estimated spreading of long-crested second order waves with calibration error on gauge in position (x_1, y_1) compared to value determined based on data without calibration error.

Figure I.11 shows a large deviation of 7.97° on the estimated mean wave direction for the target direction of 40° for Case D2. It seems like the cases containing the largest amount of second order energy A2, D2, G2 and H2 give largest errors on the direction compared to the results for the analyses without calibration error. The size of the errors for all other cases than D2 are approximately 3 to 4° .

The inclusion of calibration error makes the estimated spreading of the waves increase for cases G2 and H2, with a maximum deviation for Case H2 of 2.77° .

Calibration Error Gauge 1 and 2

For this test 5% is again added to the second order signal of the surface elevation, but added to two of the measured signals as in the second test to investigate how the errors accelerate according to calibration errors added to more wave gauges.

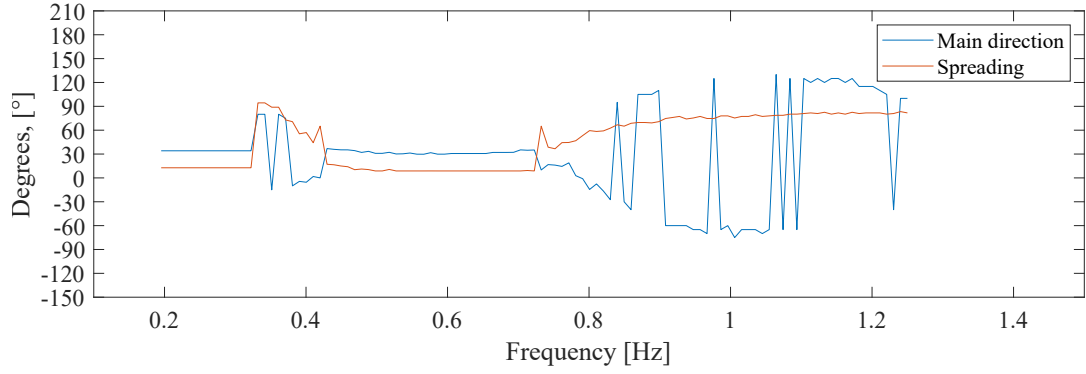


Figure I.13: Estimated direction for components in the wave field with target direction of 30° , Case D2 with error due to calibration added to two wave gauges in position (x_1, y_1) and (x_2, y_2) .

The results of the estimated mean wave direction in the figure seem to deviate less from Figure 6.3 compared to the results in Figure I.10 where only the scatter at the the highest frequencies above 1.2 Hz is left and the results at the smallest frequencies below 0.4 Hz are similar to the results of the analysis of the estimated mean wave direction for the second order wave field without any calibration error added.

The analysed directions for all the cases appear from Table I.5 for the directions from 0° to 90° .

Table I.5: Estimated values of the wave direction for second order waves with two wave gauge in position (x_1, y_1) and (x_2, y_2) with calibration error.

| | Generated direction, θ , [°] | | | | | | | | | | |
|--------------------------------------|-------------------------------------|-------|-------|-------|-------|-------|-------|-------|-------|-------|-------|
| Analysed direction, θ_0 , [°] | | 0 | 10 | 20 | 30 | 40 | 50 | 60 | 70 | 80 | 90 |
| | Case A2 | 1.66 | 10.68 | 20.96 | 30.98 | 40.53 | 50.62 | 59.85 | 68.87 | 79.62 | 89.73 |
| | Case B2 | 1.05 | 11.31 | 21.18 | 31.05 | 40.73 | 50.31 | 59.92 | 69.57 | 79.42 | 89.21 |
| | Case C2 | 0.93 | 11.11 | 21.24 | 30.98 | 40.76 | 50.46 | 60.01 | 69.64 | 79.36 | 89.19 |
| | Case D2 | -6.61 | 18.55 | 19.12 | 24.84 | 49.39 | 59.77 | 58.15 | 63.27 | 85.20 | 87.71 |
| | Case E2 | 1.04 | 11.23 | 21.18 | 31.17 | 40.79 | 50.34 | 60.12 | 69.58 | 79.28 | 89.22 |
| | Case F2 | 0.89 | 11.19 | 21.32 | 31.5 | 40.78 | 50.33 | 59.97 | 69.58 | 79.28 | 89.22 |
| | Case G2 | 5.58 | 14.04 | 22.81 | 33.32 | 40.63 | 52.15 | 59.53 | 68.06 | 76.52 | 86.41 |
| | Case H2 | 4.38 | 13.28 | 23.19 | 33.40 | 43.11 | 51.27 | 60.52 | 69.31 | 78.28 | 86.27 |

The results show that some of the cases and directions are worsened and some of them are not if the results of the estimated directions are compared to the results from Table I.4 for second order waves with only one wave gauges exposed for calibration error. This might be because of the positions of the two wave gauges, that they are placed next to each other.

The differences compared to the analysis without calibration error appears from Figure I.14 and I.15

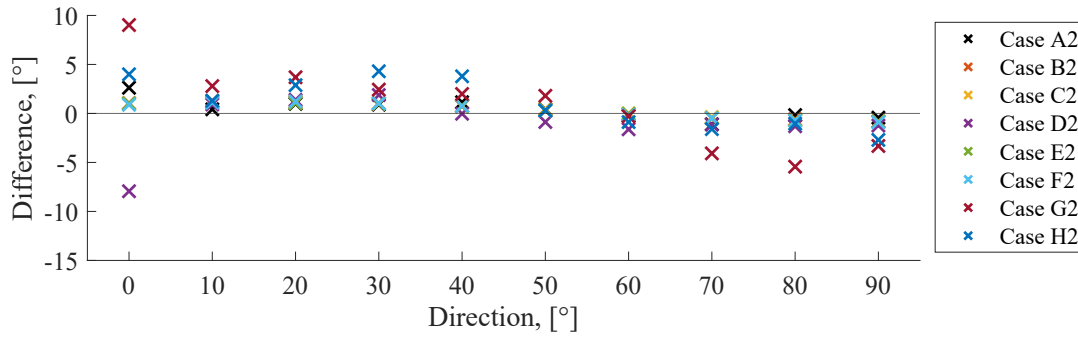


Figure I.14: Difference in mean direction of long-crested second order waves compared to value determined based on data without calibration error.

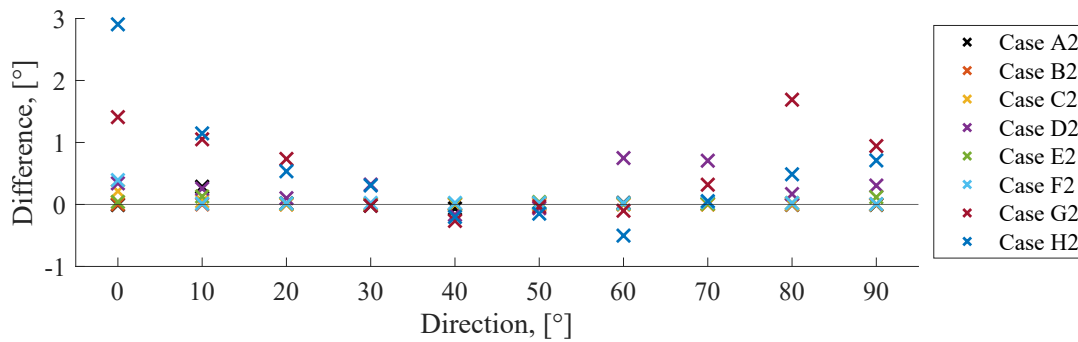


Figure I.15: Difference in estimated spreading of long-crested second order waves compared to value determined based on data without calibration error.

Calibration Error Gauge 1 and 4

This test investigate the situation where the 5% is again added to the signal of the surface elevation at two measured signals which are not placed next to each other. The two wave gauges are placed in the position of (x_1, y_1) and (x_4, y_4) . The estimated mean direction and spreading are plotted in Figure I.16.

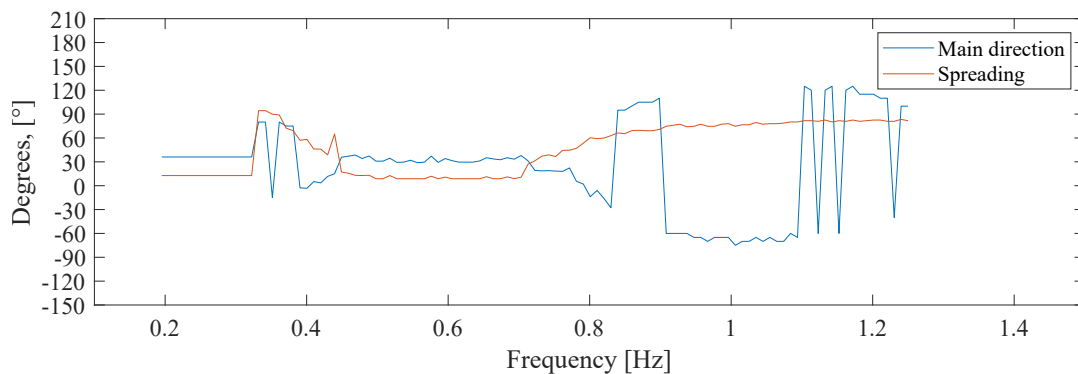


Figure I.16: Estimated direction for components in the wave field with target direction of 30° , Case D2 with error due to calibration added to two wave gauges in position (x_1, y_1) and (x_4, y_4) .

The results of the weighted directions for each case and in the span of direction from 0 to 90° are shown in Table I.6.

Table I.6: Estimated values of the wave direction for second order waves with two wave gauge in position (x_1, y_1) and (x_2, y_2) with calibration error.

| Analysed direction, θ_0 , [°] | Generated direction, θ , [°] | | | | | | | | | | |
|--------------------------------------|-------------------------------------|-------|-------|-------|-------|-------|-------|-------|-------|-------|-------|
| | | 0 | 10 | 20 | 30 | 40 | 50 | 60 | 70 | 80 | 90 |
| | Case A2 | 0.81 | 10.41 | 20.75 | 31.92 | 43.20 | 52.86 | 62.04 | 70.78 | 78.74 | 88.02 |
| | Case B2 | -0.23 | 9.85 | 19.91 | 30.03 | 40.15 | 50.28 | 60.23 | 70.06 | 80.06 | 89.91 |
| | Case C2 | -0.22 | 9.84 | 19.86 | 30.03 | 40.17 | 50.29 | 60.23 | 70.05 | 80.06 | 89.98 |
| | Case D2 | -8.89 | 16.90 | 16.53 | 23.44 | 35.49 | 58.45 | 57.80 | 63.90 | 85.77 | 96.60 |
| | Case E2 | -0.29 | 9.96 | 19.98 | 30.11 | 40.24 | 50.30 | 60.38 | 70.11 | 79.96 | 90.09 |
| | Case F2 | -0.30 | 9.87 | 19.98 | 30.10 | 40.19 | 50.25 | 60.34 | 70.11 | 80.02 | 89.89 |
| | Case G2 | 4.67 | 13.30 | 21.99 | 33.51 | 41.74 | 53.69 | 62.53 | 70.77 | 79.10 | 87.36 |
| | Case H2 | 2.87 | 12.77 | 22.82 | 32.94 | 42.86 | 53.36 | 64.25 | 71.86 | 77.63 | 86.57 |

The results of the weighted estimated mean directions show the sensibility of the analysis when adding errors related to calibration combined with including second order energy. The deviation of results are increased further when the calibration errors are added to the two wave gauges in position (x_1, y_1) and (x_4, y_4) compared to both the case with calibration added to 1 and the two gauges next to each other. The largest deviation from the estimated direction found from the analysis of second waves with up to 14.87° .

The differences compared to the results without calibration error appears from Figure I.17 and I.18.

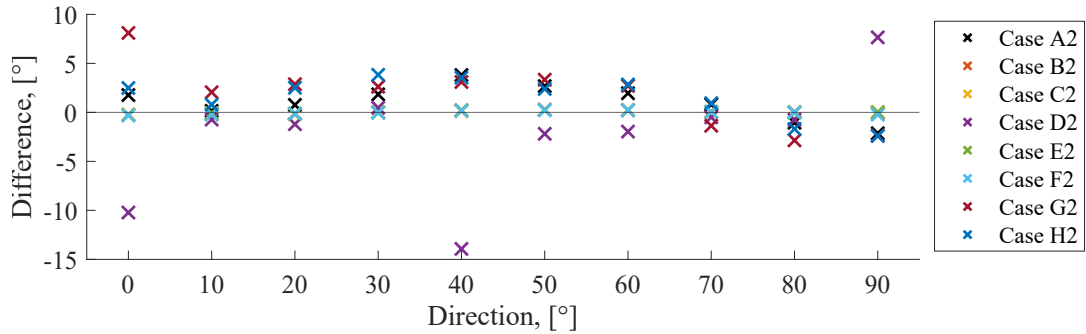


Figure I.17: Difference in mean direction of long-crested second order waves compared to value determined based on data without calibration error.

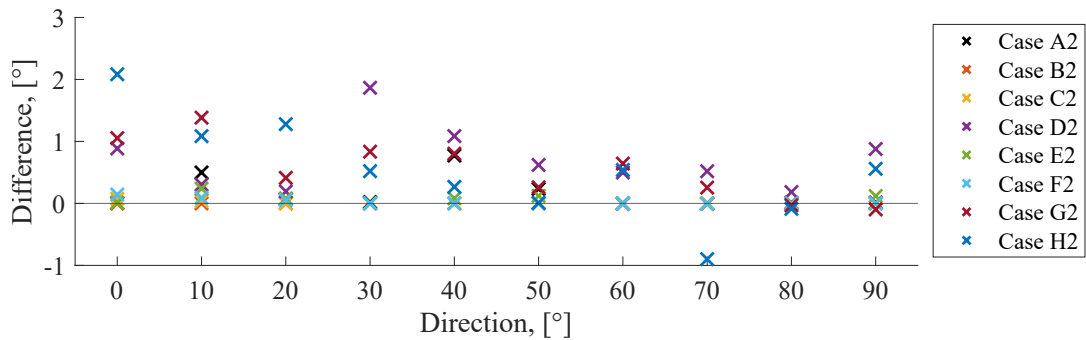


Figure I.18: Difference in estimated spreading of long-crested second order waves compared to value determined based on data without calibration error.

Figure I.17 shows the results of the weighted estimated mean directions and the deviations show

the sensibility of the analysis when adding errors related to calibration combined with including second order energy. The deviation of results are increased further when the calibration errors are added to the two wave gauges in position (x_1, y_1) and (x_4, y_4) compared to both the case with calibration added to one and the two gauges next to each other. The largest deviation from the estimated direction found from the analysis of second waves with up to 13.93° for Case D2. The other errors for all other cases are all within an accuracy of $\pm 5^\circ$, with a tendency of the largest error for Case A2, G2 and H2, which are the remaining cases containing an amount of second order energy above 12 % as stated in chapter 4.

I.1.3 Waves with Amplitude Dispersion

For the analysis of effects related to errors of calibration in combination with influence from amplitude dispersion based on stream function theory, the same data as used in section 6.3 is considered. As mentioned in the previous section, an error of calibration is then added to one or more of the wave gauges before performing the analysis. The results are here presented in the same way as for the waves of first and second order theory, with specific results of the directional analysis shown for Case D3.

Calibration Error Gauge 1

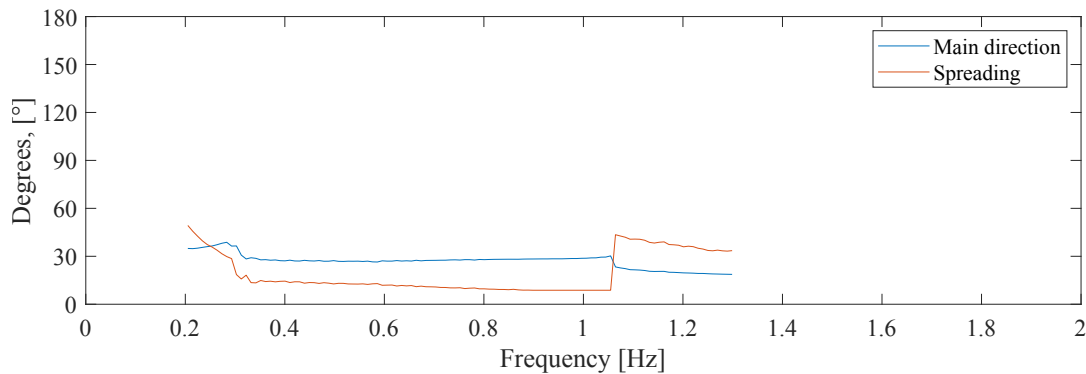


Figure I.19: Estimated direction for components in the wave field with target direction of 30° , Case D3 with error due to calibration added to one wave gauges in position (x_1, y_1) .

The results of the weighted directions for each case and in the span of direction from 0 to 90° are shown in Table I.7.

Table I.7: Estimated values of the mean wave direction and spreading parameter for higher order waves with calibration error on gauge in position (x_1, y_1) .

| | | Generated direction, θ , $^\circ$ | | | | | | | | | |
|-----------------------|----|--|-------|-------|-------|-------|-------|-------|-------|-------|-------|
| | | 0 | 10 | 20 | 30 | 40 | 50 | 60 | 70 | 80 | 90 |
| θ_0 , $^\circ$ | A3 | -0.00 | 10.00 | 20.12 | 30.41 | 40.75 | 50.87 | 60.94 | 70.92 | 80.65 | 90.07 |
| | D3 | 0.26 | 9.06 | 17.90 | 27.03 | 37.48 | 47.03 | 57.07 | 67.85 | 79.34 | 90.01 |
| | G3 | 0.00 | 9.87 | 19.79 | 29.84 | 39.91 | 49.98 | 60.01 | 70.09 | 80.09 | 90.04 |

The differences compared to the results without calibration error appears from Figure I.20 and I.21.

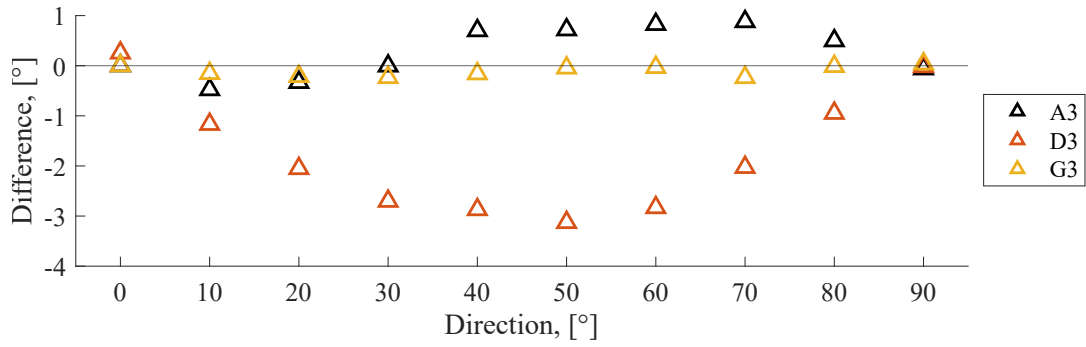


Figure I.20: Difference in mean direction of long-crested waves with amplitude dispersion compared to value determined based on data without calibration error.

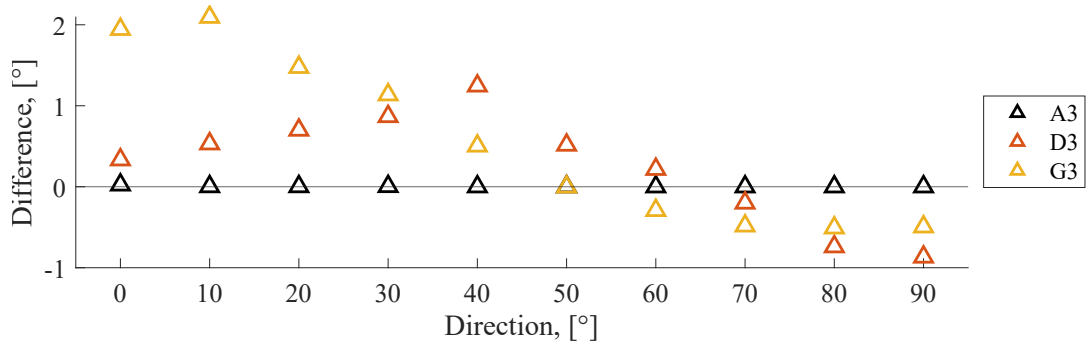


Figure I.21: Difference in estimated spreading of long-crested waves with amplitude dispersion compared to value determined based on data without calibration error.

Figure I.20 shows how Case D3 is the most affected by the calibration error for waves with amplitude dispersion, which has the largest error of -3.13° . This case shows a tendency of increasing errors when the angle relative to the gauge array increase, which peak around 50° and then decrease again. This pattern might be due to the affected gauge. The other cases seem almost unaffected and do only reach an error of 0.88° .

Calibration Error Gauge 1 and 2

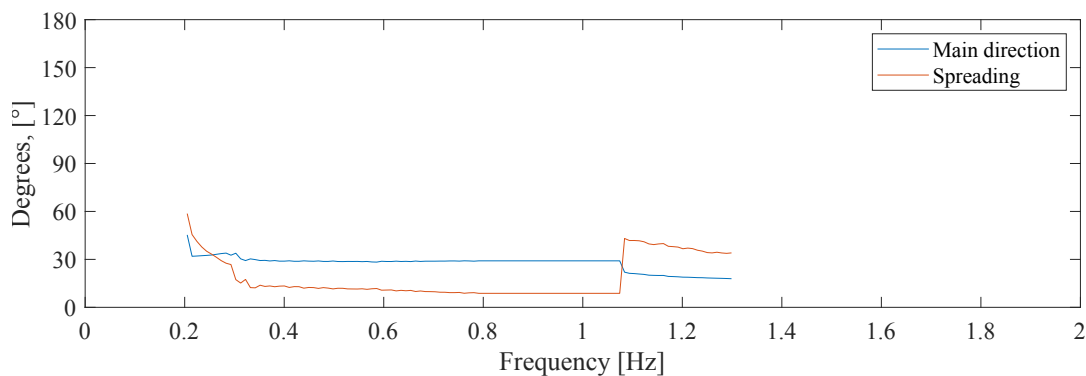


Figure I.22: Estimated direction for components in the wave field with target direction of 30° , Case D3 with error due to calibration added to two wave gauges in position (x_1, y_1) and (x_2, y_2) .

The results of the weighted directions for each case and in the span of direction from 0 to 90° are shown in Table I.8.

Table I.8: Estimated values of the mean wave direction and spreading parameter for higher order waves with calibration error on gauge in position (x_1, y_1) and (x_2, y_2) .

| | Generated direction, θ , [°] | | | | | | | | | | |
|------------------|-------------------------------------|-------|-------|-------|-------|-------|-------|-------|-------|-------|-------|
| | | 0 | 10 | 20 | 30 | 40 | 50 | 60 | 70 | 80 | 90 |
| θ_0 , [°] | A3 | 0.36 | 10.69 | 20.85 | 30.98 | 40.94 | 50.37 | 59.99 | 69.68 | 79.52 | 89.57 |
| | D3 | -1.54 | 8.27 | 18.26 | 28.62 | 39.83 | 49.99 | 60.08 | 70.33 | 81.46 | 91.80 |
| | G3 | 0.44 | 10.58 | 20.55 | 30.55 | 40.40 | 50.16 | 59.90 | 69.68 | 79.56 | 89.52 |

The differences compared to the results without calibration error appears from Figure I.23 and I.24.

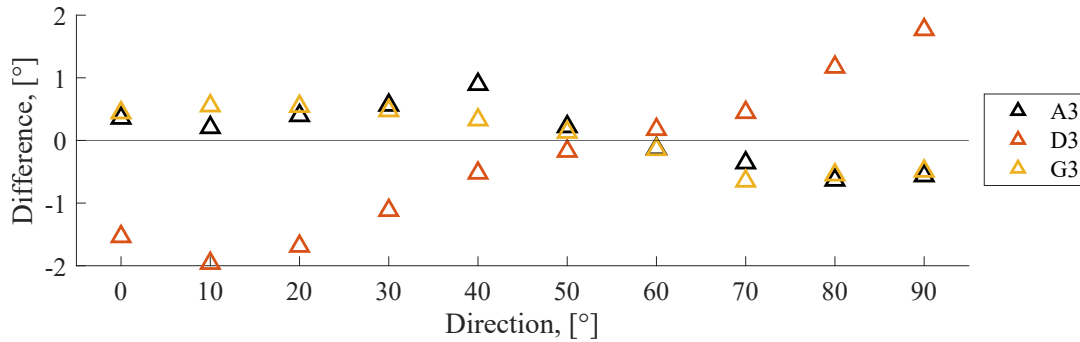


Figure I.23: Difference in mean direction of long-crested waves with amplitude dispersion compared to value determined based on data without calibration error.

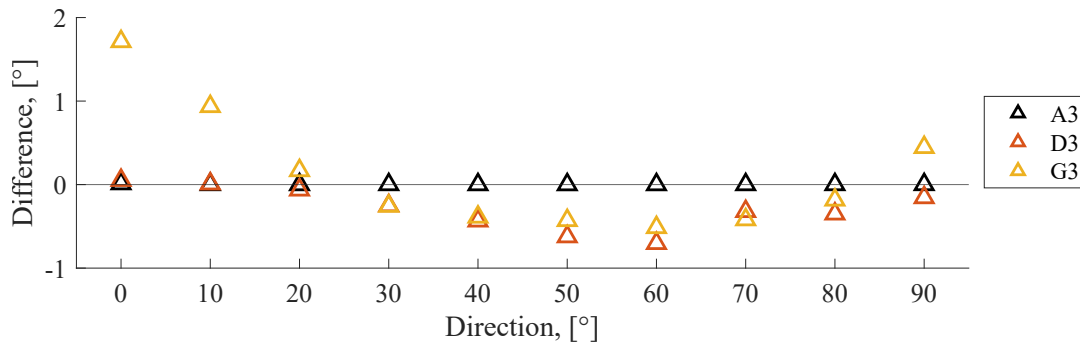


Figure I.24: Difference in estimated spreading of long-crested waves with amplitude dispersion compared to value determined based on data without calibration error.

Figure I.23 shows similar to Figure I.20, that it is Case D3, which is affected the most by the calibration error. Case A3 and G3 again seem to deviate less and do not have any errors above 1°. The pattern are just like for the analysis of calibration error of first and second order waves seems to change according to which gauges that are affected by calibration error. The largest errors appear near the angles of the axes in the coordinate system and the maximum value is -1.96° for Case D3.

Calibration Error Gauge 1 and 4

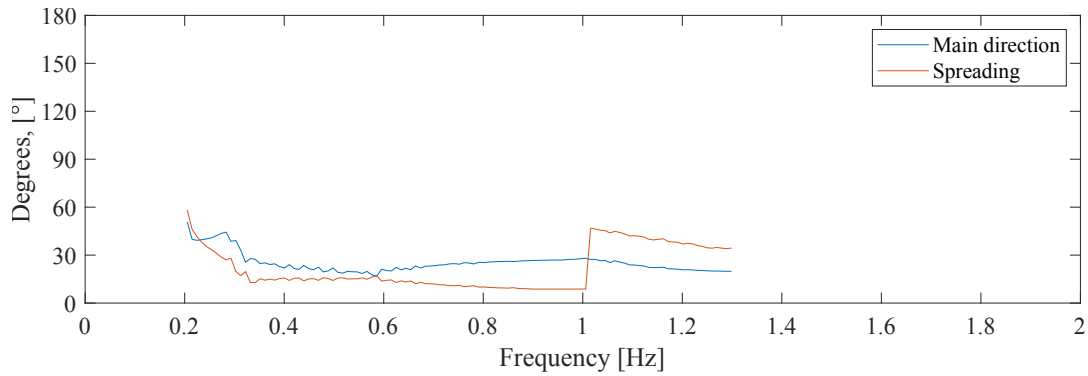


Figure I.25: Estimated direction for components in the wave field with target direction of 30° , Case D3 with error due to calibration added to two wave gauges in position (x_1, y_1) and (x_4, y_4) .

The results of the weighted directions for each case and in the span of direction from 0 to 90° are shown in Table I.9.

Table I.9: Estimated values of the mean wave direction and spreading parameter for higher order waves with calibration error on gauge in position (x_1, y_1) and (x_4, y_4) .

| | | Generated direction, θ , $^\circ$ | | | | | | | | | |
|-----------------------|----|--|------|-------|-------|-------|-------|-------|-------|--------|--------|
| | | 0 | 10 | 20 | 30 | 40 | 50 | 60 | 70 | 80 | 90 |
| θ_0 , $^\circ$ | A3 | -0.67 | 9.89 | 20.40 | 31.16 | 41.91 | 52.23 | 61.75 | 70.39 | 79.18 | 88.55 |
| | D3 | -2.46 | 5.78 | 13.69 | 21.24 | 26.70 | 31.05 | 38.36 | 69.56 | 102.36 | 110.20 |
| | G3 | -0.69 | 9.13 | 19.14 | 29.33 | 39.65 | 49.81 | 59.91 | 69.99 | 80.13 | 90.27 |

The differences compared to the results without calibration error appears from Figure I.26 and I.27.

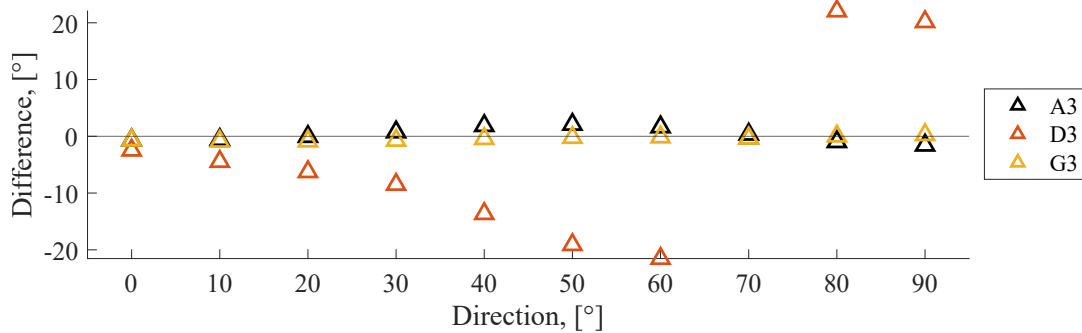


Figure I.26: Difference in mean direction of long-crested waves with amplitude dispersion compared to value determined based on data without calibration error.

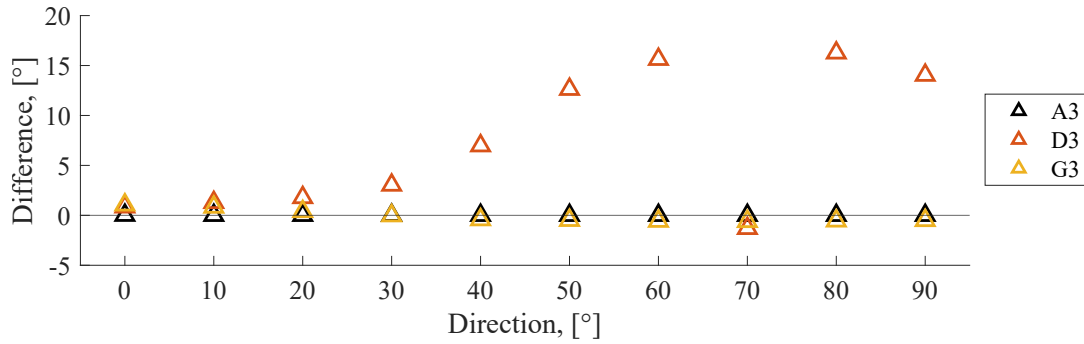


Figure I.27: Difference in estimated spreading of long-crested waves with amplitude dispersion compared to value determined based on data without calibration error.

Figure I.26 shows, that just as for the other situations with affected gauges, this seems to be the worst-case scenario of the investigated situations including calibration error. The largest error in the figure is for Case D3 and reaches a size of 22.07° , which is the largest of all errors due to calibration errors. The spreading parameter for Case A3 has an almost unchanged estimated spreading parameter at around 85 equal to a spreading in degree of 9° . Case D3 has, on the contrary, the largest change in the estimated spreading parameter at around 40 to 50 equal to a spreading in degree of 11 to 13° compared to the one from the analysis of amplitude dispersion waves. The estimated spreading parameters for Case G3 deviate from 50 to 85 equal to a spreading in degree of 9 to 11° .

I.2 Short-Crested Waves

The effect of calibration errors for analysis of short-crested waves is performed based on the same data as chapter 7, though here with an error included for one or more gauges. The analysis is therefore only performed for a single direction under the assumption, that other directions will show the same behaviour.

The errors related to calibration added to wave gauges are evaluated by generating a short-crested wave field by both a single and double summation model. The direction parameters of wave field are then analysed with an added error of 5% of the signal at one and further at two wave gauges. The single wave gauge is again the gauge with the position of (x_1, y_1) and the two wave gauges are the two with the positions of (x_1, y_1) and (x_4, y_4) , which appeared to be the most critical situation based on errors of the mean directions in the long-crested wave analysis.

I.2.1 First Order Waves

In this section first order wave fields are generated first by a single summation model which is followed by a wave field generated by a double summation model.

Calibration Error Gauge 1

In Figure I.28 the results of the estimated mean wave direction and the spreading are shown. Compared to Figure 7.6 there is a small visible variation at the estimated mean direction and spreading, which deviations are a bit larger.

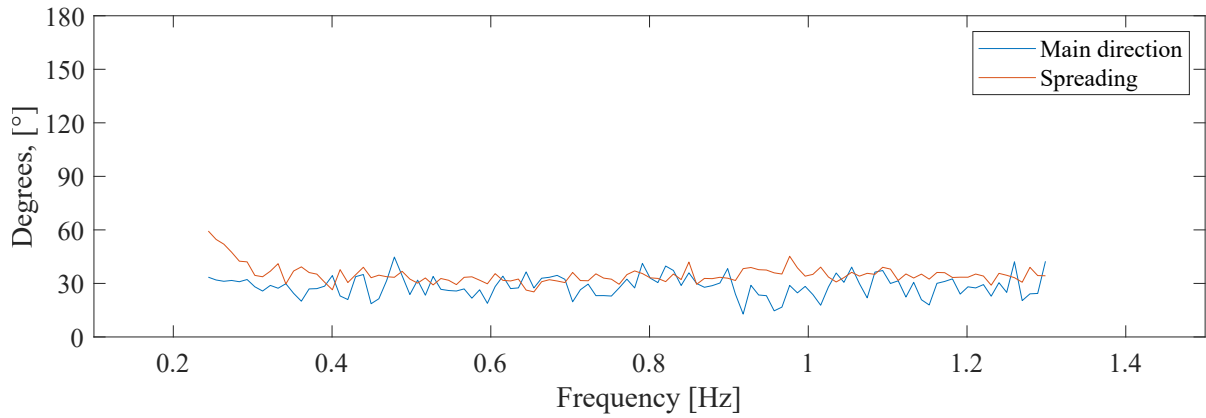


Figure I.28: Estimated direction with target direction of 30° , Case D1 with error due to calibration of 5 % added to a wave gauge in position (x_1, y_1) . Single summation.

The results of the weighted estimated mean wave direction and the spreading parameter are stated in Table I.10 together with its deviation from the short-crested waves analysed without calibration error from Table 7.2. The wave field is generated from a single summation model with calibration error added to one gauge.

Table I.10: Results of MLM estimation of directional spreading of short-crested waves based on linear wave theory with target values $\theta_0 = 30^\circ$ and $s = 5$.

| Single Summation | | | Deviation from first order theory. | | |
|------------------|---------------------------------------|---------------------------|------------------------------------|---------------------------------------|------------------|
| Case | Mean wave direction θ_0 [°] | Spreading σ [°] | Case | Mean wave direction θ_0 [°] | Spreading [°] |
| A1 | 26.89° | 32.31° | A1 | 0.33° | 0.08° |
| B1 | 29.09° | 32.54° | B1 | -0.50° | 0.40° |
| C1 | 28.60° | 31.67° | C1 | -0.52° | 0.53° |
| D1 | 28.74° | 32.67° | D1 | -1.14° | -1.24° |
| E1 | 28.56° | 32.53° | E1 | -0.51° | 0.45° |
| F1 | 27.05° | 33.71° | F1 | -0.29° | 0.43° |
| G1 | 25.09° | 32.67° | G1 | -0.29° | 0.44° |
| H1 | 27.25° | 32.92° | H1 | -0.36° | 0.47° |

The results from the table show a deviation of the weighted estimated mean wave direction in the range of $\pm 1.14^\circ$ and a deviation of the weighted spreading of up to -1.24° . From the results stated in the deviation table it is not larger compared to the difference results for the same analysis for long-crested waves. Based on the results from section I.1 about the errors related to calibration analysed for long-crested waves, the knowledge about the number and which wave gauges which are affected by calibration error are resulting in the largest error are applied in this section. Accordingly, the further analysis will consider a wave field based on first a single summation model followed by a double summation model, where two gauges are affect by calibration error. The two gauges are chosen to be placed in the position of (x_1, y_1) and (x_4, y_4) based on the deviation of the results in the previous section were largest for this case.

The corresponding results for the data generated based on the double summation model appears from Table I.11.

Table I.11: Results of MLM estimation of directional spreading of short-crested waves based on linear wave theory with target values $\theta_0 = 30^\circ$ and $s = 5$.

| Double Summation | | | Deviation from first order theory. | | |
|------------------|---------------------------------------|------------------|------------------------------------|---------------------------------------|------------------|
| Case | Mean wave direction θ_0 [°] | Spreading [°] | Case | Mean wave direction θ_0 [°] | Spreading [°] |
| A1 | 27.11° | 30.99° | A1 | -2.80° | -1.21° |
| B1 | 23.99° | 29.96° | B1 | -5.95° | -0.74° |
| C1 | 24.11° | 30.29° | C1 | -5.83° | -0.67° |
| D1 | 27.11° | 30.99° | D1 | -2.80° | -1.21° |
| E1 | 24.08° | 29.96° | E1 | -5.89° | -0.75° |
| F1 | 24.07° | 30.34° | F1 | -5.87° | -0.66° |
| G1 | 24.12° | 29.94° | G1 | -5.81° | -0.80° |
| H1 | 24.16° | 30.27° | H1 | -5.82° | -0.66° |

The differences compared to the analysis of waves without calibration error appears from Figure I.29.

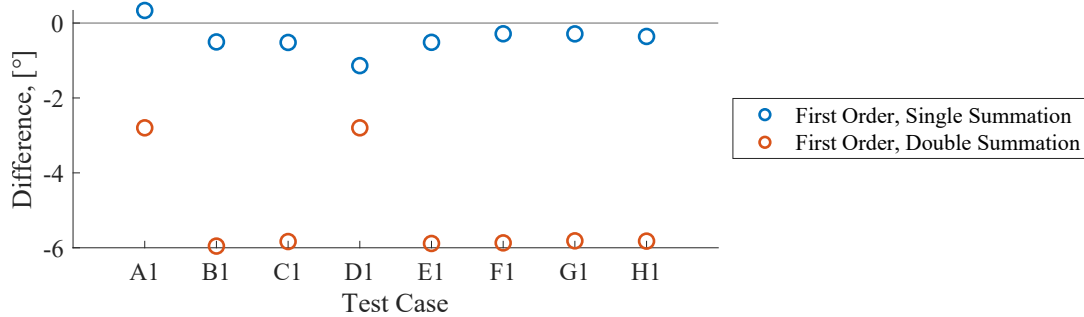


Figure I.29: Difference in mean direction of short-crested first order waves compared to value determined based on data without calibration error.

Figure I.29 shows that the directional analysis of the surface elevation generated from single summation model is in general less affected by the calibration error compared to the signal generated from the double summation model. The errors are in the size of -1.14° for the wave field based on single summation while the errors are in the size of -5.95° for the wave field based on double summation.

Calibration Error Gauge 1 and 4

In Figure I.30 the results of the estimated mean wave direction and the spreading are shown for Case D1 with calibration error added to two gauges.

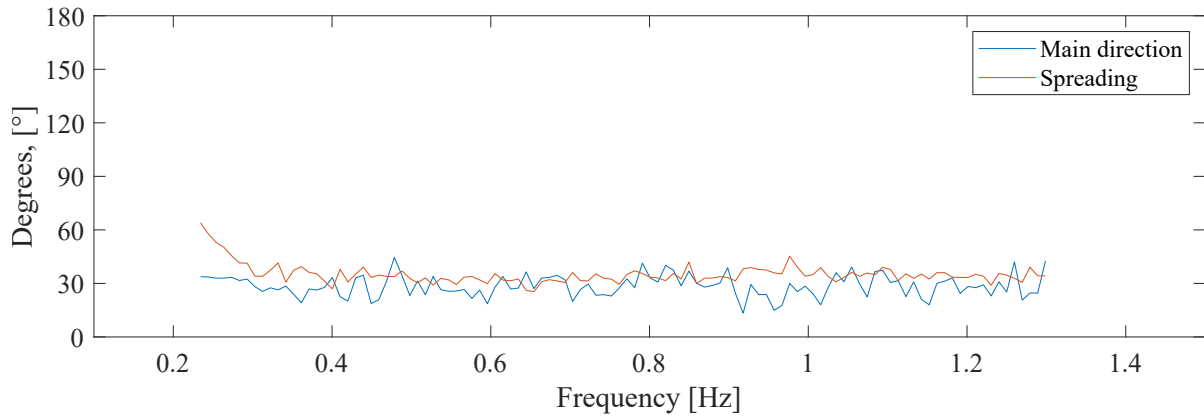


Figure I.30: Estimated direction for components in the wave field with target direction of 30° , Case D1 with error due to calibration of 5 % added to two wave gauges in position (x_1, y_1) and (x_4, y_4) . Single summation.

Table I.12: Results of MLM estimation of directional spreading of short-crested waves based on linear wave theory with target values $\theta_0 = 30^\circ$ and $s = 5$.

| Single Summation | | | Deviation from first order theory. | | |
|------------------|---------------------------------------|------------------|------------------------------------|---------------------------------------|------------------|
| Case | Mean wave direction θ_0 [°] | Spreading [°] | Case | Mean wave direction θ_0 [°] | Spreading [°] |
| A1 | 26.65° | 32.50° | A1 | 0.10° | 0.27° |
| B1 | 27.60° | 33.68° | B1 | -1.99° | 1.55° |
| C1 | 27.10° | 32.88° | C1 | -2.02° | 1.74° |
| D1 | 28.59° | 32.80° | D1 | -1.29° | -1.10° |
| E1 | 27.09° | 33.77° | E1 | -1.98° | 1.69° |
| F1 | 25.73° | 34.93° | F1 | -1.60° | 1.66° |
| G1 | 23.89° | 33.84° | G1 | -1.49° | 1.61° |
| H1 | 25.96° | 34.08° | H1 | -1.64° | 1.64° |

The results from the table show a maximum deviation of the weighted estimated mean wave direction is -2.02° and a deviation of the weighted spreading is up to 1.74° .

In Figure I.31 the results of the estimated mean wave direction and the spreading are shown for case D1. This figure are comparable to Figure 7.7, where a visible deviation of the estimated mean direction is shown consisting of The estimated mean direction is placed some lower. The spreading deviates a bit and is most visible at the smallest frequencies.

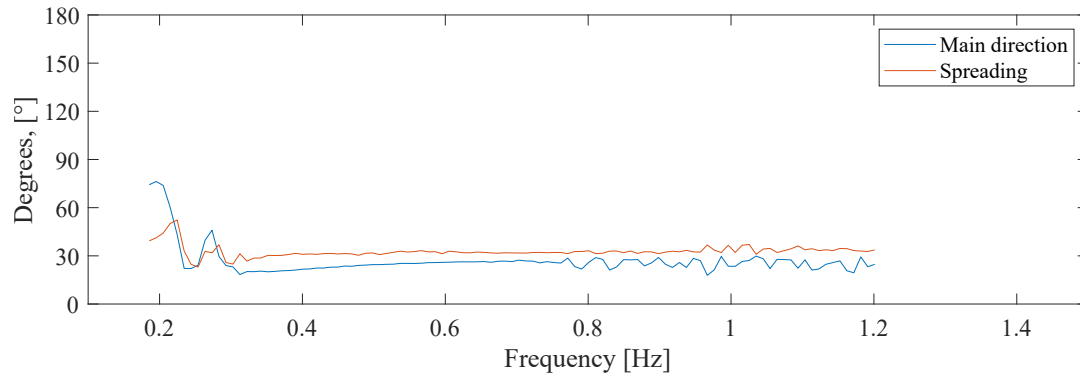


Figure I.31: Estimated direction for components in the wave field with target direction of 30° , Case D1 with error due to calibration of 5 % added to two wave gauges in position (x_1, y_1) and (x_4, y_4) .

The results of the weighted estimated mean wave direction and the spreading parameter are stated in Table I.13 together with its deviation from the short-crested waves analysed without calibration error from Table 7.3. The wave field is generated from a double summation model with calibration error added to two gauges.

Table I.13: Results of MLM estimation of directional spreading of short-crested waves based on linear wave theory with target values $\theta_0 = 30^\circ$ and $s = 5$ and $N = 2^{10}$.

| Double Summation | | | Deviation from first order theory. | | |
|------------------|--|---------------------------|------------------------------------|--|---------------------------|
| Case | Mean wave direction θ_0 [$^\circ$] | Spreading [$^\circ$] | Case | Mean wave direction θ_0 [$^\circ$] | Spreading [$^\circ$] |
| A1 | 24.65° | 31.72° | A1 | -5.26° | -0.48° |
| B1 | 16.86° | 31.06° | B1 | -13.09° | 0.36° |
| C1 | 17.04° | 31.36° | C1 | -12.90° | 0.40° |
| D1 | 24.65° | 31.72° | D1 | -5.26° | -0.48° |
| E1 | 17.05° | 31.05° | E1 | -12.92° | 0.34° |
| F1 | 16.98° | 31.41° | F1 | -12.96° | 0.41° |
| G1 | 17.20° | 31.02° | G1 | -12.73° | 0.29° |
| H1 | 17.14° | 31.32° | H1 | -12.84° | 0.38° |

The results from the table show that when introducing errors in the magnitude of 5% at two gauges the weighted mean wave direction is difficult to estimate in the analysis where the largest deviation is -12.96° . The weighted spreadings are in a magnitude of ± 0.5 .

The differences from the analysis of waves with calibration error appears from Figure I.32.

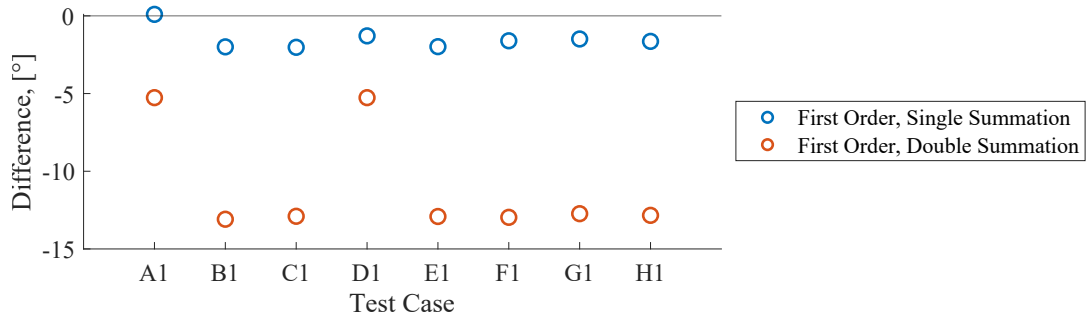


Figure I.32: Difference in mean direction of short-crested first order waves compared to value determined based on data without calibration error.

The figure shows the errors are increased for both models. Especially, the errors for the double summation model are high, and they have an maximum error of -12.96° , while the analysis of the single summation model only reach an error of -2.02° . From Figure I.29 and Figure I.32, it appear that Case A1 and D1 have in both situations of calibration error a significantly smaller error compared to the other cases.

I.2.2 Second Order Waves

The directional analysis of errors related to calibration are continued by including second order energy at the two cases presented for first order waves.

Calibration Error Gauge 1

In Figure I.33 the results of the estimated mean wave direction and the spreading are shown. This is compared to Figure 7.9, where the progress of the estimated curves a quite similar.

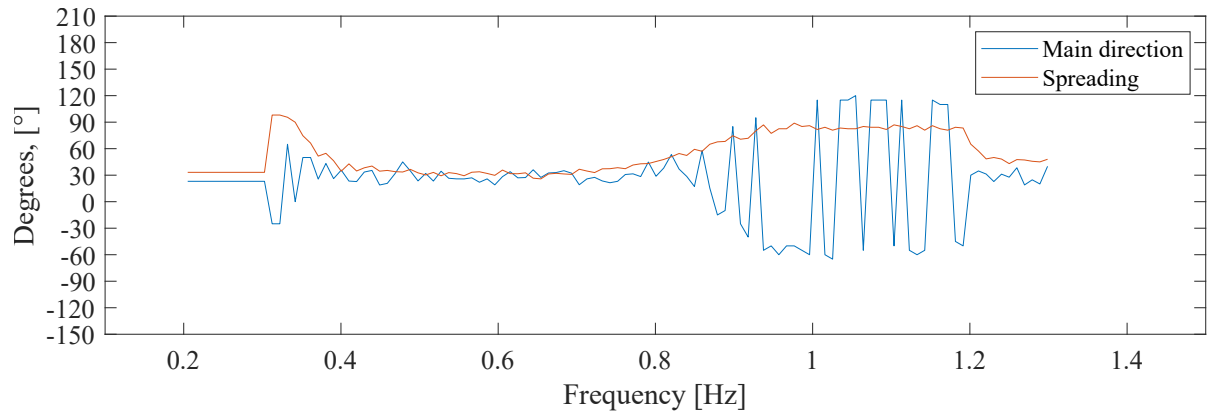


Figure I.33: Estimated direction for components in the wave field with target direction of 30° , Case D2 with error due to calibration of 5 % added to a wave gauge in position (x_1, y_1) , single summation.

The results of the weighted estimated mean wave direction and the spreading parameter are stated in Table I.14 together with its deviation from the short-crested waves analysed without calibration error from Table 7.4.

Table I.14: Results of MLM estimation of directional spreading of short-crested waves based on linear wave theory with target values $\theta_0 = 30^\circ$ and $s = 5$.

| Single Summation | | | Deviation from second order theory. | | |
|------------------|---------------------------------------|------------------|-------------------------------------|---------------------------------------|------------------|
| Case | Mean wave direction θ_0 [°] | Spreading [°] | Case | Mean wave direction θ_0 [°] | Spreading [°] |
| A2 | 26.90° | 32.90° | A2 | 0.41° | 0.08° |
| B2 | 29.09° | 32.54° | B2 | -0.50° | 0.40° |
| C2 | 28.60° | 31.67° | C2 | -0.52° | 0.53° |
| D2 | 27.39° | 38.99° | D2 | 0.12° | 0.09° |
| E2 | 28.53° | 32.59° | E2 | -0.51° | 0.45° |
| F2 | 27.07° | 33.74° | F2 | -0.29° | 0.43° |
| G2 | 25.58° | 34.68° | G2 | 0.05° | 0.59° |
| H2 | 27.59° | 34.47° | H2 | -0.03° | 0.62° |

The results show a deviation of maximum 0.50° for the weighted estimated mean wave direction and a maximum increase of the spreading of 0.62° , which is almost in the same level as the deviation for the analysis of first order waves with calibration error at one gauge.

The corresponding results for the data generated based on the double summation model appears from Table I.15.

Table I.15: Results of MLM estimation of directional spreading of short-crested waves based on linear wave theory with target values $\theta_0 = 30^\circ$ and $s = 5$.

| Double Summation | | | Deviation from second order theory. | | |
|------------------|---------------------------------------|------------------|-------------------------------------|---------------------------------------|------------------|
| Case | Mean wave direction θ_0 [°] | Spreading [°] | Case | Mean wave direction θ_0 [°] | Spreading [°] |
| A2 | 27.19° | 32.13° | A2 | -2.17° | -1.19° |
| B2 | 24.00° | 29.96° | B2 | -5.95° | -0.74° |
| C2 | 24.13° | 30.29° | C2 | -5.83° | -0.67° |
| D2 | 29.97° | 38.87° | D2 | -2.71° | -1.02° |
| E2 | 24.14° | 29.98° | E2 | -5.87° | -0.73° |
| F2 | 24.08° | 30.34° | F2 | -5.86° | -0.65° |
| G2 | 24.01° | 30.59° | G2 | -5.70° | -0.78° |
| H2 | 23.98° | 30.61° | H2 | -5.76° | -0.66° |

The difference in the estimated mean direction compared to the results from analysis without calibration error appear from Figure I.34.

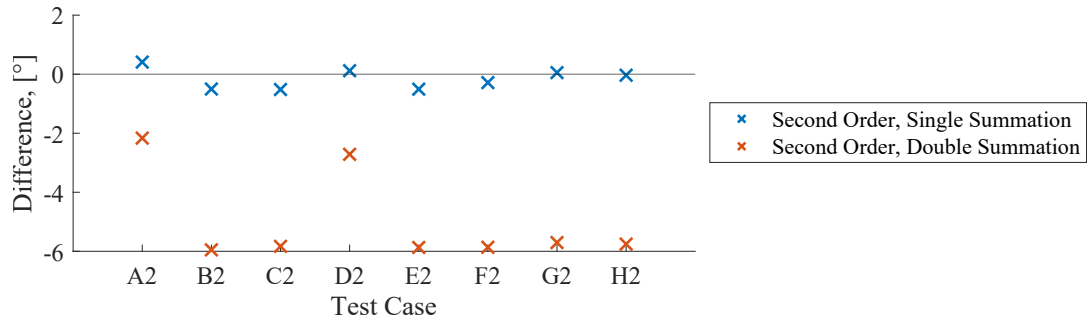


Figure I.34: Difference in mean direction of short-crested second order waves compared to value determined based on data without calibration error.

Figure I.34 shows all cases having almost no error for analysis of the data based on the single summation model. And up to approximately 6° for the data based on the double summation model.

Calibration Error Gauge 1 and 4

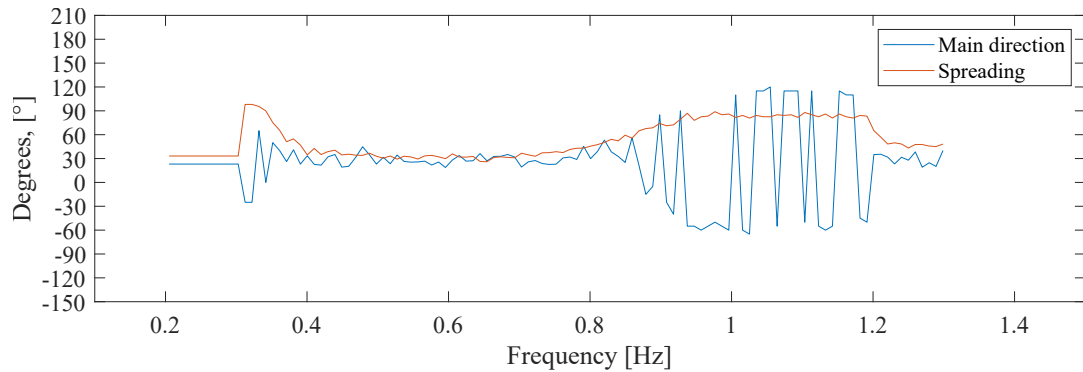


Figure I.35: Estimated direction for components in the wave field with target direction of 30° , Case D2 with error due to calibration of 5 % added to two wave gauges in position (x_1, y_1) and (x_4, y_4) , single summation.

Table I.16: Results of MLM estimation of directional spreading of short-crested waves based on linear wave theory with target values $\theta_0 = 30^\circ$ and $s = 5$.

| Single Summation | | | Deviation from second order theory. | | |
|------------------|---------------------------------------|------------------|-------------------------------------|---------------------------------------|------------------|
| Case | Mean wave direction θ_0 [°] | Spreading [°] | Case | Mean wave direction θ_0 [°] | Spreading [°] |
| A2 | 26.71° | 33.08° | A2 | 0.21° | 0.26° |
| B2 | 27.60° | 33.69° | B2 | -1.99° | 1.55° |
| C2 | 27.10° | 32.88° | C2 | -2.02° | 1.74° |
| D2 | 27.21° | 39.10° | D2 | -0.06° | 0.19° |
| E2 | 27.07° | 33.83° | E2 | -1.98° | 1.69° |
| F2 | 25.75° | 34.96° | F2 | -1.60° | 1.66° |
| G2 | 24.49° | 35.96° | G2 | -1.04° | 1.87° |
| H2 | 26.30° | 35.80° | H2 | -1.32° | 1.96° |

The results from the table show a deviation of the weighted estimated mean wave direction up to -2.02° for Case C2 and a deviation of the weighted spreading of up to 1.96° .

In Figure I.36 the results of the estimated mean wave direction and the spreading are shown. Compared to Figure 7.10 the estimated mean wave direction are more unsteady and placed in general lower, while the estimated spreading more similar to the one from the analysis without including calibration error.

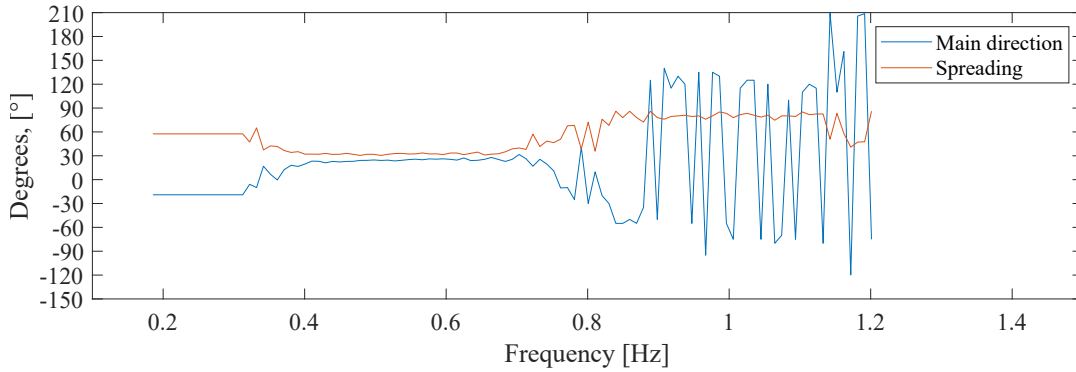


Figure I.36: Estimated direction for components in the wave field with target direction of 30° , Case D2 with error due to calibration of 5 % added to two wave gauges in position (x_1, y_1) and (x_4, y_4) , double summation.

The results of the weighted estimated mean wave direction and the spreading parameter are stated in Table I.17 together with its deviation from the short-crested waves analysed without calibration error from Table 7.5.

Table I.17: Results of MLM estimation of directional spreading of short-crested waves based on linear wave theory with target values $\theta_0 = 30^\circ$ and $s = 5$ and $N = 2^{10}$.

| Double Summation | | | Deviation from second order theory. | | |
|------------------|---------------------------------------|------------------|-------------------------------------|---------------------------------------|------------------|
| Case | Mean wave direction θ_0 [°] | Spreading [°] | Case | Mean wave direction θ_0 [°] | Spreading [°] |
| A2 | 24.74° | 32.85° | A2 | -4.62° | -0.46° |
| B2 | 16.87° | 31.06° | B2 | -13.08° | 0.36° |
| C2 | 17.06° | 31.36° | C2 | -12.90° | 0.40° |
| D2 | 26.12° | 39.45° | D2 | -6.56° | -0.44° |
| E2 | 17.16° | 31.05° | E2 | -12.85° | 0.34° |
| F2 | 17.01° | 31.41° | F2 | -12.94° | 0.41° |
| G2 | 17.13° | 31.66° | G2 | -12.58° | 0.29° |
| H2 | 16.91° | 31.68° | H2 | -12.83° | 0.41° |

The results from the table above show that when including possible errors related to calibration in a magnitude of 5% at two gauges and combine this with including second order wave theory, the analysis of the weighted estimated mean wave direction deviates with up to -13.08° and deviates overall more than the weighted estimated mean wave directions from the investigation with errors related to calibration at two gauges without second order energy. The weighted spreading deviates with up to $\pm 0.44^\circ$, which is in the same magnitude as for the cases without including second order energy.

The deviations compared to the similar waves without calibration error appears from Figure I.37.

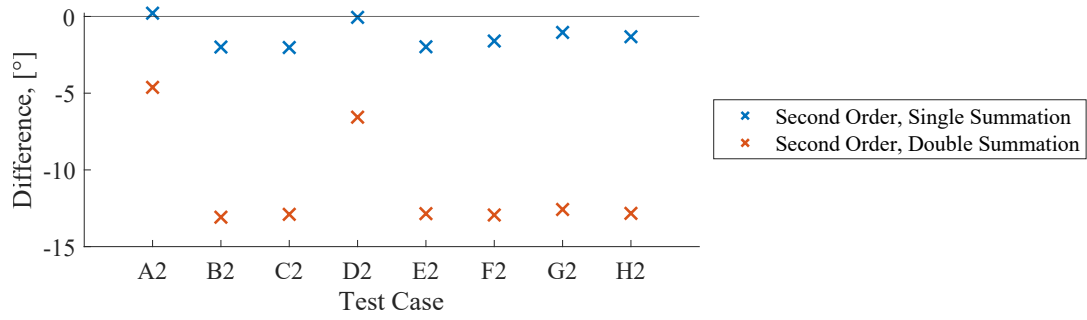


Figure I.37: Difference in mean direction of short-crested second order waves compared to value determined based on data without calibration error.

Figure I.37 shows the same pattern of error as seen from Figure I.34 just with larger errors in Figure I.37. But again the cases seems to have the same size of error at maximum -13.08° expect Case A2 and D2. The same tendency of case A2 having a smaller error than the other cases appear, while Case D2 has a large error compared to the other cases. In this situation, it is clear for the analysis of the mean directions from both generation models which case stands out. The largest error is for Case D2 from the analysis of the data generated from the double summation model which reach -37.37° .

I.2.3 Waves with Amplitude Dispersion

The amplitude dispersion related to three of the cases is considered in this section, where the investigation cover errors related to calibration added to 1 and 2 wave gauges, respectively. These analyses are performed for both a wave field based on a single and a double summation model.

Calibration Error Gauge 1

In Figure I.38 and Figure I.39 the results of the estimated mean wave direction and the spreading are shown. Compared to Figure 7.11 and Figure 7.12, respectively, there is almost no variation at the estimated mean direction nor the estimated spreading.

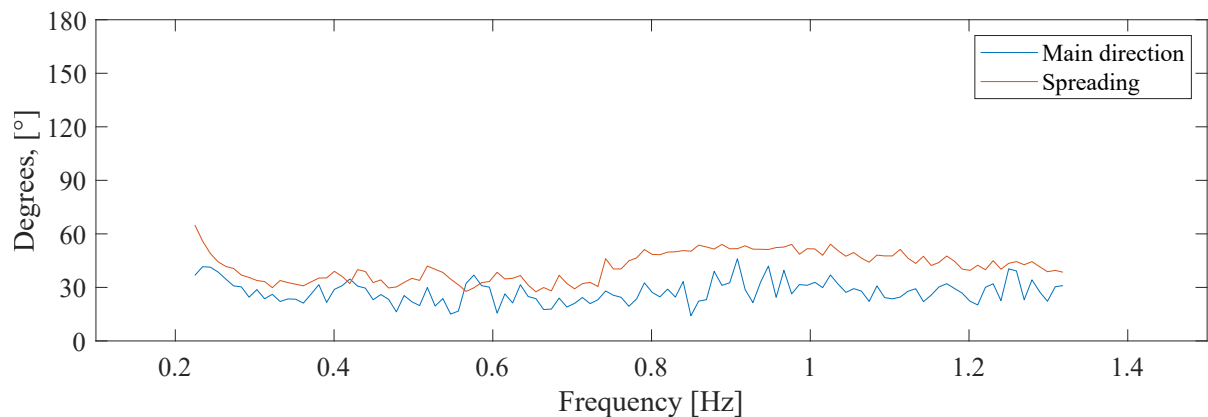


Figure I.38: Estimated direction with target direction of 30° , Case D3 with error due to calibration of 5 % added to a wave gauge in position (x_1, y_1) , single summation model.

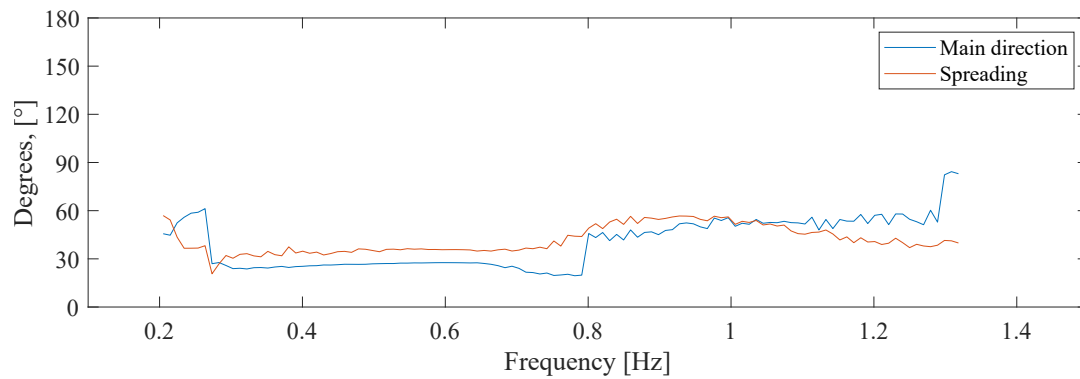


Figure I.39: Estimated direction with target direction of 30° , Case D3 with error due to calibration of 5 % added to a wave gauge in position (x_1, y_1) , double summation model.

The results of the weighted estimated mean wave direction and the spreading parameter are stated in Table I.18 analysed from a single summation model and in Table I.19 analysed from a double summation model, together with its deviations from the short-crested waves analysed without calibration error from Table 7.6 and Table 7.7, respectively.

Table I.18: Results of MLM estimation of directional spreading of short-crested waves based on linear wave theory with target values $\theta_0 = 30^\circ$ and $s = 5$.

| Single Summation | | | Deviation. | | |
|------------------|---------------------------------------|------------------|------------|---------------------------------------|------------------|
| Case | Mean wave direction θ_0 [°] | Spreading [°] | Case | Mean wave direction θ_0 [°] | Spreading [°] |
| A3 | 27.38° | 34.38° | A3 | 0.25° | 0.04° |
| D3 | 24.55° | 36.39° | D3 | -0.07° | -0.33° |
| G3 | 26.94° | 33.16° | G3 | -0.75° | 0.26° |

Table I.19: Results of MLM estimation of directional spreading of short-crested waves based on linear wave theory with target values $\theta_0 = 30^\circ$ and $s = 5$.

| Double Summation | | | Deviation from higher order results. | | |
|------------------|---------------------------------------|------------------|--------------------------------------|---------------------------------------|------------------|
| Case | Mean wave direction θ_0 [°] | Spreading [°] | Case | Mean wave direction θ_0 [°] | Spreading [°] |
| A3 | 27.02° | 31.20° | A3 | -2.80° | -1.21° |
| D3 | 27.90° | 36.59° | D3 | -0.90° | -1.03° |
| G3 | 23.68° | 31.23° | G3 | -6.19° | -0.93° |

The deviations of the weighted estimated mean wave direction and spreading show further that calibration error at one gauge at a size of 5% effect the results with up to -6.19° for the weighted estimated mean wave direction and with 1.21° for the weighted estimated spreading. The largest variations are related to the analysis of the waves generated from the double summation model.

The differences compared to the analysis without calibration error appears from Figure I.40.

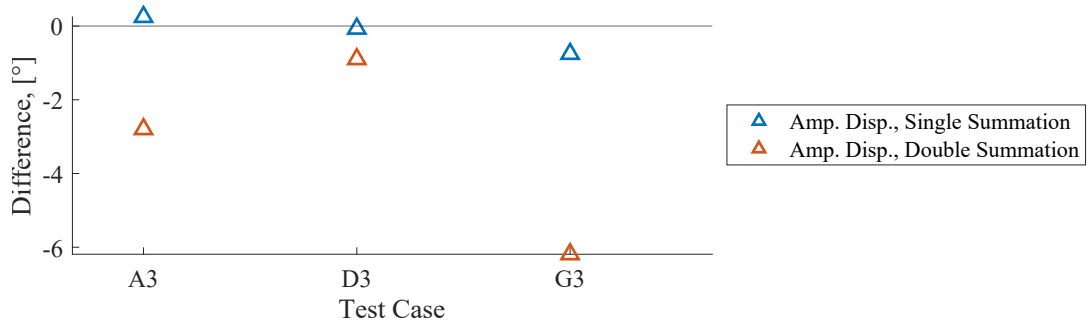


Figure I.40: Difference in mean direction of short-crested waves with amplitude dispersion compared to value determined based on data without calibration error.

Figure I.40 shows a kind of pattern between the analysed mean directions from the single and double summation model, with a vague tendency to a larger error of the mean direction for analyses of waves generated based on the double summation model. The largest error appear from Case G3 with a size of -6.19° . Based on the present analysis, there does not seem to be correlation between amount of amplitude dispersion and size of error on the mean direction.

Calibration Error Gauge 1 and 4

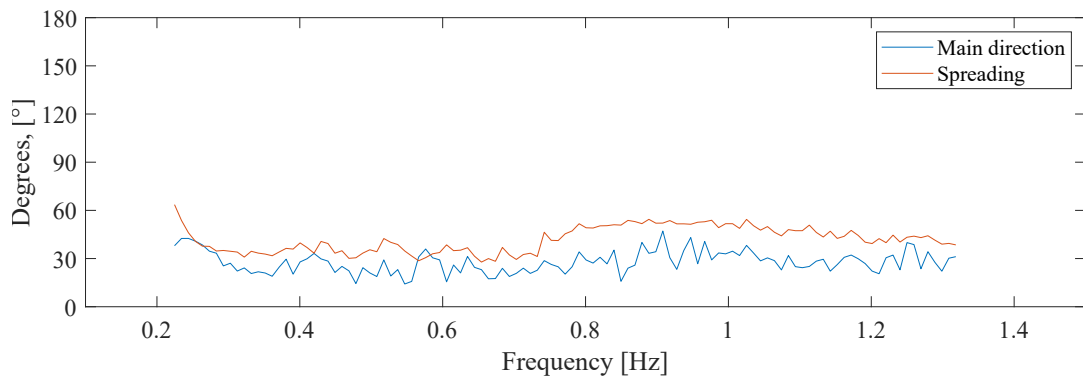


Figure I.41: Estimated direction for components in the wave field with target direction of 30° , Case D3 with error due to calibration of 5 % added to two wave gauges in position (x_1, y_1) and (x_4, y_4) , single summation model.

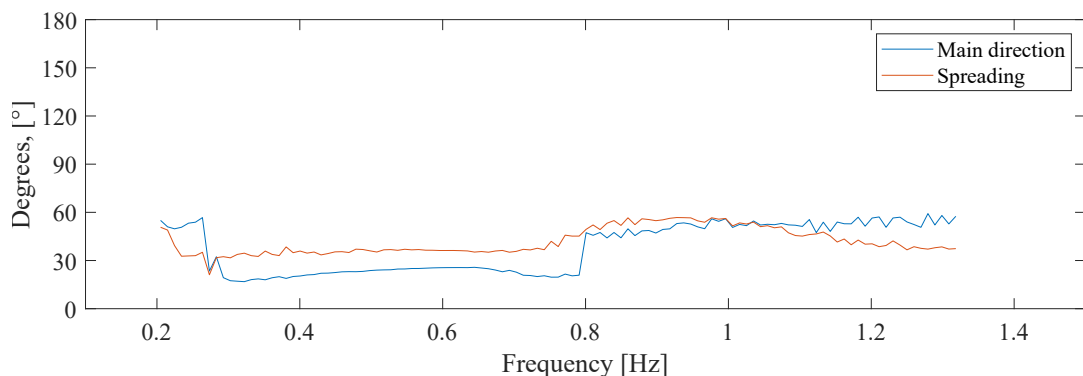


Figure I.42: Estimated direction for components in the wave field with target direction of 30° , Case D3 with error due to calibration of 5 % added to two wave gauges in position (x_1, y_1) and (x_4, y_4) , double summation model.

The results of the weighted estimated mean wave direction and the spreading parameter are stated in Table I.20 analysed from a single summation model and in Table I.21 analysed from a

double summation model., together with its deviations from the short-crested waves analysed without calibration error from Table 7.6 and Table 7.7, respectively.

Table I.20: Results of MLM estimation of directional spreading of short-crested waves based on linear wave theory with target values $\theta_0 = 30^\circ$ and $s = 5$.

| Single Summation | | | Deviation. | | |
|------------------|---------------------------------------|------------------|------------|---------------------------------------|------------------|
| Case | Mean wave direction θ_0 [°] | Spreading [°] | Case | Mean wave direction θ_0 [°] | Spreading [°] |
| A3 | 27.17° | 34.53° | A3 | 0.04° | 0.19° |
| D3 | 24.00° | 36.77° | D3 | -0.62° | 0.05° |
| G3 | 25.26° | 34.42° | G3 | -2.43° | 1.53° |

Table I.21: Results of MLM estimation of directional spreading of short-crested waves based on linear wave theory with target values $\theta_0 = 30^\circ$ and $s = 5$.

| Double Summation | | | Deviation. | | |
|------------------|---------------------------------------|------------------|------------|---------------------------------------|------------------|
| Case | Mean wave direction θ_0 [°] | Spreading [°] | Case | Mean wave direction θ_0 [°] | Spreading [°] |
| A3 | 24.60° | 31.93° | A3 | -5.21° | -0.49° |
| D3 | 25.28° | 37.30° | D3 | -3.21° | -0.32° |
| G3 | 16.33° | 32.36° | G3 | -13.54° | 0.20° |

The differences compared to the analysis without calibration error appears from Figure I.43.

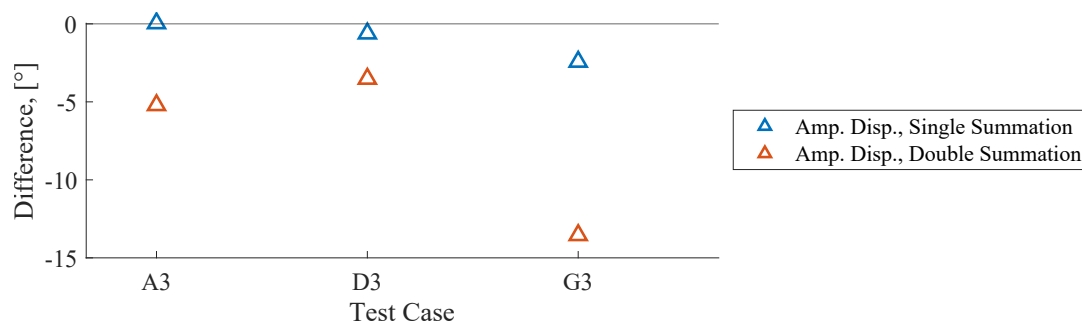


Figure I.43: Difference in mean direction of short-crested waves with amplitude dispersion compared to value determined based on data without calibration error.

From Figure I.43, it appear that the errors of the mean direction are worsened when also adding calibration error to gauge 4. The largest error are related to Case G3 of the mean directions analysed from data based on the double summation model. This error is -13.54° , which also appears as the largest error related to calibration error for the waves with amplitude dispersion.

Appendix J | Improvements Related to Calibration Error

As errors related to calibration have shown to be of great influence in the directional analysis based on the main analysis of this paper, it is here investigated what can be done to avoid this type of error. It will therefore be investigated whether it is possible to first of all detect calibration errors.

J.1 Detection of Calibration Error

To evaluate on the detection of calibration errors, the same data sets with and without calibration error on gauges in position (x_1, y_1) and (x_4, y_4) are considered, as these turned out to be of most significant influence according to the main report. The analyses included in this part have already been performed in previous parts of this project with determination of the direction and directional spreading in focus. During the analyses, the spectral density is determined based on a frequency domain analysis of the surface elevation signal for each gauge position of the CERC6 array. The spectra for a selection of analyses covering long- as well as short-crested waves appear from Figure J.1 to J.3.

For the long-crested waves in Figure J.1 and the short-crested waves based on the single summation model in Figure J.2, the spectral density determined based on the two measurements from the positions (x_1, y_1) and (x_4, y_4) seem to stand out from the spectral densities from the four other positions. For these type of analyses it therefore seems possible to detect calibration errors based on comparison of the spectral densities determined for each wave gauge position.

From Figure J.3, no significant difference between two analyses with and without calibration error respectively is noticed. The spectral densities determined based on the different gauge positions are however not equal due to poor quality of the generated data, which might be the reason that the calibration error is not detectable based on the spectral densities.

For the long-crested waves and the short-crested waves generated based on the single summation model, the generated data seems to be of high enough quality in order to determine an allowable difference in the zero moment of the spectral density, $m_0 = \int_0^\infty S_\eta(f)df$, determined from each gauge position. The amount of the difference relative to the zero moment of each gauge position is calculated, with the maximum values for the examples given in Figure J.1 to J.3 appear from Table J.1.

If the difference in the zero moments between two gauge points exceeds 10 % of the lowest of the two, the present analysis states that caution should be made, as it can be caused by calibration errors, which will lead to wrong estimations of the mean wave direction. The difference in the zero moment of the spectral densities does not necessarily mean that the estimated mean direction is wrong, since the analyses of the calibration errors showed significantly different results if the calibration errors were present at the gauges in position (x_1, y_1) and (x_2, y_2) . It will though lead to wrongful estimation of the significant wave height, which is also often of interest when analysing wave fields.

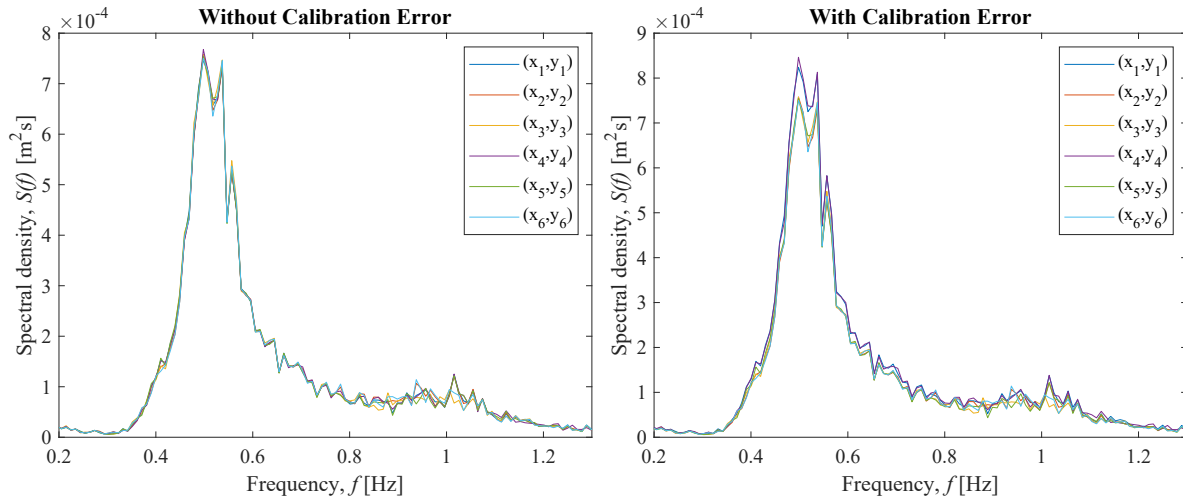


Figure J.1: Spectral densities for each wave gauge position of CERC6 array for long-crested second order wave field, with target direction 30° , Case D2.

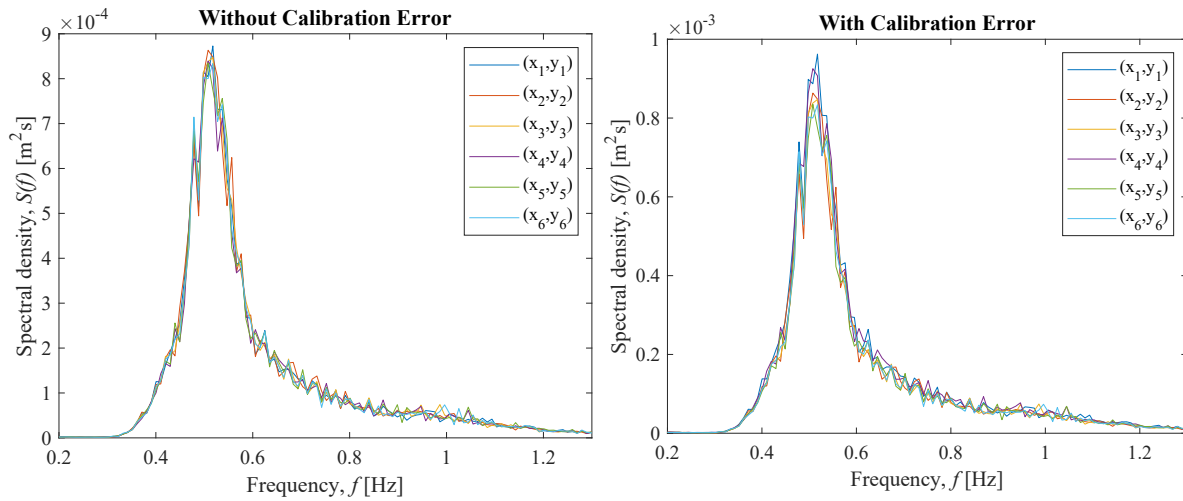


Figure J.2: Spectral densities for each wave gauge position of CERC6 array for short-crested second order wave field generated based on the single summation model, with target mean direction 30° and spreading parameter $s = 5$, Case D2.

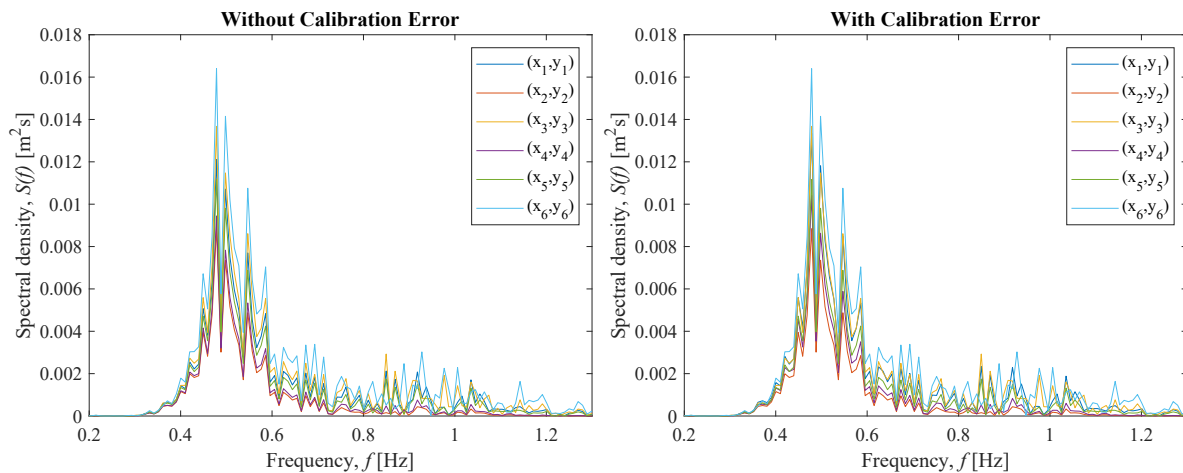


Figure J.3: Spectral densities for each wave gauge position of CERC6 array for short-crested second order wave field generated based on the single summation model, with target mean direction 30° and spreading parameter $s = 5$, Case D2.

Table J.1: Difference between lowest and highest estimated zero moment of the spectral density as the amount relative to the lowest zero moment of the data set.

| Type of wave field | Calibration Error | Max. amount of difference |
|------------------------------------|-------------------|---------------------------|
| Long-crested | No | 0.5 % |
| | Yes | 10.8 % |
| Short-crested, Single Summation | No | 2.1 % |
| | Yes | 10.7 % |
| Short-crested, Double Summation | No | 157 % |
| | Yes | 157 % |

Considering all spectra without prior knowledge about the inclusion of calibration error and generation model, the difference in spectral densities determined based on different wave gauge positions can be interpreted in the way that the considered wave field is not ergodic. Thereby the assumptions of the analyses are no longer fulfilled.

VI

Appendix II - Data

| | |
|--|-----|
| Appendix AA Data: Long-Crested Waves - Method 1 | 173 |
| Appendix AB Data: Long-Crested Waves - Method 2 | 287 |
| Appendix AC Data: Short-Crested Waves | 359 |
| Appendix AD Data: Long-Crested Waves incl. Noise | 373 |
| Appendix AE Data: Short-Crested Waves incl. Noise | 436 |
| Appendix AF Data: Long-Crested Waves incl. Errors Related to Calibration | 449 |
| Appendix AG Data: Short-Crested Waves incl. Errors Related to Calibration | 655 |
| Appendix AH Data: Wave Gauge Arrangement | 678 |
| Appendix AI Data: Variability of Double Summation Model | |